BARRIER WINDS OFF SOUTHEAST GREENLAND AND THEIR IMPACT ON THE OCEAN

A thesis submitted to the
School of Environmental Sciences
of the
University of East Anglia
in partial fulfilment of the requirements for the degree of
Doctor of Philosophy

By
Benjamin Harden
29 February 2012

Abstract

Barrier winds off southeast Greenland have been investigated through high resolution numerical models, reanalysis data and meteorological and oceanic observations.

A 20 year climatology has been conducted based on winter months from the ECMWF ERA-Interim reanalysis. Barrier wind events were shown to occur predominantly at two locations along the coast, both experiencing events stronger than 20 $\mathrm{m\,s^{-1}}$ on average once per week. Two classes of barrier winds – warm and cold – were investigated and found to develop in different synoptic-scale situations. Warm barrier winds developed when there was a blocking high pressure over the Nordic seas, while cold barrier winds owed their presence to a train of cyclones through the region.

One barrier wind event has been examined as a case study through high resolution simulations and in-situ observations. These data showed a complex spatial and temporal evolution of the wind field, temperatures and heat fluxes associated with the barrier wind. This case had many characteristics of a warm barrier wind and was shown to exhibit large ageostrophic forcing.

Through idealised modelling, the cause of the two locations of frequent barrier wind activity was shown to be the interaction of the flow with the promontories along southeast Greenland; the wind speed maxima were not maintained for a modified topography with no promontories. Two mechanisms important for wind speed enhancement were found: a tip-jet-like acceleration and downslope winds.

An investigation into mechanisms for the production of the Greenland Spill Jet has been conducted through mooring data from the Greenland shelf break and the ERA-Interim reanalysis. Barrier winds were important for spilling through two mechanisms: locally forced downwelling and the triggering of offshore flow in conjunction with shelf waves. Denmark Strait eddies were readily apparent in the observational record and also appeared to trigger spilling.

Acknowledgements

A huge thank you goes to Ian Renfrew for being a great supervisor. I'd like to thank him for all the time and effort he has given me and for playing such a large role in my scientific development. I am also completely indebted to Bob Pickart for his inspiring supervision and the multitude of opportunities he has given me over the past few years which have really expanded my horizons. Guðrún Nína Petersen also deserves a great deal of praise and thanks for her tireless, expert input into my work as do the other members of the department who have given me their time and insight over the years. I would also like to thank the Natural Environment Research Council for funding me and the Department of Environmental Sciences at UEA for having me to stay.

To my Mum, my Dad, my brother Tom and my wider family I say a massive thank you for years of support and encouragement, not least over the duration of this work. In so many ways you have made me a better scientist and a better person. I'd like to thank my friends, both in Norwich and further afield, for all the amusing diversions and supporting conversations. Two people I'd like to thank in particular are Hannah and Lauren. You guys have been awesome and an unfailing source of fun and strength.

Contents

Chapter 1

Introduction

Greenland is massive. It is the size of western Europe and its ice sheet is responsible for the Greenland plateau rising over 3000 m above sea level with very steep sides, especially along the southeast coast. Greenland is therefore cold, tall, steep and large as can be seen in Figure 1.1. It is these features that allow Greenland to radically alter the atmospheric flow over and around it on a range of temporal and spatial scales.

Greenland's impact on synoptic scales

On the largest scale, Greenland acts to reinforce the stationary wave field over the Atlantic Ocean by lowering the geopotential height of the 500 hPa level (Petersen et al., 2004; Junge et al., 2005). This is thought to be the result of cold air blocking of westerlies along the west coast causing an increase in density below mountain height. Westerly winds blowing towards Greenland also trigger large scale gravity waves (Doyle et al., 2005). These have a large effect on the atmospheric momentum budget of the northern hemisphere as well as producing local strong downslope winds. This type of feature is only accurately represented in numerical weather prediction models if the orography of Greenland is sufficiently resolved. Ólafsson (1998) showed that this has implications for models' abilities to predict the weather of the whole north Atlantic.

Greenland has a significant impact on the individual weather systems around its coastline (Scorer, 1988; Renfrew et al., 2008) located as it is on the north side of the North Atlantic storm track (Blender et al., 1997; Hoskins and Hodges, 2002). In fact, there is evidence that Greenland's location is influential in the precise latitude of the storm track, as the orography restricts the northward progression of storms (Petersen et al., 2004). In addition, the region to the east of Cape Farewell is, somewhat paradoxically, a region of both cyclogenesis and cyclolysis (Hoskins and Hodges, 2002). The cyclogenesis occurs

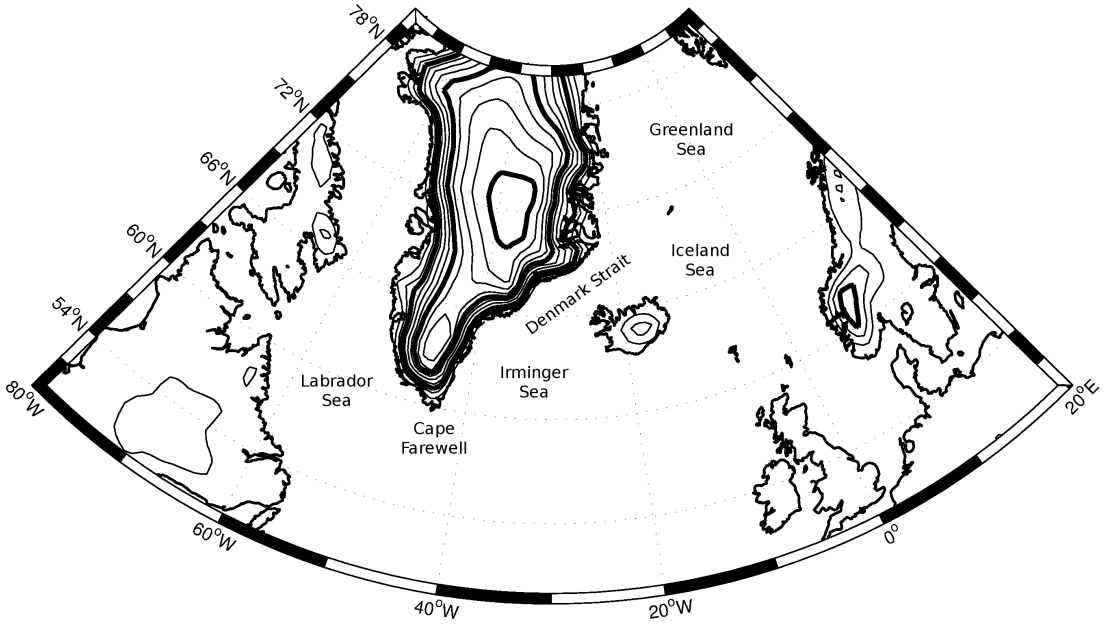

Figure 1.1: Map of the wider study region including names of key locations. Height contours every 250 m with bold contours every 1000 m.

primarily due to the production of cyclonic vorticity in the lee of Greenland due to one, or both, of low-level deflection (Petersen et al., 2003; Våge et al., 2009) and vortex stretching of downslope flows (Doyle and Shapiro, 1999; Klein and Heinemann, 2002). Serreze et al. (1997) suggests that in this region, 10 – 15 % of cyclones which are observed are generated locally. In some cases, the lee cyclones generated in this manner can couple to upper-level troughs and develop into major weather systems (Skeie et al., 2006). Cyclogenesis can also occur on smaller scales too – polar lows develop in the lee of Greenland due to katabatic winds (Klein and Heinemann, 2002), low-level ice edge baroclinicity (Douglas et al., 1995) and through the bifurcation of cyclones impinging on the southern tip of Greenland (Martin and Moore, 2006). On the other hand, cyclolysis is also common in this region and appears to occur for two main reasons. Firstly, the presence of Greenland, although allowing warm advection from the south, restricts cold advection from the north and destroys the baroclinicity of a developing cyclone. Secondly, the flow pattern in the lee of Greenland has been suggested to have the effect of 'capturing' cyclones that move into the region forcing them to decay in situ (Petersen et al., 2003).

High velocity winds

It is Greenland's amazing range of strong wind conditions though which makes this mountain so unique. Most of these are low-level, intermittent, mesoscale features, but their

influence on the large scale circulation of the atmosphere and ocean should not be underestimated. The most devastating to the inhabitants of Greenland are the downslope katabatic winds or 'Piteraqs' as they are known locally. These form due to radiative cooling of low-level air over the Greenland ice sheet and consist of strong downslope gravity-driven density jets. Through numerical modelling, Heinemann and Klein (2002) showed that katabatic forcing occurs all around the ice covered slope of Greenland although it is strongest along the steepest orographic gradients along the southeast coast. Heinemann and Klein (2002) showed that katabatic winds can be enhanced or degraded by the synoptic pressure gradient. It was one such storm, enhanced by the synoptic pressure system, that resulted in wind gusts of 72 m s^{-1} at Angmagssalik on Greenland's southeast coast (Rasmussen, 1989). van den Broeke and Gallée (1996) demonstrated that Katabatics can also be enhanced due to the thermal gradient at the ice-tundra boundary along west Greenland. Downslope flows around Greenland are not only devastating to local communities, but as mentioned previously, influence local mesocyclone production (Klein and Heinemann, 2002) and theoretically could generate large ocean heat fluxes due to their cold, dry properties.

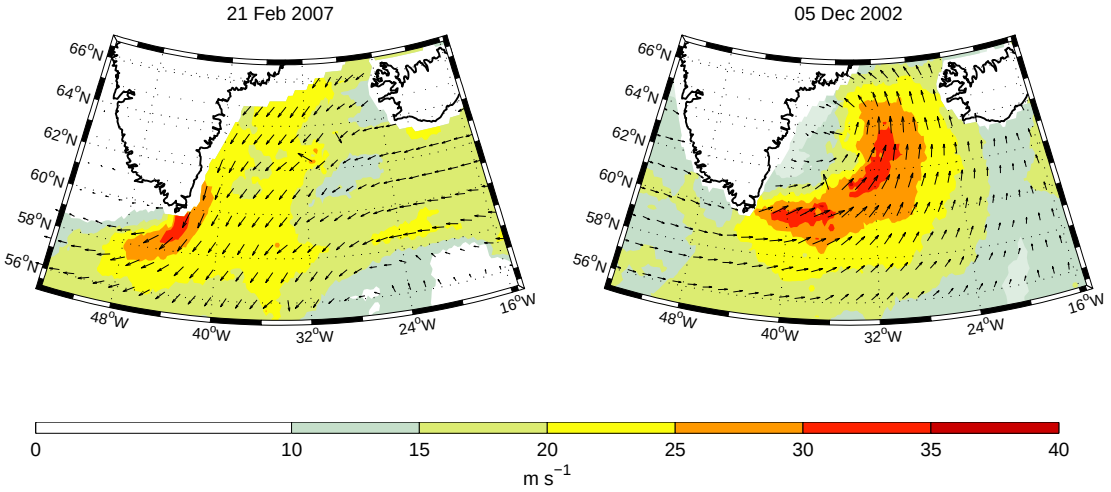

Figure 1.2: Examples of easterly (left) and westerly (right) tip jets as measured by QuikSCAT. Wind vectors shown every 5th grid point.

A region of Greenland which is particularly influential in the production of low-level, high velocity wind events is Cape Farewell, at the southern tip of Greenland. In fact, the winds are so strong and frequent that they make this the windiest location in the world's oceans (Sampe and Xie, 2007; Moore et al., 2008). Within the region there is a bimodal distribution in wind direction particularly for the highest wind speeds. These relate to the two main low-level wind jets formed – Easterly and Westerly Tip Jets (Moore, 2003; Moore and Renfrew, 2005) referred to in earlier work as forward and reverse tip jets.

Examples of each of these are shown in Figure 1.2. The synoptic forcing for Easterly Tip Jets comes from low pressure systems to the south of Cape Farewell (Moore and Renfrew, 2005). The flow towards southern Greenland is blocked and forced into a northeasterly flow upstream of Cape Farewell. When this reaches Cape Farewell, the end of the barrier, the pressure gradient produced by the orography is removed and the air enters an inertial regime which accelerates the flow westward (Outten et al., 2009, 2010). The result is a strong anticyclonic jet extending out into the Labrador Sea. The winds in the jet have been measured in situ at over 30 $\mathrm{m\,s^{-1}}$ at 40 m above the surface (Renfrew et al., 2009a), a value corroborated by modelling studies that showed winds in excess of 30 $\mathrm{m\,s^{-1}}$ at the surface (Outten et al., 2009, 2010). The region that these winds blow into, the Labrador Sea, is a vital region of deep convection in the north Atlantic (Lavender et al., 2000). More so, the precise location where easterly tip jets prevail is over a small ocean gyre, shown to be one of the hot spots of deep convection in the Labrador Sea (Lavender et al., 2002). It was therefore hypothesised by Martin and Moore (2007) that these winds could be vital in triggering overturning, however Sproson et al. (2008) refuted this hypothesis showing instead that westerly cold air outbreaks were more important.

Westerly Tip Jets, by contrast to their easterly cousins, extend eastward from the tip of Cape Farewell out into the Irminger Sea. They were initially thought to be the result of the conservation of Bernoulli function as westerlies descended over the Greenland peninsula (Doyle and Shapiro, 1999). Although this mechanism is likely to contribute part of the acceleration observed, it is probable that low-level blocking and deflection of westerlies around the southern tip of Greenland is the main driver of the wind velocity signal (Petersen et al., 2003; Moore and Renfrew, 2005). Composites of westerly tip jet events showed mean velocities in excess of 25 $\mathrm{m\,s^{-1}}$ occurring on average once every two weeks during the winter months (Våge et al., 2009). These were typically forced by a low pressure system centred in the northwest Irminger Sea, roughly in the location of the climatological Icelandic Low. Their unique combination of cold advected air and cyclonic wind stress curl allow the westerly tip jets to trigger deep convection in the Irminger sea (Pickart et al., 2003; Våge et al., 2008). This shows that even though the westerly tip jets are intermittent, their properties and strength, even on short timescales, allows them to influence the circulation of the entire Atlantic Ocean. This result piqued interest in the oceanic impact of Greenland's high velocity wind events which will be discussed in more detail shortly.

Barrier winds

Finally we come to the subject of this thesis, barrier winds, which are triggered frequently along the southeast coast of Greenland (Moore and Renfrew, 2005). Barrier winds are a well established phenomena, having first been observed and described over 40 years ago by Schwerdtfeger (1975) along the Antarctic Peninsula. They occur when stable air is forced towards a steep and high topographic barrier. The air, unable to ascend the barrier, is dammed along the coast. The resulting pressure gradient, which develops perpendicular to the coastline, supports an along-barrier jet confined below mountain height called a barrier wind. To first order these flows exist in geostrophic balance. This configuration is shown in Figure 1.3 through the use of a 2D numerical model of flow towards a ridge. This clearly shows the blocking of the lower level flow and the development of an along-barrier jet. Since they were first described, barrier winds have been observed at numerous locations worldwide; California (Cui et al., 1998), New Zealand (Revell et al., 2002), the Rockies (Colle and Mass, 1995), the Sierra Nevada (Parish, 1982), the Appalachians (Bell and Bosart, 1988), and the Alps (Chen and Smith, 1987) and have been the subject of a number of idealised numerical studies (Parish, 1982; Braun et al., 1999; Petersen et al., 2003, 2005).

Some of the most detailed studies of barrier winds have take place along the southwest coast of Alaska. As with barrier winds in many other coastal locations, the driving synoptic conditions come from maritime cyclones impinging on the coast. In their five-year climatology of coastal barrier winds, Loescher et al. (2006) showed that the locations of the strongest barrier winds (forced by onshore flow) occurred at the highest orography found along the coast – Mount Fairweather being responsible for the most persistent strong winds. They also found that not all barrier winds had the same forcing mechanisms – specifically there appeared to be two classes of wind: 'classical' and 'hybrid'. Classical barrier winds are, as described previously, the along-coast deflection of onshore directed flow. In contrast, hybrid jets source their air from a cold inland pool. The coastal outflow of this inland air is bent coast parallel by the prevailing onshore atmospheric conditions. Whereas classical jets are strongest near the highest terrain, hybrid jets are strongest downstream of a gap in the coastal terrain. This information was built upon using case study observations (Olson et al., 2007) and detailed idealised numerical modelling (Olson and Colle, 2009). These showed that not only were hybrid jets distinctively colder than classical jets, but that the hybrid jets are in general wider and less coastally confined. The modelling study of Olson and Colle (2009) also showed some more general features of barrier winds. Experiments with a wide barrier forced stronger and wider barrier winds than experiments with a narrow barrier even though the near coast terrain

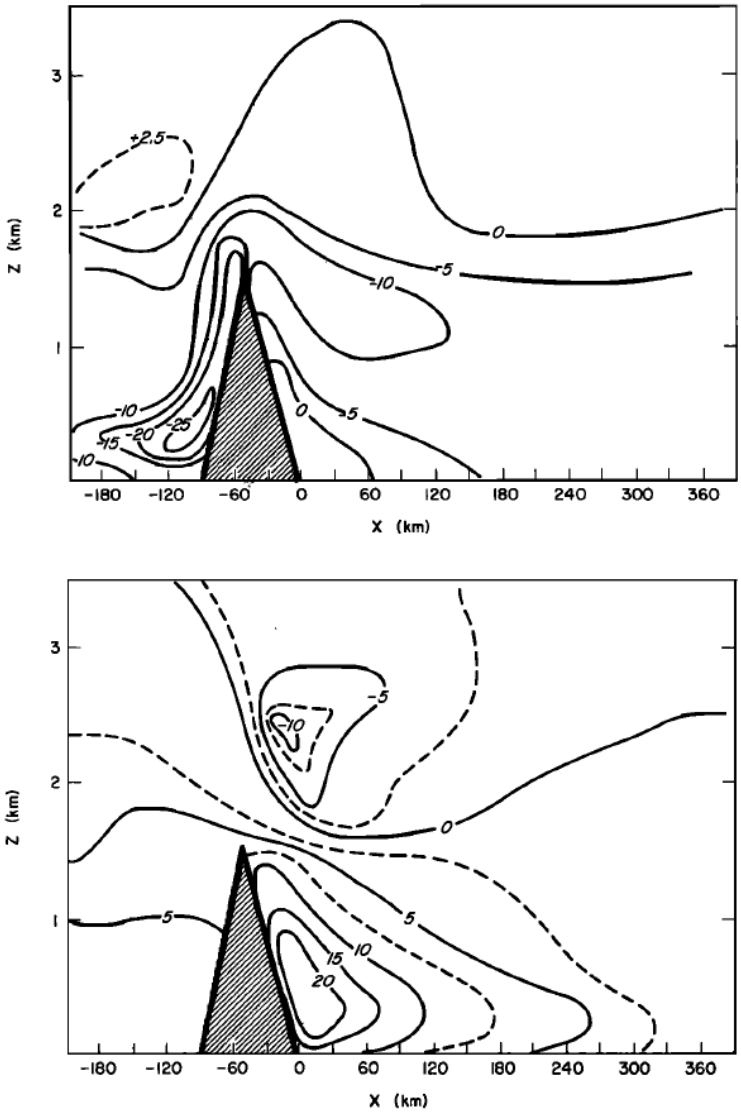

Figure 1.3: Idealised 2D modelling of flow towards a ridge from Parish (1983) demonstrating barrier wind formation through ridge perpendicular (top) and parallel (bottom) flow. Units are $\mathrm{m\,s^{-1}}$.

had the same gradient. This was explained by the deflection of the upstream flow to become more coast parallel, aiding low-level blocking. The onshore wind angle appears to be vital in determining both the strength and width of a barrier wind. Unless the angle of onshore wind incidence becomes very shallow, the wind speed enhancement and jet width will both increase as the onshore wind becomes more coast parallel.

Returning to Greenland, there is anecdotal evidence of barrier winds along the southeast coast from 1000 years ago, as recorded in the Icelandic Sagas, but it wasn't until 2003 that the first mention of these strong winds were published (Moore, 2003). It was Moore and Renfrew (2005) though who provided the first comprehensive overview of bar-

rier winds using five years of QuikSCAT 10-m wind speed data. They found that barrier winds occur predominantly at two locations along the Greenland coast, one to the south and one to the north of the Denmark Strait [dubbed Denmark Strait South (DSS) and Denmark Strait North (DSN) respectively]. At DSS, barrier winds in excess of 25 m s^{-1} were an almost weekly fixture whereas upstream at DSN they were somewhat less frequent. It is likely though that the frequency of winds at DSN was affected by the prevalence of sea ice in this location, over which no QuikSCAT measurements are possible. An example of a barrier wind as measured by the QuikSCAT product is shown in Figure 1.4.

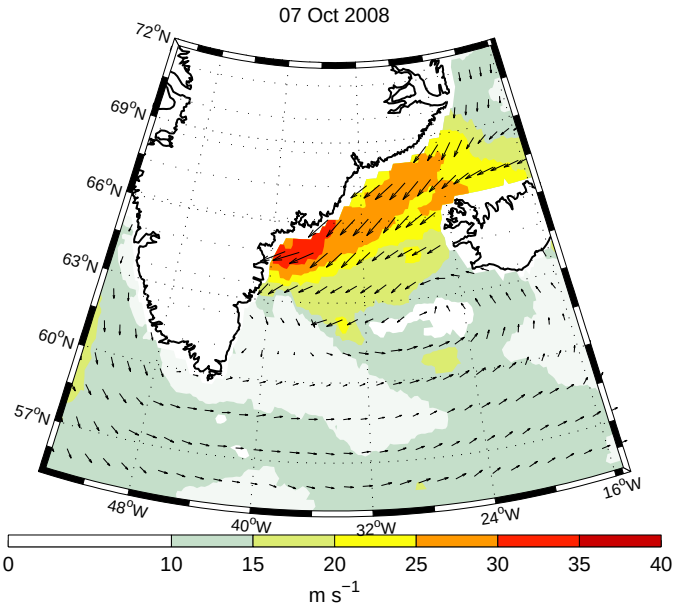

Figure 1.4: As Figure 1.2 but for a barrier wind on 7 October 2008.

In 2007, the Greenland Flow Distortion Experiment (GFDEx) set out to provide the first set of comprehensive in situ measurements of low-level strong wind events around Greenland (Renfrew et al., 2008). The main observational platform for GFDEx was the Facility for Airborne Atmospheric Measurements (FAAM), an instrumented BAe146 jet. Over the three weeks of the field campaign in February and March, 12 flights were made to investigate, amongst other things, polar lows, tip jets, and barrier winds. Several barrier winds were observed during the experiment through the aircraft mounted instruments and the use of dropsondes. These events were investigated by Petersen et al. (2009) through the observations collected and modelling work. They showed that the barrier winds were contained below 2000 m with well mixed cores of cold air. In all cases, there appeared to be two different sources of air contained within the barrier wind system; cold, dry, northerly sourced air and warmer, moist air pulled in from the south, typically residing above the jet core. They saw that the barrier winds were forced by a synoptic low pressure system to the southeast of Greenland and that the position of barrier wind formation was

determined by the precise position of this low. Through numerical simulations, they were able to show that the effect of the orography was to double the wind speed in the regions of barrier wind formation. The force balance in the domain was also investigated and shown to have large ageostrophic components in isolated regions. It appears, as in Alaska, that Greenland barrier winds also exhibit complex forcing mechanisms.

Petersen and Renfrew (2009) used the experimental data from the GFDEx campaign to investigate the surface fluxes from the range of weather events sampled. They showed that barrier winds were capable of producing total turbulent heat fluxes of up to 500 $\mathrm{W\,m^{-2}}$ and surface stresses in excess of 1 $\mathrm{N\,m^{-2}}$. These are large fluxes by regional standards. An investigation into the impact of these barrier winds on ocean circulation (Haine et al., 2009) showed a similar heat flux estimate (600 $\mathrm{W\,m^{-2}}$), a peak current of nearly 2 $\mathrm{m\,s^{-1}}$, and a ocean boundary layer depth that responded quickly to the wind forcing with mean values of around 100 m and maximum values as large as 500 m.

Potential ocean impact

Now that Greenland barrier winds have been introduced it is probably pertinent to ask the question: Why is it important to study them? From an atmospheric perspective, the seas around Iceland are rich fishing grounds so accurate prediction of strong winds is vital for the safety of vessels in this region. One feature that is important in this endeavour is that many barrier winds have strong gradients in wind speed along their boundaries [for example the shock fronts observed in Loescher et al. (2006)]. Accurate modelling of the precise position of these fronts will therefore be vital in determining what weather a vessel will experience. It has also been shown that accurate representation of strong local wind forcing around Greenland and Iceland can be important for the prediction of weather system evolution downstream (Irvine et al., 2009, 2010). A greater understanding of Greenland barrier wind dynamics will aid weather prediction throughout western Europe.

In addition to the above, further motivation for this thesis comes from the impact that barrier winds have on ocean circulation in the region. The seas around Greenland form a vital component of the overturning circulation for the entire Atlantic ocean and there are number of local processes that are likely to respond to strong wind forcing by barrier winds. Currently these interactions are poorly understood.

Transformation of surface waters through deep convection takes place at a number of locations around Greenland (Marshall and Schott, 1999) including the Labrador Sea (Lavender et al., 2000), Greenland Sea (Schott et al., 1993), Iceland Sea, and the Irminger Sea (Pickart et al., 2003; Våge et al., 2008). Although deep convection at all these locations requires strong wintertime atmospheric forcing, it is only the Irminger Sea which

has been shown to be forced by one of Greenland's low-level, intermittent wind phenomena – the Westerly Tip Jet. These can force intense deep convection, even though they are relatively short lived, due to their combination of high wind speed, cold and dry air, and cyclonic wind stress curl (Våge et al., 2009). This latter attribute forces a weak ocean gyre which domes the isopycnals and aids the onset of convection. It is possible that barrier winds could generate similar conditions to those found in Tip Jets and could be aiding deep convection around Greenland.

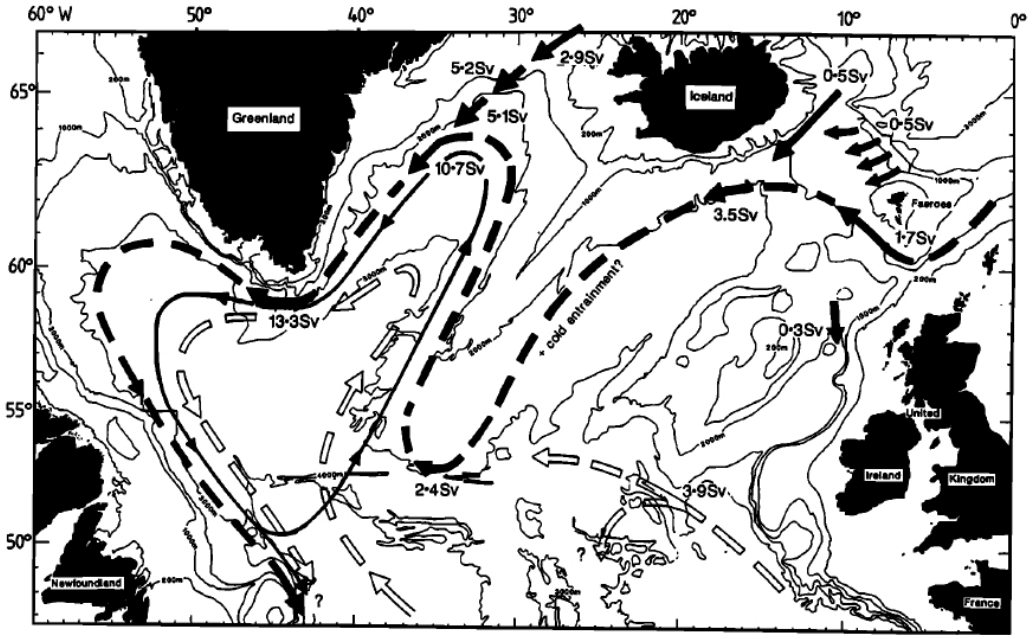

Figure 1.5: Schematic of North Atlantic circulation of water denser than 27.8 kg m^{-3} as Dickson and Brown (1994).

Deep convection in the Northern latitudes produces dense, cold water masses which can then spread equatorward to balance the poleward flow of warm water in the surface of the Atlantic. It is therefore vital in maintaining the ocean circulation of the entire Atlantic. Most of the dense water is formed in the Nordic Seas to the east of Greenland. To enter the deep ocean and return equatorward it has to cross the ocean ridge that joins Greenland, Iceland, the Faroes and Scotland. It does so through a number of gaps in this ridge. The pathways and downstream evolution of these flows are shown in Figure 1.5. As can be seen, the route which has the largest flux of dense water is through the Denmark Strait, between Greenland and Iceland, over a sill at a depth of 650 m (Hansen and Østerhus, 2000). The current best estimates of the mean volume transport of water denser than 27.8 kg m^{-3} (defined as Denmark Strait Overflow water, DSOW)[1] through the strait is

[1] Actually 1027.8 kg m^{-3}, but oceanography convention is to subtract 1000 kg m^{-3} for brevity.

about 3 Sv (Macrander et al., 2005). This dense water, having passed though the strait, cascades down the continental slope to the depths in the Denmark Strait Overflow where it then goes on to form the major limb of the Deep Western Boundary Current which flows southward along the eastern coast of North America (Figure 1.5). As it overflows it entrains more water into the current so by the time it has reached its maximum depth and meets with dense water that has reached the deep ocean through different pathways, the current transports 5–6 Sv equatorward (Dickson and Brown, 1994).

The Denmark Strait Overflow is one way in which dense water leaves the near surface environment through the Denmark Strait. There is a related body of dense water though which could be more susceptible to forcing by barrier winds. It has been shown recently (Brearley et al., 2012) that an amount of water denser than that required to be classed as DSOW stays on the East Greenland continental shelf as it passes southward though the Denmark Strait. This water subsequently spills off the shelf downstream of the sill to form what has been called the East Greenland Spill Jet (Pickart et al., 2005), a density driven gravity current which descends and traverses the southeast Greenland continental slope above the DSOW. This current was only discovered through high resolution hydrographic surveys which were capable of resolving the relatively narrow jet (Pickart et al., 2005). An estimate of the transport in the Spill Jet was generated through repeated sections south of the Denmark Strait and shown to be 4.8 ± 2.4 Sv, equivalent to the volume transport of the Denmark Strait Overflow at the same position (Brearley et al., 2012). Magaldi et al. (2011) showed, using high resolution numerical modelling of a summer month, that much of the spilling (about half) could be attributed to cyclonic eddies streaming down the shelf break from the Denmark Strait (Bruce, 1995; Spall and Price, 1998), but these simulations were under weak meteorological forcing. It is conceivable that the downwelling favourable sense of Greenland barrier winds could be contributing to the spilling of dense water off the continental shelf into the Spill Jet. Pickart et al. (2005) even hypothesised as much in their paper.

Downwelling and convection in the ocean give just two reasons why the study of barrier winds could be so potentially crucial. In addition to these, the other components of the complex current system along the southeast coast of Greenland (shown in Figure 1.6) could be susceptible to wind forcing by barrier winds. Above the Spill Jet and Denmark Strait Overflow waters there are a number of near surface currents including the retroflected, warm and salty Irminger Current and the cold fresh East Greenland Current. There is still a great deal to be learnt about these surface currents and the hydrographic front between them. A better knowledge of wind forcing will aid the development of our understanding of this current system as more is learnt about it.

It is likely that barrier winds will also influence local ocean–ice sheet processes. Bar-

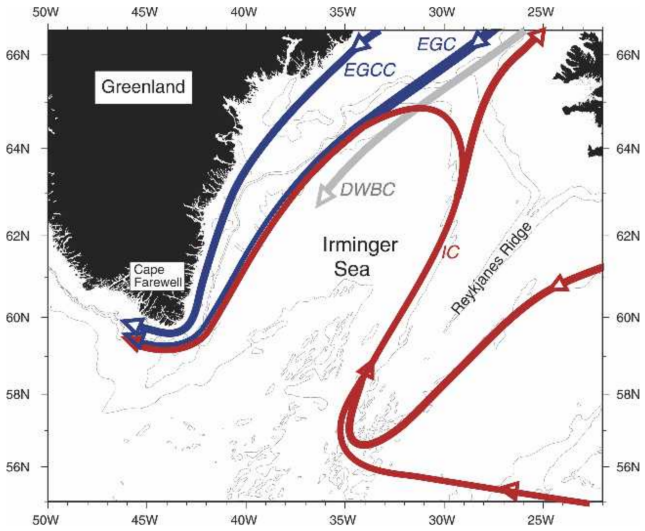

Figure 1.6: Schematic of the current system along the southeast coast of Greenland from Pickart et al. (2005).

rier winds have already been shown to force the recirculation of warm water up glacial fjords, undercutting glacial tongues and speeding up the glaciers' decent into the ocean (Straneo et al., 2010). The export of sea ice and bergs along the southeast coast is also likely to be influenced by strong coast parallel wind forcing.

As has been demonstrated, there are a large variety of potential ocean impacts of barrier winds in the region. In addition, it is especially important to understand ocean forcing in this region given the rate at which the picture of ocean circulation is changing in recent years. In the past six years, not only has the Spill jet been discovered but also a completely new pathway of water towards the Denmark Strait – The North Icelandic Jet (Steingrimur and Valdimarsson, 2004; Våge et al., 2011). It has been hypothesised that this current could supply the densest half of the total volume transport into the Denmark Strait Overflow. It is possible that the North Icelandic Jet might be influenced by local meteorological conditions.

Thesis outline

There is a clear importance in the better understanding of barrier winds off southeast Greenland from both meteorological and oceanographic perspectives. To that end, the following will be presented in this thesis:

- Chapter 2: The first comprehensive climatology of barrier winds based on 20 years of winter months from the ERA-Interim reanalysis product. Special attention will

be given to examining the range of ocean impacts observed and the reasons for any differences seen.

- Chapter 3: Unique data from a barrier wind event in October 2008 along with numerical modelling work. This case study will be compared with the case studies of Petersen et al. (2009) and the differences discussed in light of the climatological findings of Chapter 2.

- Chapter 4: Idealised modelling of barrier flows along the southeast Greenland coast to determine the reason for spatial distributions seen in observations and reanalysis.

- Chapter 5: The first observational insight into the mechanisms for the production of the East Greenland Spill Jet based on a year of hydrographic and velocity data from the southeast Greenland shelf break. This includes an investigation into the impact that barrier winds have on this cross slope transport of dense water.

- Chapter 6: Conclusions and closing remarks.

Chapter 2

A wintertime climatology of southeast Greenland barrier winds

2.1 Introduction

Greenland presents a high, steep and cold topographic barrier to the atmosphere. Its ice sheet, which covers 80% of the land mass, is responsible for the Greenland plateau being higher than 3000 m above sea level. This large, cold mass is capable of diverting and distorting atmospheric flow around it, forcing a number of intermittent, low-level, high velocity wind events such as westerly and easterly tip jets (Doyle and Shapiro, 1999; Moore, 2003; Moore and Renfrew, 2005; Våge et al., 2009; Renfrew et al., 2009a; Outten et al., 2009, 2010), barrier winds (Moore and Renfrew, 2005; Petersen et al., 2009) and katabatic/downslope winds (Heinemann and Klein, 2002; Klein and Heinemann, 2002). It also has influences on the development of polar lows, cyclogenesis (Petersen et al., 2003; Serreze et al., 1997), cyclolysis (Hoskins and Hodges, 2002; Serreze et al., 1997), and the properties of cyclones which pass through the region (Kristjánsson and McInnes, 1999; Skeie et al., 2006).

Not only are the low-level wind events produced by Greenland responsible for some of the stormiest seas in the world's oceans (Sampe and Xie, 2007; Moore et al., 2008), producing hazardous maritime conditions, but interest has been piqued recently into the possible influence that these intermittent events have on the ocean in a region that is vital for the thermohaline circulation. For example, westerly tip jets (produced around the southern tip of Greenland) have been shown to be capable of triggering deep convection in the Irminger Sea (Pickart et al., 2003; Våge et al., 2008). The knowledge that intense, but intermittent, wind phenomena can have a protracted impact on the slow overturning

A more concise version of this chapter has been published in the American Meteorological Journal of Climate. The reference, Harden et al. (2011), is included in the thesis references.

circulation of the Atlantic ocean points to the importance of understanding the prevalent atmospheric conditions and ocean forcing in the region.

The subject of this study is barrier winds – low-level jets produced when air is forced towards a high and steep topographic barrier (such as Greenland) with a large non-dimensional mountain height, Nh/U, where N is the Brunt-Väisälä frequency, h is the mountain height and U is the upstream wind speed (Schwerdtfeger, 1975; Parish, 1983; Pierrehumbert and Wyman, 1985). The air, unable to ascend the barrier, is dammed and a pressure gradient perpendicular to the barrier develops leading to geostrophic flow along the barrier (to first order). When the upstream winds are produced by a synoptic-scale cyclone, the separation of 'synoptic' and 'perturbation' pressure gradients is difficult [e.g. see Petersen et al. (2009)]. Barrier winds have been studied in situ and through numerical models at numerous mountainous locations around the world; the Antarctic Peninsula (Schwerdtfeger, 1975; Parish, 1983), Alaska (Loescher et al., 2006; Olson and Colle, 2009), California (Cui et al., 1998), New Zealand (Revell et al., 2002), the Rockies (Colle and Mass, 1995), the Sierra Nevada (Parish, 1982), the Appalachians (Bell and Bosart, 1988), and the Alps (Chen and Smith, 1987) and have been the subject of a number of idealised numerical studies (Braun et al., 1999; Petersen et al., 2003, 2005).

Along the coast of Greenland, barrier wind events were comprehensively observed by instrumented aircraft during the Greenland Flow Distortion Experiment (GFDEx) field campaign (Renfrew et al., 2008). Petersen et al. (2009) provide an overview of two barrier wind events, including jet cross sections from dropsonde soundings, numerical simulations and trajectory analysis. They showed that the presence of Greenland caused up to a doubling in the maximum wind speed along the coastline – with the precise synoptic-scale situation being critical for the location and magnitude of the associated barrier winds. GFDEx showed how potentially important these winds could be for the ocean. In the two and a half weeks of the field campaign, three barrier wind events were observed, in one case measured total turbulent heat fluxes exceeded 600 $\mathrm{W\,m^{-2}}$ and surface stresses reached 1.5 $\mathrm{N\,m^{-2}}$ (Renfrew et al., 2009b).

An investigation of their effects on the ocean was conducted through very high resolution numerical modelling of the Irminger Sea and Denmark Strait by Haine et al. (2009). They showed that these barrier winds were capable of producing maximum net heat fluxes of around 600 $\mathrm{W\,m^{-2}}$, a peak current of nearly 2 $\mathrm{m\,s^{-1}}$, and that the boundary layer depth of the ocean responds rapidly and sensitively with mean values of around 100 m, but maximum values as large as 500 m. Recently Straneo et al. (2010) showed that strong barrier winds off southeast Greenland are likely responsible for the recirculation of warm water up glacial fjords, increasing the melting of glaciers at their base and enhancing the speed of their descent into the ocean.

Tip jets and barrier winds around Greenland were the subject of the QuikSCAT climatology of Moore and Renfrew (2005) hereafter MR05. MR05 provided much useful information about strong wind events in the region, but was limited by only having a five year record over the ice free oceans and only for 10-m winds. A lack of wind speed data over sea-ice affects a large region in the north of Denmark Strait, where barrier winds are known to occur (Petersen et al., 2009). Tip jets have recently been the subject of climatologies using atmospheric reanalysis products (Sproson et al., 2008; Våge et al., 2009), but climatological knowledge of barrier winds in the region is still limited to that provided by MR05. Here we build upon that by compiling a climatology of barrier winds using state-of-the-art meteorological reanalyses, thus making use of a number of diagnostics throughout the atmosphere as well as over land and sea-ice.

The aims for this study can be summarised as:

- To extend knowledge about the frequency, strength, location and properties of barrier winds in the region;
- and to outline the impact these winds could be having on the ocean, providing the oceanic community with a useful tool for studying atmospheric forcing in the region.

2.2 Data

2.2.1 Description

Data from the European Centre for Medium-Range Weather Forecasts (ECMWF) product ERA-Interim (Berrisford et al., 2009) was used for this study. ERA-Interim is a global reanalysis product which covers the period from 1989 to the present. A number of improvements have been made on its predecessor ERA-40. These include many model refinements along with changes in data assimilation; most significantly a four-dimensional variational (4D-Var) data assimilation process is now used (Rabier et al., 1998).

The underlying model for ERA-Interim is ECMWF's Integrated Forecast System (IFS) cycle 31r2. This is a spectral, semi-implicit, semi-Lagrangian model with 255 spectral modes (T255) and 60 levels (L60) in the vertical. For grid point fields, a reduced Gaussian grid is used with an approximately uniform spacing of 80 km (N128). This is a marked improvement on ERA-40 which was T159, L60 and N80, so an approximate horizontal resolution of 125 km. The improvement in horizontal resolution is crucial for this study in order to adequately resolve the relatively small-scale barrier winds. The atmosphere is coupled to a ocean-wave model with 30 wave frequencies which can propagate

in 24 directions.

Re-analyses fields are produced four times daily at 00, 06, 12 and 18 UTC. Ten-day forecasts are run twice a day, initialised at 00 and 12 UTC. Data is available on the 60 model levels or, as used here, interpolated on to 37 pressure levels.

2.2.2 Verification

To appreciate the strengths and limitations of ERA-Interim, verification of the model against observations is necessary. Much work has already been conducted to verify ECMWF products. Although much of this was in verifying ERA-40 and ECMWF operational analyses and not ERA-Interim, the underlying model is largely the same so much of this verification should be applicable to ERA-Interim.

In a comparison of surface layer observations and calculated turbulent heat fluxes with equivalent fields in the ECMWF operational analysis (Renfrew et al., 2002) it was found that the ECMWF model represents the wind field accurately, has a small cold bias for sea surface temperature (which impacts on near surface atmospheric temperature) and predicts reasonably well the surface heat fluxes. The error in this last value tends to be to overestimate the heat fluxes by about 10%. Våge et al. (2009) found that the low wind speed comparisons of ERA-40 with QuikSCAT showed that the performance of the ERA-40 model was good. At high wind speeds, contributions from QuikSCAT's strong wind bias (Moore et al., 2008) and from the likely underrepresentation of strong winds in ERA-40 due to the relatively coarse resolution makes evaluating the model difficult. In comparisons with aircraft data (Renfrew et al., 2009b), ECMWF products were found to capture the high wind speed events in general terms, but failed to capture peak wind speeds by nearly 5 m s^{-1}. Near surface temperature (particularly for the higher resolution model) was found to be well represented although a systematic cold bias of 1 K was apparent. Humidity and heat fluxes were modelled well. All the above studies were conducted under similar meteorological conditions to those of this study which makes their findings particularly pertinent.

In addition to these region specific studies, Chelton et al. (2006) finds that even at high spectral resolution and low wind speeds, the ECMWF operational analysis systematically underestimates the intensity of weather systems with a spatial scale under 1000 km. Comparisons with buoy calculated surface heat fluxes in the northeast Atlantic (Josey, 2001) showed that the latent heat fluxes in the ECMWF reanalysis were overestimated most likely because of the use of a bulk formula. It should be noted that the measured sensible heat fluxes in this last study were so small that limited information could be gleaned about the model's ability to reproduce them accurately.

The conclusions from the above studies is that ERA-Interim is likely to under predict wind speeds, especially at at the high end and for mesoscale structures. It is likely that surface layer temperatures will be slightly too cool and surface fluxes will be well represented if slightly too large.

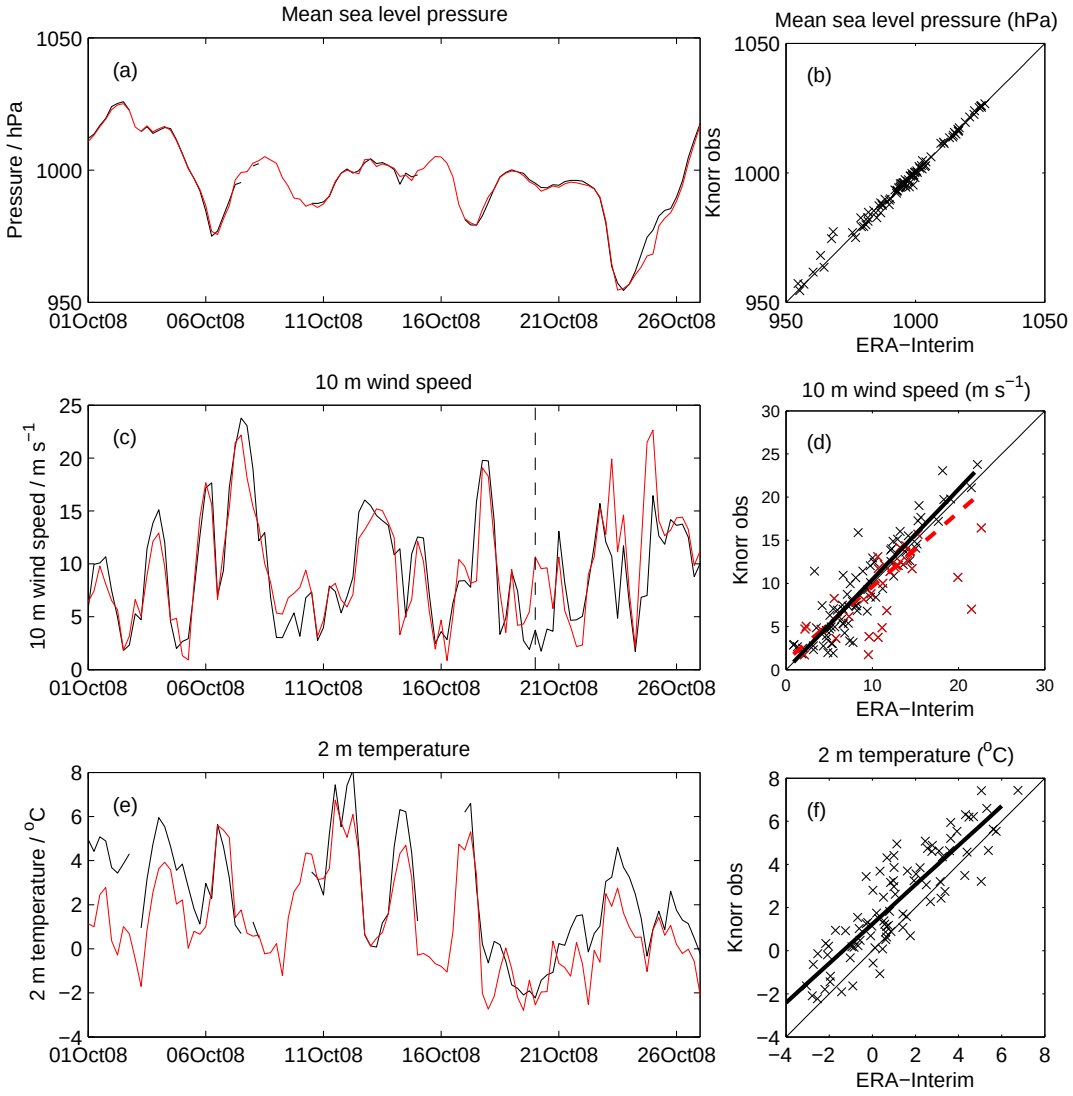

Figure 2.1: Comparison of ERA-Interim (red) near surface fields with measurements made aboard the R/V Knorr (black) in the Irminger sea in October 2008. (a-b) Surface pressure (hPa), (c-d) 10 m wind speed (m s^{-1}), (e-f) 2 m temperature (°C). The red crosses in panel (d) are for times after 20 October 2008 as indicated by the dashed line in panel (c).

Further verification will be presented based on data collected from the region of interest under barrier wind conditions. Near surface meteorological variables were collected during a research cruise in the Irminger Sea aboard the R/V Knorr in October 2008. Specifically, the variables that will be analysed are pressure and wind speed measured

by the IMET package and temperature as recorded by the Vaisala WXT5-10 system. The WXT5-10 system would have been utilised for both pressure and wind speed but due to technical issues this system was unavailable for wind speed and pressure measurements for much of the cruise so the IMET measurements were used for a more complete data set. All meteorological instruments were mounted on a tower at the bow of the ship which put them 15.5 m above sea level. In all subsequent analysis, the measurements are extrapolated to the same heights as the outputs from ERA-Interim, that is to 10 m for wind speed, to 2 metres for temperature and to the surface for pressure. This was achieved using the logarithmic neutral profile formulae for wind speed and temperature, and hydrostatic balance for pressure. Stability-dependent surface-layer formulae (Smith 1988) were also used for the wind speed and temperature reductions, but few discernible differences were seen. Due to an incomplete humidity record the neutral formulae were used below.

A number of barrier winds were observed during the cruise, making this data set ideal for verifying the performance of ERA-Interim for this study. Figure 2.1 indicates that the surface pressure and the 10 m wind speed perform well in comparison with data collected on the Knorr. The ERA-Interim pressure is in particular is in excellent agreement with the measured pressure.

Strong winds are only slightly underrepresented in ERA-Interim by around 1 $\mathrm{m\,s^{-1}}$, but the product performs better than was found in comparing ERA-40 wind speeds with QuikSCAT (Våge et al., 2009). The red dashed trend line in Figure 2.1(d) shows the regression for all data points collected, but is perhaps a little misleading. It includes points recorded after 20 October 2008 [dashed line in Figure 2.1(c)] when the Knorr spent much of its time in coastal and fjord regions where sheltering effects often lead to stronger winds in the model than were recorded on the Knorr. Those points recorded during this time are shown in Figure 2.1(d) with red crosses and a trend line excluding these points is shown as the solid line in Figure 2.1(d). The conclusion is that ERA-Interim is representing 10 m winds well. The temperature comparison and trend line in Figures 2.1(e) and (f) shows that the near surface temperature field has a cold bias of 2°C in the model, a feature seen by Renfrew et al. (2009b) when comparing observations to the ECMWF 1.125 degree operational analysis and which they attribute to low model resolution; the feature is not there for the comparison with the ECMWF T511 resolution model. As in that study, this is likely to produce an over estimation of surface turbulent heat fluxes. It seems in general though that the performance of ERA-Interim at the surface is good.

To be able to say how well ERA-Interim performs with height comparisons with radiosonde and dropsonde observations in the region of interest were conducted. Radiosondes were launched during the R/V Knorr cruise in October 2008. Figure 2.2 shows three representative soundings: (a) during low wind conditions, and (b-c) during barrier wind

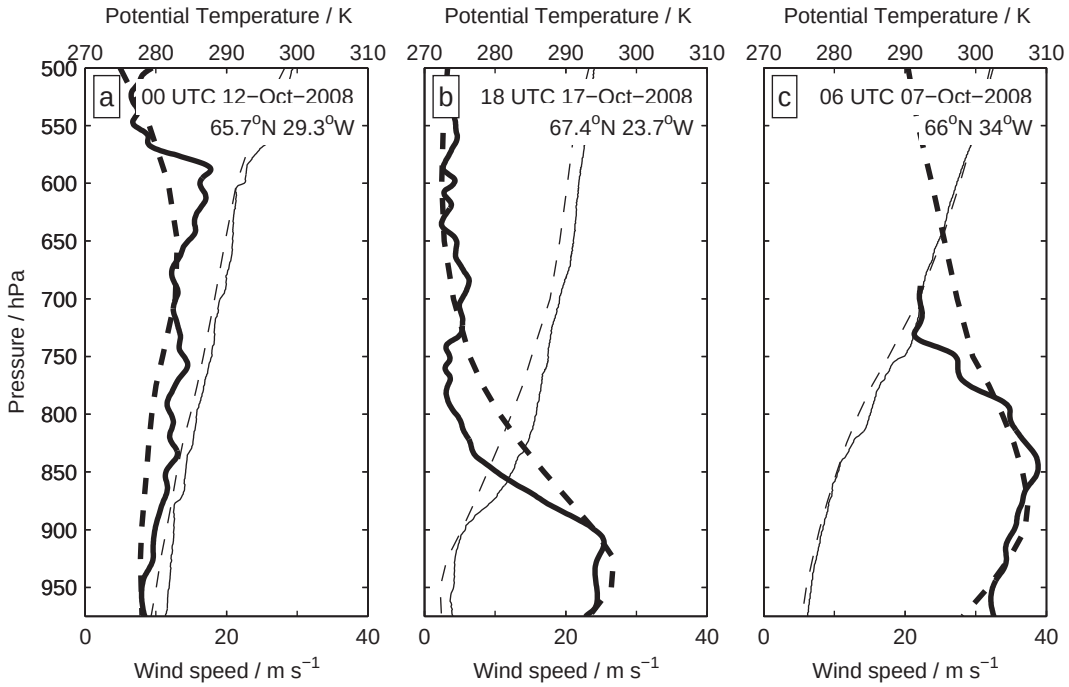

Figure 2.2: Three sample radiosonde soundings (solid lines) made aboard the R/V Knorr in the Irminger sea in October 2008 and corresponding model soundings in the ERA-Interim data set (dashed lines). Wind speed (thick, m s^{-1}) and potential temperature (thin, K) shown.

events. Under low wind speed conditions, the winds are generally well represented at all heights, while the cold bias seen at the surface extends throughout the atmospheric column. This cold bias is also observed at all heights under barrier wind conditions. The magnitude of the maximum wind speeds recorded during barrier wind conditions are mostly well captured in the ERA-Interim product, although at some times peak wind speeds are missed by as much as 5 m s^{-1}. The jets were commonly observed to be capped by a strong temperature inversion [e.g. in (b)], the gradients of which were poorly captured in the model. This results in a model jet that is too broad in the vertical. Panel (c) shows that when a barrier wind has a weaker temperature inversion, the vertical gradients in the measured wind speed are reduced and the performance of ERA-Interim improves.

Comparisons were also made between ERA-Interim and the cross sections shown in Petersen et al. (2009). These used dropsonde observations during barrier wind conditions in the Denmark Strait during GFDEx (not shown). These comparisons yielded similar features to those seen in Figure 2.2. The magnitude and vertical structure of the barrier winds were generally well represented, although peak winds in the jet core and sharp vertical gradients were occasionally too weak. The fact that the general magnitude of the jet is captured, is an indication that the horizontal resolution is sufficient to adequately

resolve these features.

What we have learnt from these verifications and from previous studies is that the ERA-Interim product is most accurate at the surface where wind speed, temperature and fluxes are modelled well. The resolution is sufficient to resolve barrier jets, although care should be taken when interpreting the vertical structure of the product which, although capturing basic features, will not necessarily capture the strength of vertical gradients in variables.

2.3 Near surface climatology

The near surface fields from ERA-Interim winters (DJF) between 1989 and 2008 were used to draw a climatological picture of the mean state in the region. Throughout, comparisons will be made to the climatology of strong wind events around Greenland compiled using QuikSCAT by MR05.

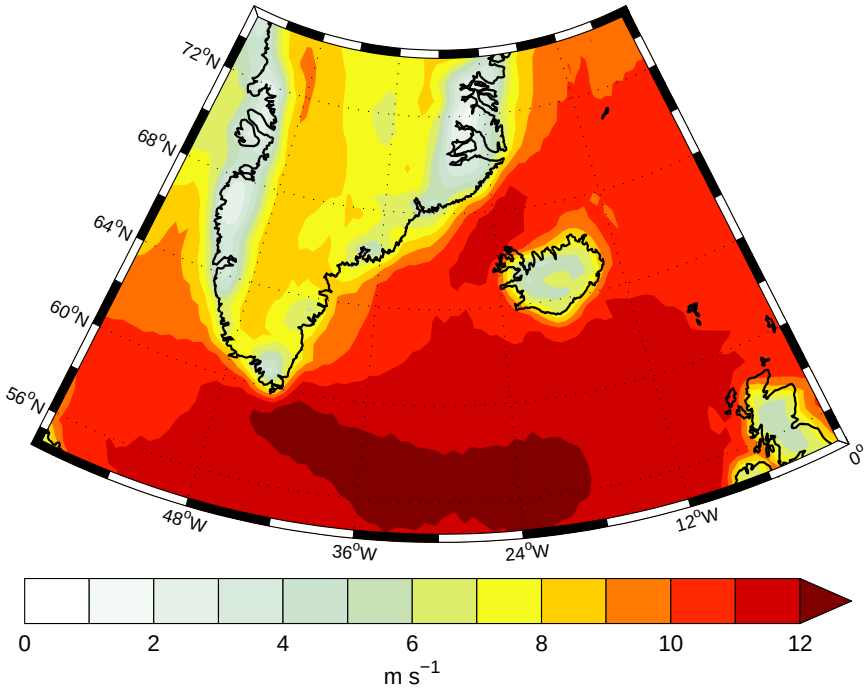

Figure 2.3: Mean of the 10 m wind speed (m s^{-1}) for ERA-Interim winter months (DJF) 1989-2008.

The mean of the 10 m wind speed for all times, displayed in Figure 2.3, shows that the region extending from Cape Farewell eastward towards Scotland experiences the strongest mean wind speed of over 12 m s^{-1}. This is likely due to the number of cyclones which pass through this region. In fact, over much of the ocean the mean wind speed seldom

falls below 10 m s^{-1}. Land is characterised by generally lower wind speeds. Although the general magnitude of the mean wind speed of the oceans agrees well with MR05, Figure 2.3 is lacking the bullets of over 13 m s^{-1} in the Denmark Strait, further south along the coast and at Cape Farewell seen in MR05. These regions frequently experience strong wind events: barrier winds along the southeast coast and tip jets at Cape Farewell. An amount of the discrepancy found here could be explained by QuikSCAT's propensity to over estimate the magnitude of high winds (Moore et al., 2008; Ebuchi et al., 2002). This would skew the mean wind speed for these regions, favouring artificially high values in the QuikSCAT analysis of MR05. Equally, models often fail to predict peak wind speeds accurately although ERA-Interim has been shown to function adequately for reproducing 10 m wind speeds. Both potential effects will act to create the differences seen.

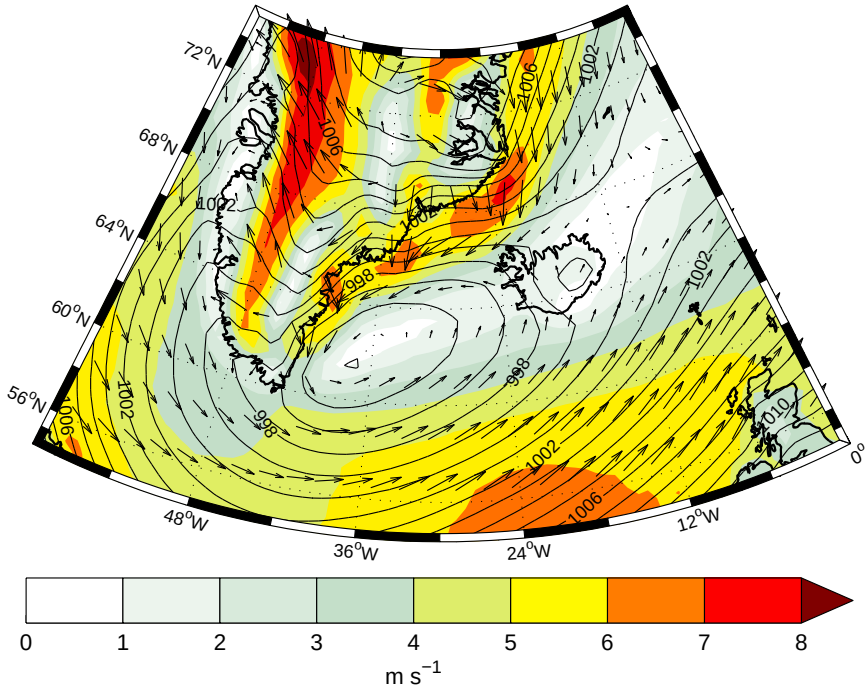

Figure 2.4: Mean of the 10 m wind field (m s^{-1}) for ERA-Interim winter months (DJF) 1989-2008. Wind vectors shown every 3rd data point.

This type of difference is also seen in the comparison of the standard deviation of the mean 10 metre wind speed (not shown) with the corresponding figure in MR05. Over much of the ocean there is good agreement, but in the regions we might expect to find strong winds, MR05 finds the standard deviation larger by more than 2 m s^{-1} at the barrier wind locations and by 4 m s^{-1} at Cape Farewell

The 10 metre mean wind field is shown in Figure 2.4, calculated by taking the mean of the easterly and northerly velocity components separately then calculating a mean speed from these values – this figure therefore shows information on predominant wind direc-

tions. It shows a climatological jet of 5 m s^{-1} running the length of the southeast coast of Greenland. This appears to be forced by a climatological low which is sitting over the central Irminger Sea. The position of this feature is consistent with the climatological Icelandic Low (Sahsamanoglou, 1990; Serreze et al., 1997). Along this wind jet sit isolated bullets in excess of 6 m s^{-1}, the site of two of which, at 66°N 34°W and 69°N 23°W, agree well with the locations for barrier winds highlighted in MR05, both having magnitudes in good agreement with those shown in MR05. A third location of high climatological wind is evident further to the southwest at 65°N 41°W, its location encroaching on the land with a larger off shore component than the other two bullets which are more coast parallel. This outflow could be partly influenced by katabatic and downslope winds that are common occurrences in this region (Heinemann and Klein, 2002; Klein and Heinemann, 2002) or be part of the downslope flow associated with westerly tip jets (Doyle and Shapiro, 1999). There is also a strong southerly flow over much of the western slopes of Greenland and a high pressure system over northeast of Greenland which acts to produce northerly winds along the east coast of Greenland

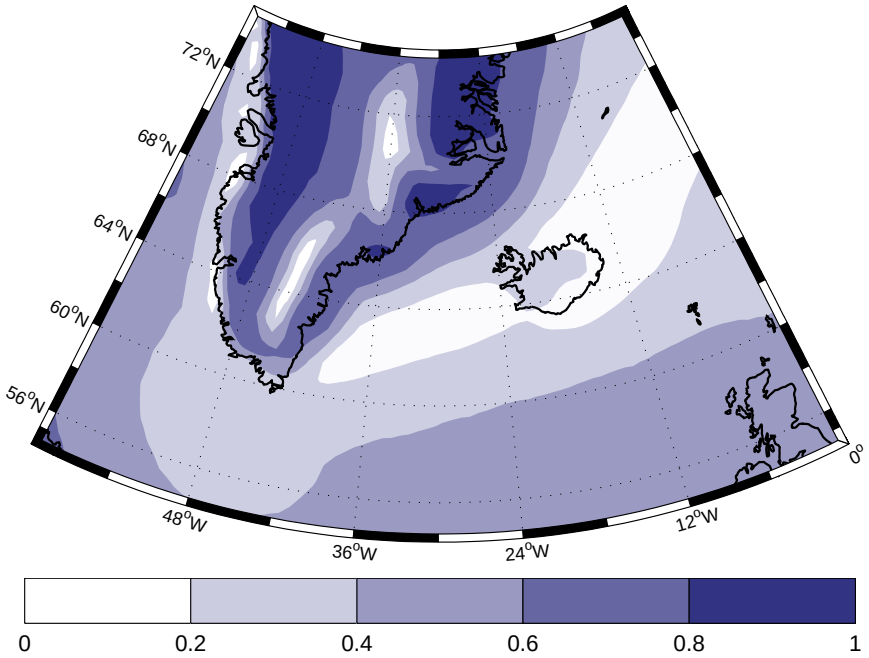

Figure 2.5: Directional consistency of the 10 m wind field for ERA-Interim winter months (DJF) 1989-2008

The directional consistency of the 10 m wind field [defined as the ratio of the mean wind field (Figure 2.4) to the the mean wind speed (Figure 2.3)] is shown in Figure 2.5. Values can range from 0, indicating no single directional preference of the flow, to 1, in which the flow is consistently from one direction. The directional consistency along

the southeast coast increases towards the coast from 0.4 at the edge of the climatological jet to nearly 0.8 along the coastline and up over the slopes. The implication is that the climatological jet shown in Figure 2.4 exists much of the time. The high directional consistency on the slope is likely due to the frequent occurrence of downslope winds, katabatic or otherwise, in these regions (Rasmussen, 1989; Heinemann and Klein, 2002; Klein and Heinemann, 2002). The low directional consistency in the central Irminger sea reflects the number of cyclones that pass through this region. The strong southerly flow over west Greenland is shown here to be very directionally consistent.

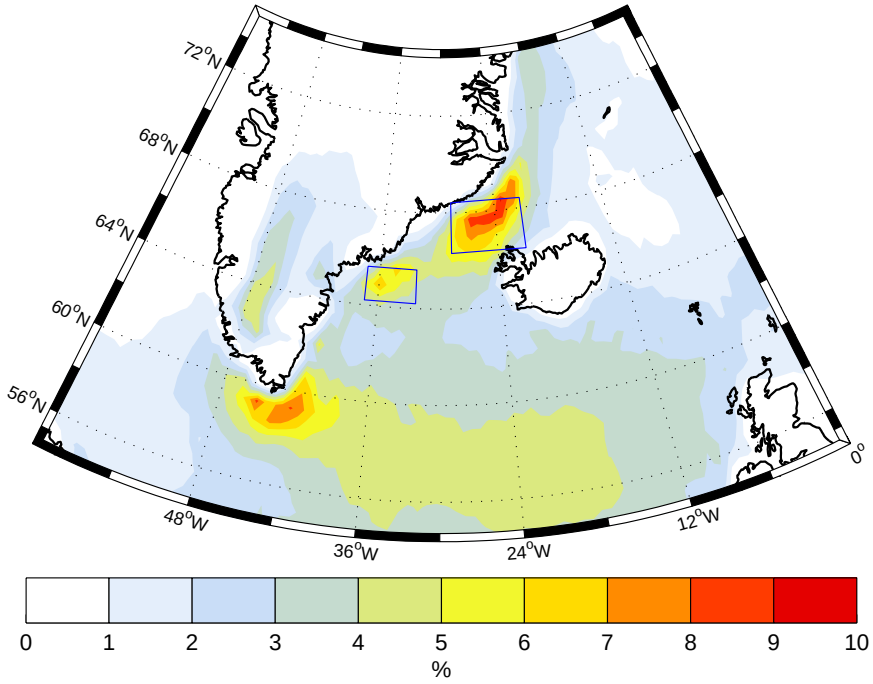

Figure 2.6: Percentage of time that the wind speed is in excess of 20 m s^{-1} at each location in the domain for ERA-Interim winter months (DJF) 1989-2008.

To complete the analysis of the climatological 10 metre wind field the fraction of time the wind speed exceeds 20 m s^{-1} at each location in the domain is shown in Figure 2.6. The threshold of 20 m s^{-1} was arbitrarily chosen as the criteria for this analysis although qualitatively similar patterns are seen for other thresholds. This is a smaller threshold than used in MR05, but chosen to take into consideration QuikSCAT's overestimation of strong winds. As with the analysis of MR05, three coastal locations become apparent, two along Greenland's southeast coast and the third at Cape Farewell. These correspond to the locations of frequent barrier winds and tip jets respectively. At each location, wind speeds exceed 20 m s^{-1} more than 6 % of the time. In the remainder of this study we focus on the northerly two sites. See MR05, Sproson et al. (2008) and Våge et al. (2009) for a climatological analysis of the Cape Farewell site.

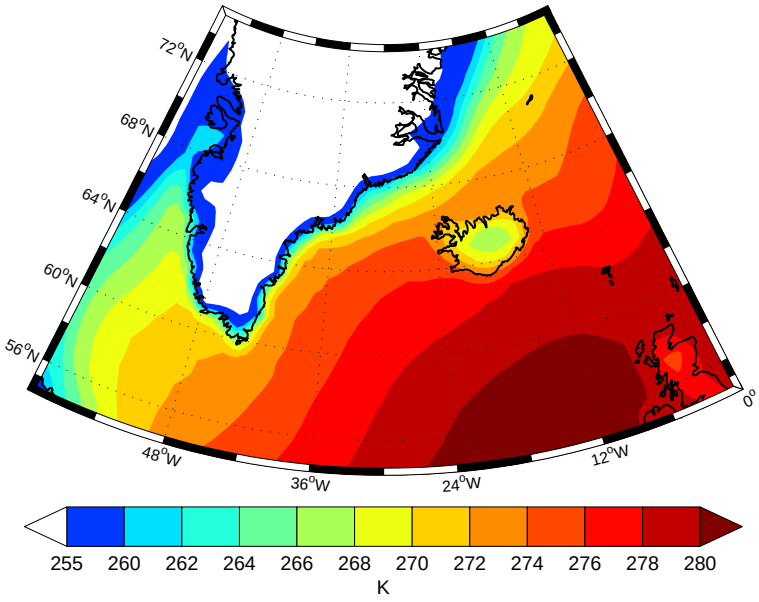

Figure 2.7: Mean of the 2 m temperature field (K) for ERA-Interim winter months (DJF) 1989-2008.

The mean two metre temperature field is shown in Figure 2.7. As might be expected, the temperatures over Greenland's high ice sheet are very low and have consequently been treated with the same colour shading. The warm air in the southeast of the domain is reflective of the heating of the warm North Atlantic Current (NAC). The temperature reduces to the north with the strongest gradient in temperature (the Arctic Front) occurring along the southeast Greenland coast where the mean 2 m temperature is below freezing in the region represented by the climatological jet in Figure 2.4. This near surface temperature distribution will be important when the ocean impact of barrier winds is considered in Section 2.4.4.

The mean total precipitation rate (Figure 2.8, sum of large scale and convective precipitation rates) shows bullets of over 0.25 $\mathrm{mm\,h^{-1}}$ located along the southeast coast of Greenland. At these locations, the total precipitation rate is dominated by the large scale precipitation as air is forced to rise as it is directed towards the coastline. The mean convective precipitation rate is maximal over the ocean to the southeast indicative of frontal weather systems that pass through the region.

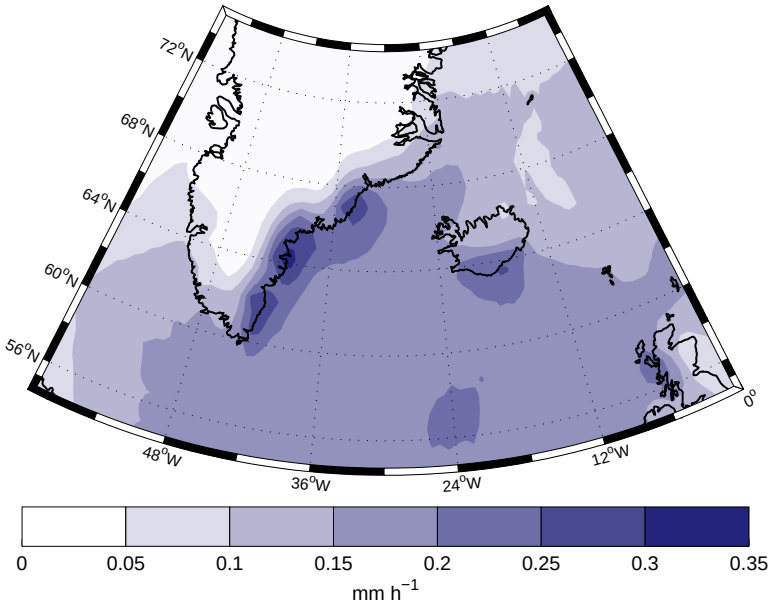

Figure 2.8: Mean of the total precipitation rate in the model (mm h^{-1}) for ERA-Interim winter months (DJF) 1989-2008.

2.4 Barrier wind detection

2.4.1 Method

Barrier winds are characterised by strong winds directed coast parallel. Therefore in this study of southeast Greenland a barrier wind event is defined if at any time the 10-m wind speed at a location is in excess of a threshold wind speed and directed between northerly (0°N) and easterly (90°N). Note that this pragmatic definition does not take into account the flow dynamics, but is nonetheless useful in capturing what have previously been shown to be barrier flows in the region [e.g. MR05, Petersen et al. (2009)]. Furthermore, the proximity to the steep topography of Greenland makes it very unlikely that strong winds detected in this way will have been produced without feeling the influence of the barrier in some way.

Following MR05, the locations that will be used for barrier wind detection are the two maxima in frequency of high wind speed events (Figure 2.6). These maxima correspond to the Denmark Strait South (DSS) and Denmark Strait North (DSN) locations identified in MR05 and for consistency, the same nomenclature will be used here. Unlike MR05, instead of using a point measurement for detecting barrier winds, a region that encompasses the maxima will be used (marked by boxes in Figure 2.6). These regions have been selected to not include any land grid points.

The steps in the detection routine for each region are as follows:

- At each time, the maximum 10-m wind speed in the region, for which the wind direction is between northerly (0°N) and easterly (90°N), is found and a time series is constructed from these values. Note that using a larger range of wind directions resulted in a similar number of detected events.

- The maxima in this time series greater than 20 $\mathrm{m\,s^{-1}}$ are selected. Different threshold values give qualitatively similar results.

- Finally, for a maximum to be defined as a barrier wind event, it must be distinct in time, i.e. separate from other maxima by over 24 hours. If wind speed maxima greater than 20 $\mathrm{m\,s^{-1}}$ are separated by less than 24 hours, the time of the peak wind speed is chosen.

2.4.2 Detection results

Applying the detection routine described above results in the detection of 252 barrier wind events at DSS and 291 events at DSN over the 60 month period (December, January and February between 1989 and 2008). This is approximately one barrier wind event a week for each location during these months. This can be compared to Våge et al. (2009) who observed roughly one westerly tip jet per two weeks in their ERA-40 based climatology. A similar number of barrier events at each location is slightly surprising, considering the difference in frequency of high winds observed between the two locations in Figure 2.6 (around 5% at DSS and 8% at DSN), the implication being that each event lasts longer at DSN than at DSS.

There exists a discrepancy between the mean frequency of barrier wind events in this study and in MR05. The 47 barrier wind events detected by MR05 in five years (one a week) at DSS agrees well with the frequency observed by this study, but MR05 only observed 19 events at DSN. This discrepancy could be partly explained by the point method of MR05 compared with the area method used here, but a more likely explanation is that MR05 is based on measurements from QuikSCAT which cannot measure 10-m wind speeds above sea ice – this is much more prevalent at DSN than DSS.

To investigate inter-annual variability, Figure 2.9 shows the number of barrier wind events detected each month and each winter season for the two locations. Both locations experience a degree of year-to-year variability, but at DSN it is larger (a standard deviation of 3.5 compared with 2.4 at DSS). There is a reasonable correlation of 0.43 (0.64) between the number of barrier wind events at each location each month (winter season). Looking at individual months, it appears that none are particularly favoured for prevalence of barrier winds.

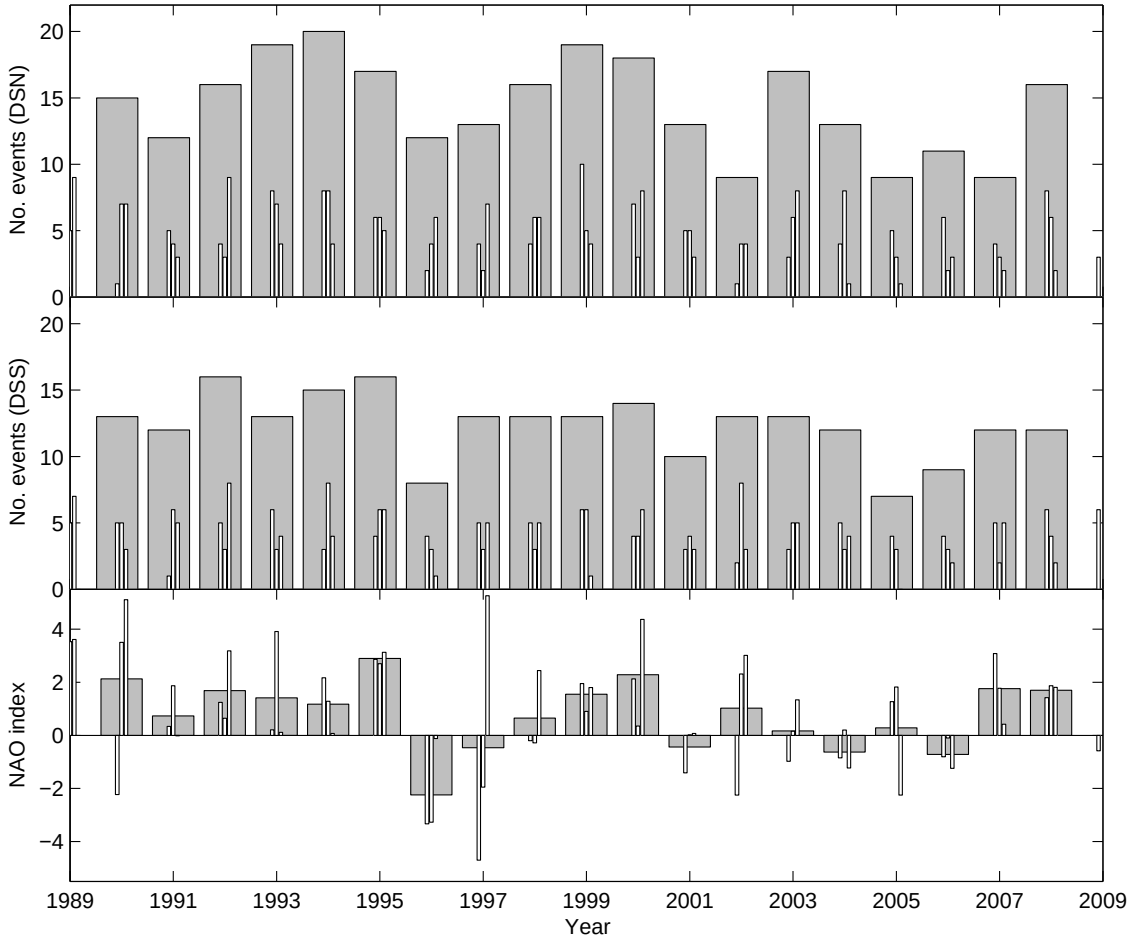

Figure 2.9: Top two panels: Number of barrier flows detected by winter month (white bars) and winter season (grey bars) for DSN (top) and DSS (middle). Bottom panel: NAO index by winter month (white bars) and winter season (grey bars).

Also shown in Figure 2.9 is the monthly and mean winter (DJF) North Atlantic Oscillation (NAO) index of Hurrell (1995). There is positive correlation between the monthly NAO index and the monthly frequency of barrier wind events at both locations with correlation coefficients of 0.31 at DSS and 0.57 at DSN, both of which are statistically significant at 99% confidence. This isn't entirely surprising considering high NAO indices are forced by a deeper Icelandic Low, the result of more frequent and deeper cyclones which are likely to produce more and stronger barrier winds. Correlation with the monthly southwest Iceland mean sea level pressure [used in calculating the NAO index of Hurrell (1995)] yields a similar result, but with slightly better correlations – coefficients of -0.37 and -0.67 are found at DSS and DSN respectively. These correlations could be useful in reconstructing barrier wind frequency for times before meteorological reanalysis coverage, but for which we have reliable NAO and mean sea level pressure data.

It has been shown that there is a correlation between the inter-annual variability at

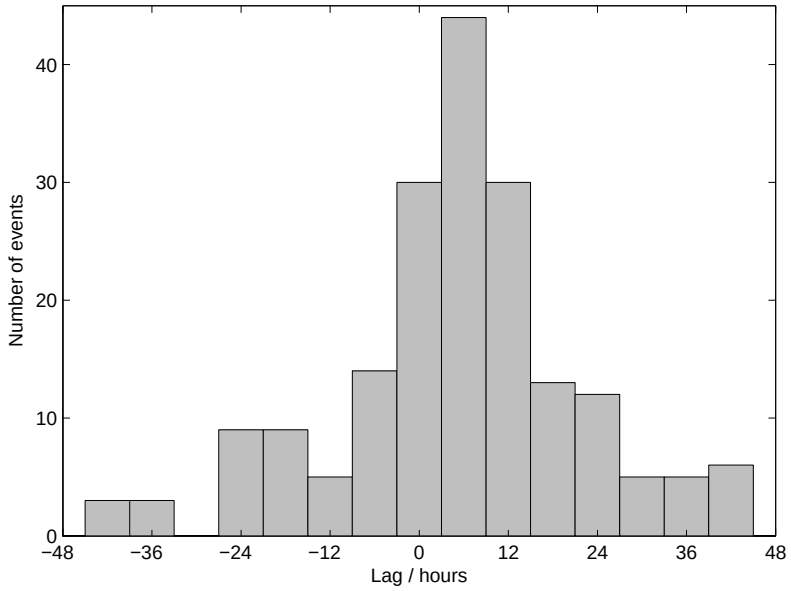

Figure 2.10: Number of events at DSS which are succeeded in lag time by an event at DSN. Positive lags indicate that the event at DSN occurred after the event at DSS.

DSS and DSN. A sensible question at this point seems to be: is there a causal relationship between events at DSS and those at DSN? Figure 2.10 shows how many events at DSS are succeeded by an event at DSN within a certain lag time. It can be seen that of the 252 detected events at DSS, 30 of them are concurrent with an event at DSN (approximately 12%). The maximum in the figure (44 events) occurs at a lag time of 6 hours. This means that 17% of the time an event at DSS is succeeded by an event at DSN by 6 hours. This implies retrograde propagation of the event; the region of strong winds travels northeastwards up the coast (seemingly against the along-barrier flow). The reason this lag exists is due to the common northeastward propagation of cyclones through the region [e.g. Hoskins and Hodges (2002)]. It is logical to suggest that as a cyclone moves through the region an event is triggered first at DSS and subsequently at DSN. This result is evidence that barrier winds off Greenland are the result of the direct influence of Greenland's topography on cyclones. The total number of events within ± 24 hours of the peak will give an upper limit on the number of causally linked events because this time period is typical of the passage of a cyclone through the region. This criterion gives 162 events (65%), meaning that the upper limit of causally linked events is around two thirds of the total number of events at DSS.

The 2-m temperature was extracted for each event at the DSN and DSS locations (Figure 2.11). The thick dashed line shows the climatological (DJF) mean for the two locations (i.e. the boxes in Figure 2.6). What is clear is that the median barrier wind event temperature isn't significantly different to the climatological mean temperature over the

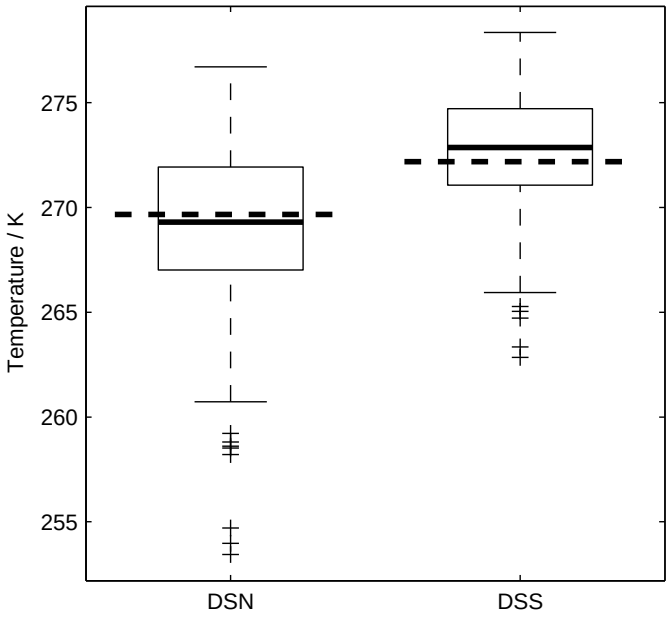

Figure 2.11: 2-m temperature (K) for all barrier wind events detected at DSS and DSN. The thick horizontal line is the median, a box indicates 1st and 3rd quartiles and bars extend to the minimum and maximum of the data set. Crosses mark outliers defined as being 1.5 interquartile ranges outside of a quartile. The climatological mean temperature for each region is shown as horizontal thick dashed line.

whole 60 month period of study at each location. Around this mean value though, both locations exhibit quite a large range. At DSS, much of the variance is contained within a 4 K range of the median value, 274 K, but temperatures can be as high as 278 K or as low as 263 K in extreme cases. At DSN, the temperatures are generally colder due to the more northerly location of the region and also the increased access to cold Arctic air that is available to the northeast of the Denmark Strait. The distribution is similar, although the range is somewhat larger; in particular a cold tail is more exaggerated at DSN with temperatures lower than 255 K in extreme cases. Not only are the median temperatures at each location comparable to their respective climatological means, but the range of barrier wind temperatures are also comparable to the climatological range observed throughout the 60 month period (not shown). This implies that barrier winds bring about no special temperature regime; they cannot be said to be generally 'cold' or 'warm' winds. A further discussion of barrier wind temperatures is addressed later, in Section 2.5.

2.4.3 Composite analysis

Mean composite fields have been produced for the 291 barrier winds detected at DSN and the 252 at DSS. Looking first at the mean 10-m wind field in Figure 2.12, we can see that at both locations the composite barrier wind speed peaks at about 20 $\mathrm{m\,s^{-1}}$ with a width

of 200 km. The lengths of the composite barrier winds are 450 km at DSN and 700 km at DSS (as defined by the 15 $\mathrm{m\,s^{-1}}$ contour). Importantly for DSS, much of the region of strong winds is located upwind of the maximum, emphasising the number of events at DSS that occur concurrently (or $\pm$ a small time lag), with events further upstream at DSN. Comparing with MR05's composites, the only substantial difference is that in this study the barrier wind composites are well defined over the sea ice, a feature that is especially important for barrier winds at DSN.

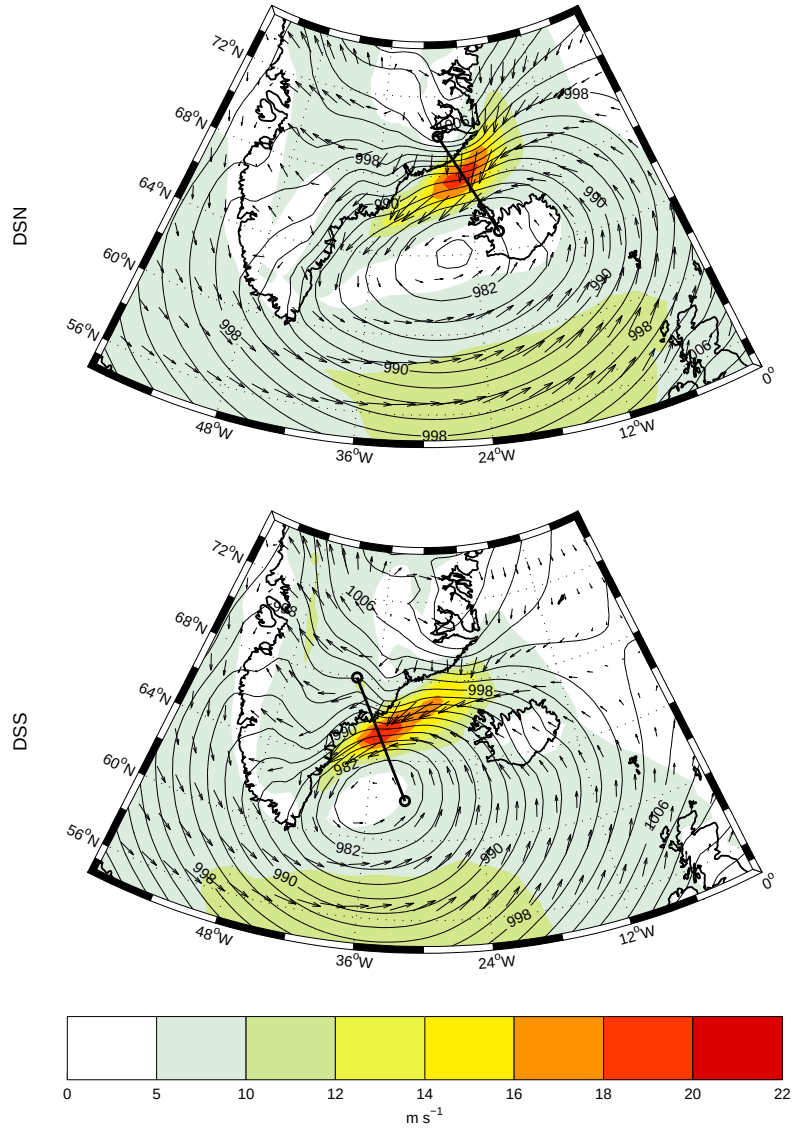

Figure 2.12: Composite of 10-m wind field ($\mathrm{m\,s^{-1}}$) for barrier wind events detected at DSN (top) and DSS (bottom) in the winter months (DJF) of the ERA-Interim dataset between 1989 and 2008. Wind vectors shown at every third data point. Composite mean sea level pressure (hPa, contours) shown every 2 hPa. Straight solid lines mark the locations for the cross sections shown in Figure 2.15

The barrier winds at both locations are forced by a composite low pressure of depth 980 hPa. For events at DSS, the location of this low is over the western Irminger Sea and for DSN it is further to the northeast off the west coast of Iceland. The translation of the composite low is comparable to the translation of the centres of peak wind speeds and is further evidence that the barrier winds are produced due to the orography distorting the flow field of the cyclone. For events at DSN the shape of the composite cyclone is more elongated along a southwest-northeast axis implying a larger distribution of the centres of action of the member cyclones along this line. The fact that the location of the composite cyclone is over southwest Iceland for events at DSN could explain why the frequency of events at DSN is better correlated with the southwest Iceland mean sea level pressure record (and subsequently the NAO) than those at DSS.

The standard deviation of the 10 m wind speed for events at DSN and DSS, Figure 2.13, shows a similar pattern for each location. The main feature is that in the detection regions there is a smaller standard deviation compared with at other locations along the coast. The low variance in each detection region will be mostly due to the small range of wind speeds that go into the composite; an artifact of the detection routine. The larger standard deviation at other regions along the coast indicates the range in size and shape of the constituent barrier winds. It appears that at both locations, barrier winds exist with a large range in upstream and downstream extent – this was confirmed by inspection of individual barrier wind events. We can see from this that a large range of barrier winds go into the composites presented in Figure 2.12 – these are not necessarily representative of the standard barrier wind.

The standard deviation of the mean sea level pressure for events at each location has one predominant feature, a large region of high variance out in the Nordic Seas. The region over which the composite cyclones sit are not the regions that experience the maximum variance. As will be seen (Section 2.5) this is likely to be caused by instances of blocking high pressure systems which are frequent in the region (Rex, 1950b; Pelly and Hoskins, 2003) or the presence of cyclones that have previously moved through the region.

Having seen already the large range of two metre temperatures (Figure 2.11) at each location, the composite mean two metre temperature field is unlikely to show a standard configuration of the temperature field for barrier winds, rather a blurring of the large range. For this reason, it is not shown. The geopotential height field on the 500 hPa level (not shown) is consistent with barrier perpendicular winds over the southeast coast of Greenland for both locations, forced by a deep trough which extends over the Labrador Sea and out over the east of Cape Farewell. Figure 2.14 shows the composite vertical profile of barrier wind speed and direction at each location. Both have jets which have their

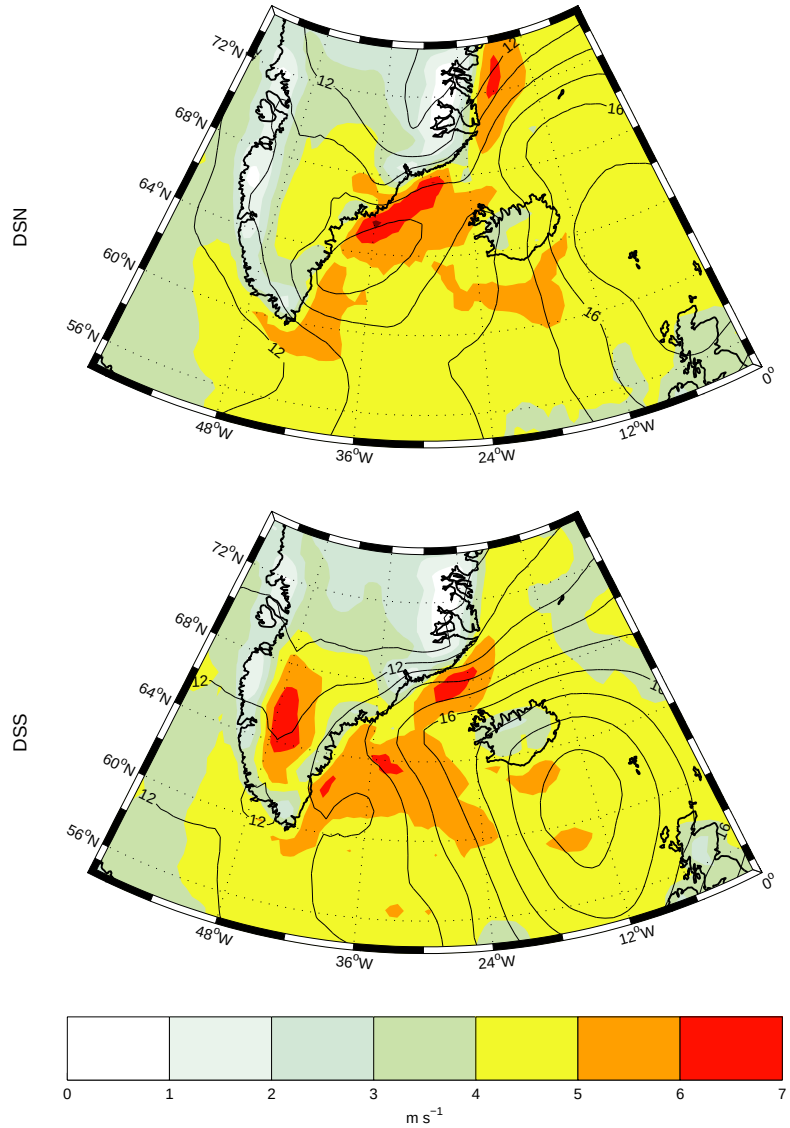

Figure 2.13: Standard deviation of 10 m wind speed ($\mathrm{m\,s^{-1}}$, colours) for barrier winds detected at DSN (top) and DSS (bottom) in the winter months (DJF) of the ERA-Interim dataset between 1989 and 2008. Contours every 0.5 $\mathrm{m\,s^{-1}}$. Standard deviation of mean sea level pressure (hPa, contours) shown every 1 hPa.

maximums at about 900 hPa. Both also have winds which veer from northeasterly (along barrier) to southeasterly (cross barrier) above mountain height. This is consistent with the standard picture of a barrier wind, i.e. a cross mountain flow at height which sustains and along barrier jet below mountain height (Schwerdtfeger, 1975). We are therefore clearly mostly sampling barrier winds and not some other high velocity events.

Cross sections of the composite wind speed and potential temperature fields for events at DSN and DSS, taken perpendicular to the direction of flow through the region of maximum wind speed (see Figure 2.12 for exact location), are shown in Figure 2.15. These

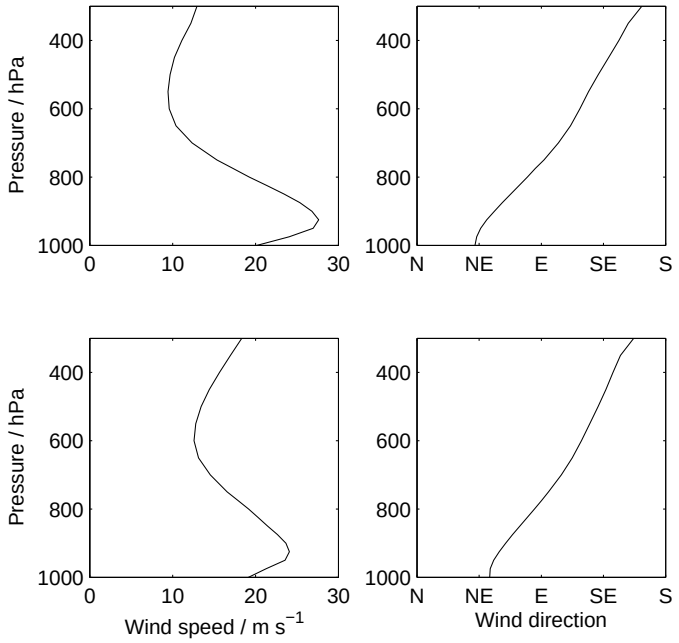

Figure 2.14: Composite vertical profiles of wind speed (left) and wind direction (right) for all events detected at DSN (top) and DSS (bottom). The location for each profile is the centre of each regions detection box.

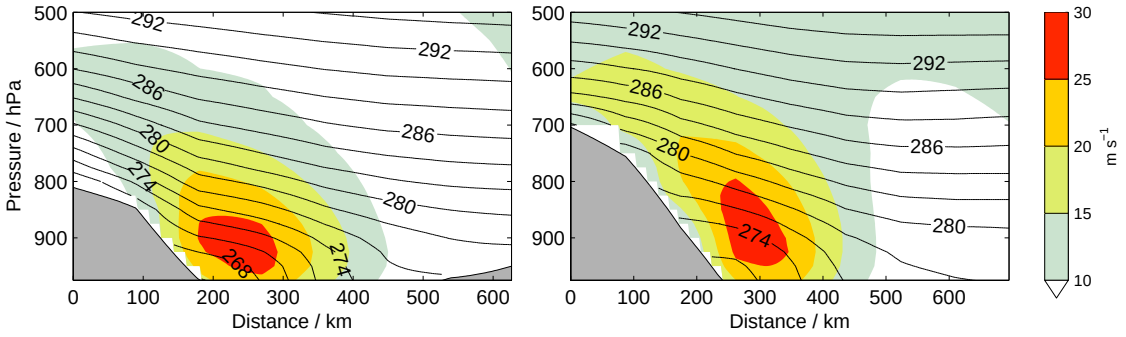

Figure 2.15: Composite cross section of the 238 barrier wind events at DSN (left) and DSS (right) for wind speed (m s^{-1}, colours, contours every 2 m s^{-1}) and potential temperature (K, solid lines, contours every 2 K). Cross section line is shown in Figure 2.12.

further show that the events detected are representative of barrier winds. The two composites show jet cores of 30 m s^{-1} at a height of 900 hPa at DSN and 875 hPa at DSS. This difference in jet core height is likely due to the 100 hPa lower topography at DSN which also produces a jet with lower overall height at DSN. The shapes of the composite barrier winds are also different. At DSN, the barrier wind structure is vertically aligned. In contrast, at DSS the barrier wind leans with height towards the coast, suggesting there is a larger cross barrier flow near the mountain top which hems the barrier wind in as seen in Figure 2.14. The shape of the composite barrier wind at DSN is reminiscent of the shape of the barrier winds observed on 2 and 6 March 2007 by Petersen et al. (2009) at

the same location.

At both locations there is evidence of a near neutral boundary layer with a stably stratified atmosphere above [as seen in Petersen et al. (2009)]. As was shown previously (Figure 2.2), ERA-Interim tends to 'blur out' the vertical structure of barrier winds, although the magnitude of the wind maxima are captured. Averaging over a number of events at each location is only likely to make this blurring worse in both wind speed and potential temperature. Indeed, manual inspection of individual cases confirmed this; many had much better defined potential temperature 'inversion layers' with a range of heights.

2.4.4 Surface Fluxes

To examine the potential impact on the ocean, surface turbulent heat fluxes, surface stress and precipitation are investigated. In ERA-Interim these fields are provided as cumulative forecast fields which are run every 12 hours. As the analyses are produced every 6 hours, some processing is required in order to extract representative values at the same time steps as the analysis. This is achieved at 00 and 12 UTC by using the cumulative values for the following three hours. At 06 and 18 UTC, cumulative totals for the following three hours are used, but extracted from the forecast fields initialised at the previous 00 and 12 UTC. Clearly this method relies on accurate forecast fields for a period of 9 hours – a reasonable assumption. Note that all variables have been normalised by the length of the forecast to give mean heat fluxes in $\mathrm{W\,m^{-2}}$, surface stresses in $\mathrm{N\,m^{-2}}$ and precipitation rates in $\mathrm{mm\,h^{-1}}$

The mean of the sensible and latent heat fluxes over each region (i.e. each box in Figure 2.6) was calculated for each barrier wind event. Figure 2.16 shows the range of values found. The median values at both locations are around 100 $\mathrm{W\,m^{-2}}$ (from the ocean into the atmosphere) for both sensible and latent heat fluxes with the medians at DSS larger by about 20 $\mathrm{W\,m^{-2}}$ than at DSN. The effect of the 3-4 K colder temperatures of barrier wind events at DSN (Figure 2.11) is being counteracted by colder seas and increased ice cover in this region (Figure 2.3). What is notable in Figure 2.16 are the large ranges. About half of these ranges are contained within ± 50 $\mathrm{W\,m^{-2}}$ of the median, but values as high as as 300 $\mathrm{W\,m^{-2}}$ (over 400 $\mathrm{W\,m^{-2}}$ in one case) or as low as -50 $\mathrm{W\,m^{-2}}$ (i.e. a flux of heat from the atmosphere) are found as well. This shows us that at each location, the winds can be extracting as much as 600 $\mathrm{W\,m^{-2}}$ from the ocean averaged over each region or at the other end of the spectrum be losing 100 $\mathrm{W\,m^{-2}}$ to the ocean. The maximum heat fluxes in each region for each event (not shown) are commonly twice as large as the box-mean values, illustrating that twice as much heat flux is possible over localised regions.

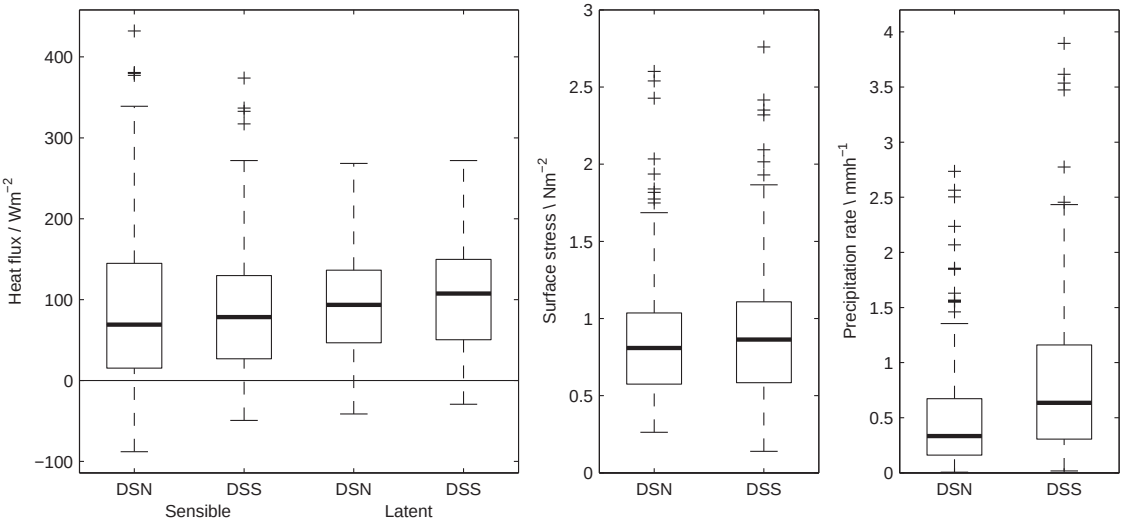

Figure 2.16: Left panel: Mean sensible (left) and latent (right) heat fluxes (W m^{-2}) for all events detected at DSS and DSN. Thick line is median, box indicates 1st and 3rd quartiles, bars extend to the minimum and maximum of the data set. Pluses for outliers defined as being 1.5 interquartile ranges outside of a quartile. A positive value indicates a flux of heat from the ocean into the atmosphere. Centre panel: Mean surface stress (N m^{-2}) for each event in regions DSN and DSS. Right panel: Mean precipitation rate (mm h^{-1}) for each event over the regions DSN and DSS.

It should be noted that the model outputs the fluxes of heat into the atmosphere and may not (due to the varying quantity of sea ice present) be interchangeable with fluxes out of the ocean. This discrepancy will be minor, as the fluxes of sensible and latent heat from the sea-ice cover are dwarfed by those from the open ocean. However this does mean that the area-average fluxes shown in Figure 2.16 will be a lower bound for the fluxes from the open ocean.

The cause of the large ranges in the heat fluxes associated with the barrier wind events is the large range in 2-m temperatures (Figure 2.11). More specifically the controlling factor for these turbulent heat fluxes appears to be the temperature difference across the air-sea interface, Δ T; correlation coefficients of 0.86 and 0.90 are found between the mean ΔT and the mean total turbulent heat flux in DSN and DSS respectively. Insignificant correlation was found between the 10-m wind speed and the turbulent heat fluxes, for the barrier wind events, despite heat fluxes being directly proportional to wind speed in the bulk formulae used to parameterise the fluxes. This is likely to be partially an artifact of the detection method; only a relatively small range of wind speeds are being sampled.

The mean surface stress and mean total precipitation rate for all barrier wind events over the DSN and DSS regions are also shown in Figure 2.16. The median surface stress for both locations is about 0.8 N m^{-2} but over a quarter of the events experience mean

stresses over 1 N m^{-2}. The precipitation rate associated with barrier wind events is generally less at DSN than DSS, with median values of 0.3 mm h^{-1} and 0.7 mm h^{-1} respectively. The reduced precipitation at DSN could be in part due to the more frequent ice cover at this location, reducing the moisture content of the air, and the smaller amount of uplift due to the lower topography. The range is also greater at DSS, the warmer location.

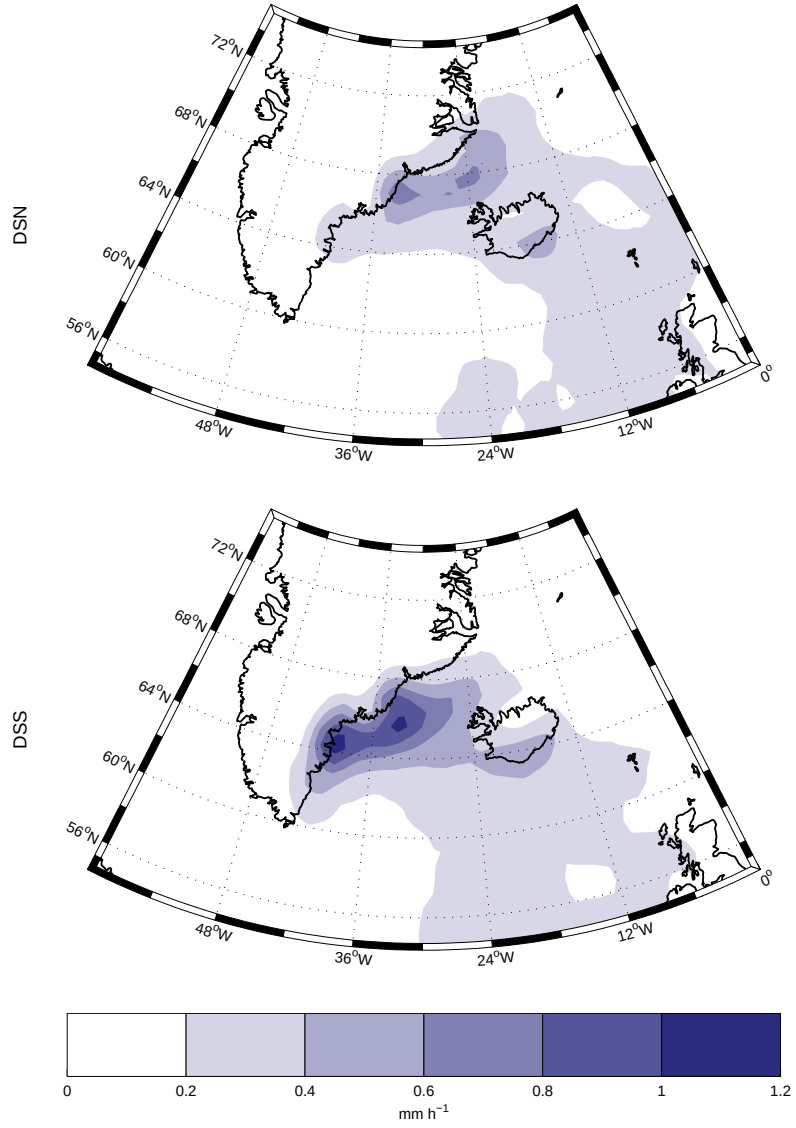

Figure 2.17: Composite of the total precipitation rate (mm h^{-1}) for barrier winds detected at DSN (top) and DSS (bottom) in the winter months (DJF) of the ERA-Interim dataset between 1989 and 2008.

Figure 2.17 shows the composite total precipitation rate for all the events at DSN and DSS. The composites for the surface heat fluxes and stress differ only slightly from the spatial distribution shown in the mean wind field composites (Figure 2.12) and for this reason they are not presented. The precipitation composites are dominated by the large

scale (strataform) precipitation rate which is a full order of magnitude greater than the convective precipitation rate. For both locations, the precipitation is concentrated in two regions, both of which are over the Greenland slopes and are therefore likely to be the result of uplift as air is forced towards the coast. The first region of enhanced rainfall at both locations is near the detection region, unsurprisingly the location that on average experiences the strongest onshore winds. The second region is at the downwind end of the barrier winds. This coincides, in both cases, with undulations in the southeast Greenland coast which put an obstruction in the way of barrier wind. This is likely to cause uplift and rainfall as the barrier wind is forced towards another slope. The implication of this is that barrier winds can have non-local precipitation patterns, more so than surface heat and momentum fluxes.

2.5 Warm and cold barrier winds

To examine the synoptic conditions that bring about the range of 2-m temperatures and hence heat fluxes, composites of 'warm' and 'cold' barrier winds were produced. There is a continuous spectrum of temperatures at both DSN and DSS (as seen via scatterplots for example, not shown) so an obvious criterion for distinguishing two classes of barrier winds from temperature doesn't present itself. Instead, we will take the extreme quartiles of the 2-m temperature time series to classify warm and cold barrier wind events and illustrate these via composites. Each composite at DSN (DSS) contains 73 (63) events.

2.5.1 Structure

Warm barrier winds at DSS (Figure 2.18, middle panels) are characterised by a composite low pressure centre nearer to Cape Farewell than average (Figure 2.12). The position of the composite cyclone channels air from the south into a band of southeasterly winds (greater than 10 $\mathrm{m\,s^{-1}}$) to the west of Iceland and into the barrier wind which is as strong as (but more localised than) the average situation in Figure 2.12.

In contrast, cold barrier winds at DSS have a composite low pressure centre which is located further northeast, closer to Iceland, and is 2 hPa deeper. This location appears to restrict the band of southeasterly winds seen in the warm composite and instead favours the channelling of air from the north through the Denmark Strait and into a long barrier wind that extends almost the whole length of southeast Greenland (from DSN to DSS). The maximum wind speeds are also greater than both the warm and the total mean composites. It is worth noting that the 2 March 2007 GFDEx case of Petersen et al. (2009) appears to be a clear example of a 'cold' barrier wind at DSS – in terms of the synoptic

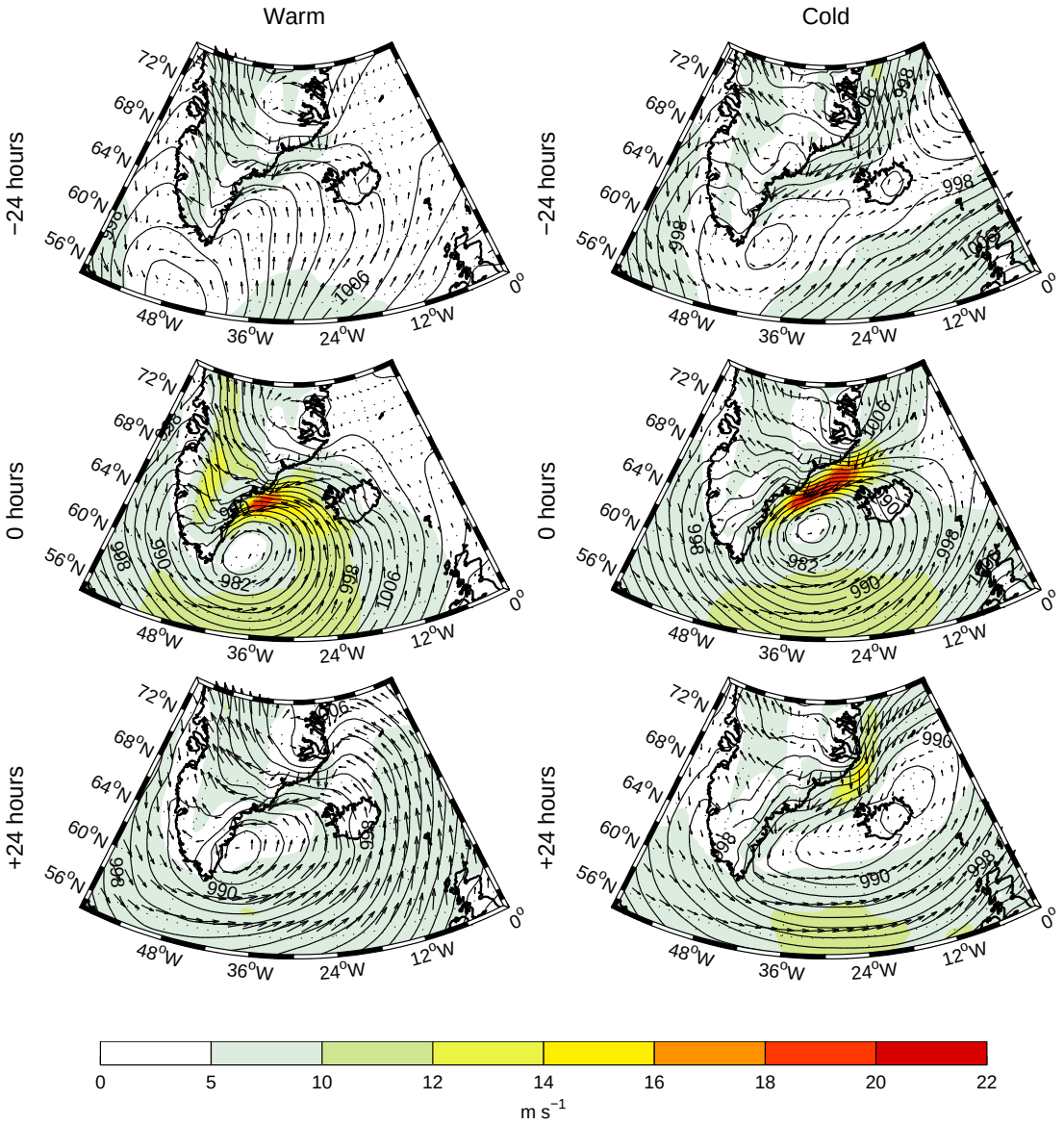

Figure 2.18: Composite of 10-m wind field (m s^{-1}) for warm (left) and cold (right) barrier winds at DSS. The middle panels show the composite barrier winds at the time of peak wind speed. The top and bottom panels show composites 24 hours before and after this time. Wind vectors shown at every 3rd data point. Composite mean sea level pressure (hPa, contours) shown every 2 hPa.

situation, barrier flow structure and observed temperatures. Further investigation into examples of warm and cold barrier winds will be conducted when further case study data and modelling work is presented in chapter 3.

The corresponding zero lag figures for DSN are very similar to those for DSS in all but location of activity (Figure 2.19). In the warm class, the composite cyclone is to the west of Iceland in a similar position to the cold DSS composite, but with a rather zonal major axis, so with significant southerly flow. In the cold class, the composite low is over

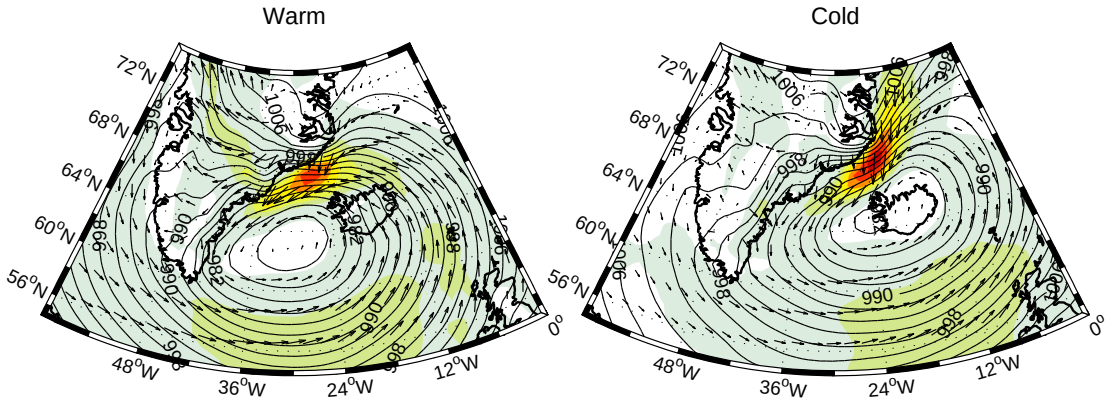

Figure 2.19: Composite of 10-m wind field (m s^{-1}) for warm (left) and cold (right) barrier winds detected at DSN at zero lag time in the winter months (DJF) of the ERA-Interim dataset between 1989 and 2008. Wind vectors shown at every 3rd data point. Composite mean sea level pressure (hPa, contours) shown every 2 hPa. Wind speed colourbar the same as Figure 2.18.

Iceland and has a more SW-NE tilt, channelling (cold) air through Denmark Strait. The 6 March 2007 GFDEx case of Petersen et al. (2009) appears to be a clear example of a 'cold' barrier wind at DSN. Similarities between DSN and DSS events persist throughout the subsequent analysis so for brevity, only barrier winds at DSS will be considered from now on. It should be presumed that results are transferable to DSN through a translation of about 500 km northeastward along the Greenland coast.

Figure 2.18 also shows the temporal evolution of warm and cold barrier winds at DSS which highlights further differences between the classifications. For warm barrier winds, the composite parent cyclone is located south of Cape Farewell 24 hours previously, before moving into the lee of Greenland for the time of the peak barrier wind, and then appearing to become 'captured' by Greenland – moving no further eastward over the next 24 hours. The lee of Greenland has been shown to be a region of cyclolysis (Petersen et al., 2003; Hoskins and Hodges, 2002). The spreading isobars at the northeast of the domain suggests this is not always the case and some cyclones do move through the region.

For cold barrier winds, the parent cyclone begins just east of Cape Farewell and moves progressively northeastwards throughout the 48 hours. The elongation and filling of the mean sea level pressure field at +24 hours is symptomatic of a range of translation speeds of the cyclones responsible for cold barrier winds. The cold barrier wind exists for a longer time, it is evident from -24 to +24 hours, initially located at DSS and then at DSN, in agreement with the calculated phase lags (Figure 2.10). In contrast, for the warm class, the barrier winds have a shorter life time.

The differing behaviour of the surface lows can be explained in part through analyses

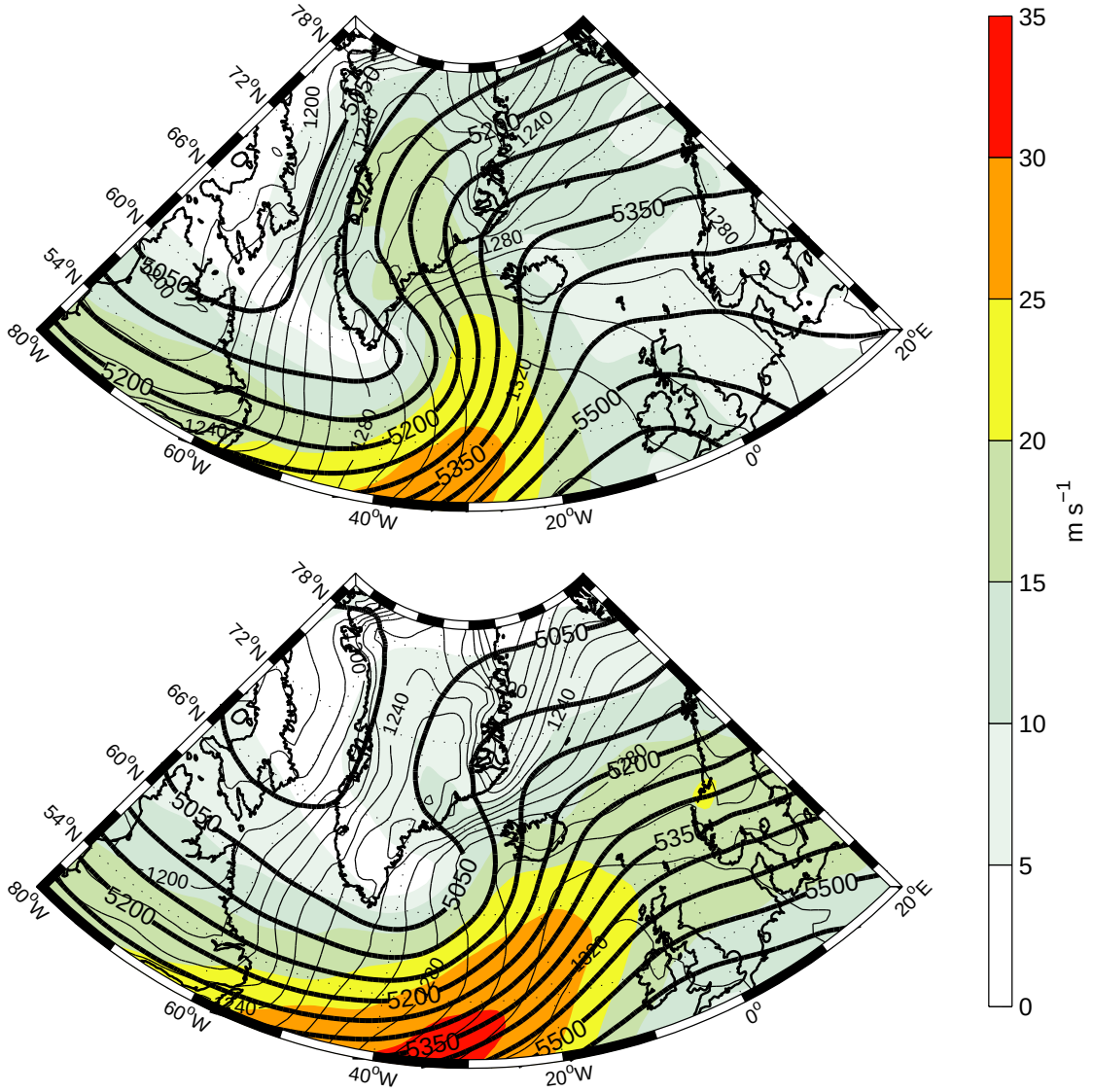

Figure 2.20: Composite of 500 hPa wind field ($\mathrm{m\,s^{-1}}$, colours) for warm (top) and cold (bottom) barrier winds detected at DSS for the winter months. Composite geopotential height (m, thick contours) shown every 50 m and 850-1000 hPa thickness (m, thin contours) shown every 10 m. Note larger domain of this figure.

at 500 hPa (Figure 2.20). Warm barrier winds have strong cross barrier flow (18 $\mathrm{m\,s^{-1}}$) above mountain height, associated with a well defined trough over the Labrador Sea and a ridge extending from the United Kingdom to east Greenland. This upper-level flow pattern would help confine a surface low to the Greenland coast and restrict its passage through the region. It will also assist in advecting warm air from the south towards DSS, resulting in barrier winds with warm cores.

For cold barrier winds, the upper level trough is located further east, over the west

Irminger Sea, and the ridge over the United Kingdom is shallower (Figure 2.20). The result is a weaker cross barrier flow at 500 hPa; the upper level winds are orientated more zonally and further to the south, aiding the surface cyclones in passing through the region.

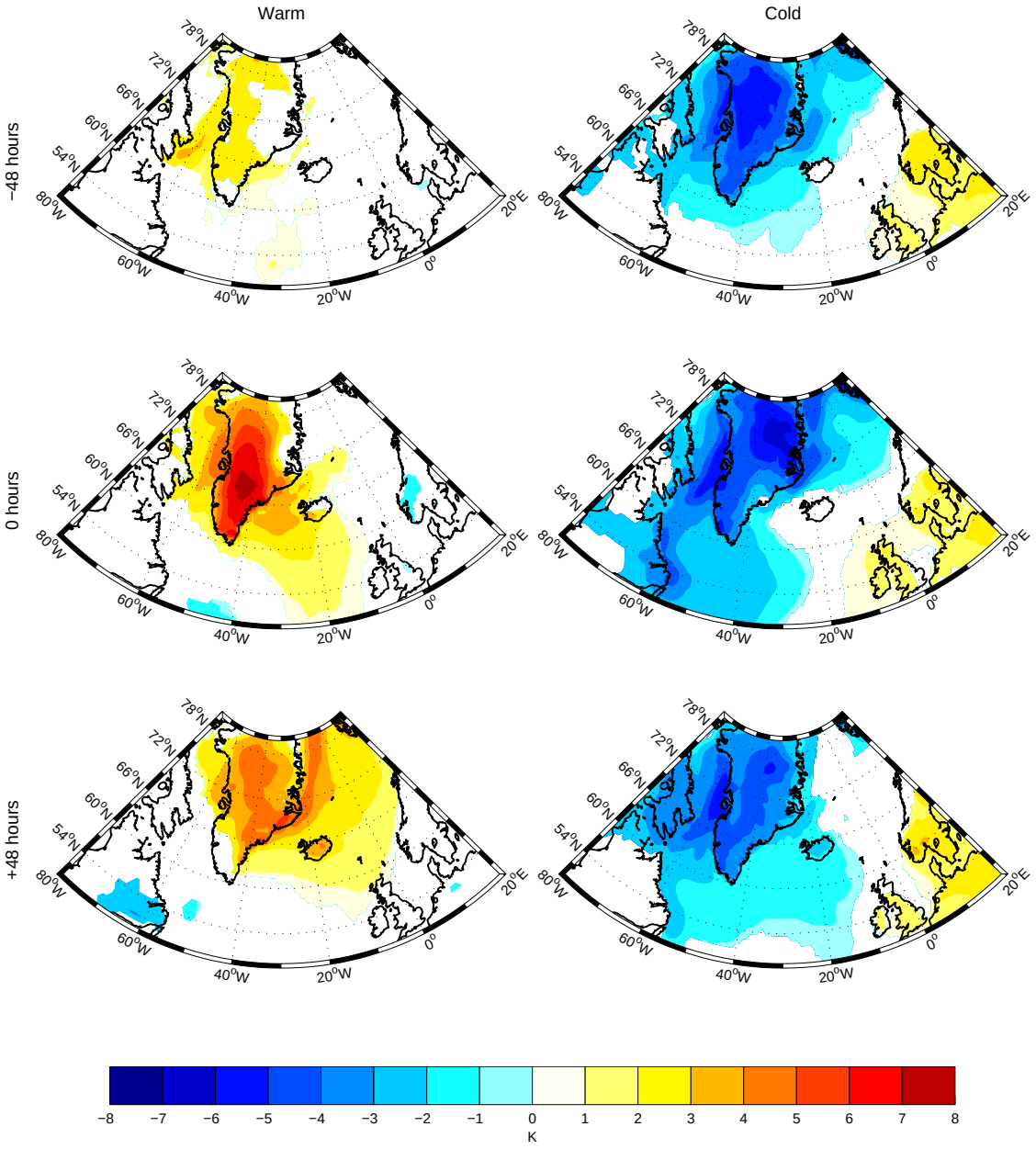

Figure 2.21: Composite of 2-m temperature anomaly (K) for warm (left) and cold (right) barrier winds, at lag times of -48, 0 and +48 hours, detected at DSS in the winter months. Only values which are statistically significant at the 95% level are shown. Note the larger domain used.

The zero lag composite 2-m temperature anomalies for the warm and cold cases is shown in the central row of Figure 2.21. In the warm composite, the region is flooded with

air warmer than the climatological mean (Figure 2.3) by as much as 3 K over the ocean and 7 K over land, the result of both the low-level flow pattern and the strong cross mountain flow at 500 hPa. This anomalously warm region extends from DSS both northwest and southeast indicative of warm advection from the southeast and is in agreement with the strong southeasterlies both over sea and land in Figure 2.18.

The cold zero lag composite is characterised by anomalously cold pool of -4 K to the north of Iceland, with a tongue extending southward through Denmark Strait to DSS. The shape of the cold anomaly, in conjunction with the cold dome of air in 1000-850 hPa thickness along east coast of Greenland (Figure 2.20) and the long barrier wind seen in Figure 2.18, is consistent with cold-air advection into the barrier wind from the north-east. These features of warm and cold barrier winds are corroborated by the 1000-850 hPa thickness composites (Figure 2.20) but are much less obvious in the 1000-500 hPa thickness composites (not shown), indicative of these features existing below mountain height.

Further differences between the warm and cold cases are seen in the lagged composites of the 2-m temperature anomaly. The cold case has a large mass of cold air residing over the Greenland ice sheet for the duration of the 96 hours. This indicates that the region is preconditioned to provide cold air in the barrier wind when the cyclone moves into the region. The warm case experiences little warming in the region 48 hours previous to the event but as the cyclone moves in then the warm air is advected northwards into the barrier wind, up over the ice sheet and even up the east coast of Greenland 48 hours after the peak barrier wind activity.

Our interpretation of this analysis is that warm barrier winds source their air from the southerly advected warm pool, whereas even though the cold barrier winds have milder air advected towards them, they are fed by an even colder source of air, i.e. from over the Greenland ice sheet and to the northeast of the Denmark Strait. It appears that the cold barrier winds in particular have an offshore (i.e. downslope) contribution (see Figure 2.18). At this stage it is not possible to say whether this minor contribution is simply a downslope deflection of maritime air or is a downslope density-driven (katabatic) flow of continental air.

These configurations are reminiscent of the classical and hybrid barrier winds along the coast of Alaska, described in Loescher et al. (2006) and Olson and Colle (2009). Our warm barrier winds are similar to their classical barrier winds which form due to the coastal deflection of onshore winds whereas our cold barrier winds have similarities to their hybrid barrier winds which have an offshore gap flow component which turns to become coast parallel as it reaches the ocean. Hybrid barrier winds are colder than classical barrier winds as they source their air from an inshore cold pool and the onshore synoptic

flow is advected over the cold core of the barrier wind. This is analogous to the maritime southeasterly flow being lifted over the cold Arctic flow seen in our cold barrier winds [see also Petersen et al. (2009), p1965]. Apart from these structural similarities though, it is unclear at this stage how similar the dynamics of barrier winds around Greenland are to those found off Alaska – this is left to further investigation.

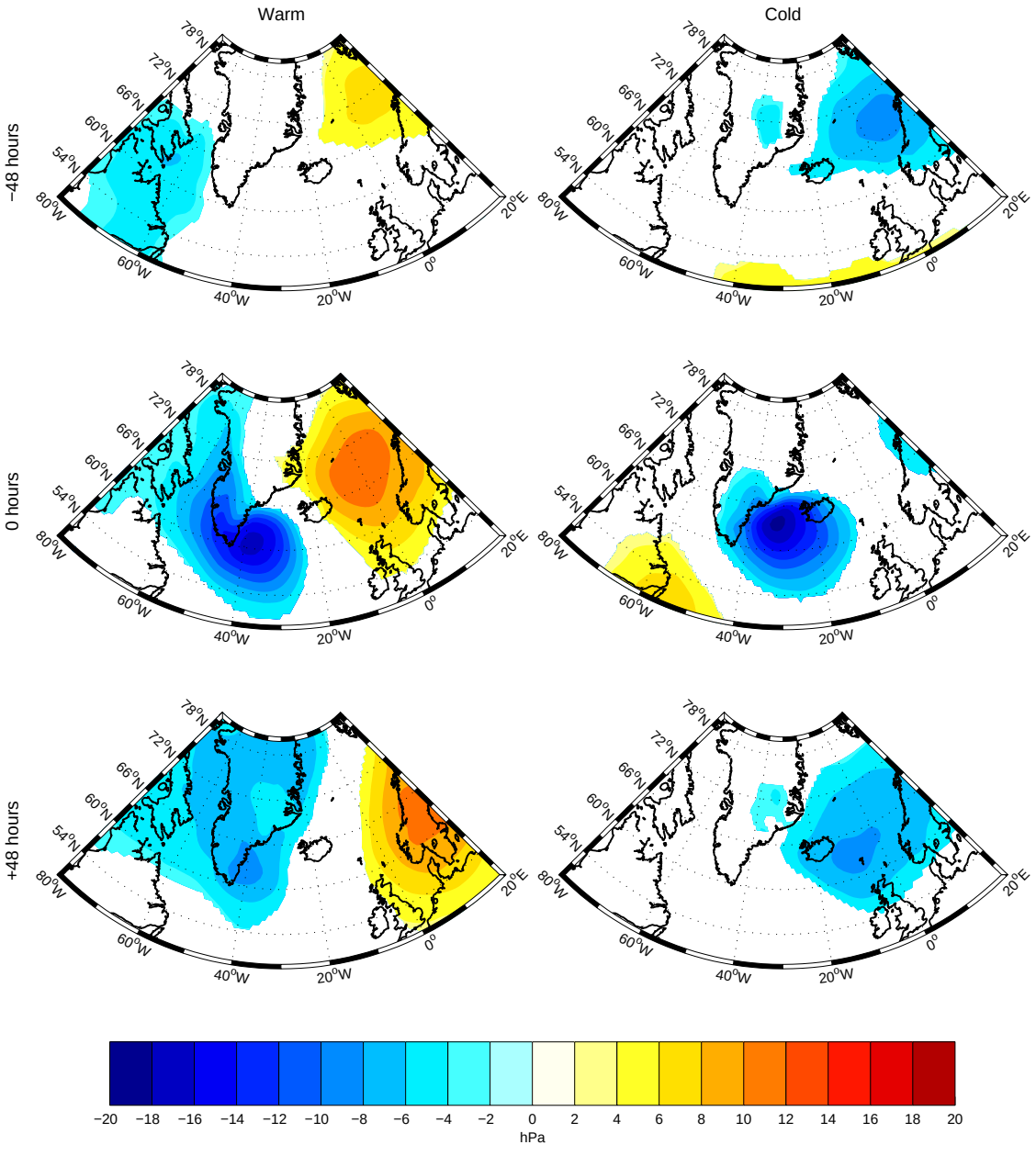

Figure 2.22: Composite of the mean sea level pressure anomaly (hPa) for warm (left) and cold (right) barrier winds, at lag times of -48, 0 and +48 hours, detected at DSS in the winter months. Only values which are statistically significant at the 95% level are shown. Note the larger domain used.

Returning to the mean sea level pressure composites (Figure 2.18) it is apparent that there is not a great deal of difference in the strength or location of the parent cyclone for the two classes of barrier wind events (at zero lag). What is it about the synoptic environment then that brings about such different local conditions? Figure 2.22 shows the composite mean-sea-level pressure anomaly for warm and cold barrier winds at the time of peak winds at DSS and 48 hours before and after. Only points which are statistically significant at the 95% level are shown. For the warm class, there is a significant high pressure anomaly of, at its peak, 10 hPa located over the Nordic Seas for the 96 hours shown. This not only blocks the passage of the low responsible for the barrier wind, but also acts to restrict cold, northerly flow along the east coast of Greenland. This configuration therefore favours warm advection from the south into the barrier winds. The fact that this anomalous high pressure can be found in a similar region throughout the 96 hour period shown is indicative of North Atlantic blocking (Rex, 1950a; Pelly and Hoskins, 2003) being important in the production of warm barrier winds. The blocking high at the surface at zero lag is consistent with the ridge at 500 hPa seen in Figure 2.20.

In contrast, the cold class is characterised by an anomalous low pressure system of -10 hPa over the Norwegian Sea 48 hours before the peak barrier winds. This likely represents the signature from a previous cyclone that moved through the region and in so doing channelled cold air down the east coast of Greenland. As the cyclone responsible for the barrier wind moves into the region, it is steered by the upper level zonal flow (Figure 2.20) and can channel this preconditioned, cold air into a barrier wind. 48 hours later, the cyclone has exited the region to the northeast. The fact that the pressure anomaly fields at lag times of $\pm$48 hours are comparable suggests that this process may be repeated, providing a 'conveyor belt' for channelling cold air from the Arctic down the southeast coast of Greenland. This 'train' of cyclones is reminiscent of the positive phase of the NAO. It is therefore unsurprising that the monthly frequency of cold barrier winds correlates (in a similar fashion to Figure 2.9) with the monthly NAO index with a correlation coefficient of 0.35. Cold events at DSN see a similar correlation of 0.39. The warm barrier winds are produced by blocking highs, consequently there is insignificant correlation between their monthly frequency and the NAO index at both locations.

2.5.2 Impact

The impact of these different temperature regimes can be seen in composites of the surface turbulent heat flux for the warm and cold barrier wind classes (Figure 2.23). The cold class has a heat flux pattern that mirrors that of the wind speed composite. Total turbulent heat fluxes of over 200 W m^{-2} are seen all the way down the southeast coast of Greenland with

bullets of nearly 400 W m^{-2} at, and upstream of, the DSS site. The largest heat fluxes are further offshore than the wind speed maximum, due to the influence of near-shore sea ice and a higher sea surface temperatures offshore. In the warm composite only a small signature of scarcely more than 100 W m^{-2} is observed at the location of strongest winds. At all other places up the Greenland coast the total heat flux is less than 100 W m^{-2}. The two temperature regimes will therefore have very different impacts on the ocean. This is also true for the surface momentum flux (not shown) which is similar to the wind speed pattern (Figure 2.18) and so quite different for the warm and cold classes. In short, the specific synoptic environment in which Greenland barrier winds form is vital in determining the range and spatial distribution of both surface heat and momentum fluxes along the coast.

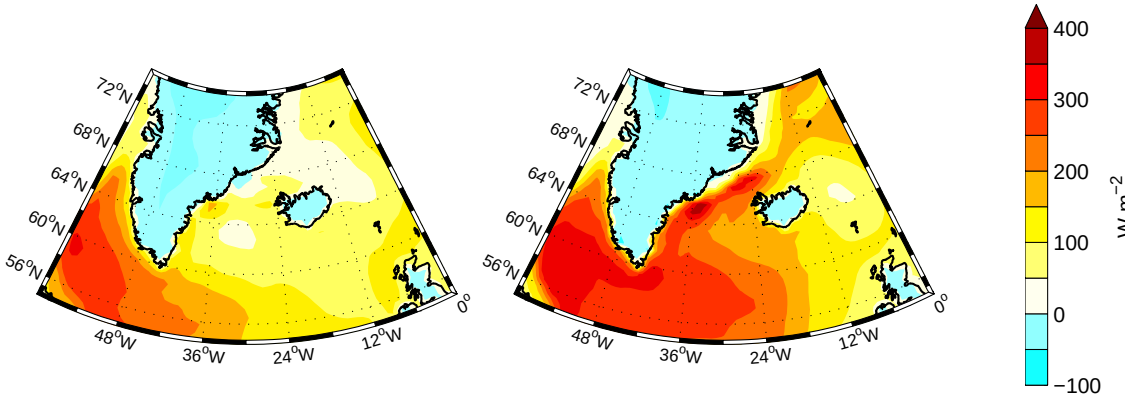

Figure 2.23: Composite of total surface turbulent heat flux (W m^{-2}) for warm (left) and cold (right) barrier winds detected at DSS at zero lag time.

2.6 Conclusions

This climatology of barrier winds along the southeast coast of Greenland has confirmed (see MR05) that there are two predominant regions where barrier winds frequently occur – referred to as Denmark Strait North (DSN) and South (DSS). During the 20 years of the climatology, barrier winds stronger than 20 m s^{-1} occur at both locations on average once a week in the winter months (DJF).

Good correlations were found between the monthly frequency of barrier winds and the monthly NAO index (especially at DSN). The relationship is explained in the following way. A high NAO index is the result of stronger and more frequent cyclones through the region which are likely to trigger more and stronger barrier winds. It is possible that this correlation will potentially allow for reconstruction of barrier wind frequency for periods

of time before reanalysis was available.

One of the most striking features of the barrier winds investigated was the large range in 2-m temperatures – southeast Greenland barrier winds can't be said to be typically cold or warm winds. An investigation into the meteorological conditions responsible for the warmest and coldest barrier winds showed that blocking highs are responsible for channelling warm air into warm barrier winds and that trains of cyclones can consecutively channel cold air down the east coast of Greenland and into cold barrier winds. A very different pattern in the surface heat and momentum fluxes is seen for each temperature regime and this shows the importance of the wider meteorological environment in understanding the local wind forcing in the region.

Chapter 3

A case study of a southeast Greenland barrier wind, October 2008

3.1 Introduction

Barrier winds are a well established phenomena and have been documented at various locations around the world. They were first described along the eastern Antarctic Peninsula (Schwerdtfeger, 1975; Parish, 1983), but have since been observed in other parts of the world, for example the Sierra Nevada (Parish, 1982) and along the western coast of Alaska (Loescher et al., 2006; Olson and Colle, 2009). These studies and additional numerical models (Braun et al., 1999; Petersen et al., 2003, 2005) have shown that barrier winds form when stable air is forced towards a steep and high topographic barrier. Unable to ascend the barrier, the air is dammed against the slopes and a pressure gradient perpendicular to the barrier develops. It is this pressure gradient that supports strong, low-level, mountain parallel flow known as a barrier wind. Generally these flows are geostrophically balanced, but more complex force balances with ageostrophic components have been documented (Olson et al., 2007; Petersen et al., 2009).

The first mention of barrier winds along the southeast coast of Greenland was made by Moore (2003) as an aside to his study of strong wind events at Cape Farewell. It was Moore and Renfrew (2005) though who provided the first comprehensive investigation into them by utilising five years of QuikSCAT data. They found that barrier winds in the wintertime predominantly form at two locations, one downstream and the other upstream of the Denmark Strait. Winds in excess of 25 $\mathrm{m\,s^{-1}}$ (as measured by QuikSCAT) were a weekly occurrence at the southerly site. The northerly site had the disadvantage of being in a region where sea ice (over which QuikSCAT can't make measurements) is prevalent in wintertime. Still, a large number of strong wind events were also found at

this location. The climatology of Harden et al. (2011) (presented in extended form as Chapter 2) used a new ECMWF reanalysis product so was able to go further than Moore and Renfrew (2005) and also discussed the typical ocean impacts of barrier wind events. A large range of surface heat fluxes was found, due to a large range of barrier wind core temperatures. These temperatures were due to very different synoptic environments; the warmest winds formed when a blocking high was in position over the Nordic Seas leading to more Atlantic maritime inflow and the coldest winds owed their presence to a train of cyclones moving up the southeast Greenland coast leading to more of a polar air mass influence. The differing source regions and shapes of the resulting composites suggests that these synoptic environments might imply different forcing mechanisms for the barrier winds.

In March 2007, the Greenland Flow Distortion Experiment (GFDEx) (Renfrew et al., 2008) set out, amongst other things, to provide the first in situ measurements of the barrier winds through the use of instrumented aircraft and dropsondes. Petersen et al. (2009) (hereafter PRM09) provides case study observations and numerical modelling output of two barrier wind events. They showed that the observed barrier winds were confined below 2000 m (below mountain height) and had a well-mixed boundary layer over the open ocean. There were typically two starkly different sources of air contained in the barrier wind; cold, dry, northerly-sourced air and warmer, moist air pulled in from the south. The driving force for the barrier winds were cyclones to the southeast of Greenland and the numerical modelling of the events emphasised the importance of the location of the cyclone centres for the precise location of barrier wind formation. Modelling also showed, in runs with and without topography, that the barrier presented by Greenland was responsible for a doubling of peak wind speeds along the coast. In addition to this study, Petersen and Renfrew (2009) presented the first surface heat flux estimates during barrier wind activity from the observations made by the instrumented aircraft. They showed that these events were capable of producing total surface turbulent heat fluxes up to 500 $\mathrm{W\,m^{-2}}$ and surface stresses in excess of 1 $\mathrm{N\,m^{-2}}$.

In this chapter, a further case study is presented based on in situ measurements from a research vessel and numerical modelling output. The dropsonde observations of PRM09 provide a good spatial picture of barrier winds but provide very limited temporal resolution due to the inability of the aircraft to be airborne for the entire period of a barrier wind event. The data presented here, although limited to a single location, are the first continuous measurements from within a barrier wind and are therefore able to chart the barrier wind through all stages of development. The measurements are also taken in a different season and, as shall be seen, exhibit very different conditions to the cases presented in PRM09. Differences between the case studies will be discussed and placed into the

climatological framework discussed in Chapter 2. As with that chapter, a special emphasis will be put on the examination of surface heat and momentum fluxes. The numerical model will also allow an examination of the force balance in these barrier winds.

3.2 Synoptic overview

The period of the study for this barrier wind case is the four days between 5 and 8 October 2008. Figure 3.1 displays the synoptic meteorological environment over this period. On 5 October, a low pressure system is approaching the Irminger Sea from the southwest. On the 6 October, the Met Office analysis charts show that this low pressure system has moved into the central Irminger Sea with a depth of 975 hPa. Its position is such that surface air is being forced northwestwards towards the southeast coast of Greenland. The QuikSCAT 10 m wind field (morning pass) shows strong southeasterly surface winds in this region associated with the tightening of the isobars here. This flow towards the coast brings with it a tongue of warm air from the southeast as seen in the ERA-Interim 2-m temperature record and delineated by an occluded front in the Met Office analysis. The QuikSCAT record also shows the development of strong northeasterly surface winds stretching 600 km along the coast with a width of around 100 km, indicating that a barrier wind has been set up. The maximum core wind speeds measure in excess of 25 $\mathrm{m\,s^{-1}}$ and the edge of the jet is characterised by a steep gradient in wind speed with a reduction of 15 $\mathrm{m\,s^{-1}}$ occurring over a 30 km distance. The geopotential height at 500 hPa shows a trough to the west of the surface low with a cut off centre along the west coast of Greenland

By 00 UTC on 7 October, 24 hours later, the low has moved eastwards to 62°N, 25°W and deepened slightly to 973 hPa. The isobars to the north of the low have tightened and become increasingly aligned with the coastline. The QuikSCAT wind speed measurements show that this is associated with an increase in barrier wind intensity with core speeds greater than 30 $\mathrm{m\,s^{-1}}$. The width of the jet has also increased to fill the entire Denmark Strait and now extends some 1000 km along the coast from Cape Tobin to 63°N. The upper level conditions are such that the cut off low has moved south to sit over the southern tip of Greenland with the trough rotated to extend eastwards. The location of this cut off low is such that it is likely to be in part responsible for the lee cyclone which has developed to the east of Cape Farewell with a depth of 980 hPa. Cyclogenesis is a common occurrence to the east of Cape Farewell and is thought to be influenced significantly by Greenland's orography (Kristjánsson and McInnes, 1999; Skeie et al., 2006).

Coupling to the upper level low could be the reason that this lee cyclone deepened over the subsequent 24 hours to 977 hPa; the original low filled to 990 hPa and has moved to settle over eastern Iceland. The location of these two lows acts to channel wind through

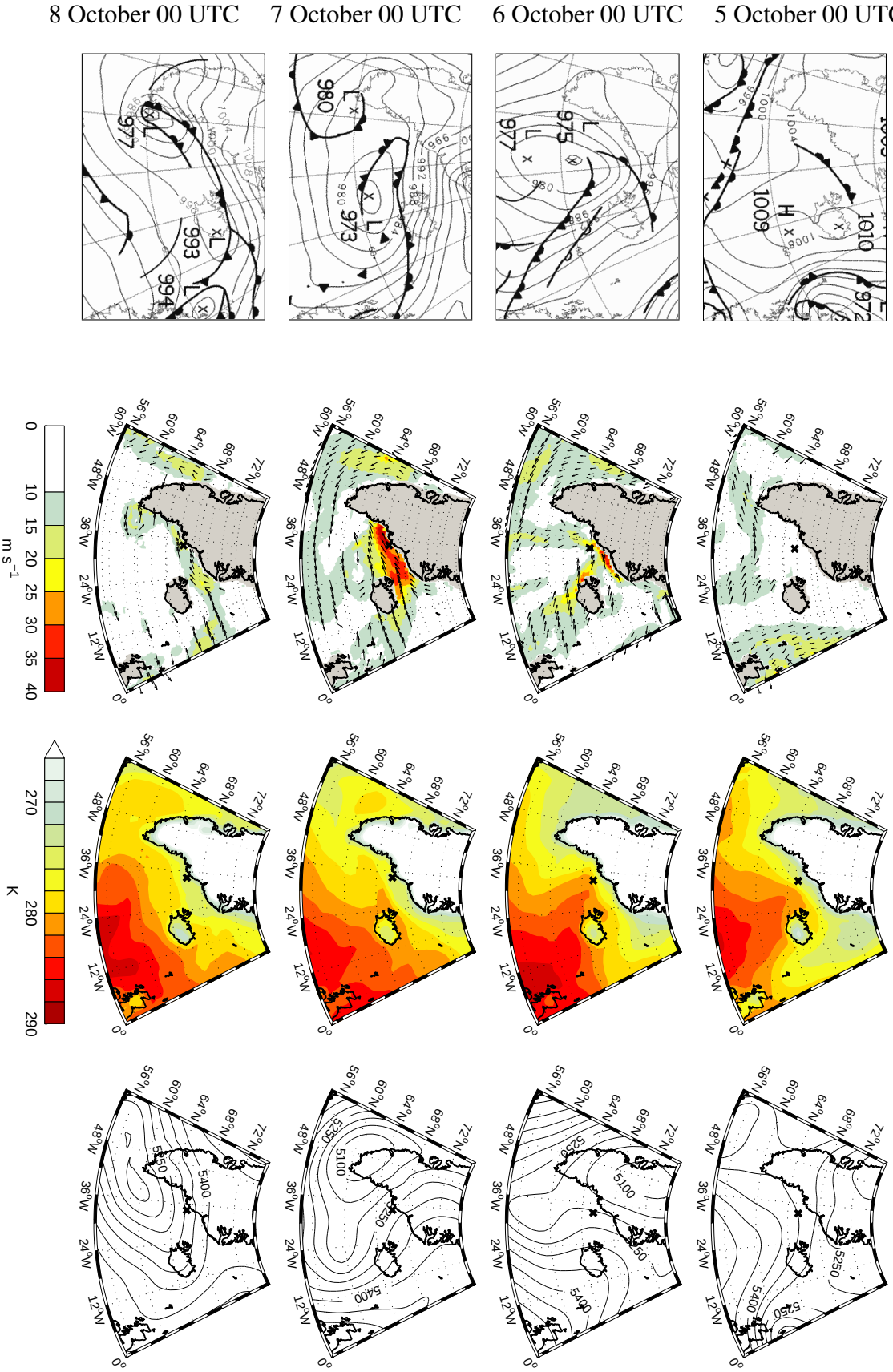

Figure 3.1: Synoptic environment between the 5 – 8 October 2008. From left to right: Met Office surface analyses for 00 UTC on each day, QuikSCAT 10 m wind field for the morning pass on each day (wind vectors only shown for winds greater that 10 m s^{-1}), ERA-Interim 2 m temperature at 00 UTC, ERA-Interim 500 hPa geopotential height (m) at 00 UTC. The black crosses indicate the location of R/V Knorr at each time.

the Denmark Strait and keep it confined to the coast. The isobars are mostly aligned along the coast, but their separation is increased and QuikSCAT confirms that the barrier flow had diminished to 10 – 15 $\mathrm{m\,s^{-1}}$ all along the Greenland Coast. The upper level flow is more coast parallel than on previous days when the upper air was being forced towards the coast from the south.

During the 8 October, a deep low moved into the region from the south, displacing the original lows to the northeast and destroying the barrier jet conditions.

3.3 Observations

3.3.1 R/V Knorr near surface measurements

The R/V Knorr was in the Denmark Strait (66°N, 34°W) for the duration of this barrier wind event on cruise number KN194-4. It was therefore well placed to sample some of the strongest winds. Its location throughout this period is shown in Figure 3.1 with black crosses. Near surface meteorological variables were measured by the ship's IMET package (wind) and by the Vaisala WXT5-10 system (temperature and humidity). All of the meteorological instruments were mounted on a tower at the bow of the ship which put them 15.5 m above sea level. For the subsequent analysis, the wind speed and temperature were extrapolated to standard meteorological heights (10 m for wind, 2 m for temperature) using the logarithmic neutral profile formulae as in Section 2.2.2.

Figure 3.2 shows the near-surface measurements taken on R/V Knorr between 5 and 9 October. The wind speed shows two periods of strong winds. One reached a maximum of 20 $\mathrm{m\,s^{-1}}$ at 06 UTC on 6 October. This is followed by a sudden reduction in wind speeds to 7 $\mathrm{m\,s^{-1}}$ in just six hours. The wind speed gradually increases again to reach a second, slightly stronger wind maximum, measuring 25 $\mathrm{m\,s^{-1}}$ at its peak at 18 UTC on 7 October. Also shown on the wind speed graph is the QuikSCAT measured wind speeds for its nearest grid point to the location of the Knorr at the time of each satellite pass. QuikSCAT agrees well with the onboard measurements during the first strong wind event, but measures consistently higher than the Knorr by as much as 10 $\mathrm{m\,s^{-1}}$ during the second event. Overestimation of 10 m wind speeds during strong winds is a feature of QuikSCAT that has been observed previously [Moore et al. (2008) and references therein]. It is thought to be caused by severe ocean roughness interfering with the scattering from the capillary waves on the surface that QuikSCAT utilises to estimate the wind speed. It is therefore not surprising that QuikSCAT should overestimate the wind speed between 06 UTC on 7 October and 00 UTC on 8 October when the surface winds are in excess of 20 $\mathrm{m\,s^{-1}}$ and the ocean state was extremely rough. QuikSCAT's tendency to overestimate

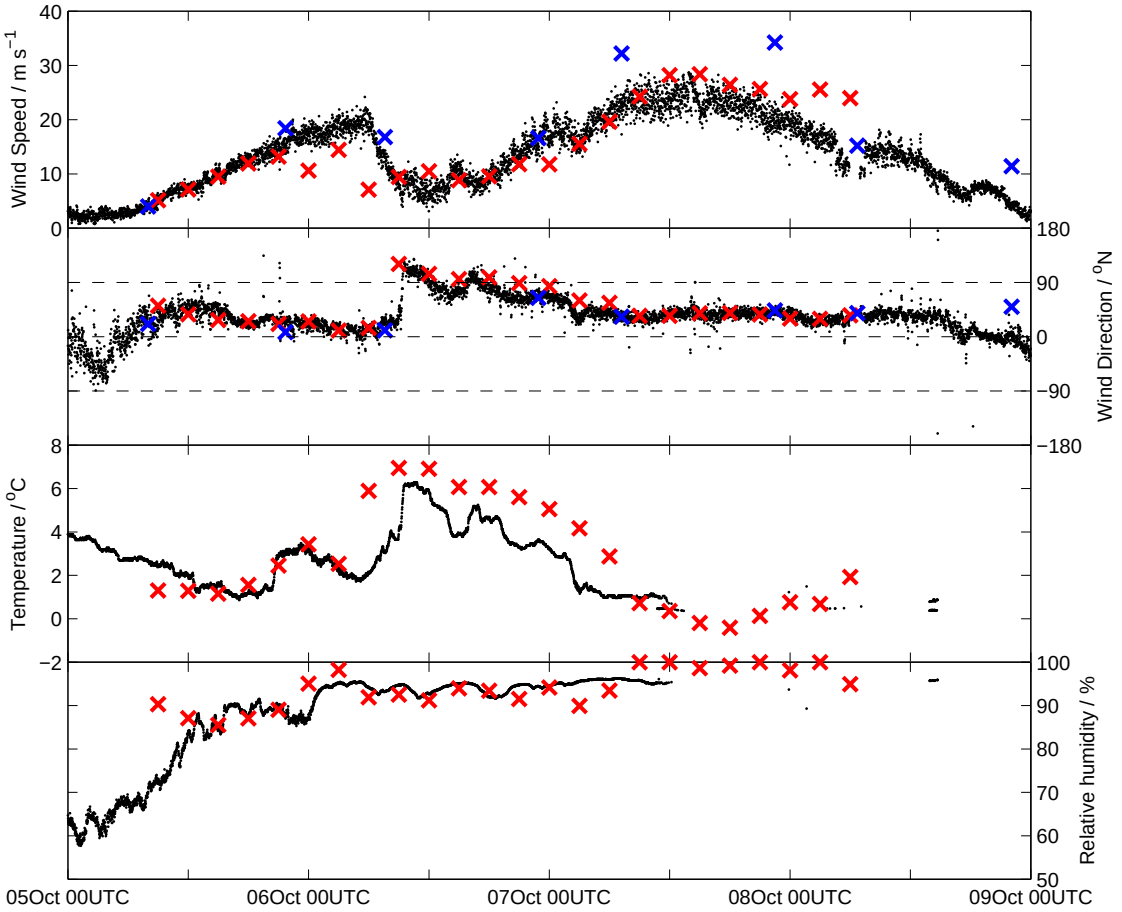

Figure 3.2: Wind speed, wind direction, temperature and relative humidity as recorded by the Knorr's meteorological equipment (black dots). Blue crosses indicate measurements by QuikSCAT of the 10 m wind speed and direction for the location of the Knorr during each satellite pass. Red Crosses show the model output (interpolated onto the same standard meteorological heights as the observational data) for each variable from the nearest grid point to the location of the R/V Knorr.

wind speeds during high winds should be kept in mind for any subsequent analysis of data from this satellite.

During the first period of strong winds, the wind direction was nearly northerly. It was only after the winds strength had dropped significantly and was at its lowest extent did the wind direction switch suddenly to become more easterly at 09 UTC on 6 October. Hereafter the wind direction gradually, but somewhat erratically, backs towards the northeast where it becomes quite consistent by the time of the second strong wind period. The QuikSCAT data for wind direction agrees well with the Knorr data for all times, even during the period when the the wind speeds from the satellite were overestimated.

For the first 24 hours of the period, the temperature is close to 2 °C on average. During

the 6 October, the temperature record increases to 7 °C in six hours. The most dramatic rise in the temperature during this period was near the end of the increase when temperatures rose 3 °C in less than an hour, coincident with the rapid wind rotation. In the subsequent 18 hours, the temperature returns by means of a fluctuant path back down to a reasonably consistent 1 °C by 06 UTC on 7 October. During the second period of strong winds the temperature sensor fell out of operation, maybe affected by the severe conditions at the time.

Initially, at 00 UTC on 5 October, the relative humidity was at 60%. By the time of the first wind maxima it had risen to more than 90% and remained above this value until the sensor fell out of operation at the same times as the temperature sensor.

3.3.2 Radiosonde soundings

Radiosondes were launched regularly from the deck of the R/V Knorr during this period. Profiles of wind speed, wind direction and potential temperature from these launches are shown in Figure 3.3. The first surface strong wind event takes the form of a low-level jet, confined below 1000 m and with a jet maximum of nearly 30 $\mathrm{m\,s^{-1}}$ at an altitude of 500 m at 06 UTC on 6 October. Above the jet, the wind speed is a reasonably consistent at 10 – 15 $\mathrm{m\,s^{-1}}$ all the way up to 5000 m. At this time, the winds in the jet are directed north-northeasterly, and gradually back with altitude to become consistently southeasterly above 2000 m. This shows that the background atmospheric conditions are southeasterly, but that near the surface this is radically altered by the presence of Greenland, accelerating and rotating the flow to be aligned along the barrier. The southeasterly flow at altitude is due to the upper level trough situated over west Greenland as shown in Figure 3.1. At this time, the potential temperature profile shows that the boundary layer is well mixed for all levels within the jet. Above this, the atmosphere is stratified.

The second surface event starts as a well-defined jet at 00 UTC 7 October but becomes much deeper and less well defined as it develops through the day. The profiles at these times show a deep jet, with the strongest winds of nearly 45 $\mathrm{m\,s^{-1}}$ (at 18 UTC on 7 October) located between 500 m and 2000 m. The strong winds of over 20 $\mathrm{m\,s^{-1}}$ at all heights and the reduced height of the soundings at this time make the definition of a jet top difficult, as does the fact that the flow is from the northeast at the surface and from the east above mountain top. It is clear that in this stage of barrier flow development, the upper and lower atmospheric flow is more aligned than previously when the flow at the surface was at least 90° to the left of the flow above mountain height. Unlike the first period of strong wind, the potential temperature profiles show little evidence of a neutral mixed layer near the surface. Distinct layers of varying stability are seen instead though.

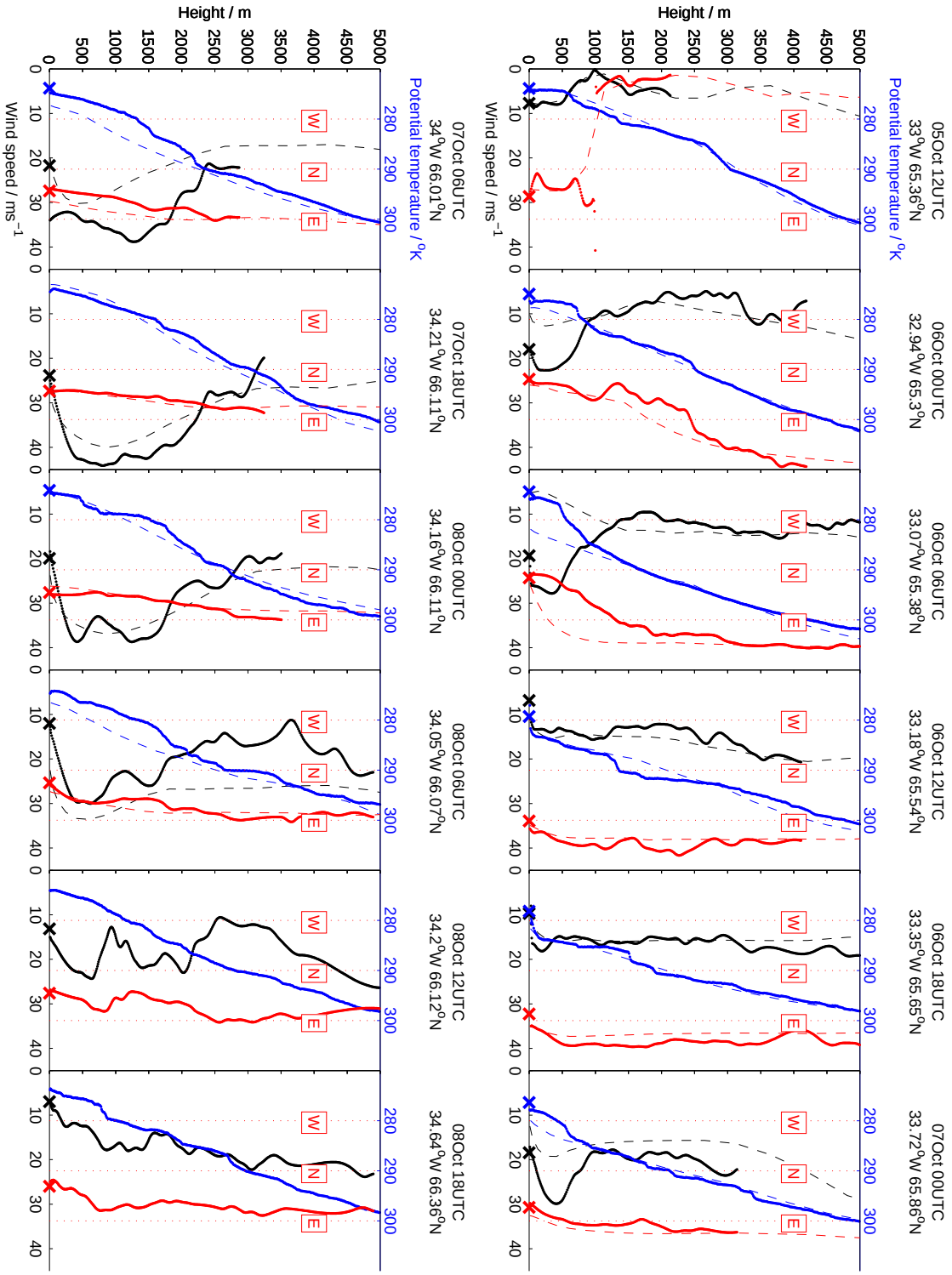

Figure 3.3: Profiles of wind speed (black), wind direction (red, indication direction the wind is flowing from) and potential temperature (blue) from radiosondes (solid) and from model output (dashed). Crosses along the bottom indicate R/V Knorr surface measurements where available.

3.3.3 Interpretation of observations

An explanation of the features seen in the R/V Knorr surface measurements and the radiosonde data can be attempted in relation to the Met Office surface pressure charts, QuikSCAT measurements and ERA-Interim fields shown in Figure 3.1. When the barrier winds first develop on the evening of 5 October, and on the follow morning, a small jet can be seen detaching itself from the Greenland coast in the vicinity of the R/V Knorr in the QuikSCAT 10 m wind field. It is likely that this feature is a result of the specific combination of upstream northeasterly flow, the shape of the barrier at this particular point, and the strong return flow to the west of the low. This is probably the specific cause of the first strong wind event as recorded on the Knorr. The vertical profiles at this time show that this region of strong winds are confined to below 1000 m and are from the north, 135 degrees to the left of the flow at altitude. This is typical of barrier flows produced by a low-level deflection of onshore wind conditions (Schwerdtfeger, 1975).

The surface wind speed subsequently decreases at 06 UTC on 6 October and the corresponding low-level jet is destroyed. The northerly flow from the coast on the western side of the low pressure centre is being restricted. This is likely due to a change in synoptic conditions such that the isobars, instead of being coastally aligned all down the barrier, cross the coast in the vicinity of the Knorr as shown at 00 UTC on 7 October. Possible causes for this include the southerly progression of the upper level cut off low which will alter the angle of wind approach to the coast at altitude, the development of the surface lee cyclone producing a competing southerly wind to the west of the original low, and the approach of the warm sector to the coast. The result is a diminution of the measured surface winds on the Knorr, but in the maintenance of their direction. This changing synoptic environment is coincidental with the approaching occluded front visible in the Met Office surface charts and also shown as a warm sector protruding towards the coast in the ERA-Interim 2 m temperature analysis. The Knorr's surface temperature and humidity increase slowly as the front approaches and the dramatic jump in the temperature at 09 UTC on 6 October marks the time at which the front passes over the Knorr. It is only at this time that the wind direction changes to become southeasterly in accordance with the winds on the warm side of the front.

Over the next 18 hours, the front must be very close to the location of the Knorr because of the semi erratic way the surface temperature, wind direction and, to some extent, the wind speed jump in steps during this period. These fluctuations in the front's position are likely due to the competing influence of the onshore wind conditions behind it and the increasingly strong barrier wind from the northeast. By 06 UTC on 7 October, the surface temperature and wind direction had become consistent; the synoptic conditions

have allowed a strong, wide barrier flow to establish itself all along the coast, channelling cold air through the Denmark Strait and moving the surface frontal temperature gradient further out to sea where it marks the southerly extent of the barrier winds.

In an idealised study, Olson and Colle (2009) showed that (everything else being equal) the width of a barrier wind increases with decreased angle of incidence of the incoming synoptic flow. They also showed that unless the angle of approach becomes very shallow, the barrier wind strength will also increase with a decrease in angle of incidence. This could help explain the widening and strengthening of the barrier wind at this time as the onshore flow becomes easterly compared to previously when it was southeasterly. This is further exemplified by the upper level conditions which have become increasingly aligned with the surface conditions; there is a less severe change in wind direction with height as observed in the radiosonde soundings at this time.

3.4 Modelling

3.4.1 Setup

The Met Office Unified Model (UM) version 6.1 (the current version around this period) was utilised in atmosphere only mode to investigate the barrier winds during this event. The UM employs a non-hydrostatic, fully compressible, deep atmosphere with a semi-Lagrangian treatment for advection of all prognostic variables except density which is given a Eulerian treatment. It has a two-time-level, semi-implicit, time integration scheme with a predictor-corrector implementation. The model has Arakawa C grid staggering in the horizontal and Charney-Philips staggering in the vertical allowing calculation of prognostic variables to be made without interpolation of values between levels. The vertical coordinates are height-based and terrain following to ease the application of lower boundary conditions. The spacing of the vertical levels is such that at upper levels the coordinate surfaces become flat.

A global run was conducted on a 640 x 481 horizontal grid in order to produce boundary conditions for a limited area model (LAM) run. The LAM was run on a 220 x 220 horizontal grid, centred over Greenland and with a rotated pole such that the latitude-longitude grid spacing (0.11°) was nearly uniform in distance producing a resolution of approximately 12 km. There were 36 non-uniformly spaced levels in the vertical, with 13 levels within the boundary layer. The initial atmospheric conditions, along with the sea surface state and sea ice concentration data, were obtained from the Met Office global analysis start files. The sea surface temperature (SST) was fixed for the entire run as the high resolution OSTIA (Stark et al., 2007) valid for the time of model initialisation.

A comparison of this product with another dataset, the weekly Reynolds SST product (Reynolds et al., 2002), yielded favourable comparisons providing evidence for the suitability of the model SST fields for the time of year. The orography was specified by GLOBE, a 30 arcsecond resolution global dataset from the National Geophysical Data Center (Hastings et al., 1999). A time step of 150 seconds was used.

Both the global and LAM runs were initialised on 5 October 2008 at 06 UTC and run for 72 hours. This length of time encompassed all of the barrier flow activity except the final stage of wind depletion. An attempt was made to conduct shorter length runs of parts of the event to negate the inaccuracies implicit after 72 hours of a limited area numerical weather prediction model run, but the model proved to be unstable during initialisation when strong winds had already formed along the coast. The length of the run should be kept in mind especially when analysing data from towards the end of the run.

3.4.2 Verification

Previous verification

Some verification of the UM in this region was undertaken by PRM09 for their case studies of barrier winds and by Outten et al. (2009) in their investigation into easterly tip jets. Both studies compared models of a similar resolution and domain to the one used here with dropsonde measurements from an instrumented aircraft (Renfrew et al., 2008). In both studies, the UM performed adequately. Petersen et al. (2009) showed that the UM captured the location and strength of the barrier winds well along with the synoptic cyclone development over the 48 hours of each run. The only noteworthy failing of the model was in its inability to properly resolve sharp vertical gradients in velocity and temperature at the top of the barrier jet.

Outten et al. (2009) investigated further the impact of the surface conditions on the shape and temperature of orographic jets near Cape Farewell by making modifications to the files used for the lower boundary conditions of the model. They found, as Petersen et al. (2009), that the marginal ice zone (MIZ) sea roughness lengths were set too high in the default UM. These were adjusted to a smaller value based on recent observations (Andreas et al., 2005) and a more representative jet was produced. In the simulations presented in this chapter this method isn't implemented due to the lack of sea ice in the region of interest. They also reconfigured the ocean surface fields to the Ocean Sea Surface Temperature and Sea Ice Analysis [OSTIA, (Stark et al., 2007)]. This is now used as standard in the UM, but at the time it was shown that this improved the wind speed, temperature and humidity profiles significantly in the barrier winds compared to the previous default UM sea surface fields.

As part of their comparison paper of aircraft data with various model products, Renfrew et al. (2009b) investigated the performance of the Met Office's North American and European (NAE) analysis. They found that the model represents the wind speeds in the region generally well although both the temperature and humidity fields experienced low-level cold, dry systematic biases which resulted in heat fluxes larger than those observed. It should be noted that this was before the high resolution OSTIA sea surface fields were implemented in the UM. As discussed previously, Outten et al. (2009) showed that this vastly improves the atmospheric temperature and humidity fields.

Verification for this case study

Further verification of the UM will be presented based on comparisons with analyses, QuikSCAT and the observations collected aboard the R/V Knorr. Figure 3.4 shows output fields from the model run for the current case study, comparable to the bottom three rows of panels in Figure 3.1. Up until 00 UTC on 7 October, the position and depth of the surface low is well modelled in point for point comparisons with the Met Office analyses. Past this time, the model's agreement with the analyses becomes less good. In the Met Office analysis, by 00 UTC on 8 October the original low is positioned over east Iceland and has filled whilst the lee cyclone at Cape Farewell has deepened dramatically and has become the dominant low pressure centre in the region. In the model, the original low has advected down the coast with the barrier flow, tightening the isobars significantly, and the lee cyclone has deepened to only 983 hPa compared with 977 hPa in the analysis. It was speculated that the reason for the development of the surface low was due to a coupling to an upper level trough. A comparison of the ERA-Interim 500 hPa height with that modelled by the UM shows very good agreement at all times in both depth and location implying that it is not a lack of upper level coupling that restricts the deepening of the lee cyclone. It may have something to do with lower level processes or the fact that nearly 72 hours have elapsed since the model was initialised – it is not entirely surprising that the model's pressure field should drift as the run time increase. Errors are introduced by inaccuracies of the initialisation data and by inadequate information coming in through the boundaries. From the comparison of Figures 3.1 and 3.4 though, it seems sensible to suggest that the model is a good representation of the synoptic surface system for at least the first 48 hours of the run. Any data past this time should be considered in light of the discrepancies between the model and the analysis.

The spatial distribution of the model's 10 m wind field compares well with the QuikSCAT wind field for most of the run. QuikSCAT is clearly measuring much higher wind speeds though – by as much as 10 – 15 $\mathrm{m\,s^{-1}}$ on 7 October. This is either due to one, or both, of QuikSCAT's overestimation of high wind speeds and a model underestimation of the bar-

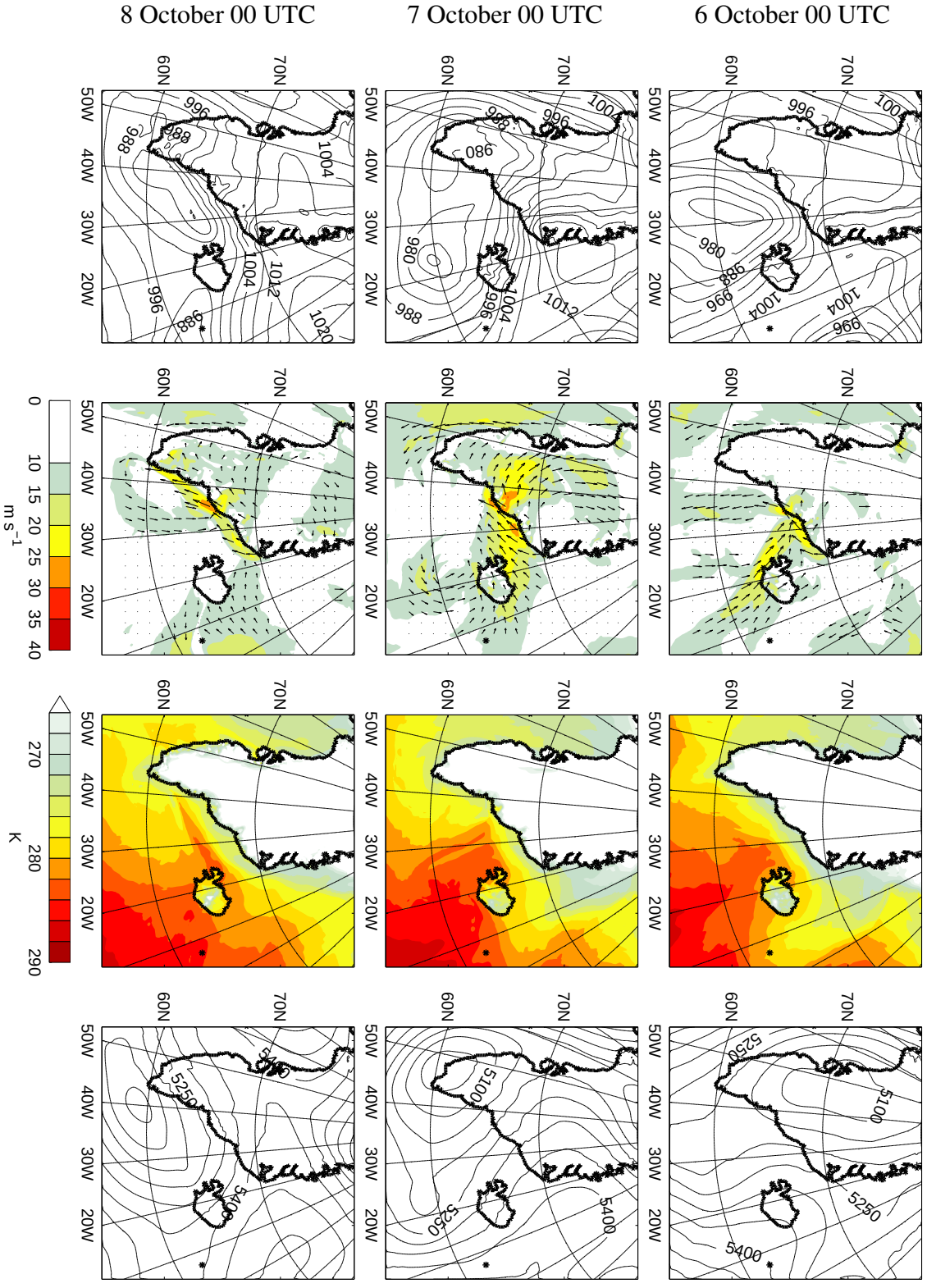

Figure 3.4: Model fields between the 5 - 8 October 2008. From left to right: Mean sea level pressure (hPa) for 00 UTC on each day, 10 m wind field for the nearest output time step to the time of the QuikSCAT morning pass on each day (wind vectors only shown for winds greater that 10 m s^{-1}), 2 m temperature at 00 UTC, 500 hPa geopotential height (m) at 00 UTC.

rier wind intensity. Along with the near surface measurements made on the Knorr and the QuikSCAT data, Figure 3.2 also shows corresponding nearest grid point model outputs for the length of the model run. The figure shows that, at least for the first 48 hours of the run, the model is doing a good job at modelling the wind speed and direction. It captures the initial rise in wind speed directed nearly from the north, the subsequent reduction in wind speed and rotation of flow to easterly and the second northeasterly wind speed maximum well. The model has stronger wind speeds than the observations after 48 hours in line with the unrealistic increase in the pressure gradient along the coast as described previously. The model agrees much better with the observations than QuikSCAT during the second high wind speed event (Figure 3.2) in agreement with the overestimation of strong winds by QuikSCAT.

The 2-m temperature panels in Figure 3.4 show a very similar picture to those in Figure 3.1. A warm tongue is advected towards the Greenland coast on the northeast side of the low during the first stage of barrier wind activity before being pushed back off shore by cold air advected down the coast when the long, wide barrier wind establishes itself. A nearest grid point comparison to the temperature measured on the Knorr is shown in Figure 3.2. In general the same form is seen – an initial rise in temperature followed by a gradual decrease. The temperature is modelled particularly well near the beginning of the model run. The temperature rise in the model occurs about three hours ahead of the observations indicating that the front arrives at the Knorr sooner in the model than in actuality. This early increase in temperature is consistent with the slightly early reduction in wind speed after the first event and shows that although the front arrives too soon in the model, the fundamental processes are being captured well in the model. The model's 2-m temperature is consistently 1–2°C higher than the observations after the front has arrived before agreeing much better after the front has been pushed back offshore. The model relative humidity (also shown in Figure 3.2) agrees reasonably well with the observations at all times.

A comparison of the soundings from the Knorr with nearest grid point vertical profiles from the model is shown in Figure 3.3. It shows that at most times, the model does an adequate job of simulating both the vertical extent and strength of the surface jets. One notable exception is during the first jet event when the model fails to capture any jet behaviour at all. Further investigations indicated that this was caused by the slight mispositioning of this jet by the model. The jet in the model is slightly to the northwest of its actual location (as shown by QuikSCAT) and due to its sharp edge this is enough to radically alter the vertical profiles in the model. This discrepancy is likely due to the early arrival of the front in the model as described above. Changing the chosen model grid point by only 60 km to the northwest has a very large effect on the profile produced

and a good representation of the jet is achieved. This applies equally well to the other times when the jet peak wind speed is missed by the slightly mispositioned surface jet in the model (for example 6 October 00 UTC and 7 October 00 UTC). In almost all cases a movement of 40 – 80 km across the jet boundary results in a much better representation of the barrier jet. This shows that although the UM is simulating representative barrier winds, the scale of the jets and their sharp edges makes it difficult for a NWP model to precisely define their location at T+24 hours and longer (at least in this case). Overall, the representation of this case study by the UM model run is deemed adequate for further investigation.

3.4.3 Barrier wind development

Now that is has been established that the model is functioning more or less satisfactorily, an investigation of other diagnostics is appropriate bearing in mind the limitations of the model described above.

Figures 3.5, 3.6 and 3.7 show the near surface development of the barrier flow with more temporal detail than Figure 3.4. As alluded to previously, and with the addition of humidity data, three stages of development can be identified which can be loosely described by the day of the simulation on which they occur:

5 October: The advection of a warm sector towards the coast.

6 October: The initial development of a narrow, coastally confined barrier wind. This is hemmed in with a strong temperature gradient associated with the warm sector on its southeastern flank. The jet core has a high relative humidity.

7 October: The widening of the barrier wind and the associated offshore advection of the temperature front. The strongest winds also move further down the coast. These are still associated with the highest relative humidities in the domain.

Figures 3.8 and 3.9 show cross sections of the horizontal wind speed, potential temperature and vertical velocity for the cross coastal lines shown in the first panel of Figure 3.5. These cross sections will be referred to as barrier flow north (BFN) and barrier flow south (BFS). BFN passes through the core of the barrier flow where it first forms during the first 6 October development stage and BFS intersects further downstream in the region of stronger winds on the 7 October. The locations for these cross sections are similar to those used in the climatology of Chapter 2 referred to as Denmark Strait North (DSN) and Denmark Strait South (DSS). The slight difference in the locations is the reason for the adoption of a different nomenclature here.

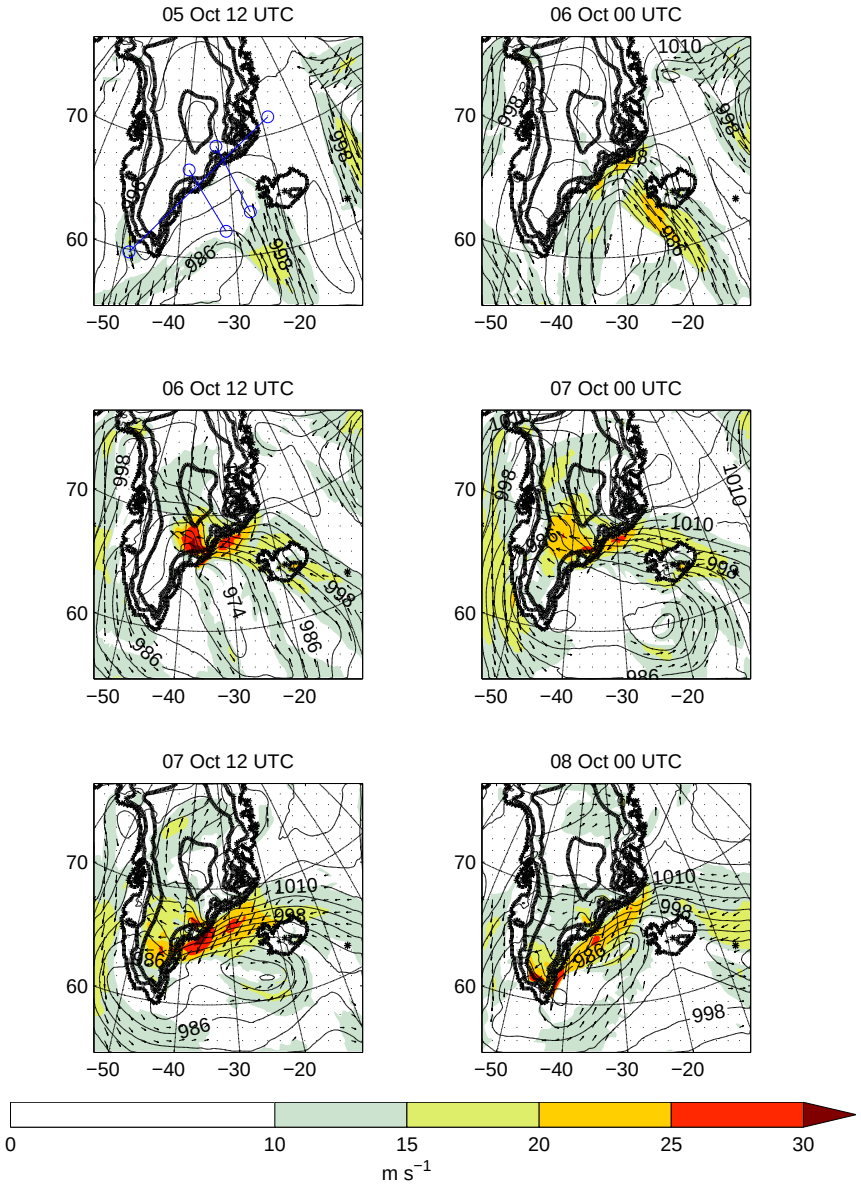

Figure 3.5: 10 m wind speed with wind vectors shown at every 10th grid point for wind speeds greater than 10 m s^{-1}. Mean sea level pressure shown every 4 hPa. First panel shows cross section lines used in Figures 3.8, 3.9 and 3.10. Orography shown every 1000 m.

The BFN cross section shows the steady build up of a barrier wind on 6 October. At 12 UTC, the jet core has a maximum wind speed of over 35 m s^{-1} at an altitude of 1000 m. The vertical profile of the barrier wind is tilted towards the coast and has a width of around 200 km as defined by the 20 m s^{-1} contour. The isentropes slope upwards towards the coast and there is a general uplift visible in the vertical velocity. All of these features are consistent with flow blocking of air directed towards the Greenland coast. Above mountain height, and offshore of the barrier, the flow is towards the coast (Figures

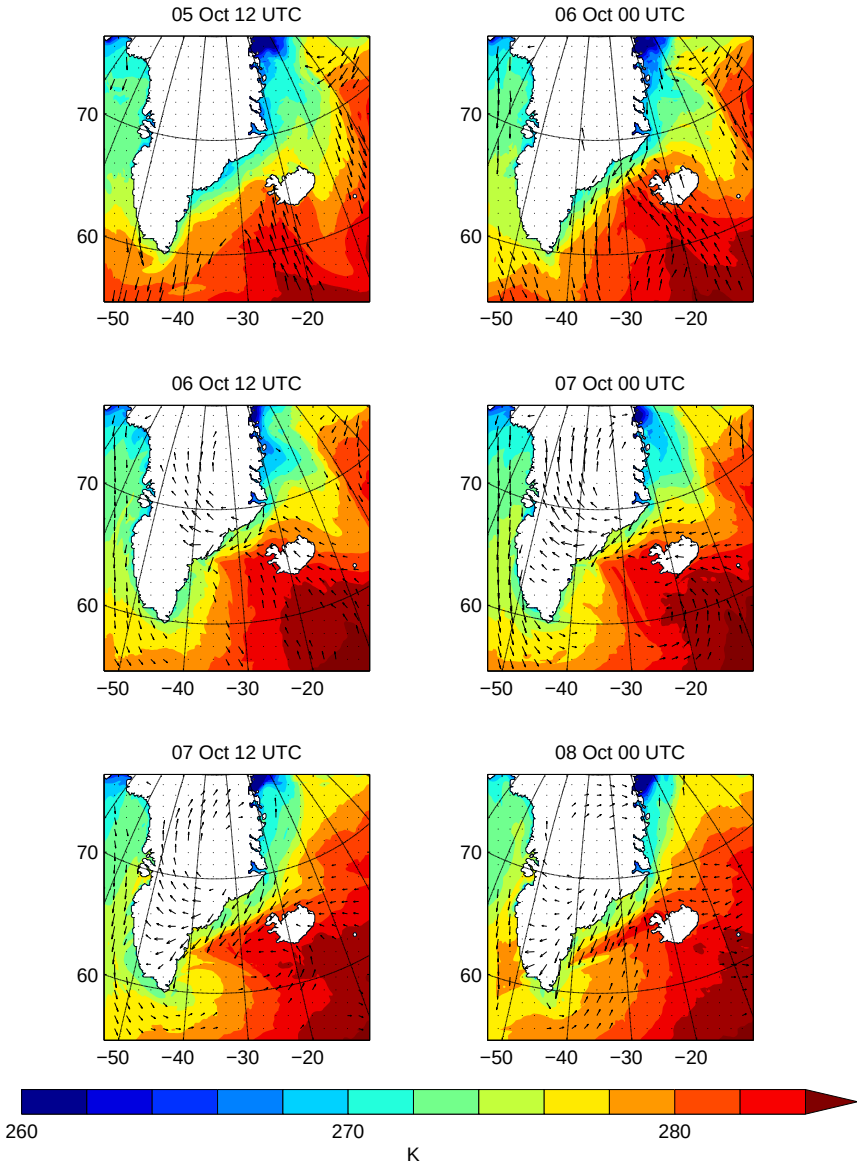

Figure 3.6: Temperature at 2 m over the ocean with 10 m wind vectors at every 10th grid point shown for wind speeds greater than 10 m s^{-1}. Orography shown every 1000 m.

3.4 and 3.5) whilst near the barrier the wind blows coast parallel, exists below mountain height and is hemmed in against the coast. This is the classic image of a barrier wind as described by, for example, Schwerdtfeger (1975) and Parish (1983).

By 12 UTC on 7 October, the barrier wind has widened and the core has moved further from the coast. The centre of the barrier wind is now exhibiting a cold, neutrally stable boundary layer. Figure 3.5 shows that the synoptic flow at this time is directed towards the barrier from the east in comparison to 24 hours previously when it was directed south-easterly. This probably accounts for a wider barrier wind which is less pushed up towards the coast in accordance with the analysis of Olson and Colle (2009) described previously.

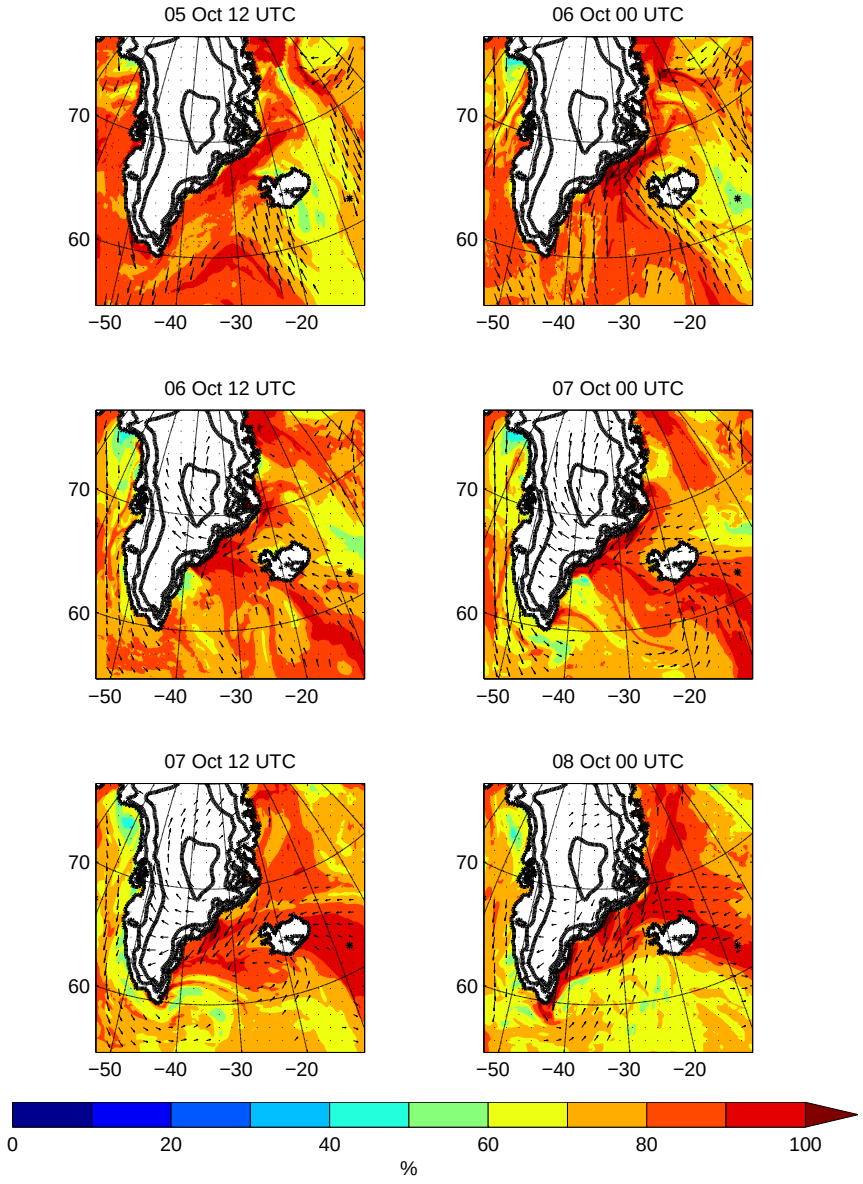

Figure 3.7: Relative humidity at 2 m over the ocean with 10 m wind vectors at every 10th grid point shown for wind speeds greater than 10 m s^{-1}. Orography shown every 1000 m.

The changed wind angle could also explain the cold air in the core of the barrier wind – colder ambient air from the east is now being funnelled through the Denmark Strait into the barrier wind. This also displaces the warm tongue offshore as shown in Figure 3.6.

Downstream at BFS, the barrier wind development is more complex. By 00 UTC on 6 October, a barrier wind similar in appearance to the one which initially forms at BFN is visible although it is much weaker. Figure 3.6 shows that BFS is more influenced by the approach of the warm sector which can clearly be seen at BFS by 12 UTC on 6 October as a region of homogeneously warm, constantly stratified air offshore of the barrier. At this time, the strongest winds of over 40 m s^{-1} are to be found high up on the Greenland

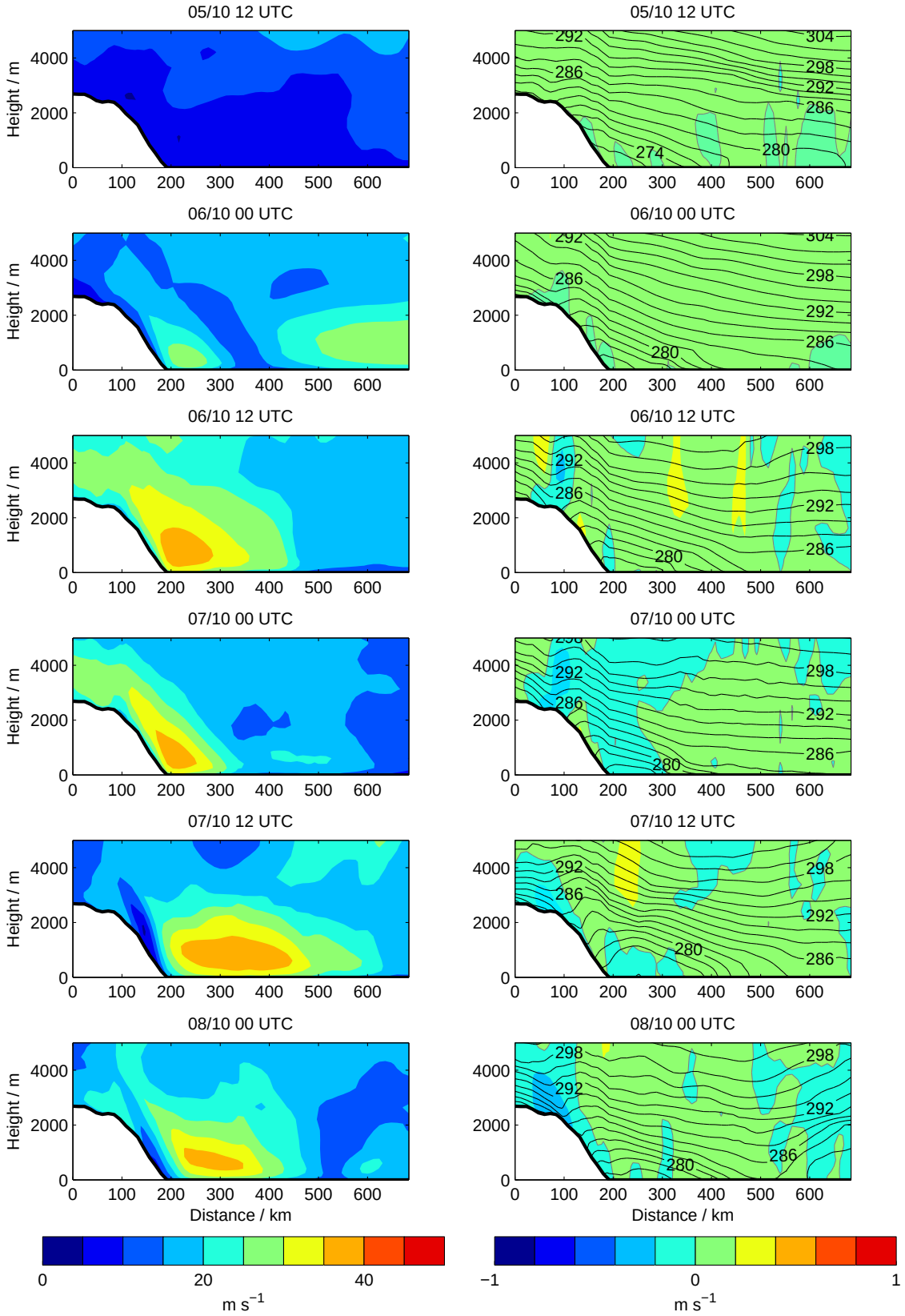

Figure 3.8: Cross section along BFN (as shown in Figure 3.5) of horizontal wind speed (left) and potential temperature (right). Also shown on right panels is the vertical velocity with red (blue) being positive (negative) and contours every 0.2 m s^{-1}.

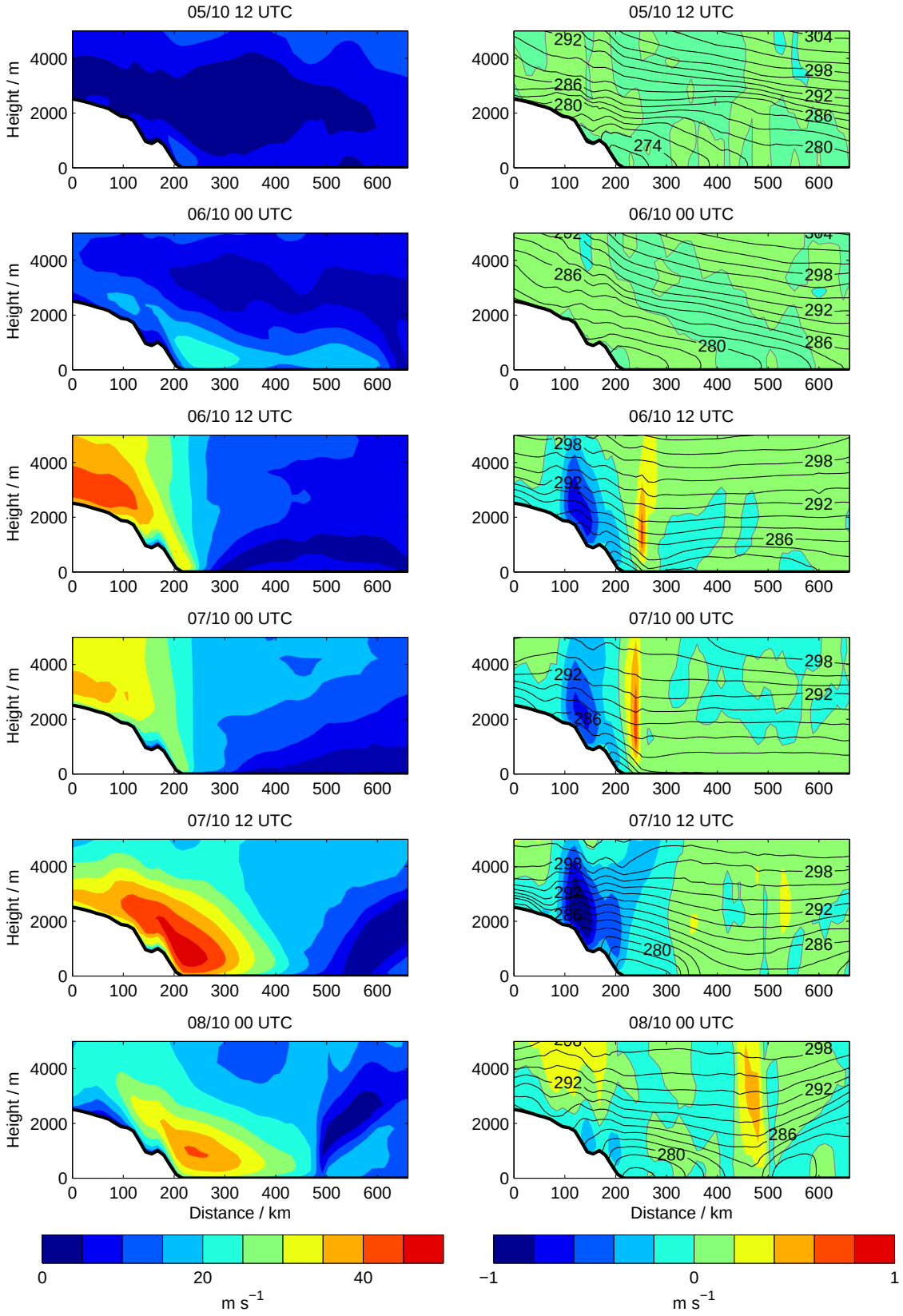

Figure 3.9: As figure (3.8) but for cross section BFS

plateau. Nearer the base of the barrier, winds are now greater than 30 m s^{-1} which appear as a tongue extending down from the plateau velocity maximum. The edge of this low-level wind is very sharp and occurs at the edge of the warm sector in conjunction with a large vertical uplift of more than 0.6 m s^{-1}. At the same time, the plateau air is strongly descending downslope. This configuration is maintained (although becoming weaker) for the next 12 hours.

By 12 UTC on 7 October, the strongest winds are back at the bottom of the slope. There is still a great deal of downslope flow on the slopes above the jet core (which now measures more than 45 m s^{-1}), but the uplift offshore of the strong winds has diminished significantly. At this time, Figures 3.5 and 3.6 show that the strongest surface winds in the region are located at this BFS cross section and that the warm sector has been advected offshore. Evidence that the localised enhancement in wind speed at this location isn't a modelling error comes from the QuikSCAT image for the morning pass of the 7 October (Figure 3.1) which clearly shows the same feature. The relative humidity (Figure 3.7) is reduced in a number of locations along the coast during this stage of development in agreement with cold, dry air being advected off the continent.

It is likely that there are two factors which have produced this wind enhancement and the offshore advection of the warm sector. Firstly, as described previously, the shallower angle of onshore wind conditions has allowed for a wider, stronger barrier wind that can advect colder air through the region and push the warm sector upwards or offshore. Secondly, it is possible that the downslope winds at BFS (as shown in Figure 3.9) are enhancing the barrier wind at this location. Katabatic winds are prevalent along this stretch of the Greenland coast (Heinemann and Klein, 2002) so could be influential in this flow, as could the downslope deflections of coast parallel flow over undulating topography as described in Parish and Cassano (2003). Another possible cause is shown in Figure 3.10, a cross section along coast for 12 UTC on 7 October (Figure 3.5 shows the along coast line for this cross section). From the angle of this cross section, it becomes apparent that the southeast coast of Greenland is seen as a series of three tall mountains by northeasterly atmospheric flow. Gravity waves are apparent over the middle of these mountains. It is well known that gravity waves are capable of forcing strong downslope winds in the lee of a mountain (Durran, 1990) and evidence of strong downdrafts and an associated increase in horizontal wind speed as the flow descends over the middle mountain can be seen in Figure 3.10. These gravity wave are seen in this cross section between 12 UTC on 6 October and 12 UTC on 7 October in accordance with the duration of the downslope winds seen in Figure 3.9 adding weight to this interpretation. To the authors knowledge, this is the first description of northeasterly downslope winds triggered by gravity waves along the southeast coast of Greenland. The degree to which they contribute to the en-

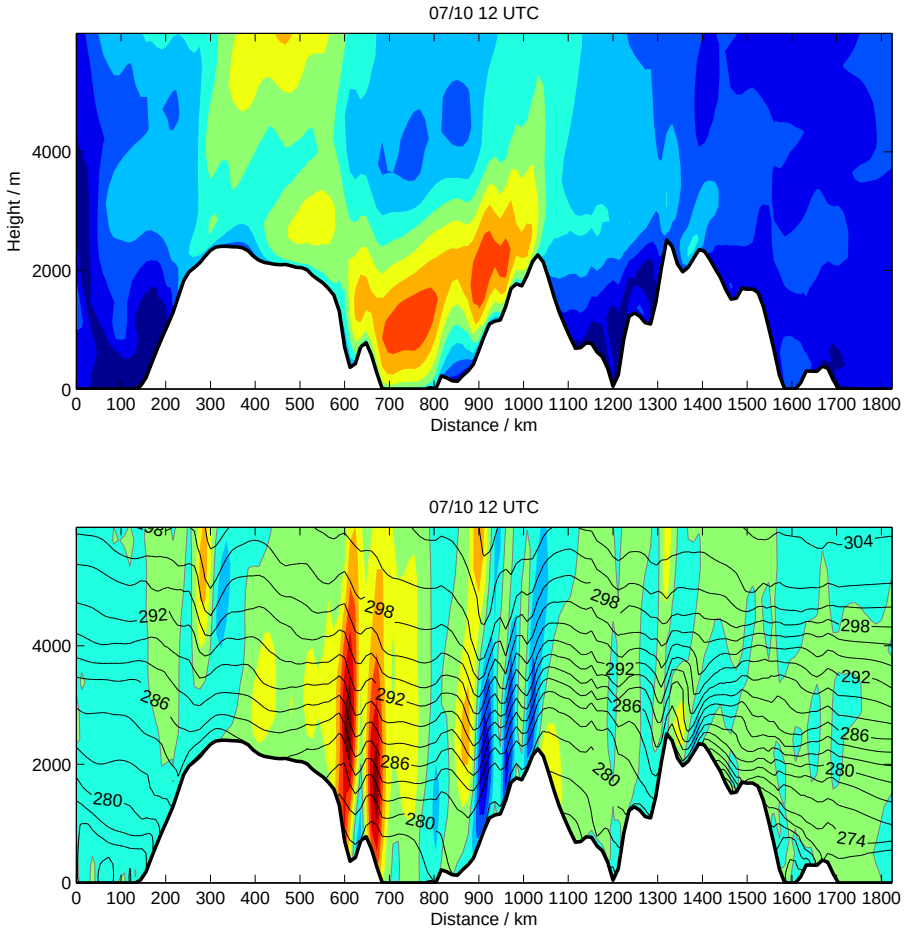

Figure 3.10: Cross sections of wind speed (left), and vertical velocity and potential temperature (right) at 12 UTC on 7 October for the along coast cross section line shown in Figure 3.5. Colourbar and contours as Figure (3.8).

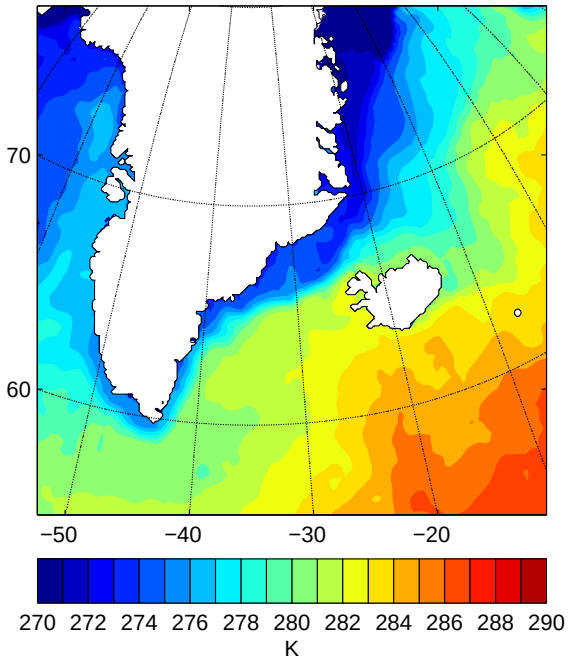

Figure 3.11: Sea surface temperature at all times during model run from OSTIA (Stark et al., 2007).

hancement of barrier winds in this region is left to further study. Some further evidence for the importance of gravity waves will be presented in Chapter 4.

3.4.4 Surface fluxes

As explained previously (see Chapter 1), the seas to the southeast of Greenland are vital for the circulation of the whole Atlantic ocean. As a result, an investigation into the surface fluxes of heat and momentum from this case study is appropriate in order to understand how important barrier winds could potentially be for local oceanic processes. One important consideration is the large variability in the sea surface temperature (SST) in the region, the result of the close proximity of the cold, northerly sourced East Greenland Current and the warm, retroflected Irminger Current (Figure 1.6). Between these is a sharp temperature gradient of around 5 K as shown in the model sea surface temperature field (Figure 3.11). The difference in temperature across this boundary is important for understanding the fluxes of, particularly, sensible heat from the ocean. Another point worth noting at this stage is that in the wintertime, a large proportion of the southeast Greenland shelf region experiences partial ice cover. This will have the effect of capping the ocean, reducing the heat fluxes through the surface and also modifying the atmospheric moisture content as the air draws less water from the ocean. In this case study there was no ice present which simplifies the situation somewhat.

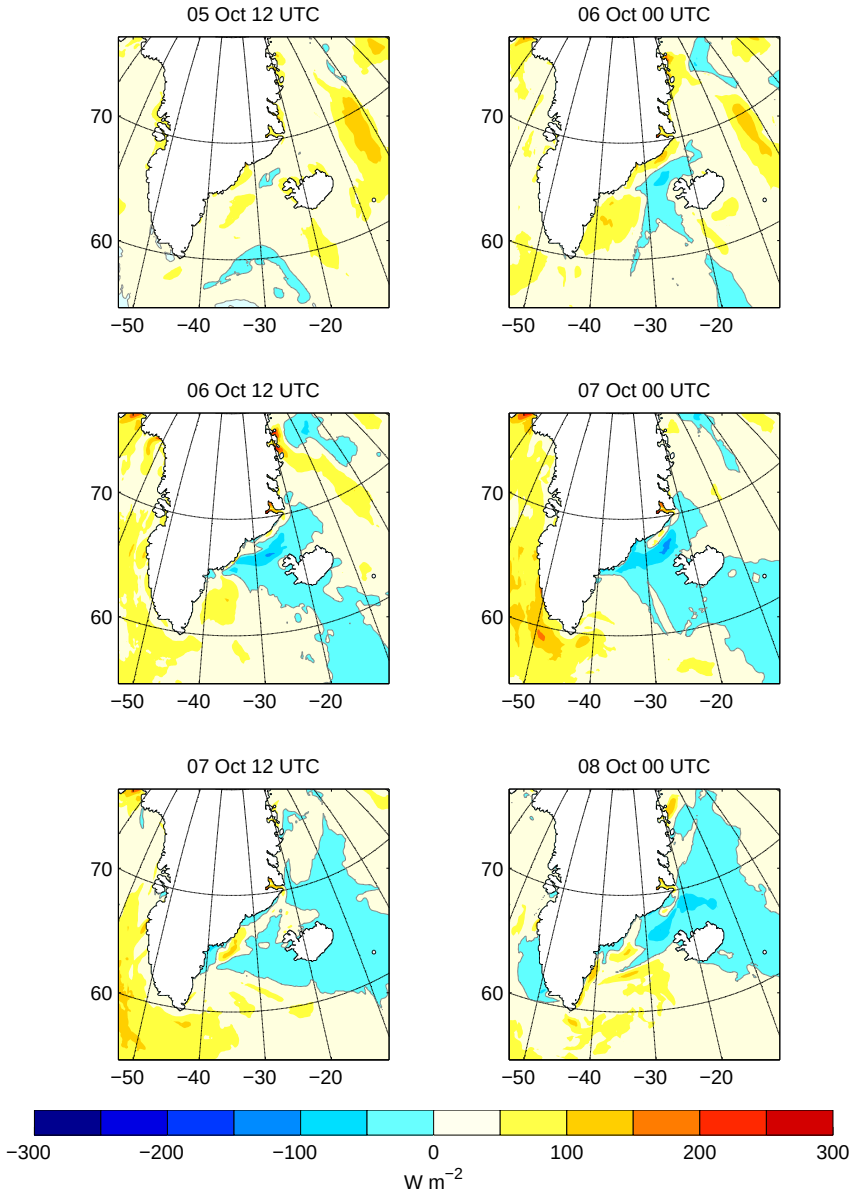

Figure 3.12: Surface sensible heat flux. Positive (red) heat fluxes indicate loss of heat from the ocean.

Looking at the sensible heat flux in Figure 3.12, it can be seen that at many times during the run negative heat fluxes (i.e. heat transfer from the atmosphere to the ocean) dominate in the region of barrier wind activity. This is due to the presence of the warm air advected up from the south. As shown in the observations and model data (Figure 3.2) temperatures at the surface ranged between 2 – 6 °C during this period at least where the Knorr was situated. This is warmer than the temperature of much of the sea surface in the region (Figure 3.11) and is the reason why the atmosphere is losing heat to the ocean. The magnitude of the strongest sensible heat fluxes into the ocean were over 100

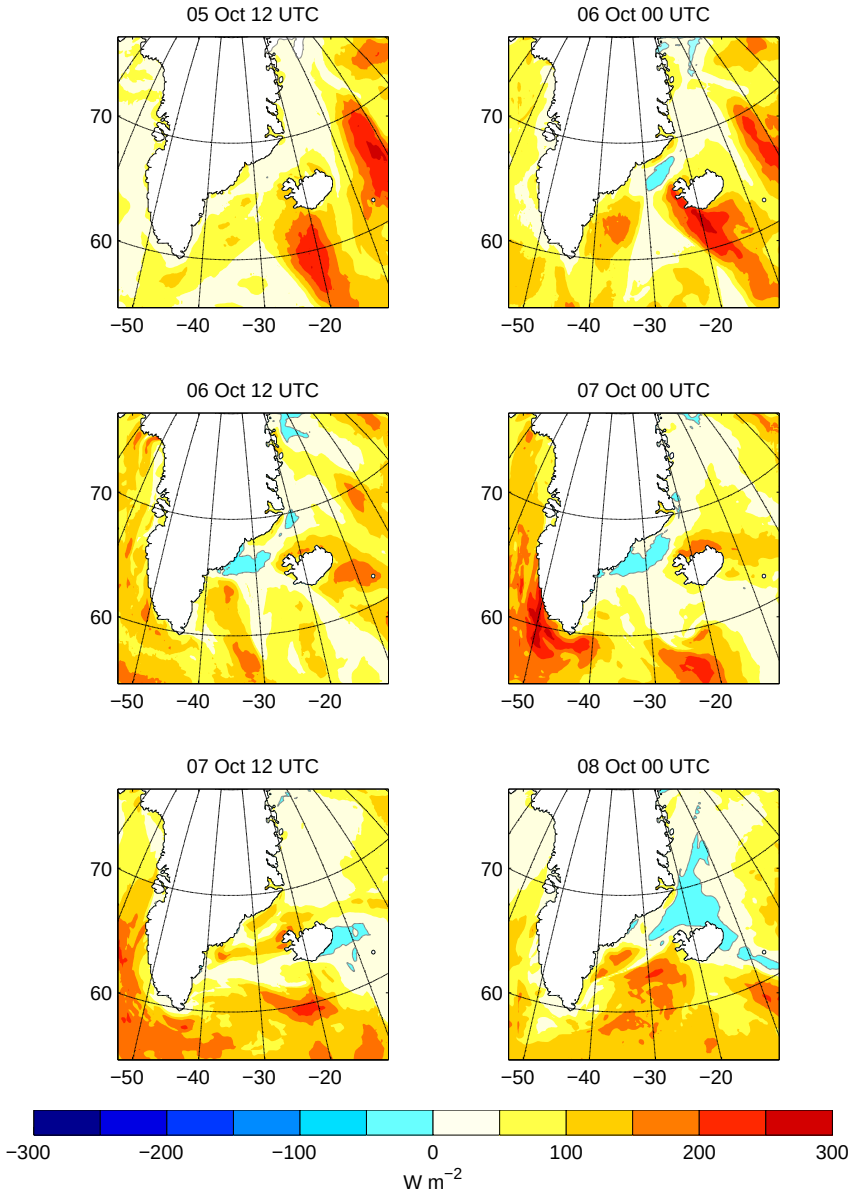

Figure 3.13: As Figure 3.12 but for surface latent heat flux.

W m^{-2}. There are also times and locations along the coast where heat fluxes out of the ocean of up to 100 W m^{-2} are found. These were typically small regions very close to the coast where the coldest winds were observed (Figure 3.6) or at the southwest extent of the barrier winds where the sea surface temperatures are higher.

Figure 3.13 shows the pattern of latent heat fluxes simulated by the model. Unlike the sensible heat fluxes, there is generally a positive flux from the ocean, due to evaporation. Up until 00 UTC on 7 October though, the regions of strong barrier wind activity show some of the smallest (and at times negative) heat fluxes. This is the result of the very moist air that can be found in these regions at this time (Figure 3.7). Once the barrier

wind has widened and extended further down the coast, the relative humidity of the air is slightly reduced and larger latent heat fluxes are seen in the vicinity of the strong winds.

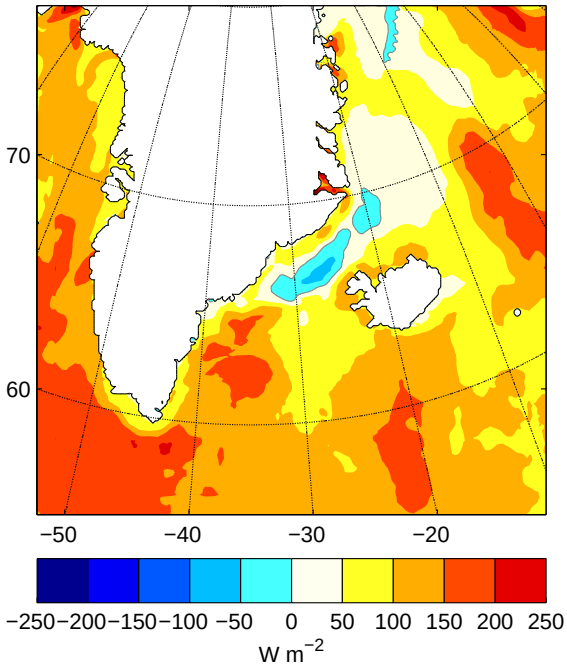

Figure 3.14: Mean of total turbulent heat fluxes over whole model run.

The mean of the combined sensible and latent heat fluxes over the length of the model run is shown in Figure 3.14. This shows a similar fragmented pattern to Figures 3.12 and 3.13. The general pattern is positive (i.e. out of the ocean) with regions of over 150 W m^{-2} scattered throughout the domain, notably, for this study of barrier winds, to the east of Cape Farewell. This is the result of colder, dryer air advected south through the barrier wind moving out over warmer waters to the east of Cape Farewell. A large region of negative heat flux (over 50 W m^{-2}) sits in the central Denmark Strait mostly due to the presence of the warm air advected north over the colder seas in this region.

The model surface stresses (not shown) follow a similar pattern to the 10 m wind field (Figure 3.5) with values of over 2 N m^{-2} found in the regions of strongest winds. Overall, the two regions which experienced the strongest winds (which were intersected by the sections BFN and BFS) exhibited surface stresses of on average over 1 N m^{-2} for the 72 hours of the run. This magnitude is comparable to that found by Petersen and Renfrew (2009) during the barrier wind events of PRM09 and indicates the large input of momentum from barrier winds to the ocean in this region.

It is clear then that, in this case, the barrier winds event has produced a spatially and temporally varying heat flux pattern containing regions of both positive and negative heat fluxes. In general, even the highest positive fluxes are modest in comparison with

other measurements from the region (Renfrew et al., 2002; Petersen and Renfrew, 2009; Våge et al., 2009), most likely because of the moist, warm air that dominates the synoptic environment in this case. This case study will now be compared with that of PRM09 in the context of the findings of the climatology of Chapter 2.

3.4.5 Classifying barrier wind events

There exist a number of similarities and some key differences between this case and the case studies of PRM09. Perhaps the most defining difference between the cases is the time of year they were observed. The barrier winds described in PRM09 were observed in early March when the Northern Hemisphere atmospheric conditions are typically cooler and sea ice can be found along much of the near coastal regions of east Greenland. The case presented here was observed in October when the region was mainly ice free. For ease of description (and to keep this important fact in mind) the case study presented here will be called the October case and those presented in PRM09 the March cases.

In both cases the location of the surface low is responsible for the location of initial barrier wind development. Importantly, there also exist for both cases two air masses - one advected from southerly regions which is warmer and moister and another colder source of air from the north. For the March cases the southerly sourced air ends up largely on top of the cold air advected in from the north whereas in the October case, the southerly advected air is more obviously abutting the colder from the south and can be represented as a front as in the Met Office analyses (Figure 3.1). In both cases though, the coldest air is to be found in the core of the barrier wind.

The March cases are typically wider and less coastally confined. They are also colder and drier – in general there are differences of about 5 – 10 K between the core barrier wind temperatures in the March and October cases. The broader cooler atmospheric conditions and the presence of sea ice may go some way to explaining the colder and drier air seen in the March cases, but the source region for the air is probably important too – Chapter 2 showed that even for the limited winter period of December to February, a climatological range of 15 K was observed along the southeast coast of Greenland. The colder, drier conditions seen in the March cases were responsible for much larger heat fluxes of between 200 and 500 $\mathrm{W\,m^{-2}}$ in the vicinity of the strongest winds (Renfrew et al., 2009b). The heat flux estimates were made along a line across Denmark Strait and it is unclear how these vary spatially further down the coast. It seems sensible, though, to suggest that these heat fluxes are likely to be much more representative of the heat fluxes throughout the entire region due to the significant difference between the air and sea temperatures all along the coast. This is in contrast to the October case where near surface temperatures

were very similar to sea surface temperatures – the result being modest turbulent heat fluxes.

The importance of the large range of near surface temperatures on heat fluxes was demonstrated in the climatology of Chapter 2. Warm and cold barrier winds were shown to develop in different synoptic environments. It appears, from the difference in the temperatures between the March and October cases, that we have two examples from the different ends of the temperature spectrum. The March cases could be said to be examples of 'cold' barrier winds and the October case a 'warm' barrier wind. As such, comparisons can be made with the composites of warm and cold barrier winds presented in Chapter 2 (Figure 2.18). The features of the warm barrier wind composite that are seen in the October case are the strong onshore winds, the more localised, weaker, barrier wind, and the presence of an anomalous high pressure to the northeast of the domain restricting northerly advection into the barrier wind. In contrast cold barrier winds are longer, stronger, less coastally confined and shows stronger northerly flow along the east coast of Greenland. All of these features are seen in the March cases. We have, on the face of it, case studies of warm and cold barrier winds.

The analysis conducted for the October case further shows that even during a single barrier wind event there is a large range in the temporal and spatial variability of the resulting heat fluxes. These scales are on the limit of ERA-Interim resolution ability. The small scale variability in heat fluxes seen suggests that to understand the surface effects of a barrier wind similar to that in the October case, a model or high resolution reanalysis product is required to fully resolve the spatial distribution of these fluxes. A single point measurement is unlikely to be sufficient to fully represent the effect of a barrier wind as the conditions may be radically different only tens of kilometres away. It also shows that although the warm and cold classifications made in the climatology are useful in describing the types of barrier winds that form, there is no guarantee that, for example, a warm barrier wind will remain 'warm' for the complete duration of strong winds or at all locations along the coast.

3.4.6 Barrier wind forcing

A question that was raised previously was whether the different temperature regimes (and differing synoptic forcings) of Chapter 2 would bring about barrier winds with different dynamics. One outcome of the discovery that the October and March cases are characteristic of warmer and colder barrier winds is that this can be partly investigated. It should be noted that these are just two cases and although there are remarkable similarities with the warm and cold cases of the climatology, there is no guarantee that they are representative

of all barrier winds that fall into these categories. Still, there is likely to be much that can be learnt from such analysis.

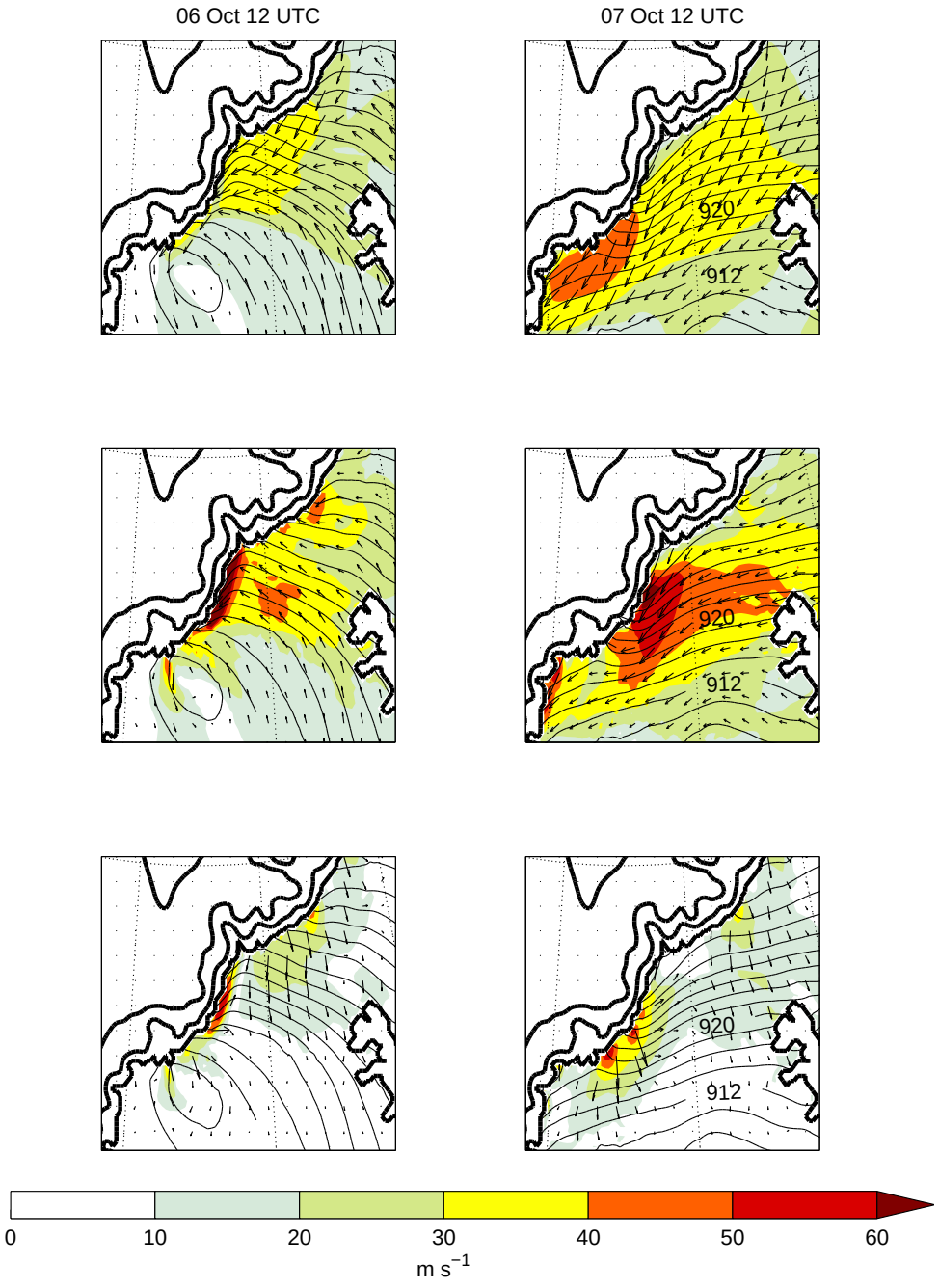

Figure 3.15: Force decomposition of wind field at model level 6 (610 m) for 12 UTC on 6 October 2008 (left) and 12 UTC on 7 October 2008 (right). Top panels: Total wind field. Middle panels: Geostrophic component. Bottom panel: Ageostrophic component (Total - Geostrophic). All panels have component wind vectors shown every 5 grid points and total model level pressure is contoured every 2 hPa.

Looking at the October case first, Figure 3.15 shows the geostrophic and ageostrophic

components of the flow field at the approximate height of the jet core (610 m) for representative times during the two stages of barrier wind development – 12 UTC on 6 October and 12 UTC on 7 October. The geostrophic wind was calculated from the model pressure and density field and the ageostrophic flow is the difference between the geostrophic and total wind fields. At both times it can be seen that the geostrophic wind alone is a poor representation of the total flow for this particular case. Both the magnitude and location of the jet core is misrepresented by the geostrophic wind and there are consequently significant ageostrophic winds at both times. There is a different distribution of geostrophic and ageostrophic winds for each stage of development suggesting different forcing mechanisms as alluded to previously. At both times, some of the ageostrophic component in the general flow can be explain by the fact that the model level in question is still in the boundary layer so experiences the effect of surface friction which will rotate the flow to the left, across the isobars. Evidence for this process can be seen in the relatively weak, cross-isobar, ageostrophic components at most locations that experience moderate total winds. There are many locations though, especially near the coastline, where the ageostrophic wind is of a comparable magnitude to the geostrophic wind. Surface frictional processes alone can't explain this.

The full horizontal momentum equation includes terms for the centrifugal force, advection, turbulent flux divergence and viscosity, not to mention the parametrised processes such as gravity wave drag. There is nothing in the calculation undertaken that distinguishes which of the components of the momentum equation is responsible for the large ageostrophic wind components observed. A complete decomposition of the force components for this flow is beyond the scope of this chapter and is left to further work, but what is clear is that this particular barrier wind is poorly represented by the geostrophic wind alone.

Figure 3.16 shows the same forcing decomposition for the 2 March 2007 case of PRM09. At this time, the location of the strongest winds in the jet core are in a comparable position to those throughout the October case simulations. In this case though, the flow field can be much better described by geostrophy with only small cross-isobar ageostrophic components consistent with the effect of friction on the boundary layer. There is by no means the magnitude of the ageostrophic terms seen in Figure 3.15. This March case is therefore much more representative of the simple orographic modification of the cyclone's near-coast isobars. The October case has a more complex flow pattern which potentially involves smaller scale interactions of strong onshore flow with the specific orographic configuration along the southeast coast of Greenland. Returning to the notion that the March (October) cases are characteristic of cold (warm) barrier winds, this analysis provides evidence that there could be significantly different dynamics associated

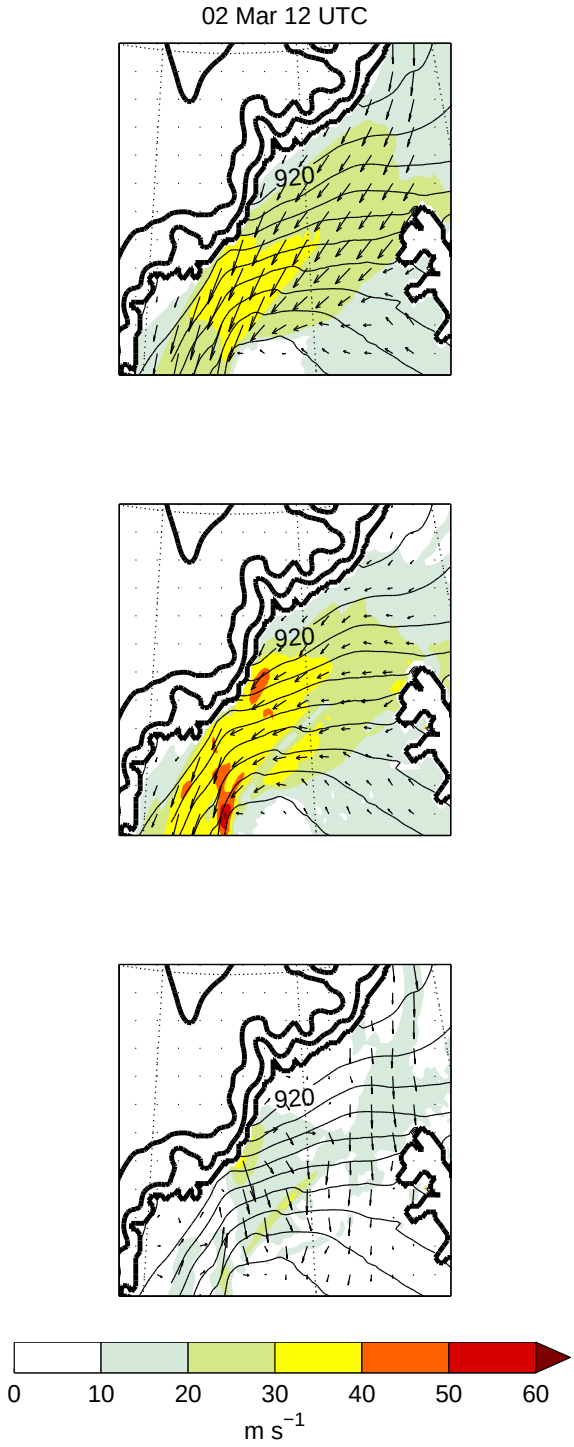

Figure 3.16: As Figure 3.15 but for the data from the UM simulations of Petersen et al. (2009) for 12 UTC on 2 March 2007 on model level 12 (620 m).

with these two classes of winds.

That said, it should be noted though that PRM09 showed that their barrier wind case on the 6 March 2007 (just 4 days after the case presented in Figure 3.16) experienced larger

ageostrophic components than the 2 March case even though this event would also be classed as a cold barrier wind. It appears that barrier wind properties and dynamics along the southeast coast are highly variable in space and time both within a single event and also between subsequent events. There are a plethora of potentially important factors in determining the configuration of any particular barrier winds including the 3D dynamics of the low impinging on the coast and the specific configuration Greenland's orography where it makes landfall, but a thorough investigation into this is beyond the scope of this chapter. Some insights will be made though through the idealised modelling of barrier winds in Chapter 4.

3.5 Conclusions

The first data from within an evolving barrier wind is presented and discussed in the context of high resolution numerical modelling of the event. The barrier wind in question occurred between 5 – 8 October 2008 and underwent two stages of development. Initially strongly onshore winds from a synoptic cyclone forced an intense, coastally banked barrier wind with warm temperatures in the core. The subsequent evolution of the cyclone leads to a second stage of development characterised by a wider and longer barrier with significantly reduced core temperatures. The spatial distribution and low-level properties of the barrier wind were therefore highly variable in time for the 3 days of strong wind activity. One result was a complex spatial and temporal pattern of surface heat fluxes along the southeast coast of Greenland, but in general these were modest in comparison to previous in situ measurements of much colder barrier winds (Petersen and Renfrew, 2009).

The barrier wind of this case study was warm and displayed many other features consistent with the warm barrier winds described in the climatology of Chapter 2, for example the strong onshore winds, the narrow barrier wind and the banking of the winds over the Greenland slope. In contrast, the barrier wind cases of Petersen et al. (2009) were described as being consistent with the cold barrier winds of Chapter 2 due to their much lower temperatures and their wider and longer extent. An examination of the geostrophic wind influence in each case showed that the Petersen et al. (2009) cold case was much better described by geostrophy whereas the warm case study of this chapter had much stronger ageostrophic components which were highly variable in space and time. It was suggested that the cold and warm barrier winds of Chapter 2 could involve different forcing mechanisms. Some more evidence for this will be discussed in the next chapter.

Chapter 4

Idealised modelling of barrier winds off southeast Greenland

4.1 Introduction

Barrier winds frequently form off the southeast coast of Greenland as a response to cyclones impinging on the coastline as has been demonstrated in this thesis and previous work (Moore and Renfrew, 2005; Petersen et al., 2009). The work presented in the preceding chapters of this thesis showed that there is a large spatial variability in the location of the strongest winds on a range of time scales. In Chapter 2, it was shown that there are two regions that experience the most frequent barrier winds over the course of 20 winter seasons (Figure 4.1). One location is to the north and the other to the south of the Denmark Strait. On shorter time scales, Chapter 3 showed a large amount of variability in the distribution of the strongest wind speed regions over the course of a single wind speed event. The force balance within simulated barrier winds was also far from geostrophic suggesting that a closer look at the formation mechanisms is required.

The two regions of enhanced barrier wind activity in Figure 4.1 (reproduced from the climatology) occur just offshore of the two major promontories along the southeast coast of Greenland. A geometrical argument therefore suggests that the precise shape of the southeast coast of Greenland may be a large factor in determining the regions of the strongest barrier wind activity. Moore and Renfrew (2005), in their paper on Greenland barrier winds, speculated that outflow from fjords may have a role to play, as might the presence of Iceland, although the latter's influence was deemed small by Petersen et al. (2009). Another potential factor could be the particular properties of the cyclones responsible for the barrier winds such as their locational preference and 3-D structure. For this study though, the hypothesis will be that the spatial distribution of barrier winds along the

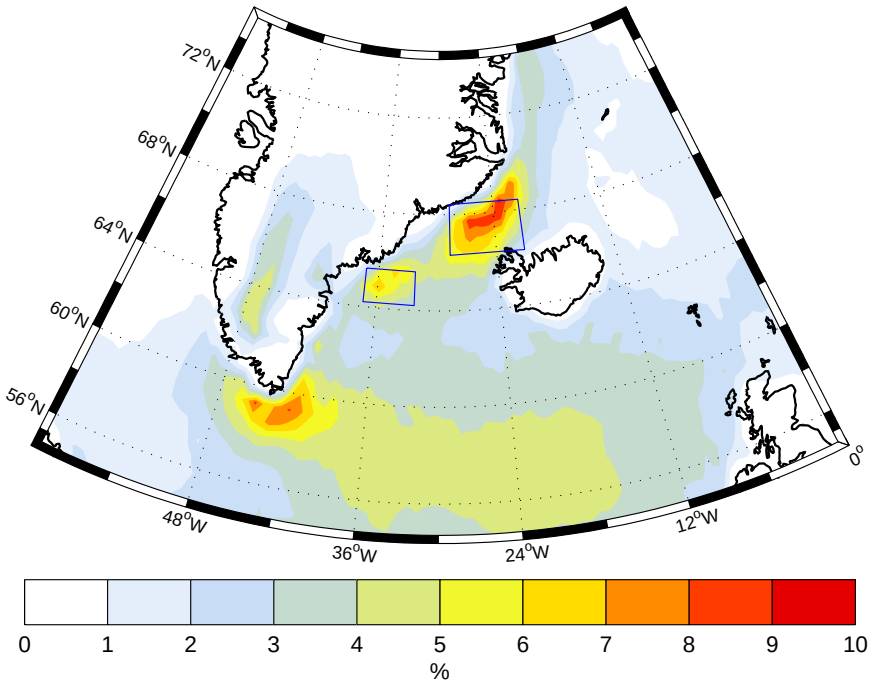

Figure 4.1: Percentage of time that the wind speed is in excess of 20 m s^{-1} at each location in the domain for ERA-Interim winter months (DJF) 1989-2008 (As Figure 2.6).

southeast coast is primarily dictated by the local orography. This will be tested through idealised numerical simulations of unidirectional flow towards an isolated mountain representative of Greenland.

In previous studies of idealised flow over isolated mountains [e.g. Smith (1989); Ólafsson and Bougeault (1996, 1997)] the character of the wind conditions over and around the orography was shown to be dictated by the value of the non-dimensional mountain height $\hat{h} = hN/U$ where h is the mountain height, N is the Brunt-Väisälä frequency and U is the upstream wind speed. Combinations of mountain waves, flow splitting (blocking) and wave breaking are seen for different values of $\hat{h}$ and mountain aspect ratio. Smith (1989) developed a diagram that related these two factors to the observed flow regime for non-rotational, non-frictional flow over idealised mountains, but it has since been shown that the flow behaves very differently with the effect of Earth's rotation. For example, geostrophic flows reduce the blocking potential of a mountain (Ólafsson and Bougeault, 1997) and generate an asymmetry in the flow over and around the mountain leading to eddy shedding and a deflection of much of the upwind flow to the left along the upwind slope of the mountain (Barstad and Grønås, 2005; Petersen et al., 2005). This latter feature is consistent with the flow in a barrier wind.

Of particular importance to this study is the numerical simulations of Petersen et al. (2005) who subjected an idealised mountain of comparable size to Greenland to winds

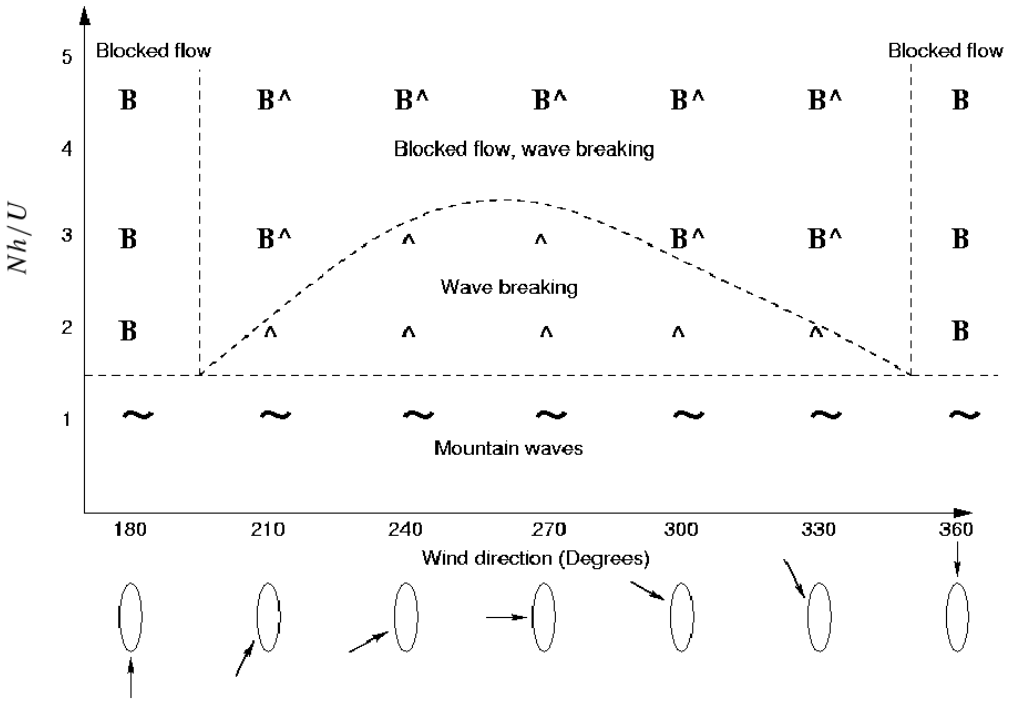

Figure 4.2: Regime diagram for rotational flow towards an idealised mountain from a range of incident angles taken from Petersen et al. (2005).

from a range of angles. Although the focus of their experiments were in the pressure drag and the downstream flow evolution, features consistent with barrier winds upstream of the mountain are seen in many of the simulations. A flow regime diagram was constructed from the experiments and is presented here in Figure 4.2. It shows that the degree of blocking experienced by the upstream flow is dependent on both the inflow angle and non-dimensional mountain height. It will be this regime diagram that will be very instructive in determining the parameters explored in the simulations of this study.

The aims of this chapter are therefore to extend the work of Petersen et al. (2005) by conducting idealised numerical simulations of flow towards an isolated mountain with orography representative of Greenland. In this way, the hypothesis that Greenland's orography is a primary driver in the spatial distribution of barrier winds can be tested. An analysis into potential mechanisms for barrier wind enhancement can also be examined.

4.2 Experimental Setup

The Met Office Unified Model (UM) version 7.5 was run in idealised mode for this study. This version employs a non-hydrostatic, fully compressible, deep atmosphere with a semi-Lagrangian treatment for advection of all prognostic variables except density which is

given a Eulerian treatment. The model is discritised with Arakawa C grid staggering in the horizontal and Charney-Philips grid staggering in the vertical. Time stepping is through a predictor-corrector, two-time-level, semi-implicit scheme. The model is fundamentally the same as that used in Chapter 3.

The model was set up in Cartesian coordinates on an f-plane (latitude 68°N, f = 1.35 x 10^{-4}) with a horizontal resolution of 48 km spaced over 100 x 100 grid points. Even though a higher resolution was computationally viable, it was deemed unnecessary due to appearance of the two distinct areas of enhanced winds speed under investigation in a lower resolution model (ERA-Interim, the 80 km resolution reanalysis product used in Chapter 2). A higher resolution model was attempted (12 km), but many small scale features such as fjord-scale jets were seen that could not explain the wind speed maxima seen in ERA-Interim due to this model's relatively coarse resolution. A model with 48 km resolution was therefore chosen in order to remove the complexity of resolving these superfluous small scale processes. There were 72 non-uniformly spaced, terrain-following sigma levels in the vertical. A time step of 60 seconds was used for all the experiments. The model was run with no moist processes. The lower boundary conditions were no flux and free slip, and a gravity wave damping scheme was employed at the upper boundary to limit reflections off the rigid ceiling.

The model domain is shown in the left panel of Figure 4.3 along with the isolated mountain representing the 48 km resolution orography of Greenland derived from GLOBE (Hastings et al., 1999) used in the experiments. The model was initialised everywhere (i.e. at all horizontal positions and heights) with a constant velocity in geostrophic balance with the pressure and temperature fields. The setup of this balance in the idealised UM required that the surface pressure was 1000 hPa at the southwest corner of the domain. This resulted in the large values of surface pressure (and the range between runs of different wind angle) seen in the vicinity of the barrier (e.g. Figure 4.5). There was an initial constant static stability throughout the domain and at all heights defined by a Brunt-Väisälä frequency. This initialisation also provided the lateral boundary conditions for the entire run – the mountain was deemed far enough from the boundaries for any discontinuities at the boundaries downstream of the mountain to not have a significant impact on the flow upstream of the barrier on the time scales that the model was run over.

4.3 Experimental design

It is hypothesised that the precise shape of Greenland's orography is the cause of the two locations of barrier wind preference. To test this hypothesis, two sets of experiments were run, one with the realistic Greenland orography and the other with modified orography.

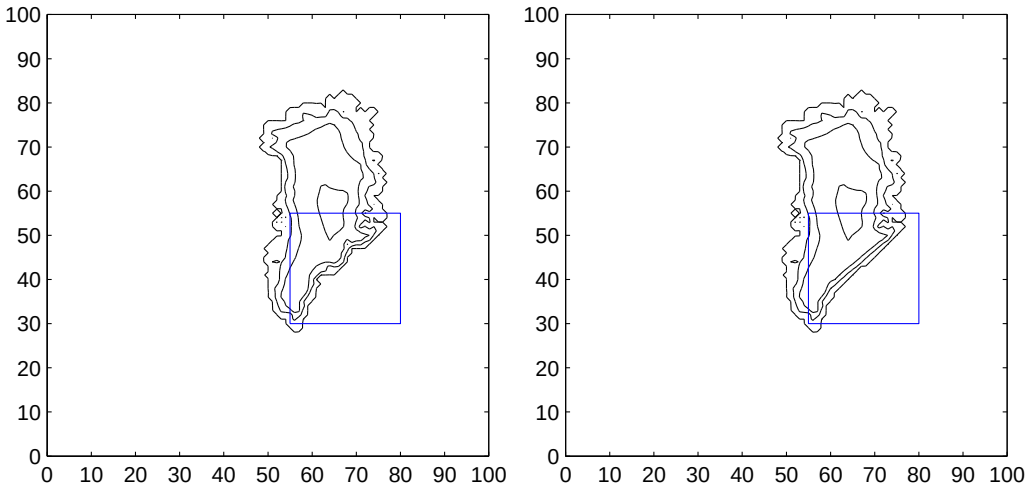

Figure 4.3: Domain and isolated mountains used for the idealised experiments with realistic (left) and modified (right) orography. Orography contoured every 1000 m. Blue box indicates the domain analysed in most of the figures in this chapter. Greenland has an approximate mountain height of 3000 m so for simplicity we use h = 3000 m in the expression for calculating the non-dimensional heights ($\hat{h}$) for all experiments.

In the experiments with modified orography, the lateral undulations in the topography of the southeast coast of Greenland were 'filled in' to present a more uniform coastline to the atmospheric flow (see Figure 4.3). A comparison of the results from corresponding runs with realistic and modified orography were then used to investigate the reason for the particular regions of barrier wind formation.

The flow regime presented for an idealised mountain in Petersen et al. (2005) (shown here in Figure 4.2) shows that the important factors for rotational flow over topography are the wind angle and non-dimensional mountain height, $\hat{h}$. A range of both were therefore investigated to probe the full parameter space. Experiments were conducted for wind incident wind angles between 45° (coast parallel) and 180° (beyond coast perpendicular) and $\hat{h}$ varied between 1.5 and 4.5. The range of $\hat{h}$ was achieved through a change in the Brunt-Väisälä frequency. It is hard though to determine ahead of time which regime a particular experiment will fit into from Figure 4.2 due to the idealised nature of the mountains in Petersen et al. (2005). It appears likely though that winds approaching the coast from shallower angles are likely to be blocked more easily for intermediate values of $\hat{h}$ and that upstream flow will be blocked independent of wind incidence angle for $\hat{h} > 4$.

In all experiments, the model was run for 72 hours. An approximately steady state upstream of the mountain was reached by 48 hours. Many experiments exhibited eddy shedding in the lee of Greenland, but these non-steady state features downstream of the mountain did not have a significant impact on the flow upstream. For each experiment, an average of the final 24 hours of the model run was analysed.

4.4 Results

Results will be presented from two sets of experiments of different non-dimensional mountain height which together demonstrate the key flow features seen throughout all the experiments. Firstly, experiments with a Brunt-Väisälä frequency of 0.01 s^{-1}, a wind speed of 10 m s^{-1} and incident wind angles of 75°, 105° and 135° are discussed. These experiments have a $\hat{h}$ of approximately 3 and the angles ranging between nearly coast parallel (75°) and coast perpendicular (135°). Secondly, experiments with the same incident wind speed and angles but a larger $\hat{h}$ (achieved through an increase in Brunt-Väisälä frequency to 0.015 s^{-1}) will be discussed. Figure 4.4 shows a boxplot of the Brunt-Väisälä frequency averaged over the bottom 7000 m of the atmosphere for all 52 radiosondes launched from the R/V Knorr near the southeast coast of Greenland in October 2008 (See Section 3.3 for more details). The soundings have values ranging from 0.01 s^{-1} to 0.015 s^{-1} demonstrating that the range of Brunt-Väisälä frequencies discussed in this chapter is representative of the range of values seen in real-world conditions off Greenland. As stated previously, experiments were also conducted for other wind angles and a wider range of non-dimensional mountain heights, but only experiments itemised in Table 4.1 will be explicitly discussed as they cover the range of real world values adequately and exhibit all the key features of the flows seen in the other experiments.

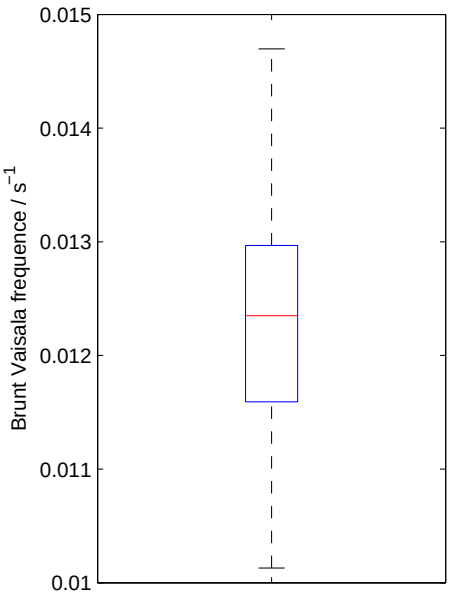

Figure 4.4: Boxplot of Brunt-Väisälä frequency (averaged over the bottom 7000 m of the atmosphere) for the 52 radiosondes launched from R/V Knorr throughout the month of October 2008. All soundings are from the Denmark Strait region under both calm and barrier wind conditions. Red line is the median, blue box covers 1st to 3rd quartile and dashed lines extend to cover the total range of the dataset.

Experiment name	Non-dimensional mountain height ($\hat{h}$)	Brunt Vaisala frequency / s^{-1}	Orography	Wind direction / °
r075h30	3	0.010	Realistic	75
r105h30	3	0.010	Realistic	105
r135h30	3	0.010	Realistic	135
m075h30	3	0.010	Modified	75
m105h30	3	0.010	Modified	105
m135h30	3	0.010	Modified	135
r075h45	4.5	0.015	Realistic	75
r105h45	4.5	0.015	Realistic	105
r135h45	4.5	0.015	Realistic	135
m075h45	4.5	0.015	Modified	75
m105h45	4.5	0.015	Modified	105
m135h45	4.5	0.015	Modified	135

Table 4.1: Table itemising upstream parameters for all idealised experiments discussed in the text. All experiments initialised with a wind speed of 10 m s^{-1} at all heights. The experiment name identifies the key properties of the experiment i.e. whether it has realistic or modified orography, the wind direction and approximate non-dimensional mountain height.

4.4.1 Small non-dimensional mountain height, $\hat{h} = 3$

General features

The lowest model level wind fields for experiments with realistic and modified orography and a range of wind angles are shown in Figure 4.5 (The first six experiments in Table 4.1). The three wind angles were chosen as they were representative of the processes observed – intermediate angles in general have flow fields intermediate between the results presented. What can be seen is that in all experiments, the mountain influences the flow upstream of the mountain and creates a coast-parallel jet reminiscent of a barrier wind. Cross mountain sections through the jet (shown for the modified experiments in the left hand panels of Figure 4.6) show that the jets are banked up on the Greenland slope and often strongest below mountain height providing further evidence that the model is simulating something comparable to a barrier flow upstream of the mountain. As with the idealised barrier wind experiments of Olson and Colle (2009), the jet width increases as the angle of incidence is reduced in experiments with both real and modified orography, as does the magnitude until the angle becomes very shallow.

In all the experiments with realistic orography, two locations of increased wind strength

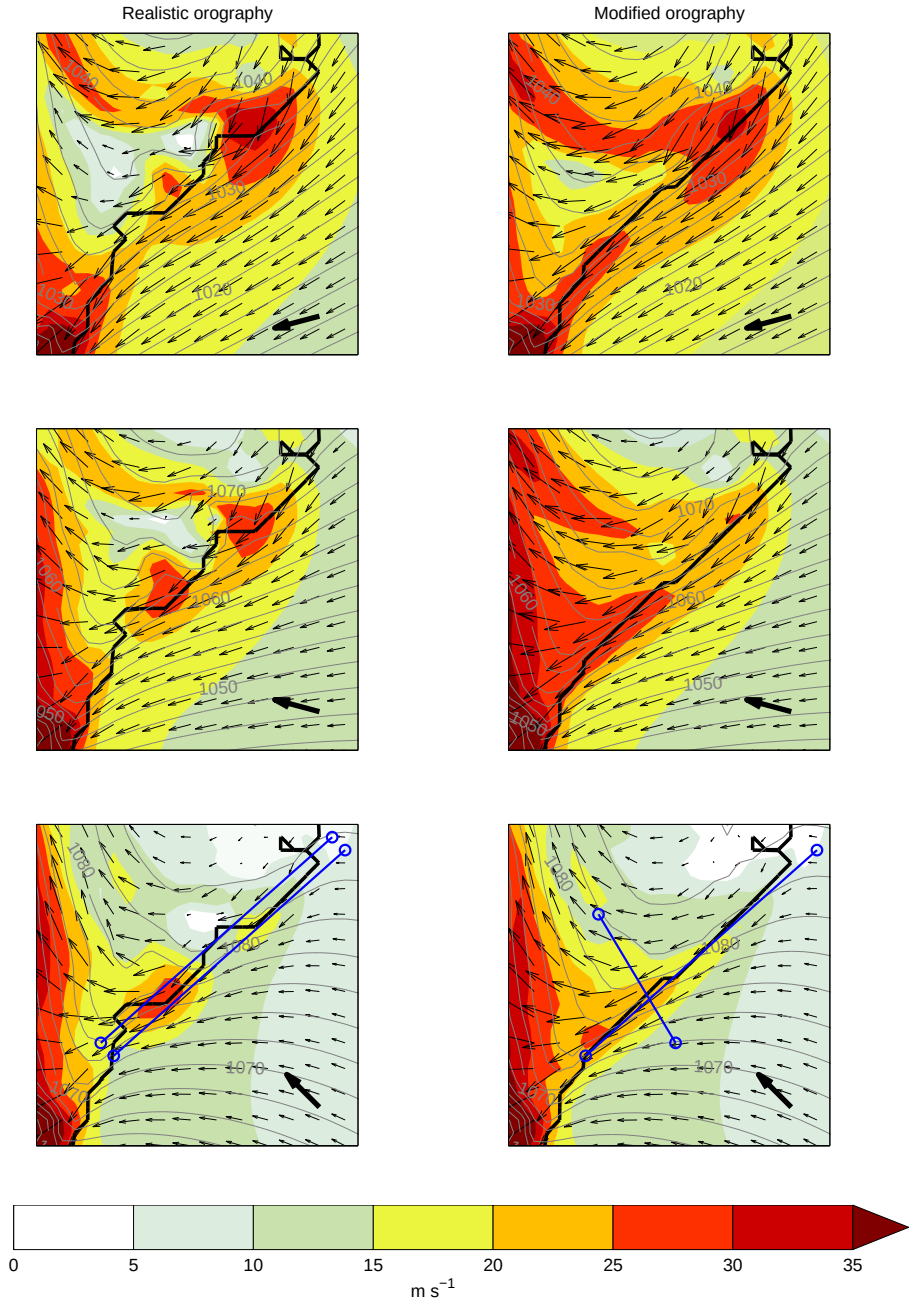

Figure 4.5: Lowest model level wind speed (colours) and mean sea level pressure (grey contours) for experiments with a Brunt-Väisälä frequency of 0.01 s^{-1} with realistic (left) and modified (right) orography. The inflow angles are shown with solid arrows and are (from top to bottom) 75°, 105° and 135°. The lowest level wind vectors are shown every second grid point. Coastline shown in solid black. The location of the reduced domain is shown in Figure 4.3. The blue cross section lines are for Figures 4.6, 4.8 and 4.9.

are apparent along the southeast coast. In addition, there exists an omnipresent wind speed maximum at the southwest extreme of the domain in all experiments which is the signal from a strong easterly tip jet (Moore and Renfrew, 2005; Renfrew et al., 2009b; Outten

et al., 2009) formed as the flow reaches the end of the barrier. This feature won't be discussed further in this chapter. The locations of the two wind speed maxima in all realistic experiments are in generally good agreement with the locations as described in Moore and Renfrew (2005) and in Chapter 2. The relative strength of the two maxima changes with the angle of wind incidence – the more northerly location dominates for more northerly (i.e. more acute) flows. In all cases both maxima occur just downstream of the two major promontories along the southeast coast.

In contrast, the results from the experiments with the modified orography show that the twin maxima disappear without these along-coast orographic variations. This finding is evidence that the undulations in the orography along the coast of Greenland appear to be the primary factor in promoting the existence of the two locations of enhanced winds observed in previous studies. This is in agreement with the original hypothesis of this chapter. Furthermore, the locations of enhanced winds appear here during a single onshore 'wind event' and therefore aren't the result of a statistical compilation of many wind events as could have been the case for the high wind frequency analysis of Moore and Renfrew (2005) and Chapter 2.

These results can also provide some insight into why these regions of enhanced wind occur under these particular flow conditions. The easiest place to start this investigation is through the experiments with modified orography – the simpler configuration. The idealised barrier winds simulated in the modified runs (right panels of Figure 4.5) have similarities with other studies of rotational flow upstream of a mountain (Ólafsson and Bougeault, 1997; Petersen et al., 2003, 2005; Barstad and Grønås, 2005). In all cases, a 'left-sided jet' is established along the southeast coast, the velocity of which increases with fetch down the barrier for all but the shallowest angle of incidence. This type of feature can be explained through the adjustment of the upstream geostrophic flow to the presence of the mountain. The decelerating affect of the obstacle reduces the Coriolis force and accelerates the flow to the left (in the Northern Hemisphere) down the pressure gradient as outlined in Barstad and Grønås (2005). The Coriolis force subsequently increases as the flow accelerates. For air that isn't 'blocked' by the mountain, the increased Coriolis force rotates the flow back towards the mountain and the air traverses and scales the barrier. For flow that is blocked below mountain height a force balance will develop along the coast and the flow will be channelled coast parallel.

There is evidence that a not insignificant amount of the flow is escaping up over the barrier in the modified experiments with $\hat{h} = 3$ especially at the downwind end of the barrier where the mountain height is lower. Evidence of this comes from the left hand panels of Figure 4.6 which are coast perpendicular cross sections through the jet core of the modified experiments with $\hat{h} = 3$. They show in all cases that the low-level horizontal

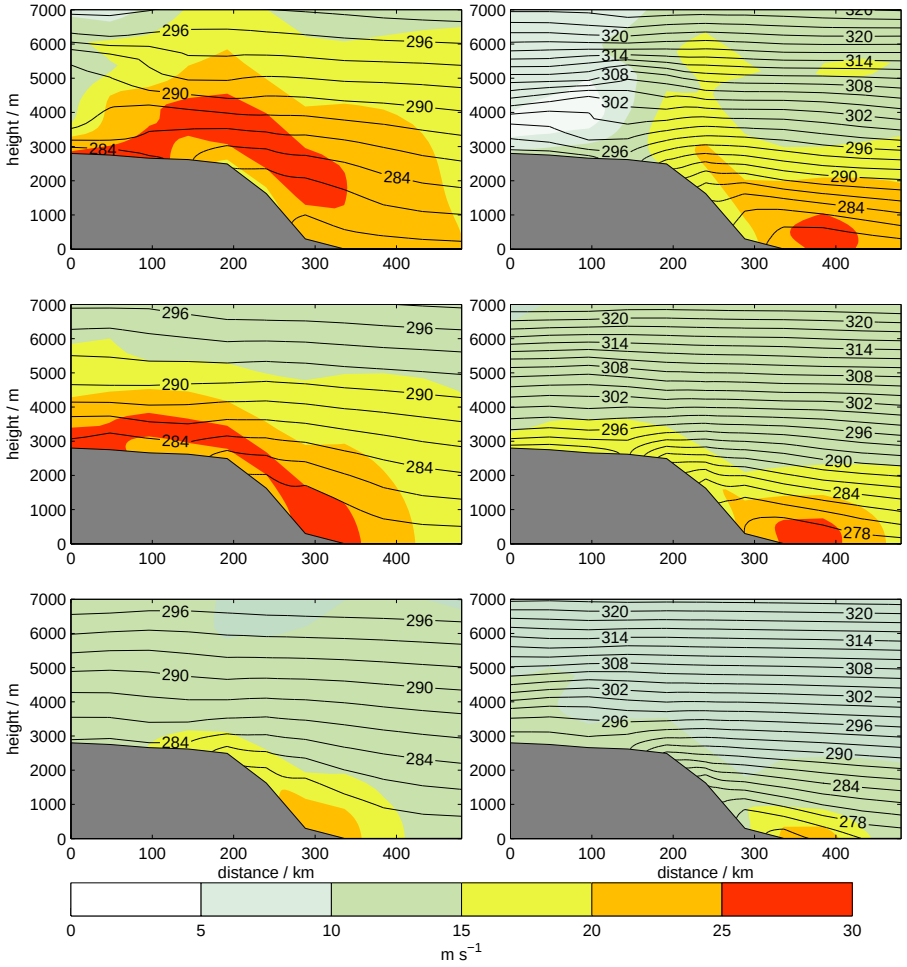

Figure 4.6: Cross sections of wind speed (colours) and potential temperature (contours) for experiments with modified orography and Brunt-Väisälä frequencies [non-dimensional mountain height] of 0.01 s^{-1} [3] (left) and 0.015 s^{-1} [4.5] (right). Flow angles (from top to bottom) 75°, 105° and 135 °. Cross section line is shown in the bottom right panel of Figure 4.5.

flow is banked up along the slope. Over these parts of the slope there are large low-level vertical velocities which increase in magnitude downstream, best exemplified by experiment m135h30 (Figure 4.7). Figure 4.7 also shows that the potential temperature along the slope and plateau show values comparable to upstream surface values, indicative of much upward advection of surface air on to the mountain top (Figure 4.7). These features are most clearly seen in experiment m135h30, but are also apparent in the other experiments with realistic and modified orography although there are complicating dynamics in many experiments that will be discussed shortly. The experiments with these flow conditions though clearly show flow distortion upstream of the mountain consistent with barrier wind formation with only weak flow blocking. This is consistent with the idealised flow regime of Petersen et al. (2005) (Figure 4.2) which states that for $\hat{h} = 3$ there is marginal

flow blocking with some angle dependence.

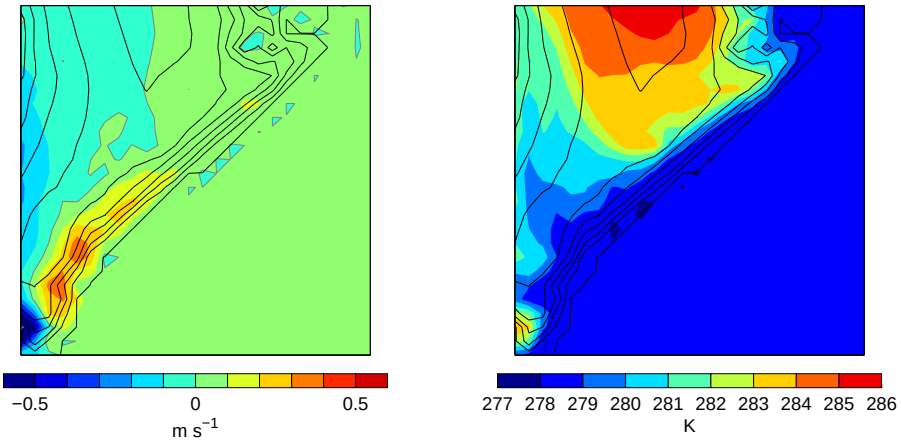

Figure 4.7: Lowest model level vertical velocity (left) and lowest model level potential temperature (right) for experiment m135h30. Orography (contours) shown every 500 m.

With these ideas in mind, a comparison of the results from the realistic orography experiments with the corresponding experiments with modified orography sheds light on the reasons for the appearance of the velocity maxima along the coast under these upstream conditions. Two main mechanisms for wind speed enhancement have been identified. These are flow entering an easterly-tip-jet regime and downslope winds associated with mountain waves. Both of these are evident to a greater or lesser degree in all experiments and will be discussed in turn.

Tip jet regime

Easterly tip jets (Moore and Renfrew, 2005; Renfrew et al., 2009a) form off the southern tip of Greenland and extend westward out into the Labrador Sea. They form when an upstream coast-parallel flow reaches the end of the barrier. At this location, the along stream pressure rapidly reduces and the flow accelerates down the pressure gradient. The increase in the Coriolis force and the collapse of the barrier perpendicular pressure gradient rotates the flow to the right until the flow readjusts to geostrophic balance on the far side of the jet (Outten et al., 2009, 2010). It is proposed that a similar flow configuration is seen at the two promontories along the southeast Greenland coast.

This easterly tip jet regime explanation is best exemplified by the experiment pair r135h30 and m135h30 (see bottom panels of Figure 4.5) through cross sections of the mean sea level pressure and the lowest model level wind speeds (Figure 4.8). The cross section from the modified experiment shows an approximately linear reduction in pressure moving southwestward along the barrier and a corresponding increase in wind speed as the air flows down the pressure gradient. In the experiment with real orography the

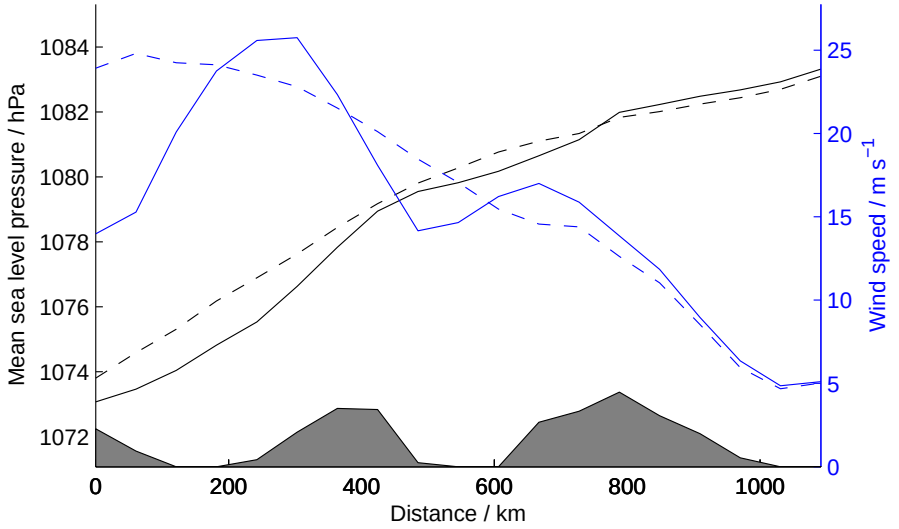

Figure 4.8: Cross section of mean sea level pressure (black) and lowest model level wind speed (blue) through the jet cores (offshore, along-coast line shown in bottom panels of Figure 4.5) of experiments r135h30 (solid) and m135h30 (dashed). The right side of the figure is to the northeast end of the cross section. Also shown is the inshore cross section of the southeast Greenland orography (no scale) to give a sense of the shape of the orography. The left of the figure is the southern end of the cross section.

general pattern is similar but superimposed on this are the undulations in pressure and wind speed that show up as the regions of enhanced wind in Figure 4.5. The two regions of enhanced winds in r135h30 occur just downwind of the promontories in the orography in conjunction with a rapid drop in the pressure. This is very similar to what occurs for the flow into the easterly tip jet at Cape Farewell (Outten et al., 2009, 2010). The pressure is reduced downstream of the promontory due to the inward undulation of the barrier and the flow consequently accelerates down this steeper-than-usual pressure gradient and a tip jet is formed. The flow in this jet will rotate to the right as the Coriolis force dominates the cross stream force balance in the accelerated jet. Evidence of this rotation can be seen in the flow field of Figure 4.5. This tip-jet-like flow can also be seen in the other experiments with reduced inflow angles although another feature becomes apparent which complicates the situation – downslope winds triggered by mountain waves.

Mountain waves

Mountain waves can be triggered when stable flow is forced over relatively steep topography (Smith, 1989; Doyle et al., 2005). They manifest themselves as static, upward propagating gravity waves in the free atmosphere and the resulting low-level flow on the lee side of the mountain is strongly downslope (Durran, 1990). These flows are often typified by relatively high temperatures due to the downward advection of upper-level air.

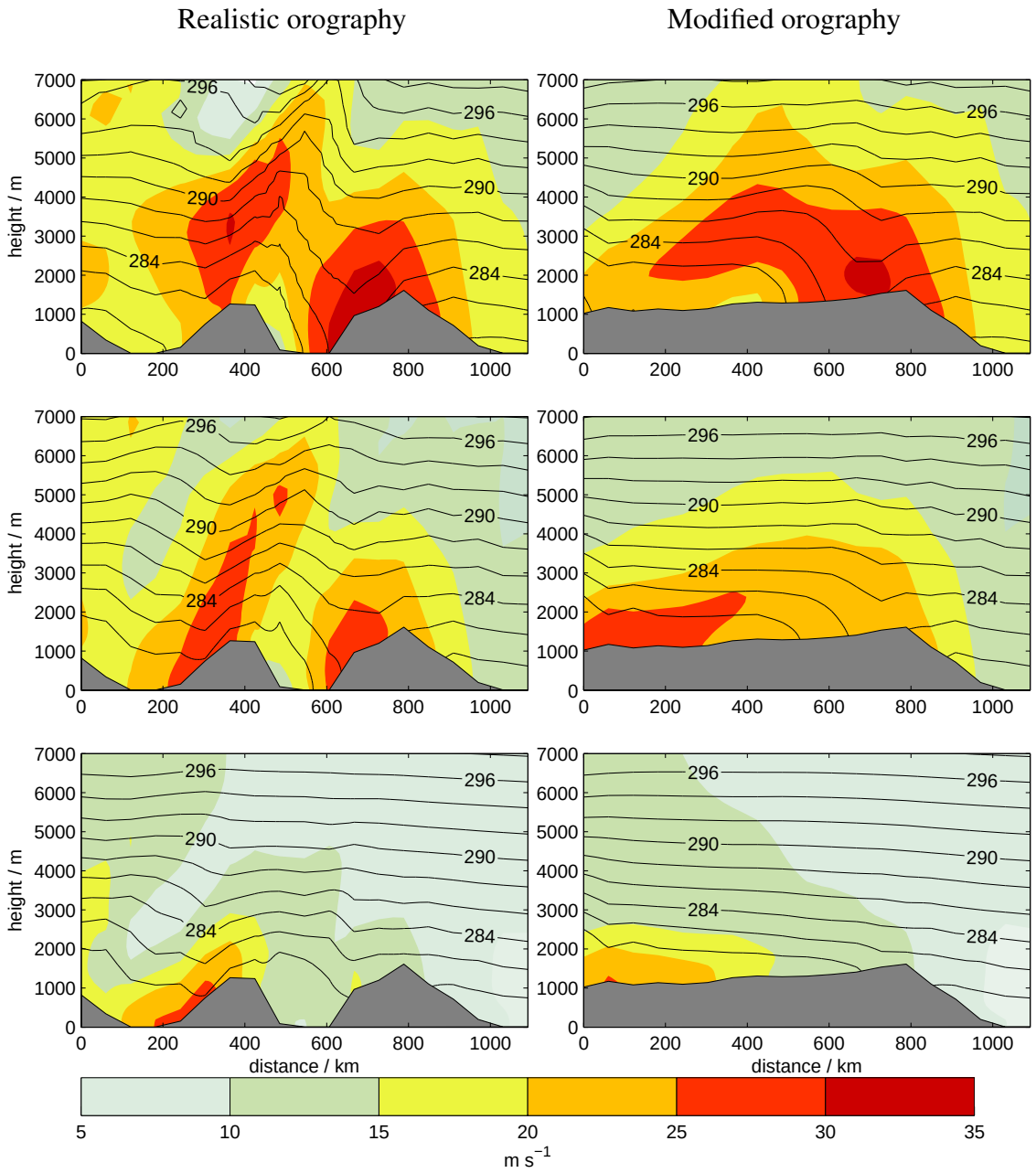

Figure 4.9: Cross section of horizontal wind speed (colours) and potential temperature (contours) taken through a line along the southeast coast of Greenland for the experiments with realistic (left) and modified (right) orography and an approximate non-dimensional mountain height of 3. Three inflow angles are shown – From top to bottom: 75°, 105° and 135 °. The cross section line is shown in the bottom left panel of Figure 4.5 by the inshore of the two along coast lines.

The large-scale impact of the mountain on upstream flow near mountain height will be to rotate it to the left (Ólafsson and Bougeault, 1997). The implication of this is an increased coast parallel component of the flow near mountain height along the southeast coast of Greenland. This is especially true for shallower synoptic wind angles for which

this adjustment requires less rotation. This is seen in plots of the mean flow direction above mountain height (not shown). From the perspective of coast parallel flow, the promontories along the southeast coast form a series of mountains as can be seen in Figure 4.9 which shows a cross section of the potential temperature and horizontal wind velocity along a line through these mountains for all experiments with $\hat{h} = 3$. All experiments with realistic orography exhibit mountain wave behaviour to some degree as seen by the coherent vertical undulations in the isentropes. The realistic experiments with shallow approach angles show the strongest mountain waves due to a more coast parallel flow at mountain height – for experiment r135h30, the mountain waves are only triggered over the middle mountain. The mountain waves in the experiments with realistic orography manifest themselves in the low-level flow as strong downslope winds in the lee of the promontories. These flow offshore and contribute to the low-level bullets of enhanced wind seen in the near surface wind field (Figure 4.5) especially for the shallower wind angles.

There is also evidence for mountain waves and downslope flow in the experiments with modified orography. This is seen most strongly in the run with the shallowest wind angle and occurs over the east corner of the mountain, where Scoresbysund would be found. The approaching flow at mountain height has been rotated to have a strong northerly component which sees the eastern corner of Greenland as an isolated mountain. It is the mountain waves and consequent downslope winds produced here that are responsible for the enhanced winds in this location for the modified experiments. No gravity wave activity is seen over the central mountain which has been removed for the modified experiments.

With this set of experiments it is not possible to isolate the gravity wave and tip-jet mechanisms. Indeed it is possible that there is a degree of interaction between the processes. For example, the reduction in pressure in the lee of the promontories produced by the mountain-wave-induced downward advection of higher potential temperature air is in the ideal location to enhance the pressure deficit the coastal winds feel when they pass the end of the promontories. This could result in a larger degree of acceleration for the tip-jet-like mechanism.

4.4.2 Large non-dimensional mountain height, $\hat{h} = 4.5$

For experiments with a Brunt-Väisälä frequency of 0.015 s^{-1}, the approximate non-dimensional mountain height is 4.5. This is large enough, in theory, to induce strong flow blocking regardless of incident wind direction (Petersen et al., 2005). The low-level wind field (Figure 4.10) from both realistic and modified experiments shows that the flow

is indeed significantly blocked by the mountain. The jet maxima are no longer banked against the slope and the vertical velocities (not show) are negligible on the slope in the lower layers too. A cross section through the jet is particularly instructive in the difference between the regimes (right hand panels of Figure 4.6). The wind jet is still surface intensified but has a smaller vertical extent and a core centred offshore.

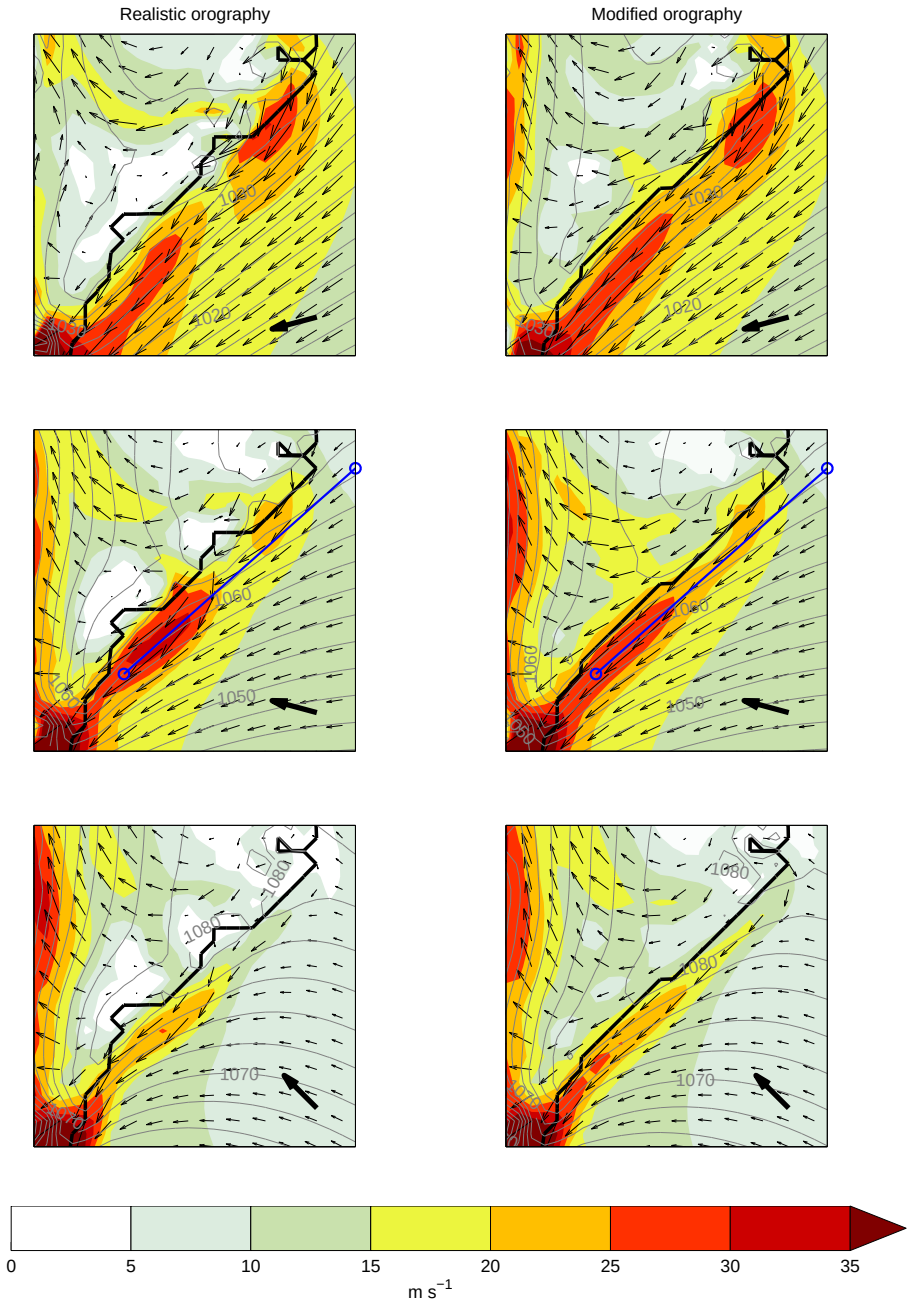

Figure 4.10: As Figure 4.5, but for the experiments with a Brunt-Väisälä frequency of 0.015 s^{-1} and a corresponding non-dimensional mountain height of 4.5. Blue cross section lines are for Figure 4.11.

The result of the blocking is that many of the features seen for the barrier flow experiments under weaker blocking conditions are less apparent. The existence of the twin maxima in the realistic experiments are less well defined especially in experiment r135h45 although they are still readily apparent in r105h45. Gravity waves have a smaller influence on the low level flow field along the coast especially at the southerly wind speed maximum location. They are generally weak or not apparent in similar cross sections to those shown in Figure 4.9. There is still evidence of their presence over the eastern corner of Greenland although the jet maxima at this location in experiments r075h45 and m075h45 have only a small downslope components and can be mostly considered classic corner jets (Barstad and Grønås, 2005).

Figure 4.11 shows a cross section of the mean sea level pressure and lowest model level wind speed through the jet core of experiments m105h45 and r105h45. The increase in wind speed in conjunction with a reduction in pressure in the realistic experiment shows that the tip-jet-like mechanism can still be seen to have some influence. In general though, the realistic and modified experiments differ by a much smaller amount than the previous experiments. It appears that the effect of blocking is therefore to reduce how much the flow is influenced by the variations in the coastline to some extent.

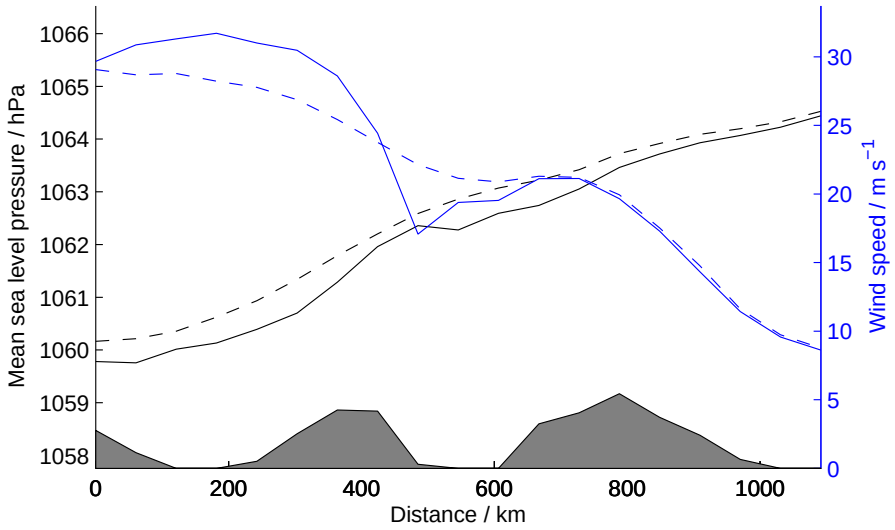

Figure 4.11: As Figure 4.8 but for the experiments with a Brunt-Väisälä frequency of 0.015 s^{-1} and inflow angle of 105°. (r105h45 and m105h45). A slightly different cross section is used to ensure this analysis is for the jet core – see Figure 4.10 for the precise position.

The strongly blocked barrier winds also appear to source their air from more northerly locations than the weakly blocked winds. This can be seen in a comparison of back trajectories from experiments r105h30 and r105h45 shown in Figure 4.12. The air entering the more weakly blocked experiment gradually approaches the barrier from offshore to

the east of the domain. In contrast, the air that enters the strongly blocked barrier winds comes from further to the north and has been channelled coast parallel down most of the southeast coast. This is because the air at this level is blocked and can't escape over the mountain as it can for the case with weaker blocking. The effect of blocking therefore goes beyond just the dynamics and shape of the barrier winds to influence the source region of the barrier wind air. These results are robust for all the other experiments with realistic or modified orography over the range of wind angles investigated. Experiments r105h30 and r105h45 were chosen for presentation because, in addition to showing the difference in source region, the trajectories of r105h45 best show the undulations associated with the two regions of tip-jet-like dynamics and reinforces the importance of this mechanism in enhancing the wind speed near to the coastal promontories.

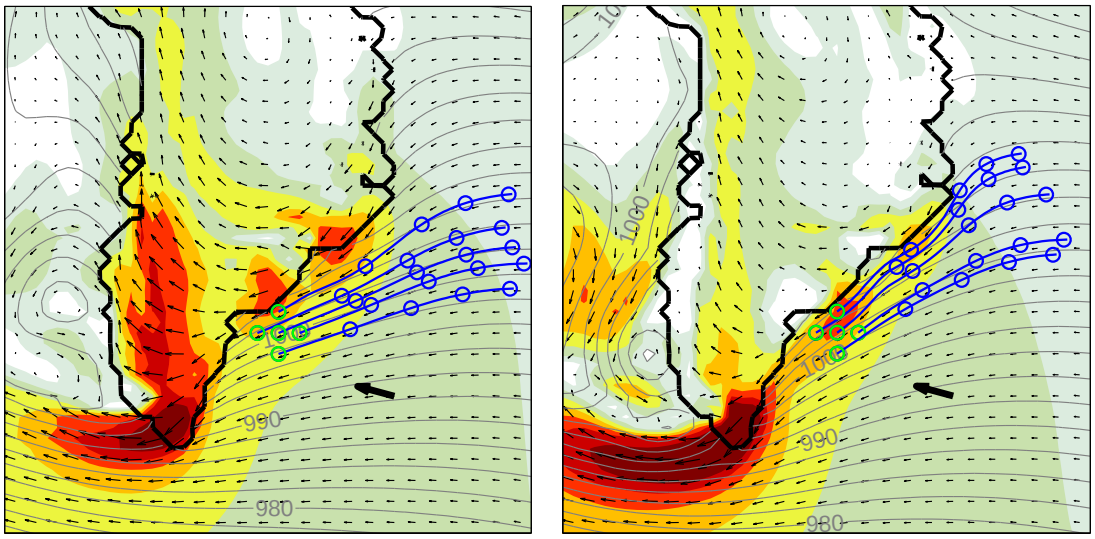

Figure 4.12: 24 hour back trajectories (blue lines) from locations on the 10th model level ($\sim$ 500 m) shown by green circles for experiments r105h30 (left) and r10545 (right). Blue circles shown for the positions of the trajectories every 6 hours. Plotted underneath is the 10th model level wind speed (colours) and pressure (grey contours, only shown over the 'sea'). The colour scale for the wind speed is the same as Figures 4.5 and 4.10. The 10th model level wind vectors are shown every 2nd grid point. The coastline is shown in thick black and the thick arrow indicates the wind incidence angle, in these cases 105°.

4.5 Conclusions and discussion

The aim of the work presented here has been to understand the reasons for their being two locations of enhanced barrier wind activity along the southeast coast of Greenland as seen in (Moore and Renfrew, 2005) and Chapter 2. Through idealised modelling, the two regions of enhanced winds have been reproduced and two mechanisms for their

existence have been determined. Firstly, low-level flow passing along the southeast coast is accelerated due to the reduction in pressure downstream of the tips of the two major promontories. This is similar to the dynamics involved in the production of easterly tip jets at Cape Farewell (Outten et al., 2009, 2010). Secondly, barrier parallel flow at mountain height is capable of triggering mountain waves and strong downslope winds in the lee of the promontories along the southeast coast, enhancing the low-level coastal winds. These mechanisms were seen most strongly in experiments with moderate static stability that only allowed for weak upstream blocking of the flow. For experiments with higher upstream static stability a large amount of blocking was observed. The flow in this regime felt the effect of the coastal undulations more weakly and evidence of the two mechanisms described previously was harder to find, especially the gravity wave mechanism. The result was a reduction in the difference between the realistic and modified experiments. The additional impact of blocking was in facilitating the inflow of more air from the north.

It is clear then that the southerly location of wind enhancement in particular requires the specific undulations in the southeast coast in order to facilitate its existence through the tip jet and mountain wave mechanisms. The northerly location though becomes apparent even for experiments with modified topography and any static stability for narrow inflow angles due to the corner in orography presented to the atmosphere at this location (equating to the location of Cape Tobin in reality). This corner is capable of producing downslope winds and corner-jet-like features in all experiments. It could be that the robustness of this feature in most experiments is the reason why it is the location which experiences the most frequent strong winds along the southeast coast in reality (Figure 4.1)

There are clearly limitations to the modelling study presented that restrict like-for-like comparisons with 'real world' barrier winds. The effect of surface friction and heat fluxes has been negated, as has the consequent production of a planetary boundary layer. The 3-D structure of mid-latitude cyclones is likely to also be important in the specific location and mechanisms for barrier wind formation as compared to the uniform flows blown at the barrier here. The study though does present some ideas for mechanisms that could be important for real barrier winds and any future investigation into them. It also provides some insights into the work already presented in Chapters 2 and 3 which will now be discussed.

The difference source regions between the blocked and unblocked cases suggests a comparison with the warm and cold barrier winds presented in the climatology of Chapter 2. The unblocked flow experiments have much in common with the warmer barrier winds; they are more coastally banked and source their air from just offshore of the barrier. The blocked barrier winds are wider over the ocean and the blocking has allowed them to draw

air in to the region from the north of the domain, consistent with the cold barrier winds. This has potential implications for other factors beyond those presented in the climatology that may influence the conditions in a real barrier wind, namely the flow parameters that determine the non-dimensional mountain height and hence the degree of blocking: the upstream wind speed and the static stability. An investigation was conducted into the typical static stabilities seen in the ERA-Interim dataset under warm and cold barrier wind conditions. No clear relation between Brunt-Väisälä frequency and temperature of barrier wind was found although this might be because of the difficulties associated with finding typical 'upstream' conditions for a complicated 3-D synoptic environment.

The case study of Chapter 3 was described as being an example of a warm barrier wind. It also has much in common with the idealised barrier winds that experience limited blocking (consistent with these being similar to the warm barrier winds of the climatology) especially in its first stage of development. For example there is significant flow escaping up over the mountain and a large amount of spatial variability in low-level wind strength associated with the undulations in the Greenland orography. In addition, it was shown that gravity waves and downslope winds were being triggered in this case study as they are in the weakly blocked experiments.

Chapter 5

The East Greenland Spill Jet and the impact of barrier winds

5.1 Introduction

In the preceding chapters, barrier winds along southeast Greenland have been examined from an atmospheric perspective through observations, reanalysis, and realistic and idealised modelling. It has been shown that barrier winds are a frequent occurrence in this part of the world and exhibit some varied dynamics and properties. Throughout, special attention has been paid to the potential impact on the underlying ocean, providing insights particularly into the typical surface fluxes produced during these events. This chapter sets out to examine one such example of the impact of barrier winds on the underlying ocean through the use of ocean observations off the southeast coast of Greenland. The region which is frequented by barrier winds is also one of the more important for the circulation of the entire Atlantic Ocean. It is also very complex, with a number of processes occurring within a relatively small region. The impact of barrier winds on these processes is currently poorly understood.

The Denmark Strait Overflow (DSO) transports on average 3 Sv of dense water from the Nordic Seas over a sill at 600 m and into the deep ocean (Macrander et al., 2005). It is a major pathway of dense water over the Greenland-Scotland ridge and contributes about half of the flow of dense water return flow out of the subarctic (Dickson and Brown, 1994). The other half flows out between Iceland and Scotland, primarily in the Faroe Bank Channel. As the DSO flows equatorward it entrains water from its surroundings, resulting in a doubling of its transport by the time it has reached the bottom of its descent (Dickson and Brown, 1994). These waters form the major equatorward pathway for dense water – the Deep Western Boundary current. The DSO therefore constitutes a vital component

of the return flow of the Atlantic Meridional Overturning Circulation. The overflow from the Nordic Seas and subsequent fate of dense waters in the Atlantic, along with transport estimates, is shown in Figure 1.5.

Above the DSO in the vicinity of the Denmark Strait there is a complex surface current system shown diagrammatically in Figure 1.6. The East Greenland current (EGC) flows equatorward in the vicinity of the continental shelf break. It constitutes a major pathway of freshwater out of the Arctic and advects a significant quantity of sea ice as well (Aagaard and Carmack, 1989). Just offshore of the EGC is the retroflected branch of the Irminger current (IC). Relative to the cold, fresh EGC, the IC water is warmer and saltier having originated from the North Atlantic Current. The result is a strong hydrographic front between these water masses that supports a geostrophic, surface-intensified jet along the Greenland shelf break south of the Denmark Strait. There is still much to understand about this front. It has been postulated that it is unstable and warm Irminger Current water is often observed inshore of the front. The mechanisms for these processes remain underdeveloped in the region.

To complicate the picture further, the shelf-slope region south of the Denmark Strait sill is frequented by cyclonic eddies which track southwards along the continental slope. Based on satellite data, a typical eddy has a diameter of 20 – 40 km and travels equatorward at a speed of 25-30 $\mathrm{cm\,s^{-1}}$ (Bruce, 1995). These eddies generally move along approximately the same path as the EGC-IC hydrographic front often giving them a distinct surface signature as the water masses are mixed by the cyclonic flow. The eddies could be partly contributing to the movement of Irminger Current water across the front.

The eddies are believed to be formed as a result of a combination of factors. Important amongst them is the fact that the DSO is not a constant flow over the sill but instead pulses intermittently with a typical frequency of a few days (Smith, 1976). The DSO therefore constitutes a string of dense boluses descending equatorward down the Greenland continental slope (Cooper, 1955). In addition, apart from a small poleward current along the north coast of Iceland, the flow through Denmark Strait is equatorward at all depths. This makes the Denmark Strait unique amongst the major overflows of the Atlantic in that is is the only one with its surface current transport in the same direction as its deep flow. According to Spall and Price (1998), the eddies are produced south of the sill because the equatorward flow at all depths allows the overflow to stretch the central water column (by up to 100%) and induce cyclonic vorticity. An eddy which has been spun up in this manner then travels downstream along the continental slope trapped above, and travelling with the speed of, a dense overflow bolus typically found below it. Spall and Price (1998) showed that eddies can be formed for steady outflow conditions through the Denmark Strait, but the natural variability at the sill is also likely to influence when, and

how frequently, eddies form.

This was the picture of the main currents in the vicinity of the Denmark Strait at the turn of the 21st century. Pickart et al. (2005) subsequently showed that there was an additional pathway of dense water through the region. High resolution CTD measurements across the Greenland continental shelf break south of the sill revealed the presence of dense water that appeared to spill off the shelf and form a gravity current along the upper slope above the DSO waters. This was named the Greenland Spill Jet. Through repeat transects of the current the Spill Jet was established as a consistent feature in the region with typical densities only slightly less dense than DSO water and an equatorward transport of on average 4.8 ± 2.3 Sv (Brearley et al., 2012). This is the equivalent to the transport of the DSO at the same latitude and therefore represents a significant contribution to the return flow of dense water from northern latitudes. Although much was learnt through these transects, there were, and remain, many questions regarding the cause of the spilling and the persistence of the Spill Jet throughout the year.

Some answers in this regard came from Magaldi et al. (2011) who implemented a high resolution ocean model over a three month summer period. Their model was capable of simulating the Spill Jet and showed that it was an intermittent feature with an average transport comparable to that of Brearley et al. (2012). They were also able to investigate the mechanisms of spilling, one of which was due to the cyclonic eddies described above. In particular, dense water residing on the shelf could be drawn off into the Spill Jet by the leading edge of a cyclonic eddy as it passed along the continental slope. About 50% of the spilling episodes observed in the model could be accounted for by this mechanism. The remaining events were believed to be triggered by a more generic instability of the shelf edge flow, leading to offshore transport of dense water.

The aim of this chapter is to investigate through observations the mechanisms by which dense water spills of the shelf south of Denmark Strait including the role of atmospheric forcing. This will be achieved through the examination of a yearlong dataset from a mooring that was in place on the continental shelf edge south of Denmark Strait. The existence and importance of eddies for spilling is investigated first. However, the main emphasis of the chapter is on the impact of barrier winds. As has been shown in previous chapters, barrier winds occur frequently at the location of the Spill Jet and are a source of potentially large heat fluxes and surface stresses. As posited by Pickart et al. (2005), the sense of the atmospheric flow is downwelling favourable providing at least one mechanism through which barrier winds could drive dense water off the shelf. It should be noted that the modelling study of Magaldi et al. (2011) was conducted during a period of weak meteorological forcing so has little to say regarding the impact of barrier winds.

5.2 Mooring Data

5.2.1 Mooring specification

The mooring that provides the data for this study (hereafter referred to as EG1) was part of a larger array of seven moorings that were deployed across the southeast Greenland shelf break and slope between September 2007 and October 2008. This was the first array designed to measure the East Greenland Spill Jet. EG1 is the most shoreward mooring in the array and resides approximately 10 km inshore of the shelf break in 248 m of water at 65.53°N, 33.15°W. Figure 5.1 shows the bathymetry of the region along with the location of EG1. The mooring design for EG1 is shown diagrammatically in Figure 5.2.

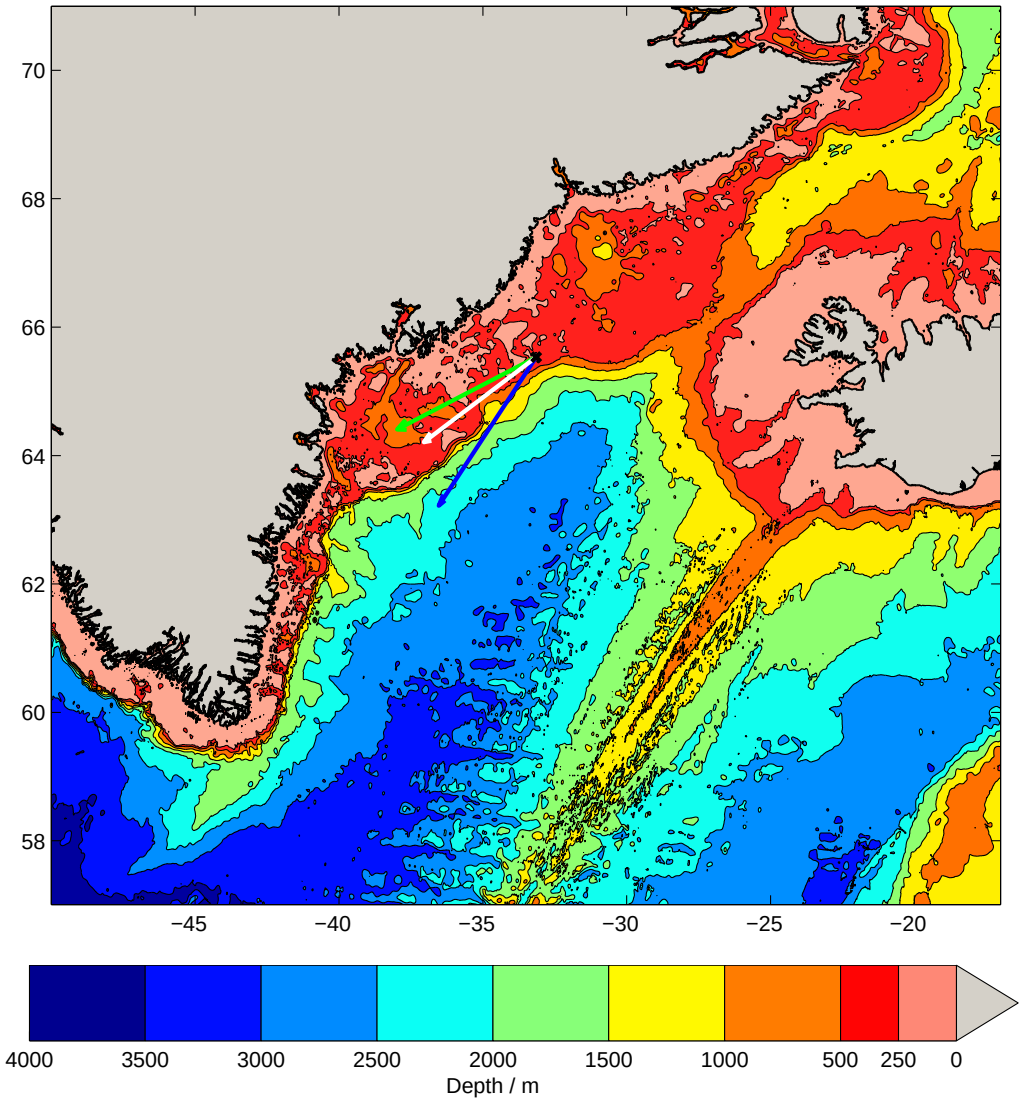

Figure 5.1: Map of region of interest and bathymetry. EG1 mooring shown by a black cross. Arrows shown are mean flow vectors for the duration of the yearlong deployment: White is the depth mean, blue is the bottom velocity bin and green is the top velocity bin.

A Coastal Moored Profiler (CMP) recorded profiles of temperature and salinity twice daily at 00 UTC and 06 UTC in the region between the anchor and the top float which was situated approximately 100 m below the surface. The data from this device covers the period between the beginning of September, when the mooring was deployed, and the end of April when the CMP motor failed and no further profiles were obtained.

To provide measurements of the hydrography above the top float, a Microcat was mounted approximately 40 m above the top float on an aluminium tube. Unfortunately, this device only remained above the top float for two months before the strong currents destroyed the buoyancy and the instrument dropped down below the top float. This can be seen from the time series of the Microcat's depth record (not shown) as a step change of approximately 85 m at the end of October 2007. This is when the Microcat falls from being 40 m above the top float (at 100 m) to 40 metres below it. A second Microcat was mounted near the base of the mooring.

To measure the velocity of the water column, EG1 had two upward looking workhorse Acoustic Doppler Current Profilers (ADCPs). One was mounted near the base of the mooring and the other on the top float. In this way, the majority of the water column was covered for the year that the mooring was in the water. The lower Microcat was mounted in the frame of the lower upward looking ADCP.

5.2.2 Processing

The individual casts of the CMP data were averaged into 2 dbar bins to remove small scale noise. The data were subsequently interpolated onto a regular depth-time grid with temporal and vertical resolutions of 6 hours and 5 metres respectively. During some periods, the mooring was 'blown down' by the strong currents to such an extent that the CMP couldn't complete full profiles between the top float and the anchor. This produced data gaps at some depths for the duration of a blow down event. These periods were not interpolated over if they lasted more than 24 hours and were left as data gaps in the final interpolated product.

The data from the two upward looking ADCPs (which will be referred to as 'top' and 'bottom') had to be concatenated together in order to produce full-depth profiles. A comparison between the current speeds measured by both ADCPs at similar depth bins is shown in Figure 5.3. The top ADCP bin is at a depth of 90 m and the bottom ADCP bin used in the comparison is from 112 m. Due to the large distance between the location of the bottom ADCP and the depth of the bin used for the comparison, there are many times when there are no measurements at this depth. In fact, only 28% of the possible times contained a measurement, but this still corresponds to over 2500 data points. The

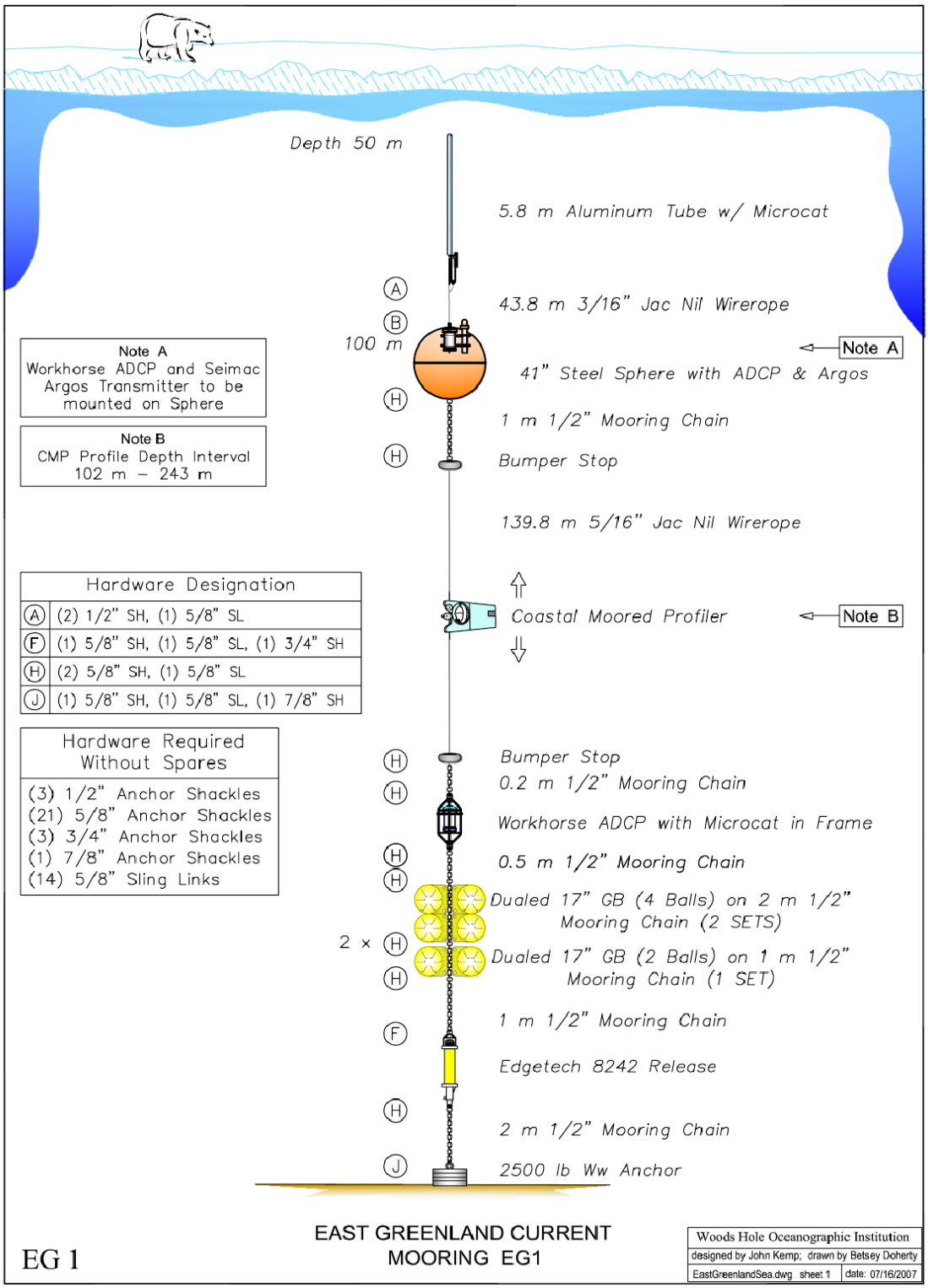

Figure 5.2: Mooring diagram for EG1 mooring.

20 m difference between the bins under comparison is a trade off between any possible systematic differences in the current speed over this range and the large reduction in the number data points if a higher bottom ADCP bin is used. As can be seen from Figure 5.3, the current speeds compare well between the two ADCP records.

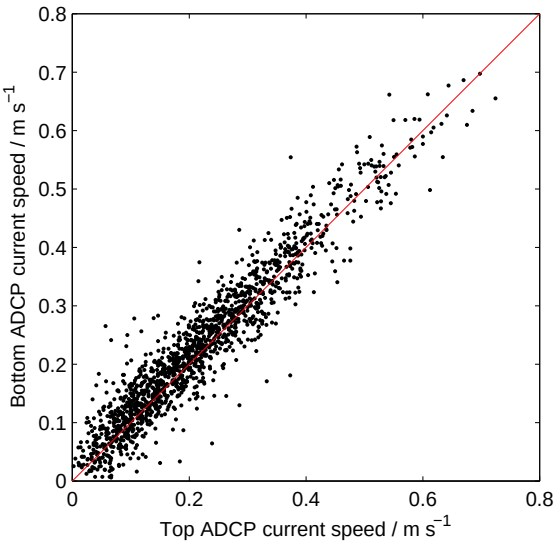

Figure 5.3: Comparison between the current speeds measured at the top and bottom ADCPs. The depth bin from which the data from the top ADCP comes is 90 m and the ADCP bin for the bottom ADCP is from 112 m.

Figure 5.4 shows the comparison between the current angles measured at the same bins. This clearly shows an angle bias between the two ADCPs which is likely the result of a systematic compass error in one of the two ADCPs. It is very likely that the top ADCP was incorrect. The reasoning for this is firstly that the top ADCP was mounted on the side of a steel top float which would give the ADCP's compass an asymmetric distribution of metal around it. This would have the affect of altering the magnetic field felt by the top ADCP's compass in line with the type of error seen in Figure 5.4 (National Geospatial-Intelligence Agency, 2004). Secondly, and in support of the top ADCP needing correction, is the fact that the depth integrated flow in the bottom ADCP follows the isobaths in the region, as expected for a predominantly geostrophic flow. This gives one confidence that the lower ADCP compass was indeed accurate.

The simplest correction that can be made (and the one that was chosen) is by fitting a sinusoidal waveform to the difference in the angles between the two ADCPs as a function of the top ADCP angle. This way, for any measured top ADCP angle, there will be a corresponding rotation angle needed to be applied to the top ADCP record. The data and the fitted sinusoid is shown in Figure 5.5. The fitting was done so as to reduce the RMS error in the velocity components after the rotation is completed.

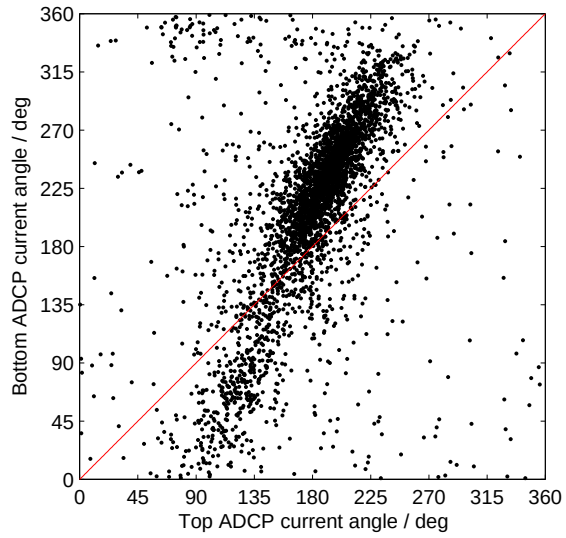

Figure 5.4: Comparison between the current angles measured at the top and bottom ADCPs for the same depth bins as for Figure 5.3.

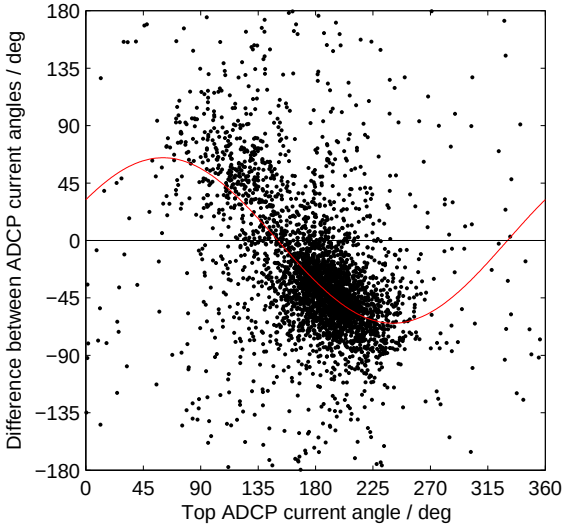

Figure 5.5: The difference between the top and bottom ADCP current angles plotted as a function of the top ADCP current angle for the same depth bins as for Figure 5.3. Red line is the best fit sinusoid to the data and represents the angle correction function applied to the top ADCP current record.

Figure 5.6 shows the result of this rotation. As can be seen, there is still a reasonable spread in the data, but in general, the angles agree much better than before the rotation was implemented. After the rotational correction was applied to the top ADCP, the processing of the data was completed by de-tiding the data, subjecting each profile to a butterworth filter to remove high frequencies, and interpolating the data onto a regular time-depth grid with resolutions of one hour and 8 metres respectively.

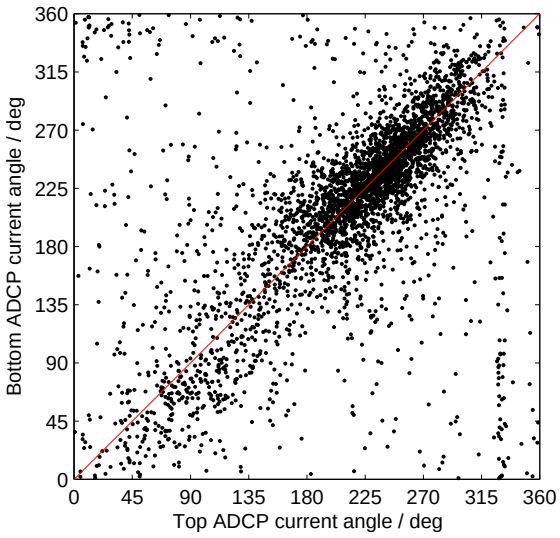

Figure 5.6: Comparison between the current angles measured at the top and bottom ADCPs for the same depth bins as for Figure 5.3 after the rotational correction shown in Figure 5.5 has been applied.

5.3 Year overview

5.3.1 Hydrography

The complete processed hydrographic record is shown in Figures 5.7 and 5.8. There is a great deal of variability on the scale of a few days. Temperature and salinity undergo in-phase oscillations, especially in the upper water column, most likely due to the proximity of the mooring to the hydrographic front between the East Greenland Current and the Irminger Current, which typically resides just offshore of the shelf break (see Figure 1.6). The cause of these oscillations in temperature and salinity are investigated further in Section 5.4.3. Near the bottom, water denser than 27.7 kg m^{-3} can typically be found although there is some of variability on the order of a few days and longer.

In addition to this high frequency variability there is a pronounced seasonal signal in the hydrographic variables, most clearly shown in Figures 5.9 and 5.10. Figure 5.9 is low-pass filtered representation of Figures 5.7 and Figures 5.8. It was obtained using a running mean method with a filter width of 30 days. The temperature and salinity panels show that there are larger scale variability than the oscillations seen in Figures 5.7 and 5.8 in both variables. The water column undergoes two periods of generally warmer and saltier conditions in October and early December. Most of this signal is towards the top of the water column. From January there is a general transition to colder, fresher water properties, but the high frequency oscillations in temperature and salinity are maintained around a lower running mean (not shown). The seasonal amplitude of the temperature

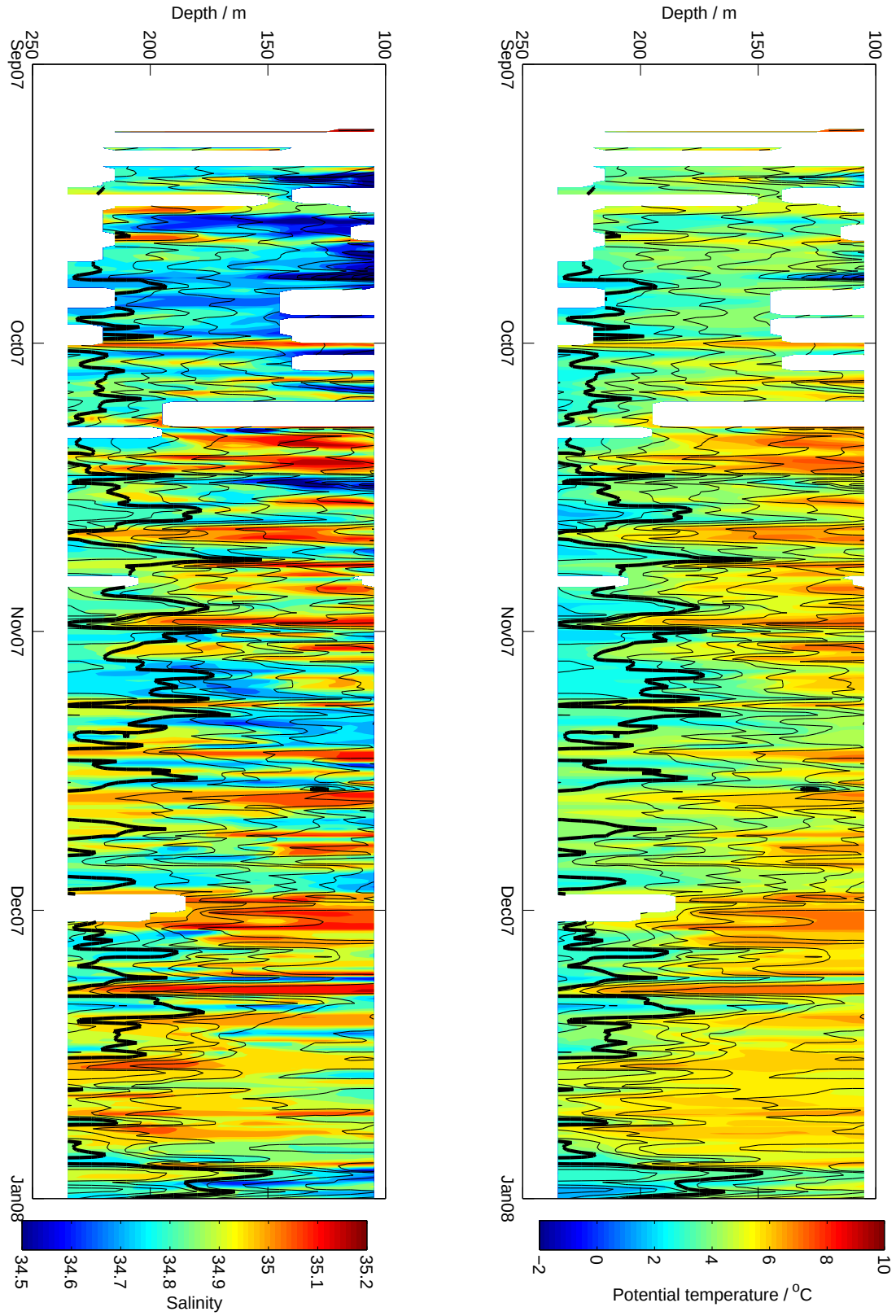

Figure 5.7: Potential temperature (right) and salinity (left) as a function of depth and time for the EG1 mooring (colours). Potential density contoured over the top and shown every 0.05 kg m^{-3}. 27.7 kg m^{-3} shown in bold for reference.

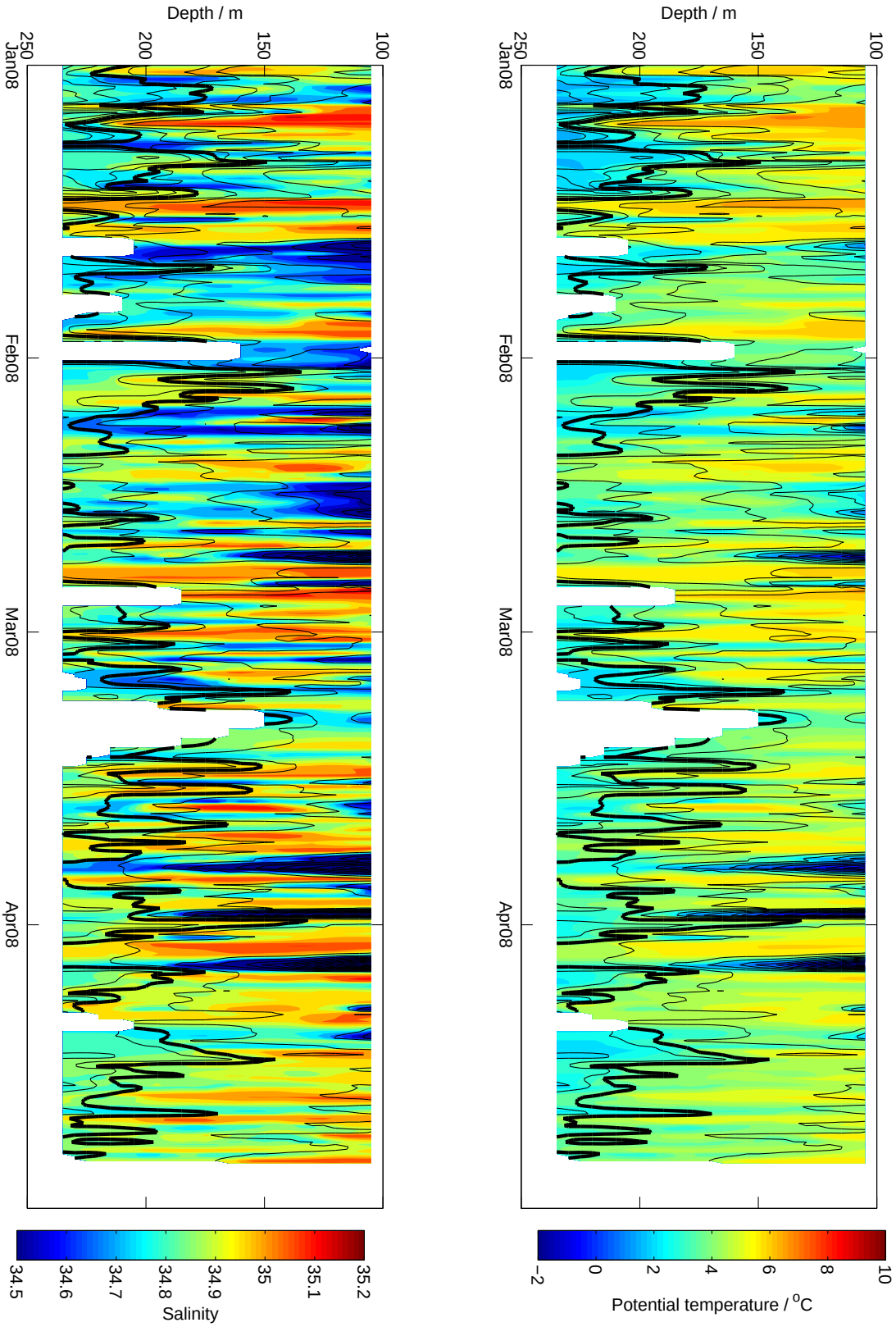

Figure 5.8: As Figure 5.7.

signal at the mooring is in accordance with the seasonal range of temperatures measured in the Irminger current as it approaches Iceland from the south (Héðinn Valdimarsson, priv. comm.)

The potential density panel shows that there is, on average, water denser than 27.7 $\mathrm{kg\,m^{-3}}$ near the bottom of the shelf for most of the record, without any clear seasonal trend. However, above this the density does vary seasonally. In particular the water starts off well stratified, but as winter progresses the upper water column becomes more dense and destratified, consistent with local or upstream wintertime convection. This densification occurs as a result of the reduction in temperature, although the salinity was also reduced. The destratification of the upper water column is clearly seen in the Brunt-Väisälä frequency panel as a sloping interface between weakly stratified water in the upper layer and well stratified water near the bottom. This can be seen as evidence for local convection to a depth of 200 m. The onset of this destratification occurs in later November but probably started earlier in the waters between the surface and the height of the top of the CMP record at 100 m.

Figure 5.10 shows mean vertical profiles of the potential density for the length of the entire record as well as for the individual seasons, offering another view of the annual signal. At the beginning of the record (between September and November) the water column is well stratified with an almost constant stratification at all depths. Moving into the period between December and February, the density and stratification of the lower water mass remains constant while the upper water column becomes denser and less stratified. This period could be classified as a two layer system with different stratifications. Between March and May, the upper water mass becomes increasingly densified and the reduction in stratification has penetrated farther down in the water column. Note, however, that the water near the bottom remains largely unaffected, consistent with the lack of a clear seasonal signal seen at the bottom in the potential density panel of Figure 5.9.

To further illustrate the differences between the upper water column and the water near to the bottom for the full year, Figure 5.11 shows the time series of the potential density from the upper (blue) and lower (red) Microcats. The depths of the two time series are 140 m and 242 m respectively. Recall that the upper Microcat was knocked down below the top float at the end of October which is why the data shown in Figure 5.11 for the upper Microcat begins at that time. It should be noted that both these time series cover the whole time the mooring was in the water and therefore extend further than the data from the CMP.

The data from the lower Microcat clearly shows that although there is some larger scale variability in the potential density near the bottom, there is no clear seasonal signal. The mean density at this depth is greater than 27.7 $\mathrm{kg\,m^{-3}}$ and there are times when

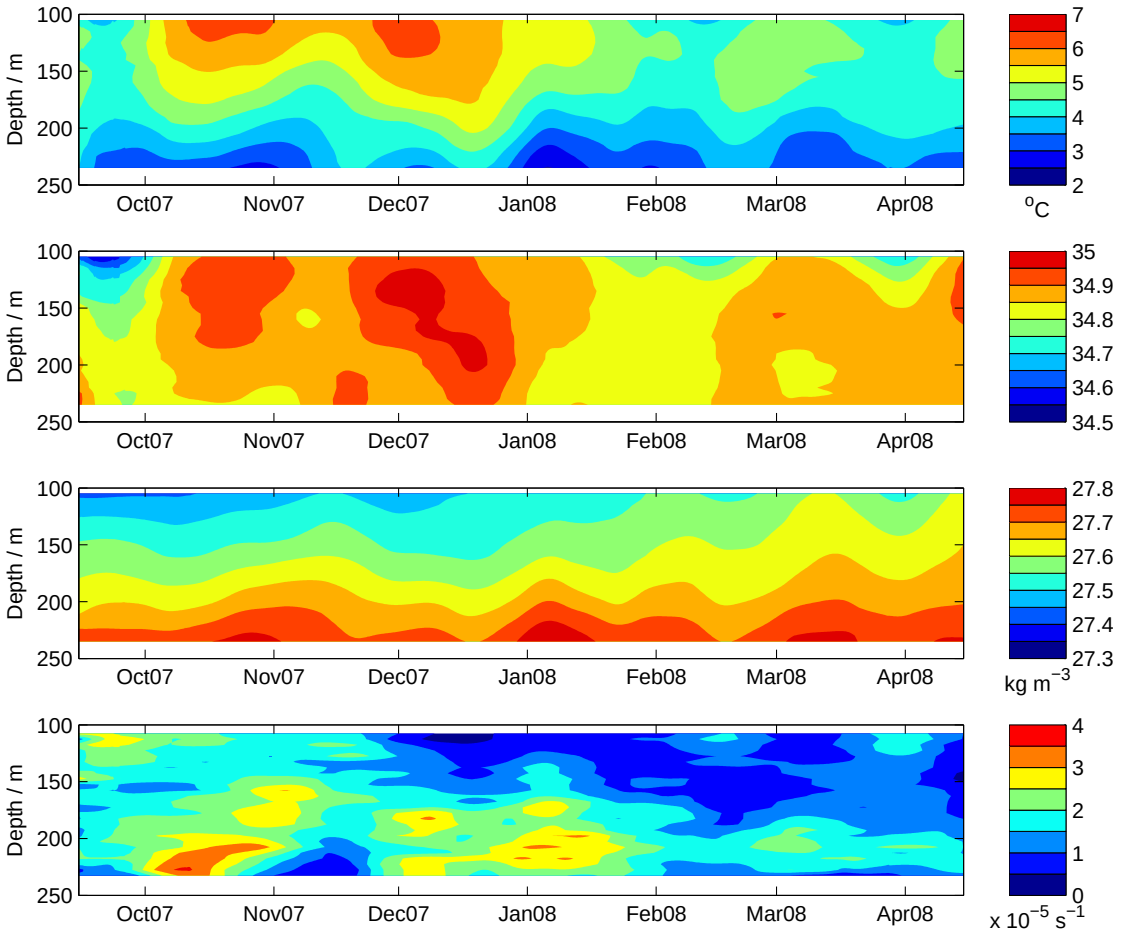

Figure 5.9: Hydrographic variables smoothed over 30 days using a running mean filter. From top: Potential temperature, salinity, potential density, Brunt-Väisälä frequency.

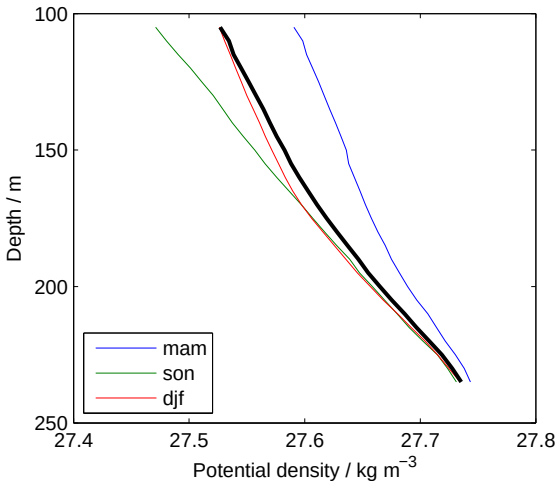

Figure 5.10: Mean of the potential density for duration of hydrographic record (thick black) along with seasonal means for September–November (green), December–February (red) and March–May (blue).

waters of the density of the DSO (27.8 $\mathrm{kg\,m^{-3}}$) are present on the shelf. This occurs about 7% of the time. Higher in the water column, there is a clearer seasonal signal as the water becomes more dense during the winter and spring before reducing in density during summer and into the fall. This suggests that at the time that the CMP failed (in late April) the water column had reached its minimum stratification and maximum upper water column density and was about to restratify most likely due to weaker atmospheric forcing, and glacial and sea ice melt.

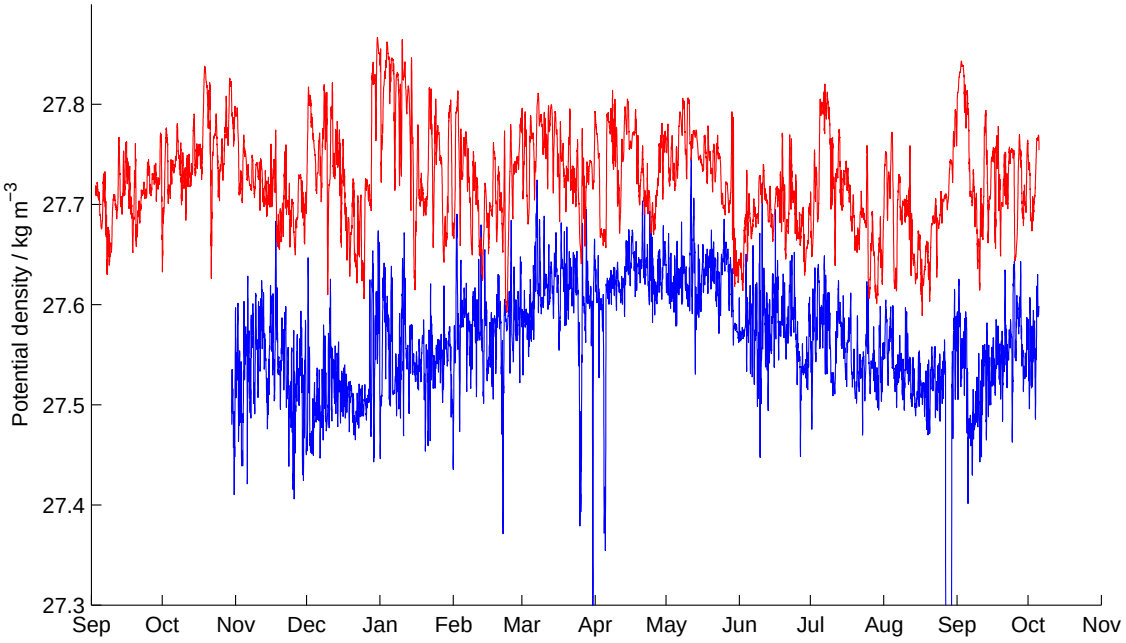

Figure 5.11: Potential density measured by the top (blue) and bottom (red) Microcats averaged into 6 hourly bins.

5.3.2 Velocity

The yearlong mean of the current speed and direction is shown in Figure 5.12. As can be seen there is both a top and bottom intensified flow. The bottom intensified flow has a mean of over 25 $\mathrm{cm\,s^{-1}}$ and veers offshore with depth. In the middle water column, the flow is approximately along isobath (which is angled at about 60°N for the location of the mooring) and as the bottom is approached the current veers offshore by about 20°. This veering with depth is also shown by the yearlong mean flow vectors in Figure 5.1. The surface intensified mean flow of nearly 25 $\mathrm{cm\,s^{-1}}$ also has a veering associated with it, this time onshore. This part of the water column is being sampled by the top ADCP. Although we have seen previously that the current speeds are likely being represented

well by the top ADCP (Figure 5.3), the direction of the current in this part of the water column had to be corrected using the method described in Section 5.2.2. Evidence of this correction can be seen by the slight discontinuity in the mean current direction at a depth of about 90 m which is the depth at which the two velocity records were concatenated. It is unlikely that this introduces a significant error into the dataset.

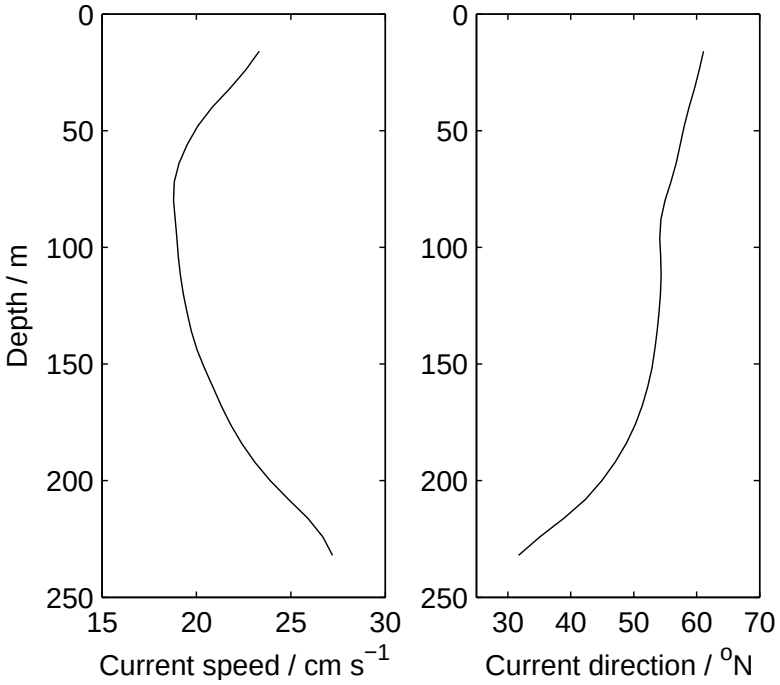

Figure 5.12: Mean of the current speed and direction (direction the current is coming from measure relative to north) for the length of time of the mooring deployment.

As has been shown, dense water resides on the bottom of the shelf for most of the year. The offshore veering of the flow in the region where dense water exists is the first indication that the EG1 mooring captures the occurrence of dense water being forced offshore and potentially spilling off of the shelf edge.

The shelf edge runs at an angle of approximately 60 °N at the location of the mooring array. The veering of the mean current with depth to an angle of 30° cross shelf therefore implies a net mass transport off the shelf. There is no reason to believe that this location is special in terms of providing a route for dense water on the shelf to be transported offshore. If it is presumed that the mean offshore flow here is representative of the offshore flow along the entire length of the East Greenland shelf break then an approximate value for the mean offshore transport can be obtained. Using an along stream length scale of 500 km (the approximate length of the wider part of the shelf south of Denmark Strait) the mean offshore transport is approximately 2 Sv. This is less than half of the typical transports of the East Greenland Spill Jet seen in hydrographic surveys (Pickart et al.,

2005; Brearley et al., 2012), but it is likely that larger transports will occur for shorter periods which may be more important in the Spill Jet production. There will also be a degree of entrainment associated with the spilling of the water off the shelf which will increase the transport in the Spill Jet. Importantly though, this figure for the transport is consistent with a measurement of the inflow of dense water on the Greenland shelf through the Denmark Strait (Robert Pickart, priv. comm.).

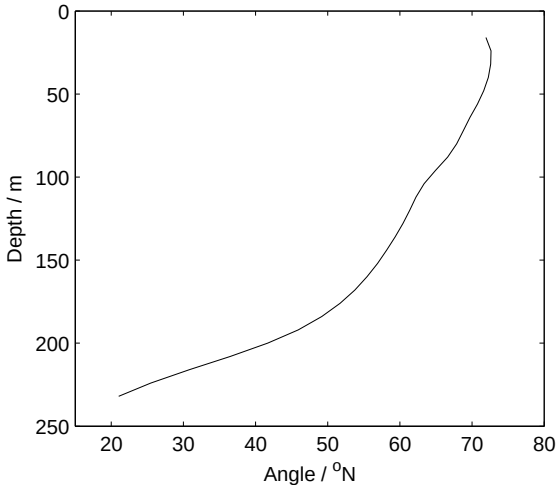

Figure 5.13: Angle of the major axis of the variance ellipses at all depths. Angles are measure relative to north.

Not only does the mean current veer with depth but the principal axis of the variance does as well. This is shown in Figure 5.13 which is the angle of the major axis of the variance ellipses calculated at all depths. The vertical shear is actually greater than that observed for the mean flow. At the bottom, the offshore flow in the mean is associated with a variance that is directed farther offshore. Near the surface, the mean flow is approximately along shore, but the variance is directed more in the onshore direction. The phenomena of veering in both the mean flow and the variance of the mean shows how baroclinic the system is. It also means it is not immediately obvious what angle to use for the rotation of the two components of the current into along and cross stream directions. After some consideration, 60°N was chosen for this angle as it corresponds to both the major axis of the variance ellipse for the depth mean flow and also the approximate orientation of the shelf edge. This latter point allows for a simple link to be made between cross stream flow and cross shelf flow. Figures 5.14 and 5.15 show the full velocity record after this transformation into along and cross stream velocities is made. The along stream flow is positive when directed down the coast to the southwest and, to maintain a right handed coordinate system, the cross stream flow is positive when directed onshore.

One immediately notices that the along stream flow looks quite barotropic in compar-

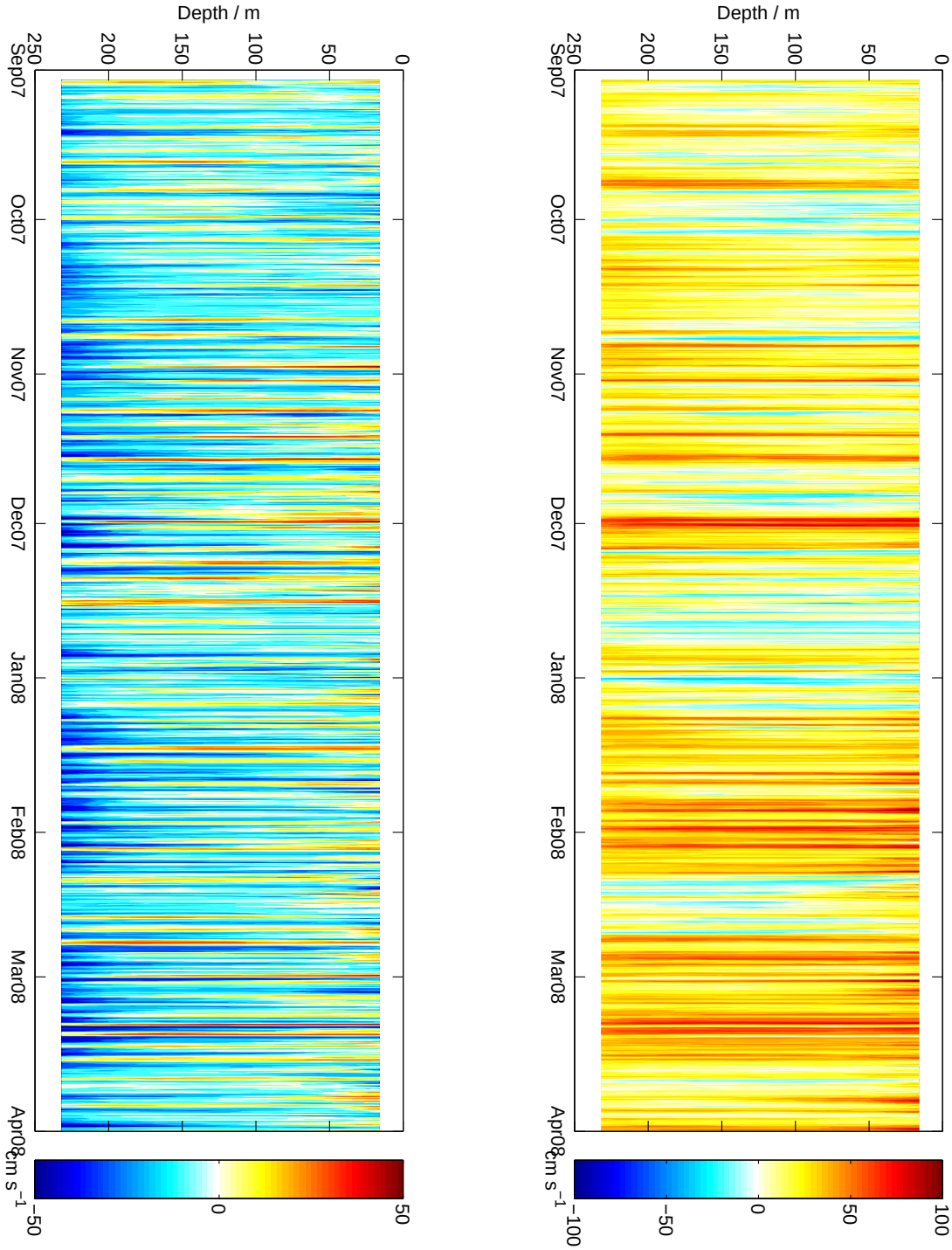

Figure 5.14: Along (right) and cross (left) stream velocity for all times during the EG1 mooring deployment. Rotation angle for along stream direction is 60 °N. For the cross stream flow, a right handed axis is maintained such that positive (negative) is onshore (offshore) flow.

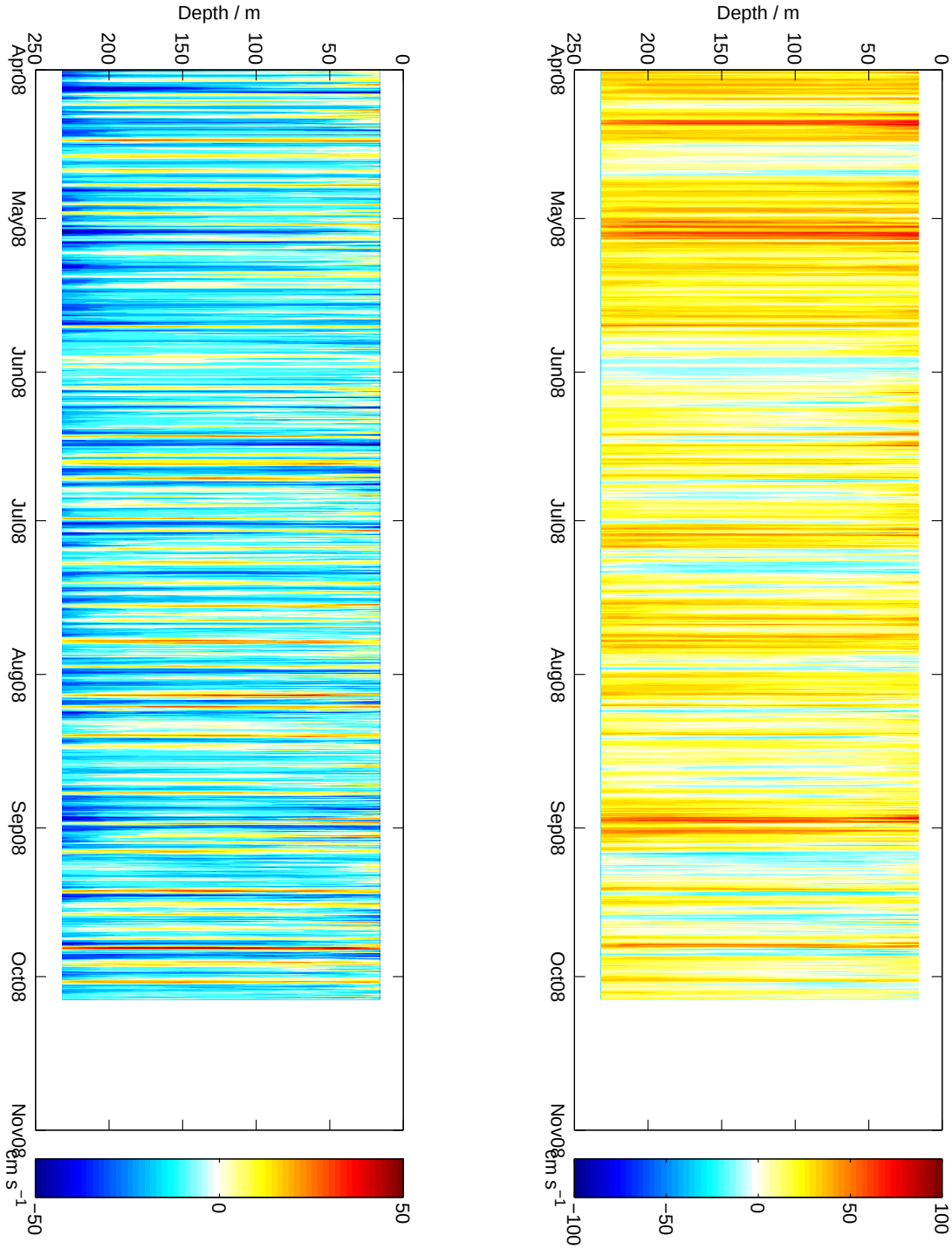

Figure 5.15: As Figure 5.14.

ison with the cross stream flow, which appears to have a stronger baroclinic signature. Near the bottom, many strong cross stream events can be observed. This indicates that, although the mean flow is directed offshore towards the bottom, this offshore flow is episodic in nature.

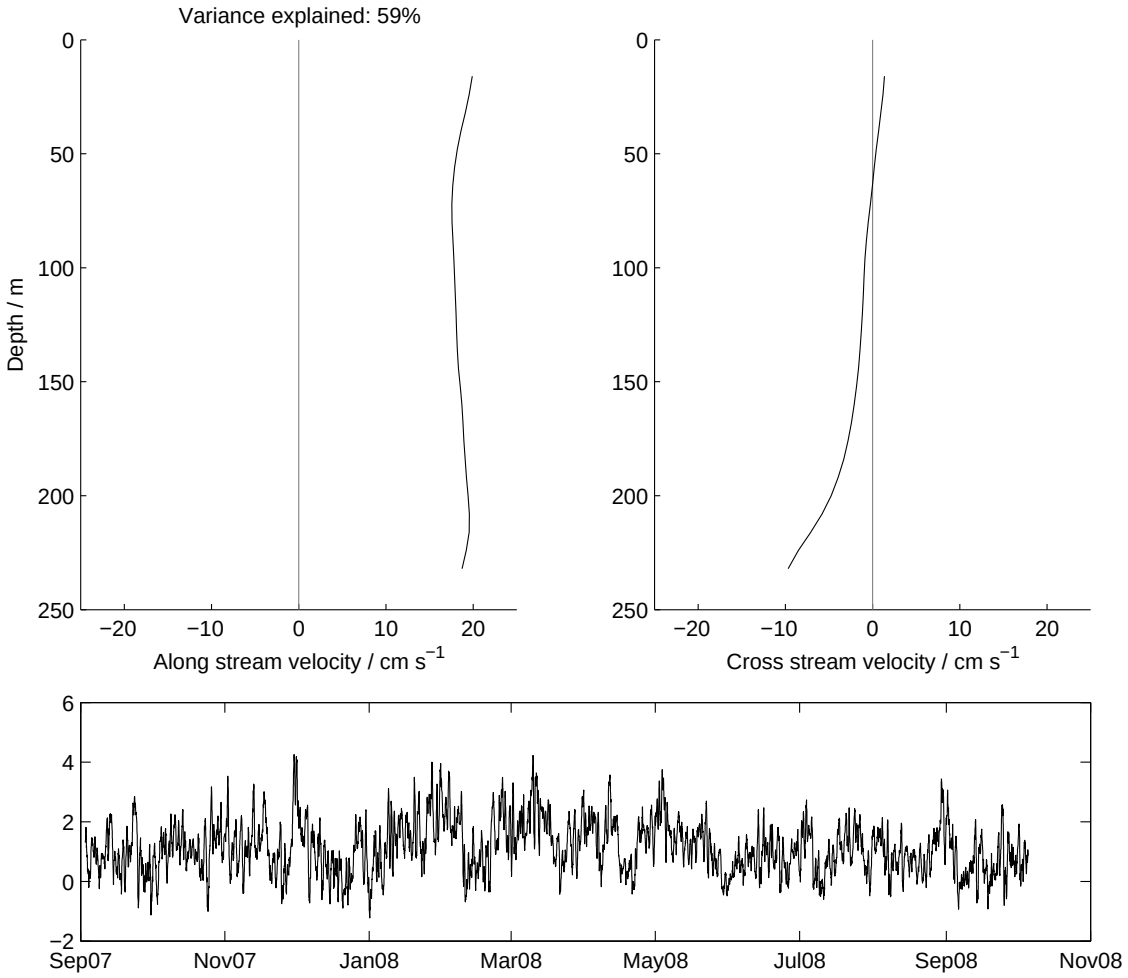

Figure 5.16: 1st mode of the coupled Empirical Orthogonal Functions (EOF) for the along stream (top left) and cross stream (top right) along with the associated time series (bottom).

To examine the typical variability in the along and cross stream currents, coupled Empirical Orthogonal Functions (EOF) were calculated, the first two modes of which are shown in Figures 5.16 and 5.17. The first mode is barotropic in the along stream flow and baroclinic in the cross stream flow with the strongest currents at the bottom. This mode explains 59% of the variability in the current components. The associated time series is almost always positive indicating that the along stream mode is a barotropic oscillation about a defined positive along stream mean, i.e. the direction of the flow

is rarely reversed. The implication for the cross stream flow is that the mean flow is offshore towards the bottom (as has been previously shown) but that whenever there is an anomalously large along stream pulse, the baroclinicity and hence the bottom cross stream velocity is increased.

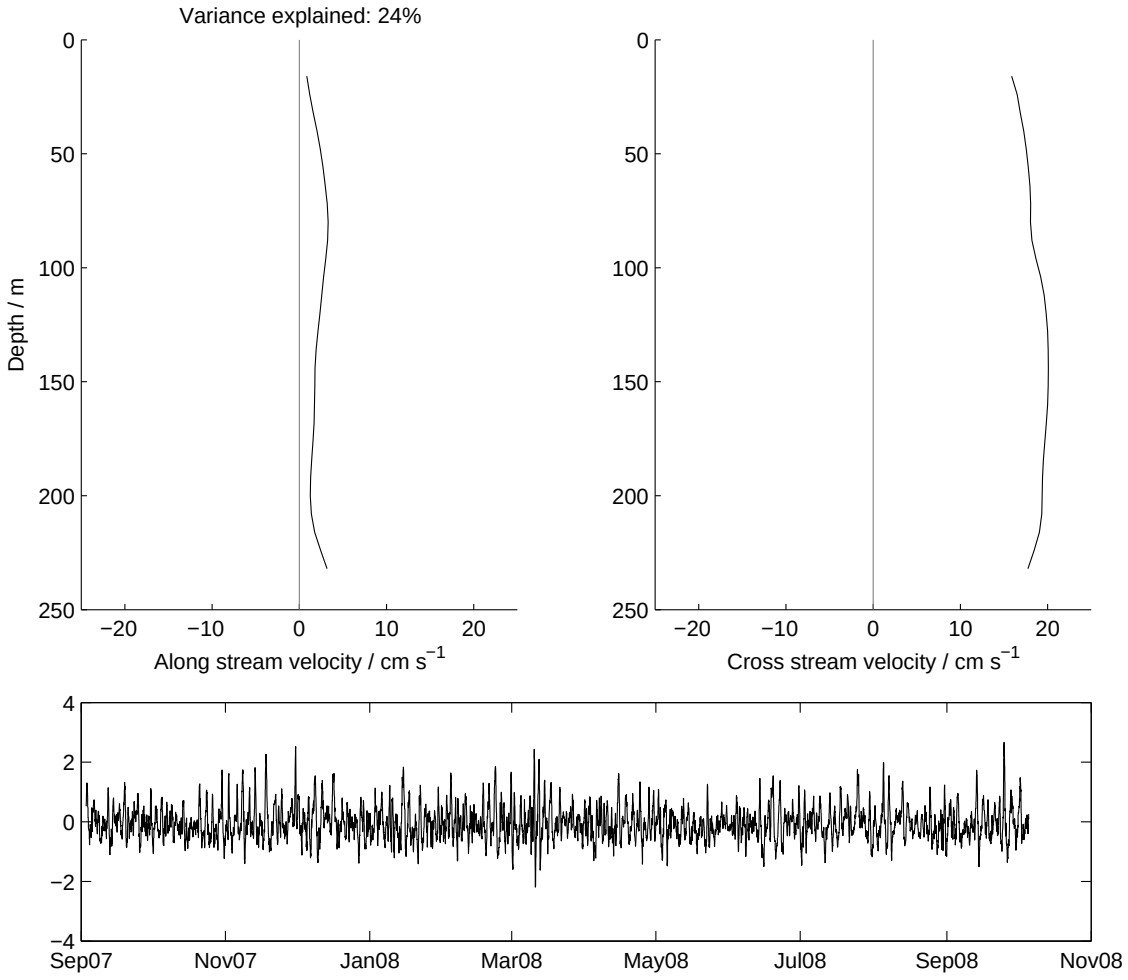

Figure 5.17: 2nd mode of the coupled Empirical Orthogonal Functions (EOF) for the along stream (top left) and cross stream (top right) along with the associated time series (bottom).

The second coupled EOF mode is a barotropic mode in the cross stream velocity with almost no signature in the along stream flow. The time series for this mode is centred on zero indicating that this mode represents a balanced onshore-offshore oscillation in the cross stream velocity. This mode explains 24% of the variability in the flow. As shown next, it is likely that this cross stream mode represents the signature of eddies that propagate along the continental slope south of Denmark Strait and brush up against the shelf region.

5.4 Eddies

Cyclonic eddies are regularly formed south of the Denmark Strait as the result of the intermittent spilling of dense water in the Denmark Strait Overflow (Bruce, 1995; Spall and Price, 1998). The intermittent nature of the overflow is thought to be the result of the internal instabilities of the flow near the Denmark Strait sill (Smith, 1976) and results in the production of a train of dense boluses south of the Strait. As a bolus of dense water cascades down the overflow, the middle water column undergoes intense stretching and, to conserve potential vorticity, large relative vorticity is generated which results in a cyclonic eddy (Spall and Price, 1998). The frequency of the production of these eddies is therefore closely tied to the frequency of spilling of dense water though overflow which has a characteristic time scale of a few days. These eddies are trapped above the boluses that produce them and are mid-depth intensified as this is the region that underwent the most stretching. Using satellite data, Bruce (1995) estimates that they travel southward along the continental slope of southeast Greenland with a speed of 25-30 cm s^{-1}, a typical radius of order 20-40 km and a frequency of 1.5-2.5 days.

Using a high-resolution ocean model, Magaldi et al. (2011) hypothesised that these eddies represent an important mechanism for causing spilling of dense water off the continental shelf. In particular, the leading edge of an eddy has an offshore velocity which is capable of pulling dense water off the shelf into the East Greenland Spill Jet. This process has yet to be observed in observational records however. This section will explore the evidence for eddies in the velocity and hydrographic records of the EG1 mooring. An analysis of their impact on the spilling of dense water off the shelf will be conducted in Section 5.6.

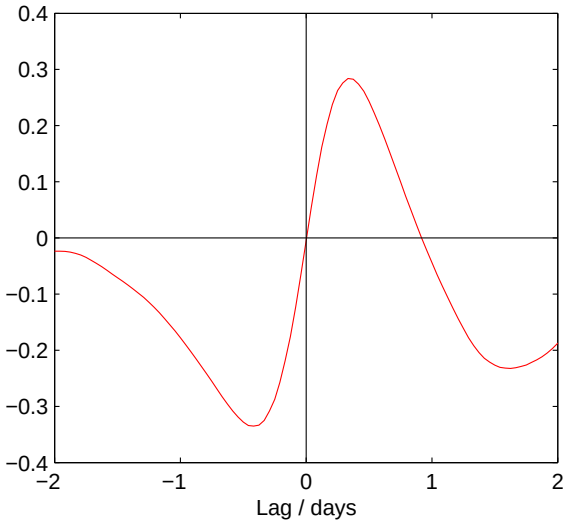

Figure 5.18: Cross correlation of depth mean along and cross stream velocity

5.4.1 Initial evidence

The first piece of evidence for the presence of eddies comes from the cross correlation of the depth mean along and cross stream velocities which is shown in Figure 5.18. This figure indicates that there is significant correlation between these two variables, not at zero lag, but at lags of approximately ± 12 hours. The negative correlation at -12 hours corresponds to an offshore directed current pulse (negative) preceding an alongstream current anomaly (positive), whereas the positive correlation at +12 hours is associated with an enhanced onshore current (positive) following the alongstream anomaly. In other words, the figure indicates a flow sequence of offshore followed by along shore followed by onshore, which is precisely the type of signature that would be expected from a mooring located on the shoreward side of a cyclonic eddy. It should be noted that such a correlation pattern doesn't uniquely describe cyclonic eddies. Being on the shoreward side of an anticyclonic eddy would produce the same correlation picture as the signs of all the velocity components would be reversed. In fact, this correlation figure, while pointing out that there are rotational features in the current record, only additionally informs us that the mooring is on the shoreward side of the eddy core, as expected. The time between the peaks in Figure 5.18 is 24 hours, indicating that the an eddy takes one or two days to pass the mooring site.

This analysis, along with the prevalent barotropic cross stream flow with zero net transport seen from the EOF analysis (Figure 5.17), suggests that eddies may be best identified through looking at the barotropic (depth mean) cross stream velocity in greater detail.

Figure 5.19 shows the wavelet spectrum for the depth mean cross stream velocity time series. As can be seen, most of the energy is centred in the 1 – 4 day band. This corroborates the time period found from the cross correlation for the translational timescale of a single eddy. In addition, the frequency of variability in the Denmark Strait Overflow (order of a few days) is also represented in this band. It is therefore likely that the wavelet spectrum picks out two timescales: the time that one eddy takes to pass the mooring and the time between subsequent eddies. The former is likely to be smaller than the latter, but resolving these two timescales from this analysis is difficult. Within this band of frequencies there is some variability in time. Not only are the periods of cross stream activity discrete, but there also appears to be a larger amount of power in the signal (especially at larger time scales) during the winter months compared with the summer months.

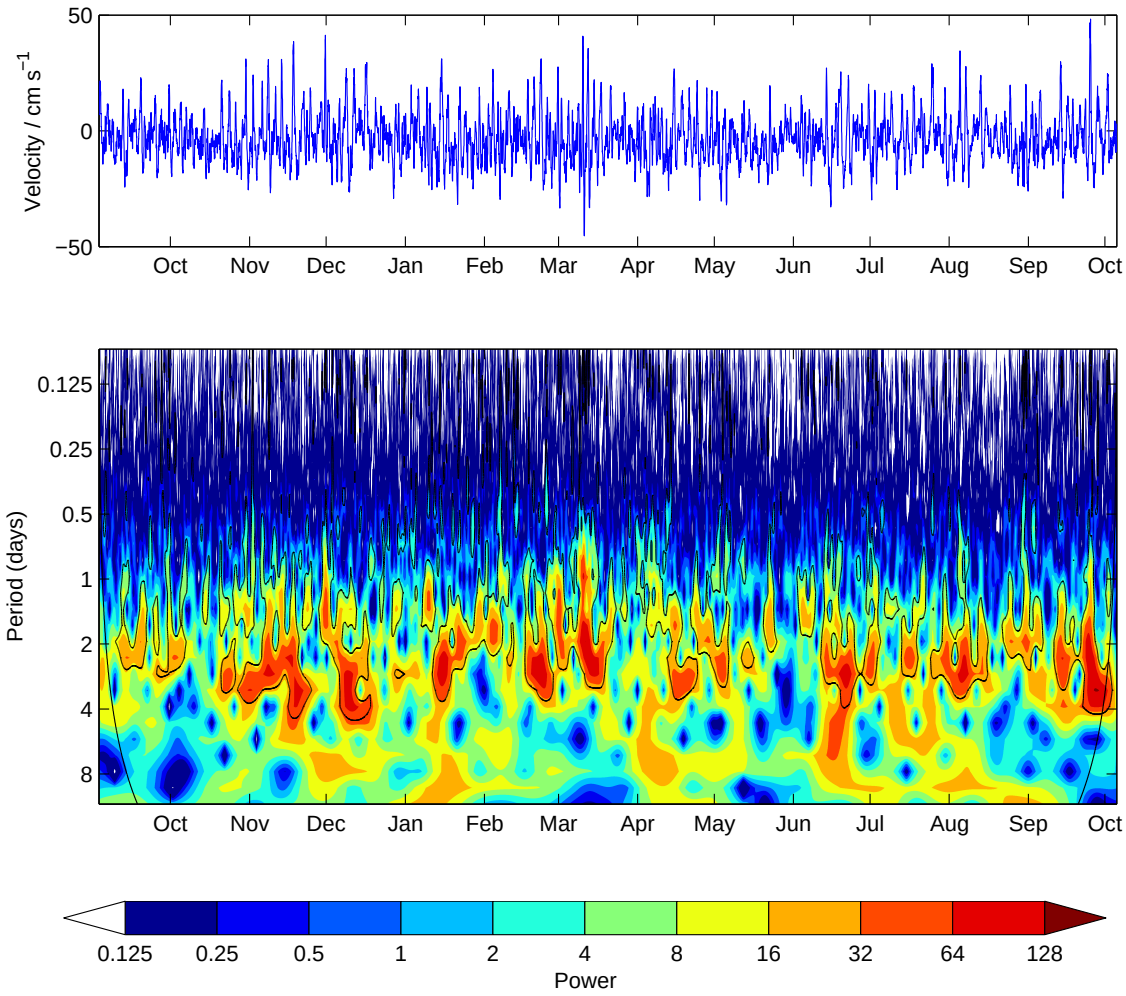

Figure 5.19: Wavelet power spectra of the depth mean cross stream velocity using a Morlet waveform. Power units are days^2 as the analysis was conducted on the velocity time series normalised by its standard deviation. The original time series is shown along the top and the wavelet spectrum is shown underneath. Black contours indicate regions which are statistically significant at 95% confidence and the curved contours at each edge indicate regions where edge effects may be important.

5.4.2 Detecting eddies

As shown above, there is good evidence for rotational flow in the depth mean velocity at the EG1 mooring site, most likely related to the passage of eddies offshore of the mooring along the continental slope. To better understand these patterns, an attempt was made to detect particular eddies. A velocity anomaly field was defined which was the result of subtracting a five day running mean from both the depth mean along and cross stream velocities. This is equivalent to high passing the velocity records with a filter width of five days. Five days was chosen as the threshold because, as Figure 5.19 shows, all the power in the eddy energy is associated with timescales smaller than that.

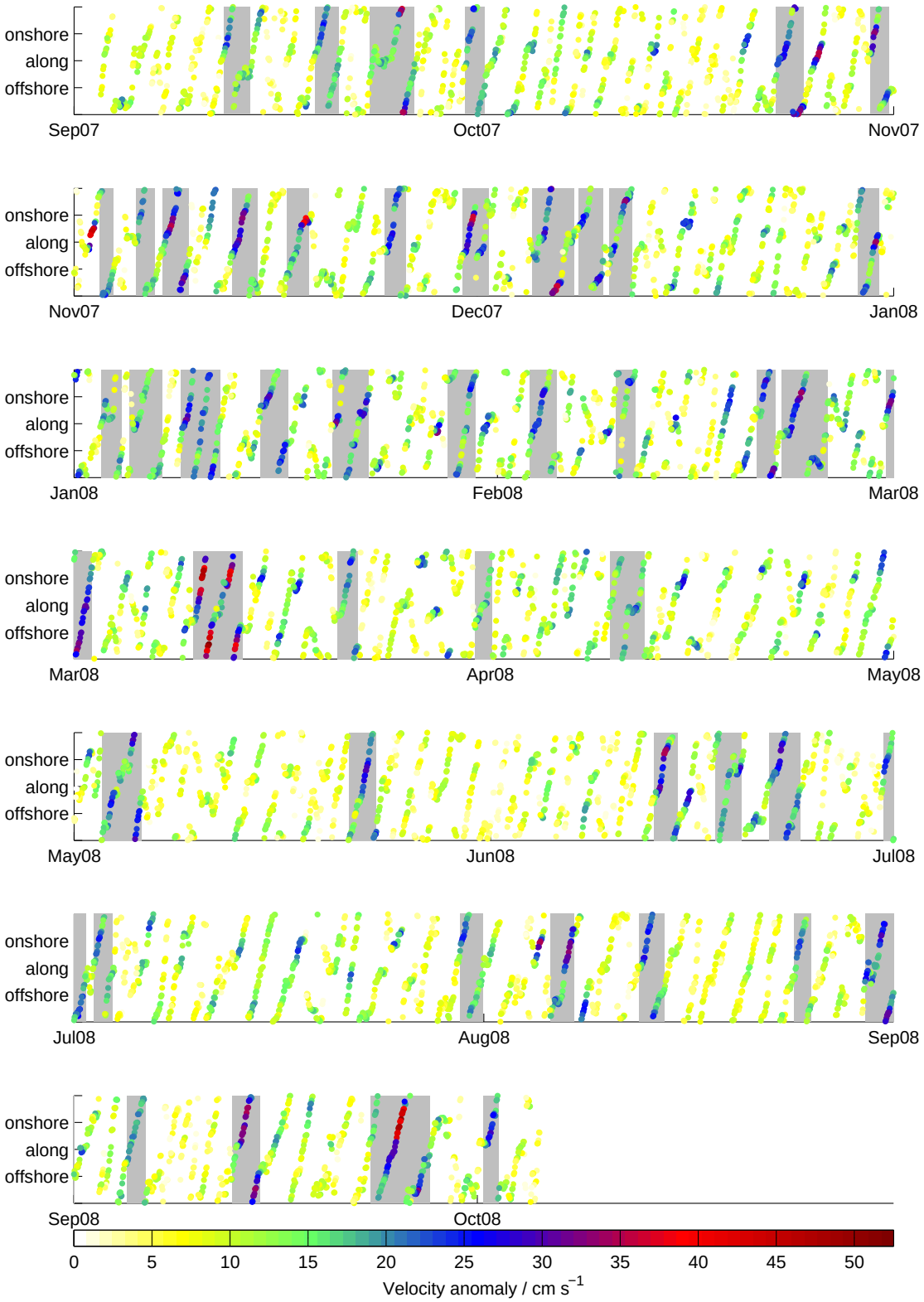

Figure 5.20: Current speed for five day high-passed depth mean velocity for all times plotted as a function of current angle and time.

Figure 5.20 shows the results of this calculation as a plot of the magnitude of the velocity anomaly as a function of time and direction. As suggested by the correlations in Figure 5.18, there is clearly rotational flow embedded in the mean flow much of the time. This rotation is overwhelmingly in the clockwise direction (again this could be representative of being on the shoreward side of cyclonic or anticyclonic eddies) and has a range of amplitudes from 5 $\mathrm{cm\,s^{-1}}$ to 50 $\mathrm{cm\,s^{-1}}$. The cross correlation of the high passed along and cross stream flows shows a similar pattern to that in Figure 5.18 but with maximum correlations nearer to 0.6 (not shown). This shows that the eddies describe a lot of the higher frequency variability, but perhaps not so much the lower frequencies.

To detect individual, strong signals from this dataset a detection routine was employed. Times were selected when the velocity anomaly magnitude was greater than a certain threshold and maintained this magnitude for over 24 hours with fewer than six consecutive hours below the threshold within this time. The specified threshold chosen was somewhat arbitrary, but taken as two thirds of the total, unfiltered depth mean current speed. Other thresholds were tried, but this one produced a good balance between the number of events detected and the quality of each event. It should be noted that there is nothing in the method for producing the anomalies nor the detection routine that require these features to be rotational; they are simply large amplitude velocity anomalies lasting at least 24 hours.

The periods for which the detection criteria were met are denoted in Figure 5.20 by grey boxes. Most of these events have very well defined rotations associated with them. The mean rotation rate for all of the events is seven degrees per hour which is equivalent to a complete rotation in 50 hours. This is in accordance with the time scale picked out from the cross correlation in Figure 5.18 and confirms that an individual eddy takes on average two days to pass the mooring.

To determine whether the eddy features detected are predominantly cyclonic or anticyclonic, a histogram of the angle that the eddy was first detected at was computed (Figure 5.21). The majority of the eddies start somewhere between the offshore and along stream directions. Seeing as it is likely that the detection routine may miss some of the ‘spin up’ part of the eddy which may have a lower magnitude than the required threshold, this result suggests that eddies start with an offshore biased flow, consistent with the features representing predominantly cyclonic eddies.

To examine the vertical structure of the eddy and assess potential asymmetries in more detail, lagged correlations of the five day high-passed depth mean along stream velocity with the five day high-passed cross stream velocity at each depth was calculated. The results of this are shown in Figure 5.22. The general pattern, as might be expected, is consistent with Figure 5.18. Anomalous along stream flow is associated with a preceding

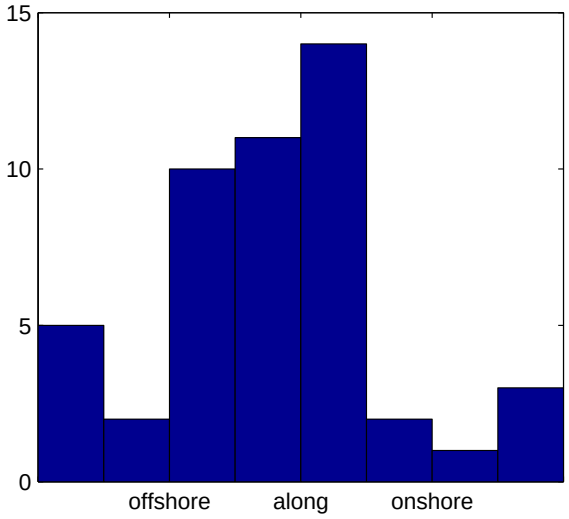

Figure 5.21: Histogram of the starting angle of the eddies detected and shown in Figure 5.20.

offshore flow and and subsequent onshore flow. The structure of this feature with depth shows that the offshore flow is strongest towards the bottom, while the onshore flow appears to be more barotropic. Of course, this crude method of extracting the eddy signal by simply using a high-pass filter doesn't take account of potential mechanisms by which the eddy could be modified by the mean flow that it is embedded in.

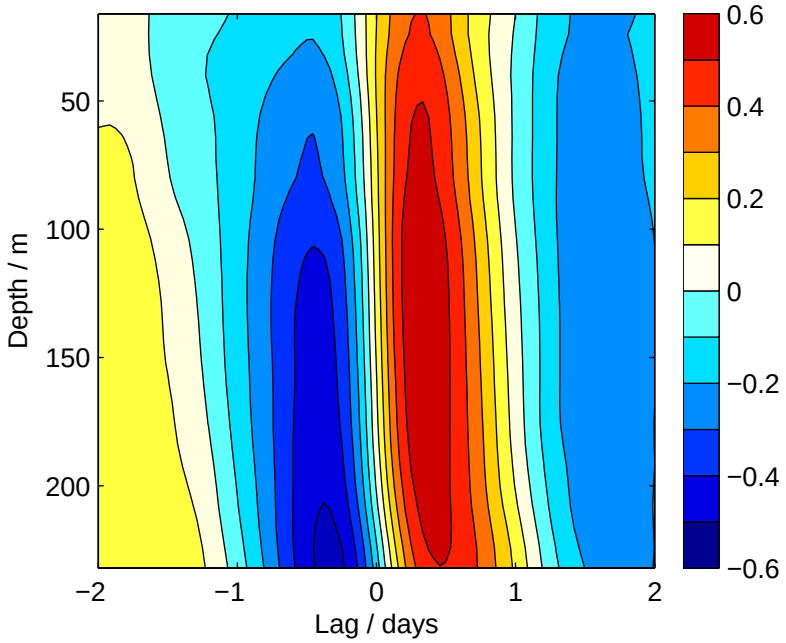

Figure 5.22: Lagged correlations of the five day high-passed depth mean along stream velocity with the five day high-passed cross stream velocity for all depth bins.

5.4.3 Impact on hydrography

It has been shown that eddies are advecting water both onshore and offshore. What is the impact of this on the hydrography at the mooring site? A hydrographic front exists just offshore of the shelf break between the warm and salty Irminger Current (IC) and the cold and fresh East Greenland Current (EGC) (see Figure 1.6). Lagged correlations of the depth mean potential temperature, salinity and potential density with the cross stream velocity (averaged over the depth of the hydrographic record) are shown in Figure 5.23. These show that there is reasonably good correlation in the temperature and salinity panels at a lag of approximately 12 hours. This is associated with an offshore flow (negative) bringing colder and fresher water to the mooring as well as an onshore anomaly (positive) preceding an increase in temperature and salinity. This is consistent with an eddy drawing cold and fresh water from the EGC offshore on the leading edge of the eddy and pulling warm and salty IC-type water onshore at the trailing edge. Thus eddies should have the effect of mixing the two water masses. The fact that the correlations aren't stronger indicates that there are other important factors in the variability of the hydrographic record. Potentially these include the lack of a well structured front in the region at some times of the year and the presence of lenses of water passing the array that were already transferred to the 'wrong side' of the front somewhere upstream of the mooring. Evidence for these can be seen in, for example, Brearley et al. (2012).

The changes in temperature and salinity serve to compensate each other in density, as there is only weak correlation between the cross stream flow and the potential density. A correlation might be expected if the density front offshore of the shelf edge is advected right the way to the mooring site and a lack of correlation suggests that this is not happening often enough.

From the results presented in this section, it is clear that cyclonic eddies are ubiquitous in the velocity record with typical time periods of 1 – 4 days. An assessment of how important eddies are in the spilling process will be conducted in Section 5.6.

5.5 Barrier winds

Barrier winds along the southeast coast of Greenland provide another potential mechanism by which dense water can be driven off the southeast Greenland continental shelf. The data that will be used to quantify the timing and location of the winds in the region come from the ERA-Interim product, a global atmospheric reanalysis from the European Center for Medium Range Weather Forecasting (ECMWF). The model specification has been described previously in Chapter 2. The important feature for the analysis of bar-

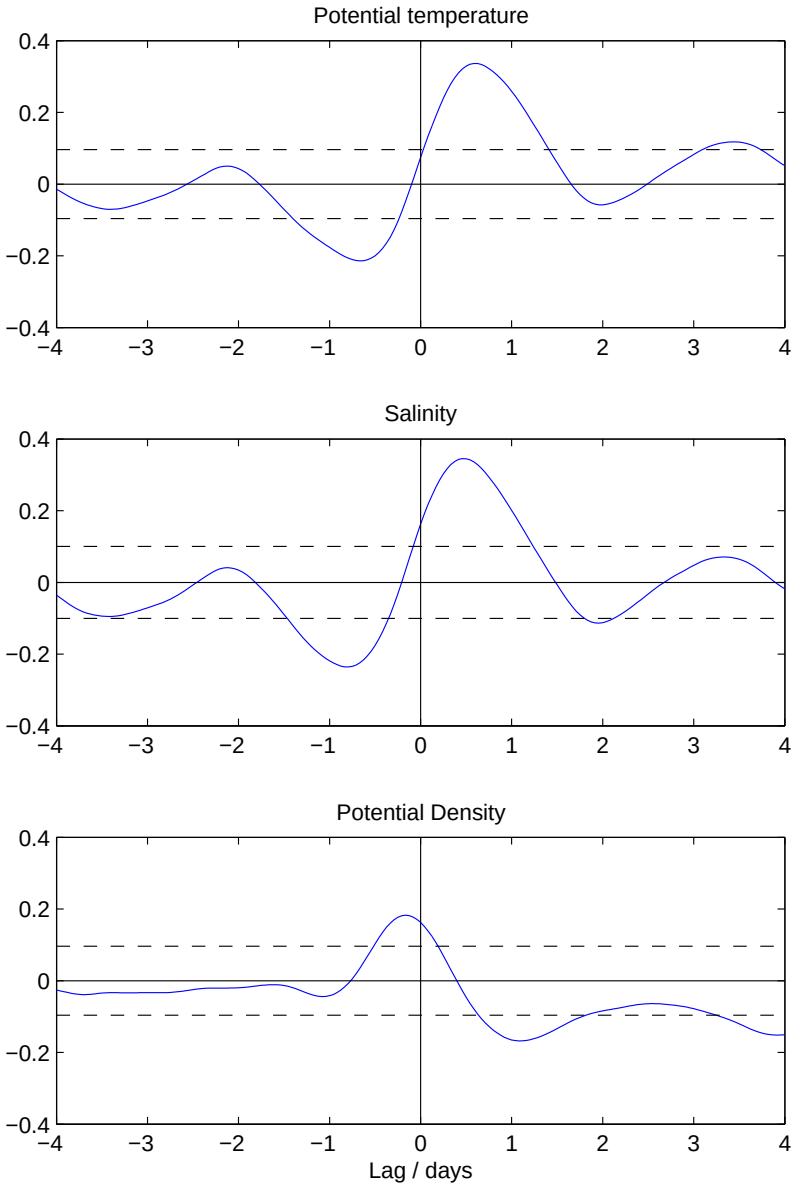

Figure 5.23: Lagged correlations of the depth mean potential temperature (top), salinity (middle) and potential density (bottom) with the depth mean cross stream velocity. The dashed lines indicate the 95% confidence intervals.

rier winds is that the horizontal resolution of ERA-Interim (80 km) is good enough to accurately resolve their spatial extent and magnitude. Although scatterometer data are available for the period that the mooring was in the water, these products don't provide data above partial sea ice which could be potentially important for the forcing of the ocean through the winter months.

5.5.1 Potential impact of barrier winds

Barrier winds are strong and coast parallel (Moore and Renfrew, 2005). The direction of flow, with the coast to the right, make them downwelling favourable winds. This means that the winds should drive Ekman transport onshore in the surface layer. Due to the presence of a coastline, the onshore directed flow will cause a positive sea surface height (SSH) anomaly to form at the coast and drive an offshore flow below the surface layer. Thus, the along shore winds should set up a cross stream, baroclinic transport cell with surface waters being transported onshore and water below transported offshore. This mechanism therefore becomes a candidate by which dense water residing on the outer shelf can be transported offshore and subsequently form the Spill Jet. Another impact of the coastal SSH anomaly is that it will set up an along stream (downwind), geostrophic balanced current (Allen, 1980). This should be barotropic in nature, but in practice is often surface intensified (Pickart et al., 2011) or otherwise due to particular stratifications. Not only will this SSH anomaly induce an along stream anomaly due to local winds, but the SSH anomaly will tend to propagate along the shelf with the coast to the right as a 1st mode barotropic shelf wave (Allen, 1980; Mysak, 1980; Brink, 1991). These modes are very fast and can travel at speeds on the order of a few hundred kilometres per day (Pickart et al., 2011). The result is an along stream velocity anomaly signal induced at locations downstream of the wind forcing region. This has potentially important implications for the velocity measured by the EG1 mooring. As has been shown in Chapter 2, barrier winds can occur all the way along the southeast coast of Greenland, both locally at the mooring site and often upstream, north of the Denmark Strait region. The EG1 mooring is therefore likely to measure along stream velocity signals from barrier winds that impact the coast both locally or many hundreds of kilometres upstream.

Returning to the local downwelling model, the two dimensional onshore-offshore response described above will have a similar coast perpendicular width to that of the wind forcing. This means that the barrier winds that force this kind of response at the mooring site need to be at least the width of the shelf – at our particular location on the order 100 km. The upstream length scale of the wind forcing is also important. The coastal SSH anomaly set up by the surface onshore flow will tend to propagate down the shelf with the coast to its right as described above. Similarly at the back end of region of wind forcing, the lack of a SSH anomaly will also propagate into the region of wind forcing. This will have the effect of degrading the coastal SSH anomaly and the associated offshore flow at depth (Allen, 1976). Essentially, the propagation of this signal is informing the wind forced region of the finite upstream extent of the wind. Hence the region in question makes a transition from a two dimensional state to a three dimensional one. The upstream

extent of the wind is therefore important in determining how long the wind forced region experiences the two dimensional response that may be associated with the spilling of dense water off the shelf.

The responses that might be expected to be seen in the EG1 velocity data are therefore:

- A two dimensional Ekman response for wide and long, local barrier winds.
- Along stream anomalies associated with barrier winds at any location along the coast upstream of the mooring site.

5.5.2 Barrier wind overview

A detection routine similar to that used in Chapter 2 for the climatology of barrier winds was employed here, with a couple of small differences. Firstly, instead of a box method for finding barrier winds, the wind record at the nearest grid point to the mooring was used. It is presumed that if a high velocity wind event were detected at this grid cell it is likely to extend onshore as well and therefore the width criterion for seeing a 2D response is met. Secondly, for this study it is the along shore component of the winds that will have the impact on the ocean, so instead of applying a directional criteria to the wind velocity time series, the velocity at the nearest grid cell was rotated into an along coast direction of 60°N. This has the additional benefit of being able to see the times when the winds are not only weak but even in the reverse direction to the prevalent barrier wind flow. A lower wind speed threshold was also used to increase the number of events detected in a single year. The complete barrier wind detection routine can be described as follows:

- The 10-m velocity time series from the nearest ERA-Interim grid point to the mooring array was selected.
- The component of the wind in the along coast direction of 60°N was computed.
- Barrier wind events were defined as maxima in this time series greater than 15 $\mathrm{m\,s^{-1}}$ and separated in time by at least 24 hours.

The results of this detection routine are shown in Figure 5.24. In total, 49 events were detected, equivalent to one a week. It is clear though, that many of the strongest events occur in the winter months and there are many more events between September and May than there are in the summer months. Times when the wind is weak and directed up the coast in the opposite direction to barrier winds are also apparent.

The composite image of the 10-m wind field for the 49 detected barrier winds (Figure 5.25) shows a picture typical of barrier winds in the region. A low pressure system is

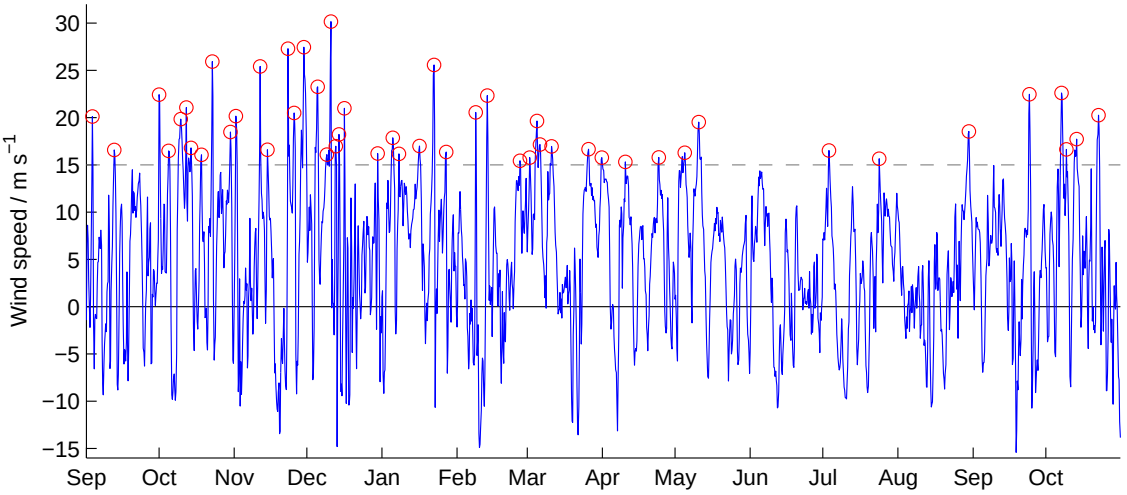

Figure 5.24: Along coast 10-m wind velocity from the nearest ERA-Interim grid point to the EG1 mooring location. Detected barrier winds shown with red circles and the threshold velocity for barrier wind detection shown as dashed grey line.

located in the central Irminger Sea with a depth of 986 hPa. This low directs air towards the southeast coast of Greenland into a composite barrier wind of strength 22 m s^{-1} at its maximum over the mooring site. The composite barrier wind is wide enough to cover the whole shelf region. As can be seen, the barrier winds for the year that the mooring was deployed are strong and frequent suggesting a high chance of detecting a response in the ocean.

5.5.3 Evidence for ocean impact of barrier winds

Evidence for some of the expected ocean impacts will now be presented. Looking first at local winds, it is hard to find specific examples of a local wind which produces the expected 2D Ekman response in the ocean. The reason for this is because, as previously shown, the velocity record at the mooring site is dominated by rotational signals from eddies. Presuming, to start with, that we can simply sum the flow patterns from the wind and the eddies, the 2D wind response would often be hidden by an eddy, potentially only manifesting itself as a 'more baroclinic' eddy.

The correlation of the local wind velocity record (shown in Figure 5.24) with the along and cross stream velocities is shown in Figure 5.26. Looking first at the cross stream correlations (bottom panel) the expected 2D structure can be seen. There is significant positive correlation between the alongshore wind velocity and the near surface cross stream velocity and a significant negative correlation at the shelf base. This implies that during periods of stronger wind there is onshore flow at the surface and offshore flow

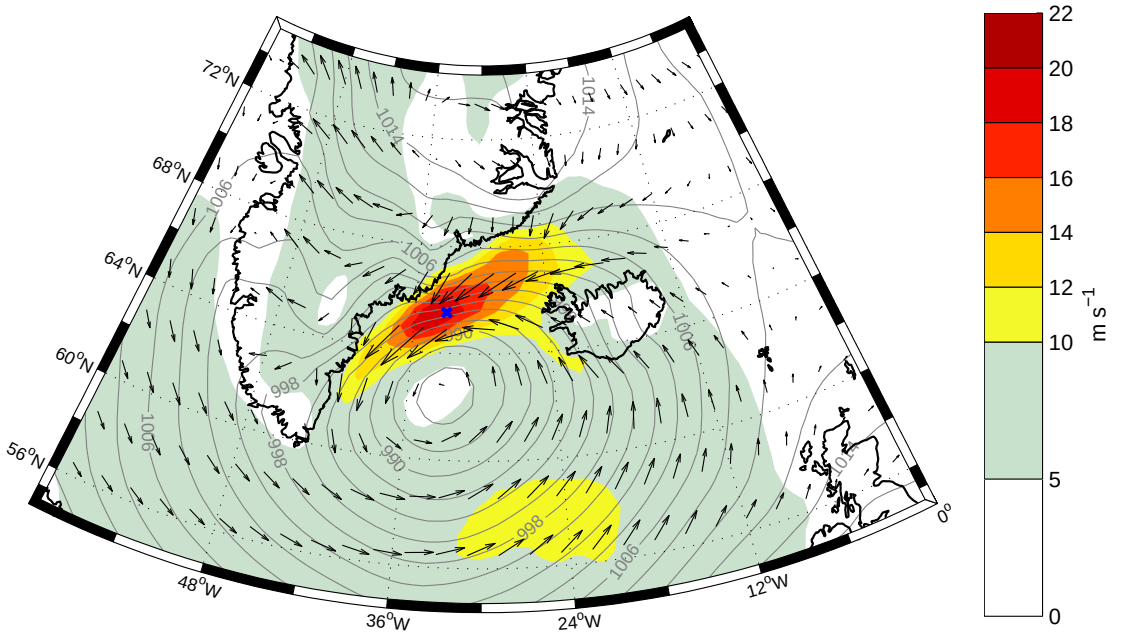

Figure 5.25: Composite of the 10-m wind speed from the 49 barrier winds detected at the location of the EG1 mooring from the ERA-Interim dataset. The composite mean sea level pressure (contours) is shown every 2 hPa and the composite wind vectors are plotted at every third grid point. The EG1 mooring location is shown with a blue cross.

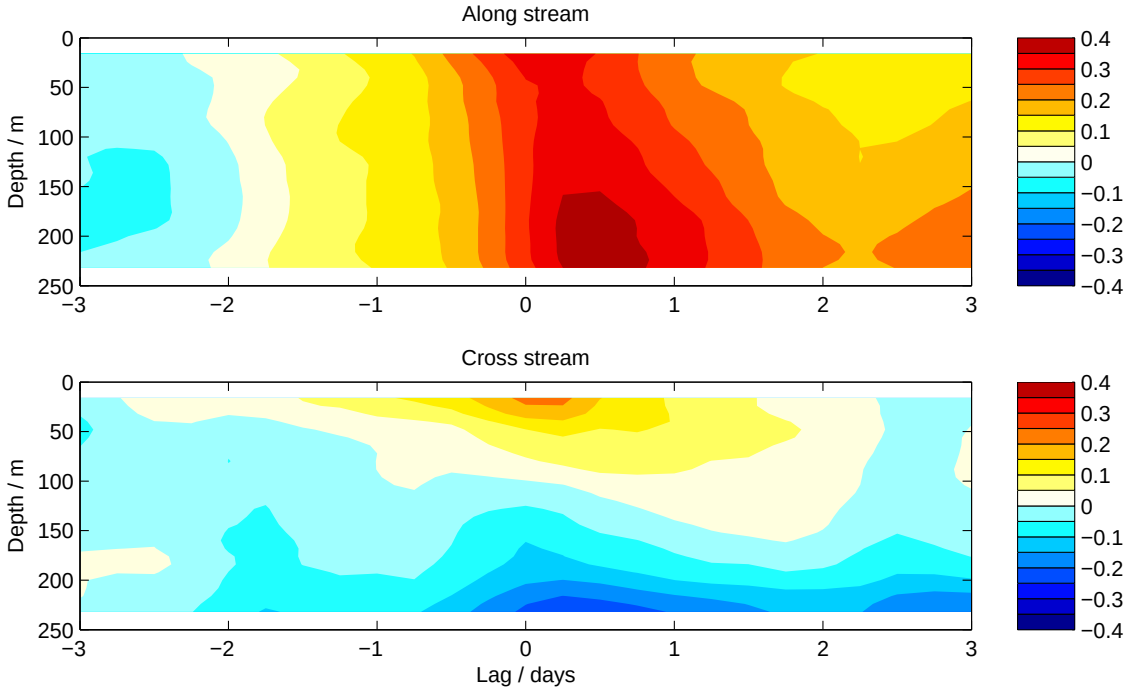

Figure 5.26: Lagged correlation of the along coast wind velocity (Figure 5.24) with the along (top) and cross (bottom) stream velocities.

at depth. The onshore flow correlation has its maximum at zero lag showing that this

process happens in phase with the wind. The return flow at depth comes after a slight lag of approximately eight hours. This is consistent with the time required to set up this return flow after the surface water has established the SSH anomaly at the coast, which should be on the order of an inertial period [on the order of half a day at the latitude of the mooring site (Webster, 1968)]. Hence, using this correlation approach, it seems that the barrier winds local to the mooring are clearly capable of producing the 2D wind response as expected. The reason why the correlations are reasonably weak is that there is a great deal of variability in the cross stream flow not explained by winds which can be attributed to eddies or other processes.

The along stream velocity lagged correlations (top panel) shows a strong, positive along stream correlation at all depths which is slightly intensified at a lag in the lower water column. This is likely the signature of the along stream flow set up at the coast due to the geostrophic adjustment process, which also happens on the inertial time scale. All the correlation signatures presented are statistically significant at 95 % confidence.

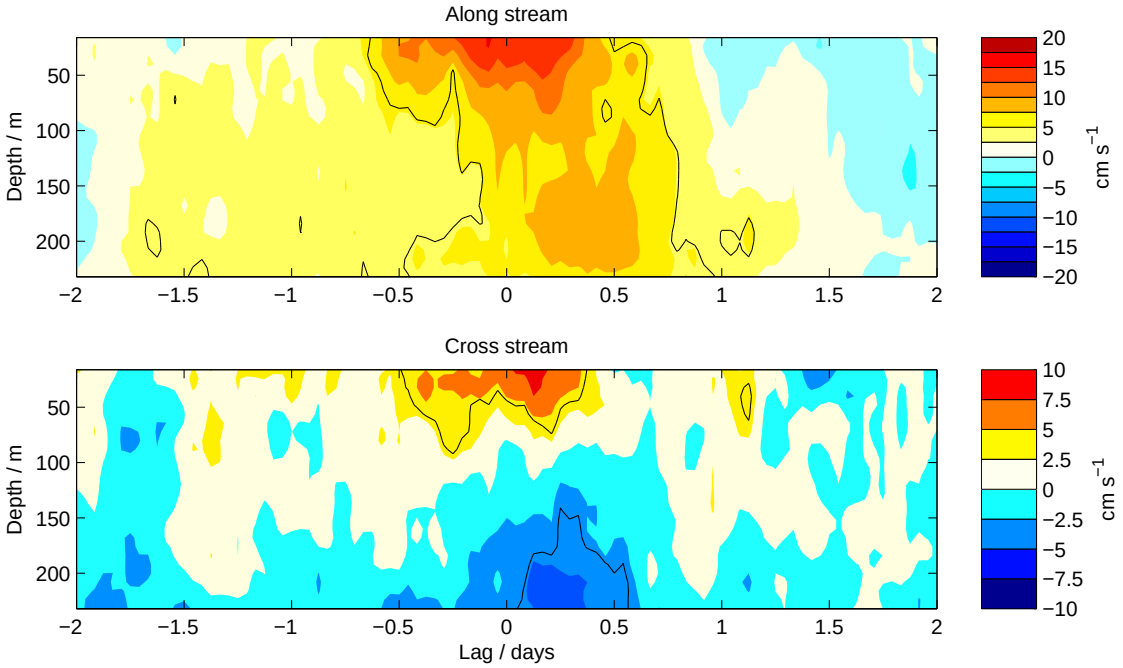

Figure 5.27: Lagged composites of along (top) and cross (bottom) stream velocity anomalies (relative to the year long mean) centred on the times of detected barrier winds shown in Figure 5.24. 49 events went in to the composite. The black contour indicates the regions which are statistically significant at 95% confidence.

To get a better idea of the magnitude of this 2D response induced in the ocean, lagged ocean composites were calculated for the times of the barrier wind events highlighted in Figure 5.24. A similar pattern to that shown in the correlation plots appears in these composites of velocity anomalies (Figure 5.27). In the cross stream direction there is an

onshore flow of nearly 10 cm s^{-1} near to the surface and a return flow at a slight lag near the bottom. This return flow is weaker than the surface onshore flow, with a magnitude of 6 cm s^{-1}, but exists over a deeper layer. In the along stream direction, there is an acceleration of the flow throughout the water column but, in contrast to the correlation plots, this is surface intensified. Again this is consistent with the build up of a SSH anomaly at the coast. This figure gives us a quantitative estimate of 15 cm s^{-1} for the magnitude of shear that is introduced to the cross stream flow during a barrier wind event.

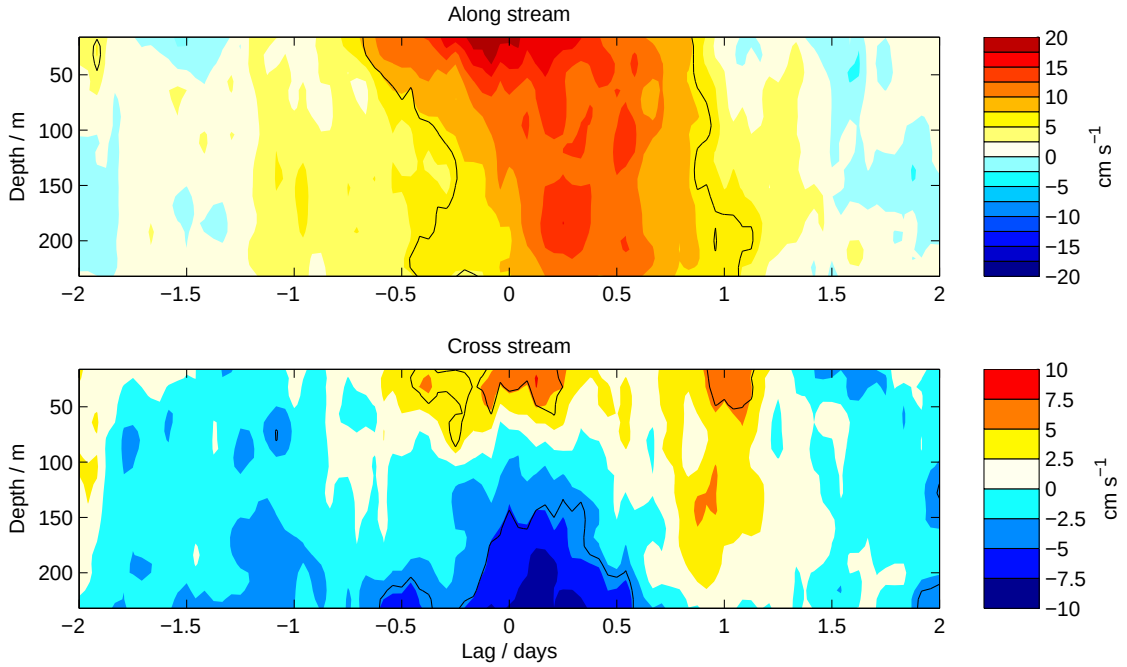

Figure 5.28: As Figure 5.27 but for a subset of local barrier wind events that also have coincidental winds stronger than 12 m s^{-1} at a location in Denmark Strait (67.7°N 25.3°W), approximately 900 km upstream of the EG1 mooring. 33 events went in to the composite.

This composite can be further enhanced by considering only those local barrier wind events that are also coincidental with a strong wind upstream. This is tantamount to only compositing the long barrier wind events and, as described previously, should be representative of events that maintain the 2D Ekman downwelling configuration for a longer time. An upstream threshold of 12 m s^{-1} was imposed at a location that was approximately 400 km upstream in the Denmark Strait at 67.7°N, 25.3°W. As a result of this subsampling of events, 15 low velocity upstream events were removed leaving 33 events in the composite which are shown in Figure 5.28. Both the along stream flow and the cross stream shear have been increased. This is in line with theory which states that longer barrier winds will be able to set up a longer lived (and hence stronger) along stream anomaly associated with the coast SSH anomaly. The 2D Ekman cell will also be stronger and longer (as observed) due to the lack of degradation of the SSH anomaly by

the signal from the back end of the storm. The onshore surface flow is the only part of the composite that has weakened through subsampling barrier wind events in this way. If the events that have weak upstream winds are used to make a composite (not shown), the 2D signal disappears altogether. These subsampling exercises give weight to the notion that what is being seen in Figure 5.27 is a 2D Ekman downwelling signal superimposed onto the mean flow.

It is of course possible that a stronger 2D response than observed could be seen for barrier winds because of two factors. Firstly, the wind data is given only every six hours compared to the ocean velocity data which is hourly. This could cause a degree of blurring in the timing of the resulting ocean response as a peak in wind speed could be wrongly located in time by up to six hours. Secondly, the method used only takes the times of peak winds and doesn't take in to account the range of timescales of the winds. Some winds ramp up quickly, others drop off quickly after they reach their peak and others maintain a reasonably strong flow for many hours. These differing characteristics of the winds are likely to play a role in the response of the ocean, but unlike the first point, it is unclear whether incorporating this information in some way would increase or decrease the composite response seen.

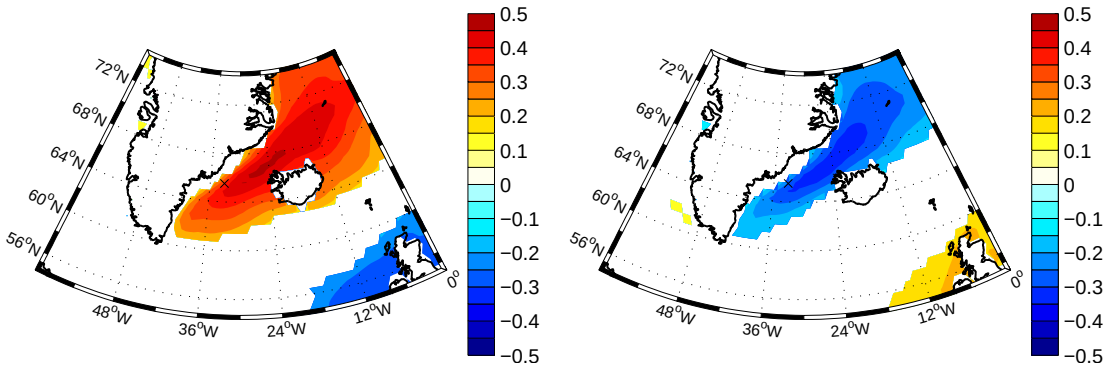

Figure 5.29: Maximum of the lagged correlations of the along coast wind velocity at all points in the domain with the depth mean along stream velocity (left) and the bottom cross stream velocity (right). Only correlations which are significant at 95% are shown. The black cross indicates the location of the EG1 mooring.

There is clearly a 2D downwelling response observed in conjunction with local winds, but is there evidence of an impact from winds upstream of the mooring? The left panel of Figure 5.29 shows the maximum of the lagged correlations between the along coast wind velocity at every point in the ERA-Interim domain with the depth mean along stream current velocity at the mooring site. As can be seen, the region where the wind has maximal correlation with the along stream velocity lies in a thin strip running from the mooring array upstream, through the Denmark Strait. The maximum correlation is 0.45, located

near to the central Denmark Strait. It is expected that along stream velocity anomalies at the mooring site are associated with a SSH anomaly either generated locally or propagated into the region from a wind disturbance upstream. There should be no impact on the velocities at the mooring site for a wind that occurs downstream of the mooring. This explains why the largest correlations are found extending upstream from the mooring site. The maximum in the Denmark Strait probably reflects that this location picks up most of the wind signals, both local and non-local which contribute to the along stream anomalies at the mooring site. The line of maximum correlation is centred offshore of the mooring and there is insignificant correlation onshore of the mooring site. This probably reflects the fact that the width of the wind generated SSH anomaly is controlled by the width of the wind; a wind signal must exist at the shelf edge (as well as onshore of this) for any effect to be seen at the mooring.

A similar figure for the depth mean cross stream velocity (not shown) yields only weakly significant correlations without any clear pattern. This implies there is no significant barotropic cross stream impact of the winds in agreement with the correlations and composites presented in Figures 5.26 and 5.27. A pattern is clearly seen, though, if only the cross stream flow at the bottom of the velocity record is used (right panel in Figure 5.29). Apart from the change in sign of the correlations (increased offshore flow is negative) the pattern is largely similar to that for the depth mean along stream flow. The maximum correlation is -0.33 located slightly north of the Denmark Strait. This means that when there is a wind along the coast upstream of the mooring, there is not only an along stream velocity set up at the mooring, but an offshore bottom current induced as well. This is in accordance with the first mode EOF (Figure 5.16) which showed that along stream barotropic velocity anomalies are associated with an increase in baroclinicity in the cross stream flow resulting in a bottom intensified offshore flow. The fact that the time series for this mode is well correlated with the wind velocity up the coast gives some confidence that some of the variability in this mode is associated with barrier winds. It is possible that the increase in baroclinicity is the result of the 2D Ekman flow shown to be in existence. A similar correlation map to those in Figure 5.29 was produced for the surface onshore flow (not shown), which showed weaker correlations centred around the mooring site – indicative of local forcing. A similar pattern to that seen in Figure 5.29 might be expected if the upstream signal were related to 2D Ekman downwelling and leads to the conclusion that there is probably a different mechanism at play.

To see this upstream influence in greater detail, Figure 5.30 shows the composite image from the 59 barrier wind events detected at a location in the Denmark Strait, 400 km upstream of the mooring (67.7°N, 25.3°W). It has lost much of the onshore flow associated with the local wind forcing, but clearly has both of the other features described

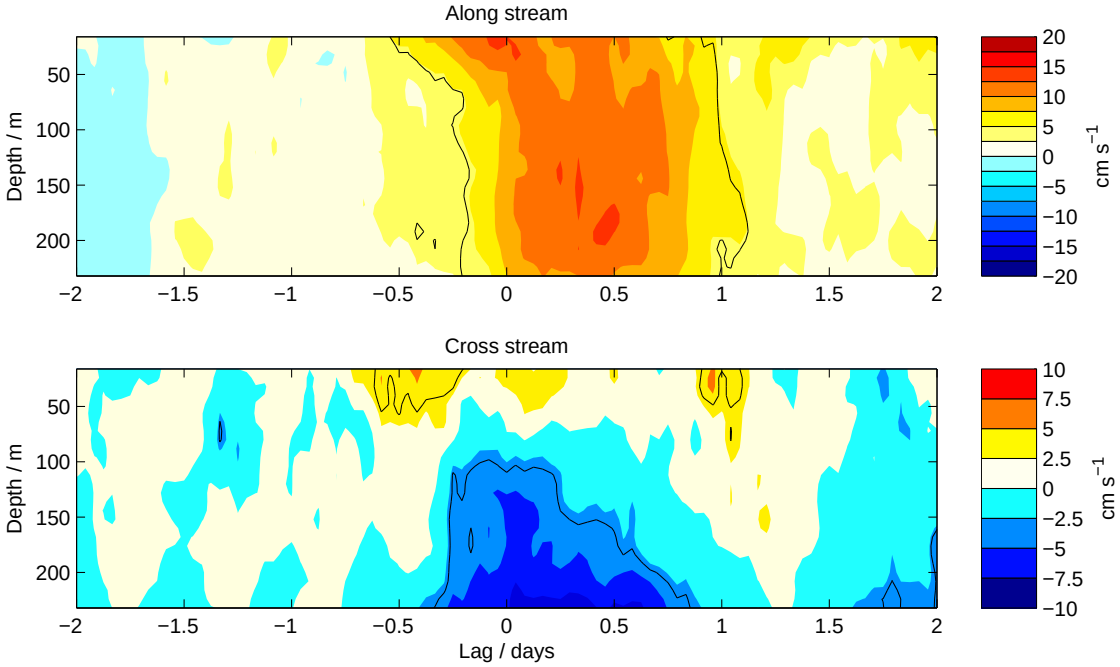

Figure 5.30: As Figure 5.27 but for a location in Denmark Strait at 67.7°N 25.3°W, approximately 900 km upstream of the EG1 mooring. 59 events went in to the composite.

previously – that is, a strong barotropic along stream current and a slightly leading bottom intensified offshore flow. When this set of events was subsampled for those that were coincidental with weaker winds local to the mooring (and hence should show only a weak 2D Ekman downwelling signature) the structure was largely unaffected. This is further evidence that the features shown in Figure 5.30 are not necessarily indicative of 2D downwelling, but potentially represent another process entirely. It also indicates that the larger response seen in Figure 5.28 for long local barrier winds might include both local downwelling and this new upstream effect. Possible explanations are explored in the discussion (Section 5.7.1).

5.6 Spilling

It has been shown that there is bottom intensified offshore flow in the mean (Figure 5.12). Figure 5.31 shows the time series of the cross stream velocity for the lowest bin in the ADCP data at a depth of 232 m. There is clearly an offshore flow in the mean, but the velocity is quite variable around this mean. These offshore anomalies shall be equated to 'spilling' even though it is possible they may not go on to actually contribute to the Spill Jet. The magnitudes of these flows, the proximity to the shelf edge (10 km) and the presence of water dense enough for the Spill Jet makes this a reasonable assumption.

The spilling appears to be episodic in nature with times of offshore flow with magnitudes larger than 50 cm s^{-1}. The wavelet spectra of this time series (not shown) is similar to that of the depth mean cross stream velocity (Figure 5.19) in that most of the energy in the signal has a period of between one and three days. As this was previously attributed to eddies, this indicates that eddies are important in producing the higher frequency variations seen in Figure 5.31 and hence the episodic nature of spilling.

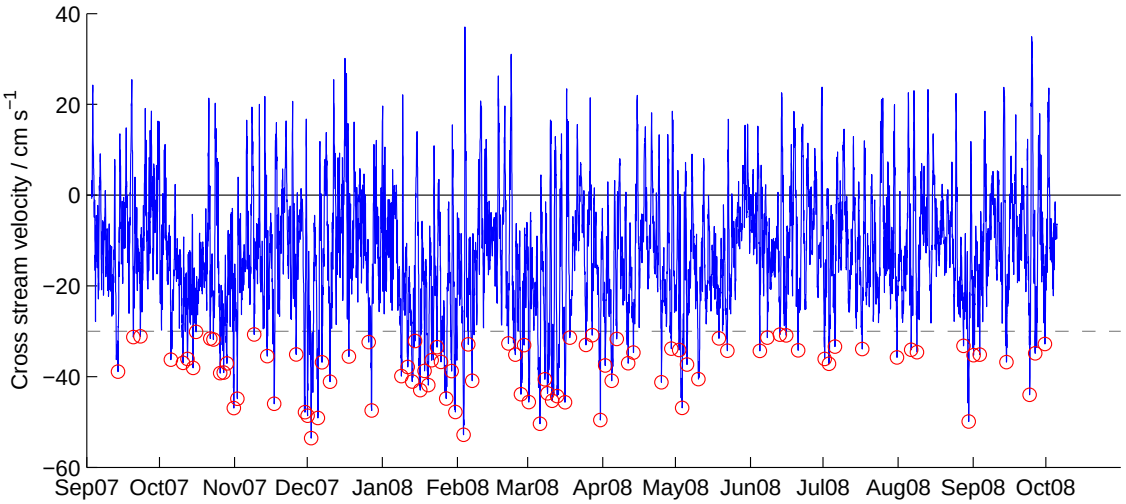

Figure 5.31: Cross stream velocity from the lowest ADCP bin at a depth of 232 m. Detected spilling events are marked with red circles and the threshold for spilling event detection (30 cm s^{-1}) is shown with a dashed line.

5.6.1 Spilling detection

To examine the spilling events in greater detail, a spilling detection method similar to that used for barrier winds was employed on the bottom bin cross stream velocity shown in Figure 5.31. The detection criteria for a spilling event is that the magnitude of the bottom cross stream velocity must be larger than 30 cm s^{-1}, directed offshore and separated from another spilling event by at least 24 hours. If two events are detected less than 24 hours apart, the larger of the two events is chosen. 92 events were found by this detection method and they are marked in Figure 5.31 by red circles.

An additional constraint was considered which required the density of the bottom Microcat to be greater than 27.7 kg m^{-3} (which is the typical density of the Spill Jet water (Pickart et al., 2005; Brearley et al., 2012). Only 23% of the 92 events are discarded if this criteria is used. Since it has been seen that there is reasonably dense water at all times on the shelf (probably denser than that found directly offshore at this depth) and there is nearly no correlation between cross stream flow and density, this was deemed an

unnecessary additional criteria especially as the subsequent analysis is unchanged and a larger number of events was afforded for subsampling.

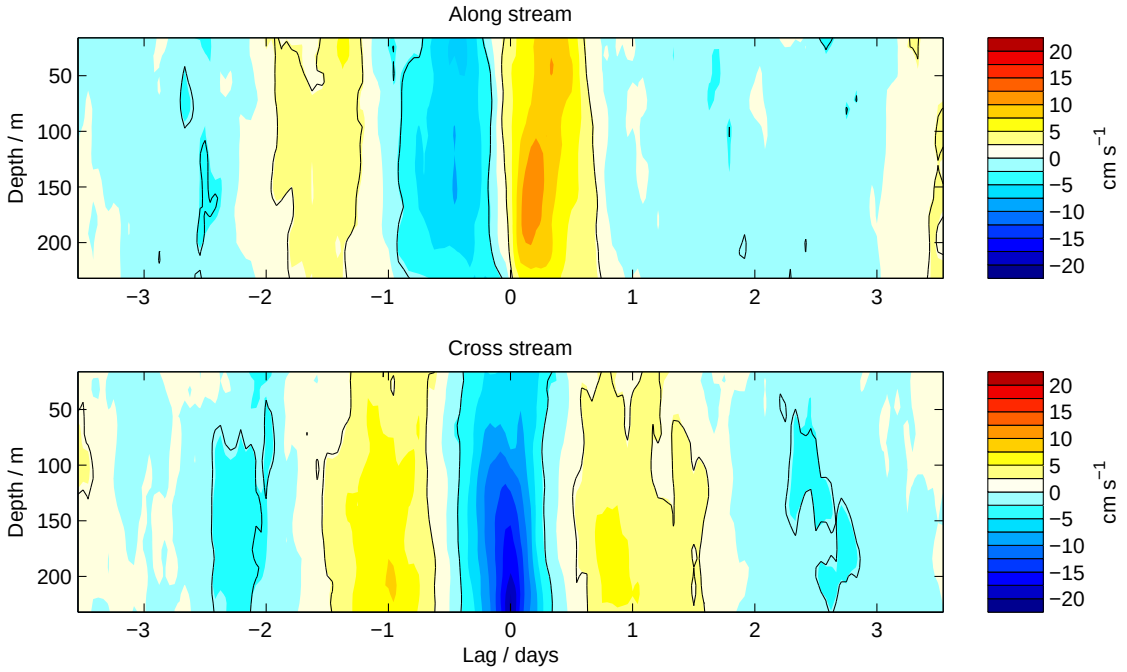

Figure 5.32: Lagged composites of five day high-passed along (top) and cross (bottom) stream currents from the times of the 92 events shown in Figure 5.31. The black contour indicates regions which are significant at 95%.

5.6.2 High frequency variability

Lagged composites of the along and cross stream velocity anomalies (relative to a 5 day running mean calculated at every depth) for the times of all detected spilling events are shown in Figure 5.32. These show the unmistakeable patterns of an eddy. The offshore flow associated with the detected spilling feature is unsurprisingly the largest feature in the figures because at zero lag this is constrained to be large. On either side of this, both at positive and negative lags, is a sequence of positive and negative cross stream anomalies with a wavelength of about two days. This time period is consistent with that attributed to eddies previously. The along stream flow has a similar pattern of positive and negative anomalies with a similar wavelength but shifted a quarter of a wavelength ahead of the cross stream flow. This pattern describes rotational flow, without being specific over whether the flow is cyclonic of anticyclonic. This particular arrangement though can be more easily described as two cyclonic eddies (which start with an offshore anomaly) rather than an anticyclonic eddy with two half cyclonic eddies either side. Consistent

with the results presented earlier (Figure 5.21), it is assumed that the eddies are cyclonic in nature for the rest of the analysis.

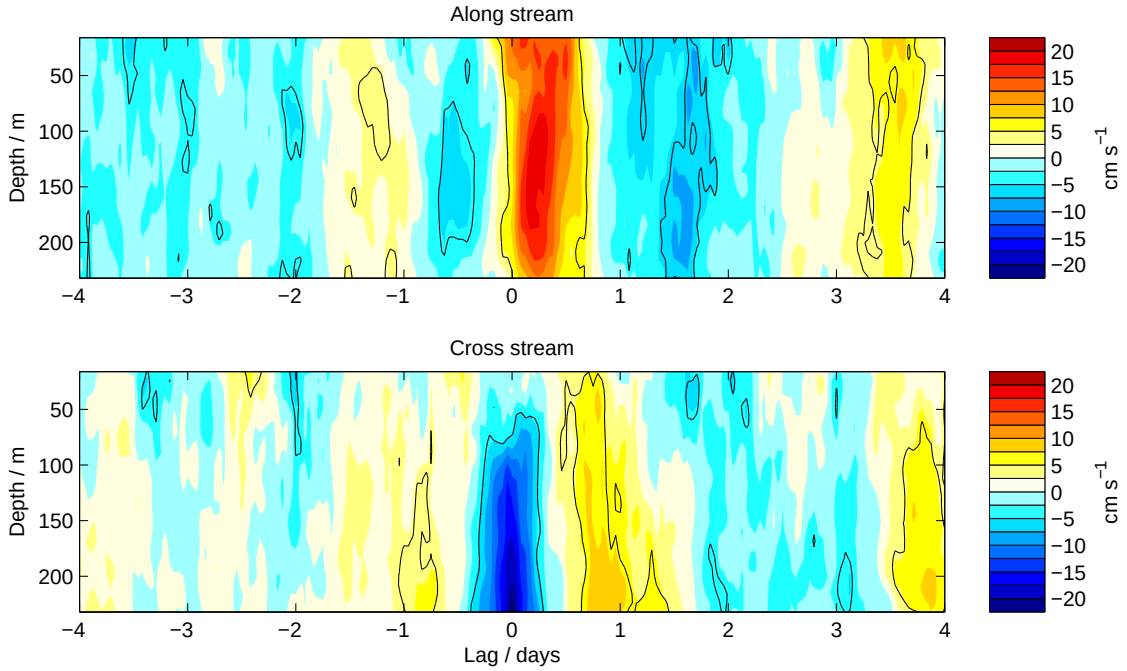

Figure 5.33: As Figure 5.32 but for the 23 events that occur at the same time as a local wind stronger than 12 m s^{-1}.

To further probe this pattern under slightly different conditions, the events were subsampled based on whether they occurred coincidentally with a strong or weak local winds. The strong wind threshold was 12 m s^{-1} which was the upper quartile of the wind velocities for the times of the spilling events which produced 23 events. The low wind criterion was that the magnitude of the wind velocity was less than 5 m s^{-1}, producing 28 events. The high wind speed composite (Figure 5.33) shows that when there is a strong local wind there is a larger offshore flow at the bottom and a high degree of baroclinicity in the cross stream flow. Both of these features are consistent with the 2D Ekman downwelling scenario (Figure 5.27) and also with the effects of an upstream wind (Figure 5.30). The along stream flow that succeeds the spilling is also much stronger in accordance with the along stream acceleration induced by the coastal SSH anomaly. The total significant pattern seen represents a single cyclonic eddy so even under high local wind speed conditions, the timing of the spilling is still dictated by the eddy. The wind appears just to amplify the effect of this single eddy by superimposing its effect on top. This shows that the local wind can force a single eddy to be able to produce some of the strongest spilling events.

When there are weak local winds the pattern is quite different (Figure 5.34). What becomes apparent is a long chain of eddies extending backwards in time from zero lag

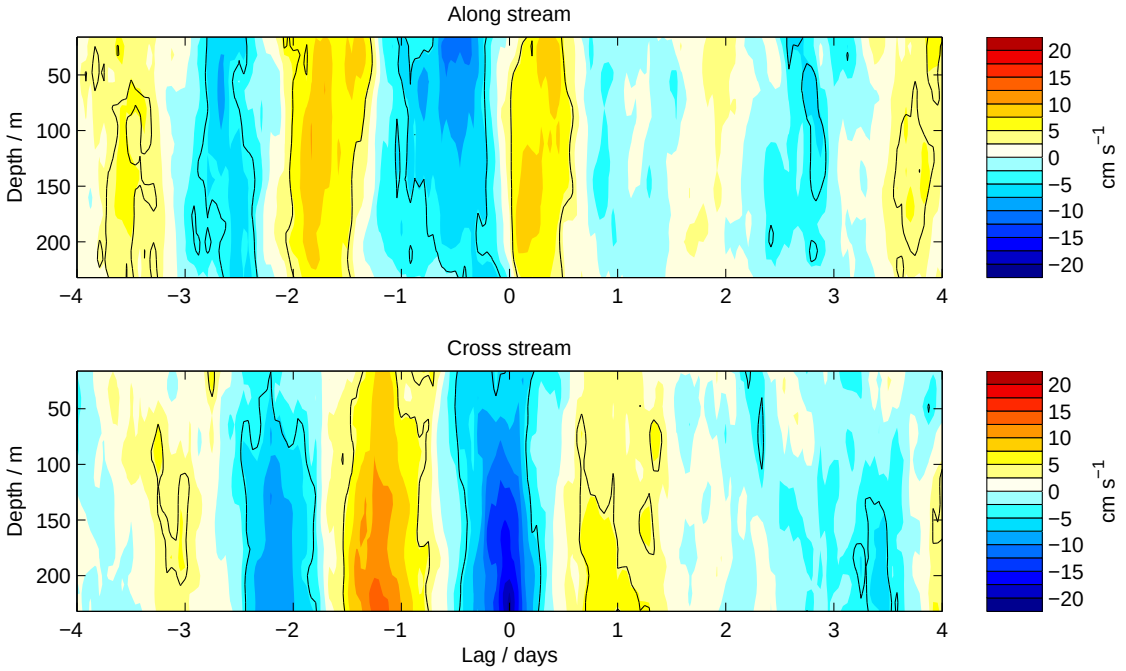

Figure 5.34: As Figure 5.32 but for the 28 events that occur at the same time as a local wind magnitude less than 5 m s^{-1}.

but not extending into positive lags. This implies that in the absence of local winds, a single eddy won't be strong enough to produce the strongest spilling events seen. Rather, it requires a chain of closely packed eddies preceding it in order for the spilling to be strong enough. It isn't known what precise mechanism allows this to occur, but some assistance is given from Figure 8 of Spall and Price (1998). The idealised simulations of Denmark Strait eddies presented show a complex flow field associated with a train of eddies, but there is evidence of an increased offshore transport for an eddy which follows closely behind another.

It should perhaps be noted that although the precise timing of spilling events has been largely attributed to eddies, there are likely to be other processes at play such as internal instabilities that will also lead to spilling as highlighted in Magaldi et al. (2011). These mechanisms may be hidden in the spilling composites by the good coherence of the eddy structures or they may be producing spilling in the region between the mooring and the shelf edge meaning they are missed entirely from the observational record.

5.6.3 Low frequency variability

It has been seen that eddies are responsible for much of the higher frequency variability in the strongest spilling events, but there is variability in spilling at scales larger than a few days as well. There are sustained periods of larger cross stream flow than average, for

example in January and early March, and also periods of reduced average cross stream flow, for example in mid February and early June. There is little change in the degree of variance between these periods (as seen from moving standard deviation analysis, not shown) indicating that the background flow doesn't significantly affect the scale of the eddy response seen in the ocean, but is merely superimposed on the eddy field.

It should be noted that the strongest spilling events detected all cluster at times of larger mean cross stream flow. This longer timescale variability is shown in Figure 5.35 which shows five day low-passed wind velocity from the upstream location used previously and the low-passed depth mean along stream and bottom cross stream velocities. Correlation coefficients between there three time series are shown in Table 5.1. As can be seen, the depth mean along stream velocity and the bottom cross stream velocity are very well anti-correlated. This is in accordance with the EOF analysis (Figure 5.16) which showed that the along stream barotropic signal had an associated cross stream flow at the bottom.

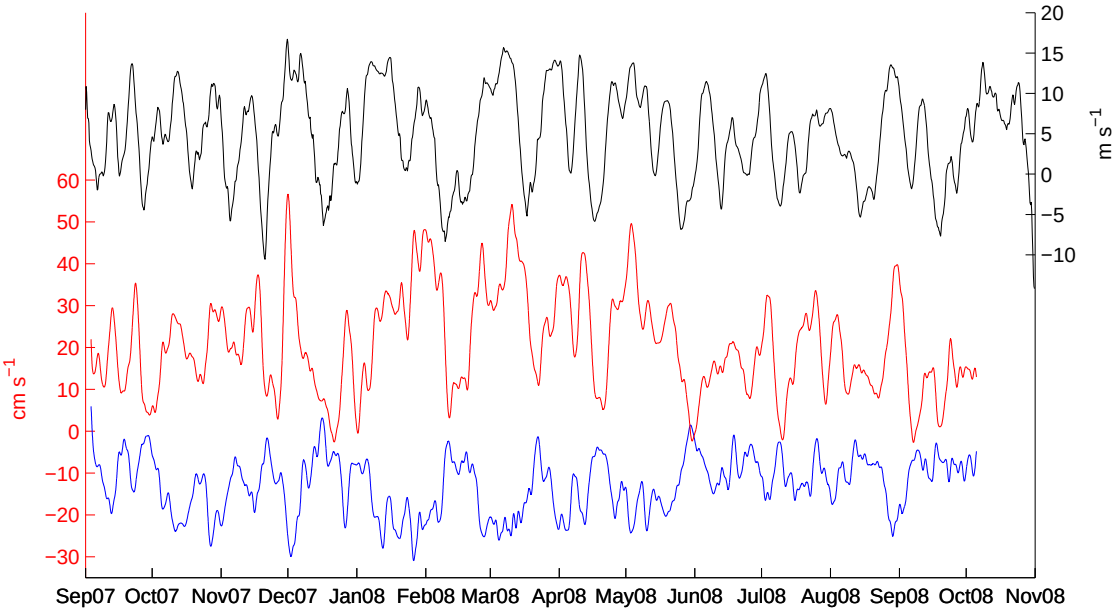

Figure 5.35: 5 day low-passed along coast wind velocity from 67.0°N, 24.6°W (black), depth mean along stream velocity (red) and cross stream velocity from the bottom most ADCP bin at 232 m (blue). The red axis on the left applies for both the red and blue lines.

As we have seen previously, the wind signal upstream of the mooring is correlated with the depth mean along stream velocity and the bottom cross stream velocity (Figures 5.29 and 5.30). Figure 5.35 shows this is the case, showing up strongly in the lower frequency components of the velocity signals. Very good correlations are found between the wind and these current velocities at lags in accordance with the typical time is would

take for this first mode wave to travel from the upstream location to the mooring site (of order one day). It also appears, at least from the timeseries presented, that the times when the wind velocity is negative is just as important as the times of positive flow for the modulation of along and cross stream velocities.

Variables	r	Lag / days
Depth mean along stream and bottom cross stream velocities	-0.68	-0.80
Wind velocity and depth mean along stream velocity	0.63	1.50
Wind velocity and bottom cross stream velocity	-0.58	1.75

Table 5.1: Table of maximum correlation coefficients between the time series shown in Figure 5.35. The lags recorded are positive (negative) if the first variable leads (trails) the second.

The timescale for individual wind events is often smaller than the threshold used for the low-pass (five days) so individual storms are unlikely to be resolved in this time series. Therefore what is shown is the average windiness of a period of time, i.e. times when there are either numerous or extended wind events. The impact seen on the ocean is thus similar, it is the cumulation of the impact of individual storms and how they impact the longer frequency variability of the ocean response. The impacts of the wind already discussed are to induce local downwelling and a barotropic along stream acceleration (with corresponding bottom intensified offshore flow). Both of these impacts will have times scales of less than 5 days, but are likely to be hidden by the variability due to eddies – the frequency bands for winds and eddies are likely to fall in the same range. It is only by looking at the wind effects averaged over a period of time, when at least the short timescale eddy signature has been removed, that we can see them. The nature of the correlation between the wind and the bottom cross stream flow (possibly via the along stream acceleration) is still unclear and will be discussed in the Section 5.7.1.

5.7 Conclusions and discussion

The EG1 mooring was deployed between September 2007 and October 2008 on the south-east Greenland shelf edge at 65.53°N, 33.15°N in 248 m of water. The hydrographic data from the mooring shows that, on average, the water on the bottom of the shelf has a density greater than 27.7 $\mathrm{kg\,m^{-3}}$, which is as dense as the water seen in previous Spill Jet observations (Pickart et al., 2005; Brearley et al., 2012). There is a degree of variability in the bottom density record, but no seasonal signal is observed. Above this bottom layer the water undergoes a seasonal cycle of densification and destratification in the winter and spring months and restratification through the summer.

The velocity measured by the mooring's ADCPs shows a yearlong mean profile which is along isobath in the central water column and veers offshore by 20° near the bottom where a climatological flow of over 25 $cm\,s^{-1}$ exists. The main modes of variability in the velocity record are an along stream barotropic oscillation, associated with a bottom intensified cross stream flow, and a cross stream barotropic oscillation without a coupled along stream mode. There is weak correlation between this latter cross shelf flow and temperature and salinity, consistent with some cross shelf advection of the IC and EGC waters past the mooring. This modest correlation, though, in conjunction with only a marginally significant correlation between the cross stream velocity and the potential density indicates that either the hydrographic front offshore of the shelf edge is poorly defined throughout the year, the cross stream flow doesn't last long enough to transport the IC-EGC front far enough over the mooring, or that the variability in the hydrography is influence heavily by isolated patches of water which have been transported to the 'wrong side' of the front upstream of the mooring.

Signals from eddies are readily apparent in the velocity record as a clockwise rotation of varying magnitude. These have a characteristic time of two days at the mooring site consistent with previous measurements of eddy radius and propagation speed. Eddies are strongest in the winter months, potentially due to the lower stratified water south of the Denmark Strait. This will induce a larger stretching of the mid-depth waters of the Denmark Strait overflow and spin up stronger eddies (Spall and Price, 1998).

Evidence of the ocean impact of barrier winds is also observed in the velocity record. Locally, winds produce a 2D Ekman cell consisting of onshore flow at the surface and a return flow offshore at depth on the shelf. Associated with this is the build up of a sea surface height (SSH) anomaly at the coast and a corresponding along stream geostrophic flow. The downwelling produces a mean offshore flow of 6 $cm\,s^{-1}$ per wind event. This effect is enhanced if the wind extends a long distance upstream of the mooring site.

Non-locally, winds can also set up SSH anomalies which propagate down the coast as a shelf wave to the mooring location. The barotropic along shore anomalies associated with these SSH anomalies appear to be accompanied by an increase in baroclinicity in the cross stream flow which manifests itself as a bottom intensified offshore flow. It seems unlikely that this process is representative of 2D downwelling because the configuration is seen to be strongest for winds which are located upstream and no onshore flow is seen at the surface in any composite or correlation analysis of upstream winds.

The precise timing of events which involve the offshore transport of water at the base of the shelf (which are equated to potential spilling events) were seen to be primarily controlled by eddies triggering the process on their leading edge. At times of strong local winds, an isolated eddy can produce a strong spilling event due to the superposition of

the wind signal over the eddy flow field. When there are no local winds, it appears that a train of closely packed eddies are needed to precede any particular eddy for some of the strongest events to be triggered.

There is a longer scale variability associated with spilling. Most of the strongest spilling events occur at times of strongest average along stream flow, themselves highly correlated to the winds upstream in the Denmark Strait. It therefore appears that upstream winds and the subsequent along stream anomalies which reach the mooring site are responsible for providing a mechanism for enhancing the spilling process. This is through the increase in offshore flow at the bottom associated with these along stream anomalies.

5.7.1 Discussion

If the bottom intensified offshore flow (associated with along stream anomalies) can't be explained through local downwelling then what other mechanisms could be at play? One explanation that can be discounted is that of a bottom Ekman layer. As the along stream anomaly is set up, bottom friction and the Coriolis force will act to cause a veering to the left (offshore) towards the bottom. The reason why this couldn't be a mechanism for this process is that in this scenario, the flow necessarily has to weaken towards the bottom – in the data, the magnitude of the flow during these events is greatest at the bottom.

It is likely that an along stream anomaly would have other secondary circulations associated with it. For example, at the front end of the anomaly would be a region of convergence in the along stream direction which would result in an offshore flow. In theory this outflow would be barotropic with a strength dependent on the degree of convergence at the front end of the anomaly. This may be playing a small part in the observed offshore flow, especially at times before the along stream anomaly arrives, but there is too much baroclinicity in the cross stream flow and much of it occurs at the same time as the along stream anomaly. It is therefore unlikely that the offshore flow can be attributed to such convergence. Additionally though, it has been shown that the local stratification is complex and varies seasonally. It could be that the precise form of the shelf wave's secondary circulations may be influenced by the local or upstream stratification.

Another potential explanation is the interaction of the along stream anomalies with the bathymetry, either locally or upstream. The southeast Greenland shelf varies greatly in width and depth, and has a number of other complex topographic features as shown in Figure 5.1. Features of potential importance to shelf waves in particular are the deep Kangerdlugssuaq trough which cuts the shelf upstream of the mooring with a depth of 1000 m, the widening of the shelf region through the Denmark Strait, and the lip in the shelf near the shelf break just onshore of the mooring. Probably one, or both, of improved

bathymetric data in the region or model experiments would be required to fully probe how these features would interact with an along stream current anomaly

The atmospheric configurations in this region are also complex and highly variable. Barrier winds can be centred at any location up the coast [although some are favoured over others (Moore and Renfrew, 2005)], their spatial and temporal scales are wide ranging, and they can transit up-coast, down-coast or remain stationary. All of these factors will influence the oceanic response, both through the degree of local downwelling and through the specific configuration, and secondary circulations, of any shelf waves which are excited. Again, it seems that modelling studies would be required to gauge, in particular, the exact structure of coastal waves excited by storms of varying scale and with different temporal evolutions. There are both not enough examples of different types of barrier wind and too many eddies in the system to probe this in any thorough way from the observational data.

The fact that the variance in the cross stream flow changes little between times of stronger and weaker mean cross stream flow indicates that the wind impact isn't to enhance the strength of the overall eddy. This information doesn't prohibit another potential mechanism by which winds could be influencing spilling – the along stream anomalies set up by the local and non-local winds could be distorting the flow pattern of an individual eddy making it more effective at spilling on its leading edge. The individual members of the upstream composites presented in Figure 5.30 will have eddies randomly superimposed on them which are averaged out in producing the composite. If the effect of the winds were to distort an eddy to produce more spilling this kind of effect would show up once all the events had been averaged in the composite and might explain some of the pattern seen.

There are multiple explanations that have been presented for the longer scale variability of spilling which seems to be controlled by the upstream wind. Which of these are important, and to what extent, will probably require modelling studies either in realistic or idealised domains. It is probable that a great deal could be learnt about the eddies, and the potential impact of winds on the eddy flow field, from the analysis of the complete mooring array. Such an investigation of the data from the full array is left to future work.

Chapter 6

Conclusions and discussion

Barrier winds off southeast Greenland have been examined through meteorological reanalysis, observations and numerical modelling (both realistic and idealised). An investigation has also been made into one potential ocean impact of barrier winds, the triggering of the East Greenland Spill Jet.

Climatology

A wintertime climatology of barrier winds off the southeast coast of Greenland has been conducted based on 20 years of ERA-Interim reanalysis data. Barrier winds were shown to be a frequent occurrence at two locations along the southeast coast of Greenland, one to the north and the other to the south of the Denmark Strait. These locations were called Denmark Strait South (DSS) and Denmark Strait North (DSN). In the winter months, events with wind speeds greater than 20 $\mathrm{m\,s^{-1}}$ were a seen on average once per week at both locations. It was shown that they were triggered by a synoptic cyclone with a centre on average directly to the south of the region of barrier wind formation. There was a degree of monthly and seasonal variability in the frequency of barrier wind events and it was shown that the monthly frequency of barrier winds correlated well with the monthly NAO index especially at DSN ($r = 0.57$). A higher NAO index is typified by more and deeper cyclones moving through the region capable of triggering more and stronger barrier winds. The reason for the especially good correlation at DSN is accounted for by the location of the centre of the composite cyclone for these events which lies directly over southwest Iceland, one of the centres-of-action of the NAO and the location of one of the stations used to define the NAO index.

Two-metre temperatures for the barrier wind events at both locations exhibited a large range which was typical of the climatological range in temperatures. In addition, the

median 2-m temperature was also similar to the climatological mean in each region. This shows that the barrier winds bring about no particular temperature regime – they can not be said to be typically warm or cold winds. One consequence of this large range in barrier wind temperatures was a large range in surface turbulent heat fluxes. The coldest barrier winds were capable of extracting up to 500 W m^{-2} from the ocean and the warmest winds actually provided a source of heat to the ocean.

Two classes of barrier wind were investigated – warm and cold – and were found to develop in very different synoptic environments. It should be noted that these classes are the extreme quartiles of a rather continuous distribution of temperatures. Warm barrier winds, which were smaller and more coastally confined, owed their presence to a blocking high pressure system over the Nordic Seas. This blocking high restricted the passage of the cyclone responsible for the barrier wind, inhibited the northerly advection of cold Arctic air down the east coast of Greenland and promoted strong southerly advection of warm, moist, maritime air into the barrier wind. The colder winds in contrast were characterised by a train of cyclones passing through the region, each drawing more cold, northerly air down the east coast of Greenland into a long and wide barrier wind. The implication is that to understand the ocean forcing during barrier wind events, one has to appreciate the much wider synoptic-scale environment.

Case study

Observational and numerical modelling data for a case study of one barrier wind event showed that the development of even a single barrier wind event can be complicated and highly variable both spatially and temporally. The barrier wind event in question occurred between 5 – 8 October 2008 and was shown to undergo two stages of development. The first of these involved a strongly onshore synoptic-scale flow which forced a barrier wind which was coastally confined with a complex spatial pattern of low-level winds that included a jet which detached itself from the coast. The temperatures during this period were higher than during any other time during the event, the result of strong southerly advection into the barrier wind. The second stage of development was associated with a reduction in the incident angle of the wind from the synoptic flow. This allowed for a longer, wider, less coastally-confined barrier wind to establish itself along the entire southeast coast of Greenland with core temperatures approximately 5 °C colder than in the barrier wind of the first stage of development.

Putting this individual event into the context of the climatology, the barrier wind was an example of a warm barrier wind. This was due to the warm temperatures observed, the strong coast perpendicular inflow and the localised, coastally-banked barrier wind that

was produced. In contrast, the barrier wind case studies of Petersen et al. (2009) were examined and similarities were seen between these cases and the cold barrier winds of the climatology – the core temperatures were much colder and the barrier winds were wider, longer and less coastally confined.

The existence of case studies from different ends of the temperature spectrum facilitated an examination of the degree in which the winds in each case were in geostrophic balance. It was shown that the barrier wind events of Petersen et al. (2009), the cold barrier winds, were much better described by geostrophy in comparison to the barrier wind event presented in this thesis which had large ageostrophic components that varied a great deal in both space and time. The suggestion is that barrier winds from the cold and warm classes could be forced by very different mechanisms.

Idealised modelling

Some insight into the forcing mechanisms for barrier winds has been provided through idealised experiments of unidirectional flow towards an isolated mountain with orography representative of Greenland. The first finding of this study was that the two regions of frequent barrier wind formation (DSS and DSN) as seen in the climatology were the result of the protrusions in Greenland's orography at these two locations. When the protrusions are smoothed out, the wind speed maxima disappear. Two mechanisms were then presented to account for the wind maxima seen in the idealised experiments at these locations. Firstly, the flow was observed to accelerate around the promontories due to the rapid reduction in pressure experienced due to inward undulation of the topography. This is very similar to the acceleration of a easterly tip jet around Cape Farewell. Secondly, mountain waves were observed for northeasterly flow along the southeast coast of Greenland. The result of these was strong downslope winds in the lee of the promontories enhancing the low level flow in these regions.

Some additional insight into the climatology and case study work was provided through examining the flow patterns from weakly and strongly blocked experiments. When the flow was weakly blocked, much of the flow could escape over the barrier and the resulting barrier wind spread upward over the slope region. The source of the air for these winds had a southerly component. When the flow was more strongly blocked the barrier winds were more confined below mountain height and channelled air from the north. These strongly blocked barrier winds were also centred offshore of the barrier. There are clearly comparisons that can be made between the weakly blocked winds and the warm barrier winds of the climatology and case study; equally, comparisons can be made between the strongly blocked winds and the colder barrier winds. This result suggests that other fac-

tors not discussed in the climatology such as static stability and upstream wind speed and direction could also be influential in determining the surface conditions in a barrier wind.

Ocean impact

The meteorological analysis presented in this thesis describes the atmospheric conditions above the water and provides a powerful motive for analysing the effect of these strong and frequent barrier winds on the underlying ocean. This was achieved through analysis of a year-long hydrographic and velocity data set from the southeast Greenland shelf break. An investigation was conducted into the mechanisms for the cross slope transport of dense water which spills off the shelf and forms the East Greenland Spill Jet, a significant pathway for dense water out of the Sub-Arctic. Barrier winds had been hypothesised as one mechanism for triggering this process because their direction of flow would be expected to force downwelling.

Waters as dense as those seen in previous Spill Jet crossings was found near the bottom of the shelf for much of the year without any clear seasonal cycle. At almost all times, the water at the base of the shelf was more dense than 27.7 $\mathrm{kg\,m^{-3}}$. The velocity record showed a strong shear – the near-surface flow travels coast-parallel, but the flow near the bottom veers offshore. This is the first evidence that near the shelf break there is dense water and it is transported offshore in the mean, confirming the hypothesis that the Spill Jet sources its water from the shelf.

As it had been established that a signature of spilling could be seen in the mooring data, potential mechanisms for spilling were then investigated. Denmark Strait eddies were prevalent in the velocity data as a strongly rotational signal with typical period of 1–2 days consistent with previous estimations of their radius and velocities. The leading (offshore directed) edge of the eddies had been previously proposed as a mechanism for the offshore advection of dense water and evidence of this process was indeed seen in the data. Denmark Strait eddies appeared to be particularly important in the high frequency variability of spilling.

The barrier winds also appeared to be influential in the offshore advection of dense water along the bottom of the shelf. Evidence of downwelling induced by local barrier wind events was seen as an onshore transport near the surface and a consequent offshore flow at depth on the shelf. In addition, a signal was also seen in the mooring velocity data from non-local wind events. This was due to the down-coast propagation of a shelf wave from upstream wind disturbances. The observed response at the mooring site was an along stream acceleration and a coincident offshore, bottom intensified flow. The precise mechanism by which the shelf waves were capable of triggering this offshore flow is still

not fully understood, but it is likely to be due to the complex bottom topography of the region or the precise wave dynamics associated with the particular stratification at the mooring site.

From the analysis of individual spilling events it was concluded that although eddies appear to be responsible for the high frequency variability in spilling, the barrier winds are hugely influential in the lower frequency variability.

Discussion

The atmospheric and oceanographic insights that this thesis provides into barrier winds and their impact progresses knowledge of these phenomena, but still leaves some open questions that will require future investigation.

From an atmospheric perspective, there is still much to learn about the dynamics of barrier winds both specifically around Greenland and at other locations around the world. The barrier winds described in this thesis are highly variable in space and time and have been shown to exhibit strongly ageostrophic behaviour in both realistic and idealised examples. Understanding these processes in greater detail will help numerical weather prediction models to accurately simulate barrier winds. Many open questions exist which include, for example, the effect of the atmospheric boundary layer, sea ice, mountain waves and internal cyclone dynamics on the formation mechanisms and consequent properties of barrier winds. The discovery of a potentially large downslope (offshore) wind component in the idealised modelling [along with any additional real-world katabatic forcing (Heinemann and Klein, 2002)] will have implications for the type of barrier winds produced. This is somewhat related to Alaskan barrier winds which were shown to form from the outflow of a cold pool of inland air (Olson et al., 2007; Olson and Colle, 2009). These barrier winds also exhibited large ageostrophic forcing and spatial and temporal variability. Any future work in describing the dynamics of barrier winds along the southeast coast of Greenland would have implications for the study of these winds off Alaska and at other locations worldwide.

A number of different ‘regimes’ for barrier winds have been investigated in this thesis including warm and cold, blocked and unblocked, and shallow and steep wind incidence angle. Although some connections between these process has been made, a concerted effort is required in order to fully understand the reasons for, and implications of, the barrier winds that form under these conditions. Considering the large range in possible surface conditions of barrier winds, depending on the synoptic environment, it appears very important that progress is made in this area. Again, this will have implications beyond Greenland be it through a better understanding of ocean forcing or in aiding the

development of theories about barrier winds around the world.

One example of barrier wind impact on the ocean has been presented, but there is still a great deal of scope for future work in this area. Even within the example given in Chapter 5 there are still open questions including the precise mechanisms for the shelf wave induced offshore flows and the degree of non-linear interactions between the ocean's response to eddies and wind forcing occurring simultaneously. Beyond this example, there are many other local processes that could be influenced by barrier winds such as the transfer of water between the Irminger and East Greenland currents, the export of sea ice and bergs along the Greenland coast and the production and fate of dense water upstream and locally to the Denmark Strait.

Given the potential importance of barrier winds for the ocean processes both locally and globally (not to mention their importance from a purely atmospheric perspective) it is perhaps pertinent to talk about the implications that a changing climate may have for barrier winds. There are a number of important changes predicted that will affect the formation and impact of barrier winds. Bengtsson et al. (2006) showed that over the course of the coming century, under a typical climate change scenario, there will be a reduction in the density and intensity of storms passing close to Greenland due to a southerly shift in the storm track. This will presumably have implications for the number and strength of barrier winds produced and the effectiveness of their impact on the ocean. For the example of the Spill Jet, it is possible that a reduction in barrier wind strength and frequency will mean a reduction in dense water transport out of the Sub-Arctic, although it is possible that another process for dense water transport may become more effective.

Another important implication of a changing climate is in the recent observed reduction in Arctic sea ice extent and the predicted further decrease over the coming century (IPCC, 2007). Although not explicitly discussed in any detail in this thesis, the impact of the sea ice on barrier winds has been shown to be important for the energy budget low down in the jet (Outten et al., 2009) and is likely to be significant for other factors including the heat and moisture content of the air and the consequent surface heat and momentum fluxes.

Greenland's ice sheet is melting rapidly, especially at its periphery (IPCC, 2007). The implications of this include a rise in global sea levels and the freshening of the North Atlantic, potentially leading to a reduction in the Meridional Overturning Circulation. Barrier winds are both important for the melting of the ice sheet and likely to be influenced by an increase in freshwater run-off. Straneo et al. (2010) showed that the impact of barrier winds is to force warm water up fjords along southeast Greenland, aiding the melt of glacial tongues and increasing the rate at which the glaciers flow into the ocean. As with changes to sea-ice concentrations, the freshening of the seas around Greenland is

likely to have an impact on the heat content of the upper ocean and hence the low-level heat and moisture content of barrier winds. The capping potential of the North Atlantic freshening is also likely to inhibit any barrier wind induced oceanic convection.

The resolution of current state-of-the-art coupled climate models (e.g. HiGEM (Shaffrey et al., 2009)) is probably still too low to sufficiently resolve realistic barrier winds in the atmosphere and hence their impact on the ocean. Many of the influenced ocean processes (e.g. the Spill Jet and the Irminger-East Greenland front) are also likely to only be marginally resolved. Work needs to be conducted to assess how barrier winds are represented in these climate models and perhaps suitable parametrisation schemes developed.

Research is therefore required to both fully understand the current barrier wind types, formation mechanisms and impacts, and to assess and improve how they are represented in climate models.

Bibliography

Aagaard, K. and E. C. Carmack, 1989: The Role of Sea Ice and Other Fresh Water in the Arctic Circulation. *J. Geophys. Res.*, **94**, 14 485–14 498, doi:10.1029/JC094iC10p14485.

Allen, J. S., 1976: Some Aspects of the Forced Wave Response of Stratified Coastal Regions. *Journal of Physical Oceanography*, **6**, 113–119, doi:10.1175/1520-0485(1976)006<0113:SAOTFW>2.0.CO;2.

Allen, J. S., 1980: Models of Wind-Driven Currents on the Continental Shelf. *Annual Review of Fluid Mechanics*, **12**, 389–433, doi:10.1146/annurev.fl.12.010180.002133.

Andreas, E. L., P. O. G. Persson, R. E. Jordan, T. W. Horst, P. Guest, A. A. Grachev, and C. W. Fairall, 2005: Parameterizing the turbulent surface fluxes over summer sea ice. *In Eighth Conference on Polar Meteorology and Oceanography. American Meteorological Society. San Diego, CA.*

Barstad, I. and S. Grønås, 2005: Southwesterly flows over southern Norway-mesoscale sensitivity to large-scale wind direction and speed. *Tellus A*, **57**, 136–152, doi:10.1111/j.1600-0870.2005.00112.x.

Bell, G. D. and L. F. Bosart, 1988: Appalachian Cold-Air Damming. *Monthly Weather Review*, **116**, 137–161, doi:10.1175/1520-0493(1988)116<0137:ACAD>2.0.CO;2.

Bengtsson, L., K. I. Hodges, and E. Roeckner, 2006: Storm Tracks and Climate Change. *J. Climate*, **19**, 3518–3543, doi:10.1175/JCLI3815.1.

Berrisford, P., D. Dee, M. a. P. Fielding, K. Fuentes, S. Kobayashi, and S. Uppala, 2009: ERA Report Series: 1. The ERA-Interim Achive. Tech. rep., European Centre for Medium-Range Weather Forecasts.

Blender, R., K. Fraedrich, and F. Lunkeit, 1997: Identification of cyclone-track regimes in the North Atlantic. *Quarterly Journal of the Royal Meteorological Society*, **123**, 727–741, doi:10.1002/qj.49712353910.

Braun, S. A., R. Rotunno, and J. B. Klemp, 1999: Effects of Coastal Orography on Landfalling Cold Fronts. Part I: Dry, Inviscid Dynamics. *Journal of the Atmospheric Sciences*, **56**, 517–533, doi:10.1175/1520-0469(1999)056<0517:EOCOOL>2.0.CO;2.

Brearley, J. A., R. S. Pickart, H. Valdimarsson, S. Jonsson, R. W. Schmitt, and T. W. Haine, 2012: The East Greenland boundary current system south of Denmark Strait. *Deep Sea Research Part I: Oceanographic Research Papers*, **63**, 1–19, doi:10.1016/j.dsr.2012.01.001.

Brink, K. H., 1991: Coastal-trapped waves and wind-driven currents over the continental shelf. *Annual Review of Fluid Mechanics*, **23**, 389–412, doi:10.1146/annurev.fl.23.010191.002133.

Bruce, J. G., 1995: Eddies southwest of the Denmark Strait. *Deep Sea Research Part I: Oceanographic Research Papers*, **42**, 13–29, doi:10.1016/0967-0637(94)00040-Y.

Chelton, D. B., M. H. Freilich, J. M. Sienkiewicz, and J. M. Von Ahn, 2006: On the Use of QuikSCAT Scatterometer Measurements of Surface Winds for Marine Weather Prediction. *Monthly Weather Review*, **134**, 2055–2071, doi:10.1175/MWR3179.1.

Chen, W.-D. and R. B. Smith, 1987: Blocking and Deflection of Airflow by the Alps. *Monthly Weather Review*, **115**, 2578–2597, doi:10.1175/1520-0493(1987)115<2578:BADOAB>2.0.CO;2.

Colle, B. A. and C. F. Mass, 1995: The Structure and Evolution of Cold Surges East of the Rocky Mountains. *Monthly Weather Review*, **123**, 2577–2610, doi:10.1175/1520-0493(1995)123<2577:TSAEOC>2.0.CO;2.

Cooper, L. H. N., 1955: Deep water movements in the North Atlantic as a link between climatic changes around Iceland and biological productivity of the English Channel and Celtic Sea. *Journal of Marine Research*, 347–362.

Cui, Z., M. Tjernström, and B. Grisogono, 1998: Idealized Simulations of Atmospheric Coastal Flow along the CentralCoast of California. *Journal of Applied Meteorology*, **37**, 1332–1363, doi:10.1175/1520-0450(1998)037<1332:ISOACF>2.0.CO;2.

Dickson, R. R. and J. Brown, 1994: The production of North Atlantic Deep Water: Sources, rates, and pathways. *Journal of Geophysical Research*, **99**, 12 319–12 341, doi:10.1029/94JC00530.

Douglas, M. W., M. A. Shapiro, L. S. Fedor, and L. Saukkonen, 1995: Research Aircraft Observations of a Polar Low at the East Greenland Ice Edge. *Monthly Weather Review*, **123**, 5–15, doi:10.1175/1520-0493(1995)123<0005:RAOOAP>2.0.CO;2.

Doyle, J. D. and M. A. Shapiro, 1999: Flow response to large-scale topography: The Greenland tip jet. *Tellus A*, **51**, 728–748, doi:10.1034/j.1600-0870.1996.00014.x.

Doyle, J. D., M. A. Shapiro, Q. Jiang, and D. L. Bartels, 2005: Large-Amplitude Mountain Wave Breaking over Greenland. *Journal of the Atmospheric Sciences*, **62**, 3106–3126, doi:10.1175/JAS3528.1.

Durran, D. R., 1990: Mountain waves and downslope winds. *Atmospheric Processes Over Complex Terrain*, **23**, 59–83.

Ebuchi, N., H. C. Graber, and M. J. Caruso, 2002: Evaluation of Wind Vectors Observed by QuikSCAT/SeaWinds Using Ocean Buoy Data. *Journal of Atmospheric and Oceanic Technology*, **19**, 2049–2062, doi:10.1175/1520-0426(2002)019<2049:EOWVOB>2.0.CO;2.

Haine, T. W. N., S. Zhang, G. W. K. Moore, and I. A. Renfrew, 2009: On the impact of high-resolution, high-frequency meteorological forcing on Denmark Strait ocean circulation. *Quarterly Journal of the Royal Meteorological Society*, **135**, 2067–2085, doi:10.1002/qj.505.

Hansen, B. and S. Østerhus, 2000: North Atlantic – Nordic Seas exchanges. *Progress In Oceanography*, **45**, 109–208, doi:10.1016/S0079-6611(99)00052-X.

Harden, B. E., I. A. Renfrew, and G. N. Petersen, 2011: A Climatology of Wintertime Barrier Winds off Southeast Greenland. *Journal of Climate*, **24**, 4701–4717, doi:10.1175/2011JCLI4113.1.

Hastings, D. A., et al., 1999: The Global Land One-kilometer Base Elevation (GLOBE) Digital Elevation Model, Version 1.0. Tech. rep., National Oceanic and Atmospheric Administration, National Geophysical Data Center, 325 Broadway, Boulder, Colorado 80305-3328, U.S.A. URL `http://www.ngdc.noaa.gov/mgg/topo/globe.html`.

Heinemann, G. and T. Klein, 2002: Modelling and observations of the katabatic flow dynamics over Greenland. *Tellus A*, **54**, 542–554, doi:10.1034/j.1600-0870.2002.201401.x.

Hoskins, B. J. and K. I. Hodges, 2002: New Perspectives on the Northern Hemisphere Winter Storm Tracks. *Journal of the Atmospheric Sciences*, **59**, 1041–1061, doi:10.1175/1520-0469(2002)059<1041:NPOTNH>2.0.CO;2.

Hurrell, J. W., 1995: Decadal Trends in the North Atlantic Oscillation: Regional Temperatures and Precipitation. *Science*, **269**, 676–679, doi:10.1126/science.269.5224.676.

IPCC, 2007: *Climate Change 2007: The Physical Science Basis. Contribution of Working Group I to the Fourth Assessment Report of the Intergovernmental Panel on Climate Change*. Cambridge University Press, Cambridge, United Kingdom and New York, NY, USA.

Irvine, E. A., S. L. Gray, J. Methven, and I. A. Renfrew, 2010: Forecast Impact of Targeted Observations: Sensitivity to Observation Error and Proximity to Steep Orography. *Monthly Weather Review*, **139**, 69–78, doi:10.1175/2010MWR3459.1.

Irvine, E. A., S. L. Gray, J. Methven, I. A. Renfrew, K. Bovis, and R. Swinbank, 2009: The impact of targeted observations made during the Greenland Flow Distortion Experiment. *Quarterly Journal of the Royal Meteorological Society*, **135**, 2012–2029, doi:10.1002/qj.499.

Josey, S. A., 2001: A Comparison of ECMWF, NCEP–NCAR, and SOC Surface Heat Fluxes with Moored Buoy Measurements in the Subduction Region of the Northeast Atlantic. *Journal of Climate*, **14**, 1780–1789, doi:10.1175/1520-0442(2001)014<1780:ACOENN>2.0.CO;2.

Junge, M. M., R. Blender, K. Fraedrich, V. Gayler, U. Luksch, and F. Lunkeit, 2005: A world without Greenland: impacts on the Northern Hemisphere wintercirculation in low- and high-resolution models. *Climate Dynamics*, **24**, 297–307, doi:10.1007/s00382-004-0501-2.

Klein, T. and G. Heinemann, 2002: Interaction of katabatic winds and mesocyclones near the eastern coast of Greenland. *Meteorological Applications*, **9**, 407–422, doi:10.1017/S1350482702004036.

Kristjánsson, J. E. and H. McInnes, 1999: The Impact of Greenland on cyclone evolution in the North Atlantic. *Quarterly Journal of the Royal Meteorological Society*, **125**, 2819–2834, doi:10.1002/qj.49712556003.

Lavender, K. L., R. E. Davis, and W. B. Owens, 2000: Mid-depth recirculation observed in the interior Labrador and Irminger seas by direct velocity measurements. *Nature*, **407**, 66–69, doi:10.1038/35024048.

Lavender, K. L., R. E. Davis, and W. B. Owens, 2002: Observations of Open-Ocean Deep Convection in the Labrador Sea from Subsurface Floats. *Journal of Physical Oceanography*, **32**, 511–526, doi:10.1175/1520-0485(2002)032<0511:OOOODC>2.0.CO;2.

Loescher, K. A., G. S. Young, B. A. Colle, and N. S. Winstead, 2006: Climatology of Barrier Jets along the Alaskan Coast. Part I: Spatial and Temporal Distributions. *Monthly Weather Review*, **134**, 437–453, doi:10.1175/MWR3037.1.

Macrander, A., U. Send, H. Valdimarsson, S. Jónsson, and R. H. Käse, 2005: Interannual changes in the overflow from the Nordic Seas into the Atlantic Ocean through Denmark Strait. *Geophysical Research Letters*, **32**, L06 606, doi:10.1029/2004GL021463.

Magaldi, M. G., T. W. N. Haine, and R. S. Pickart, 2011: On the Nature and Variability of the East Greenland Spill Jet: A Case Study in Summer 2003. *J. Phys. Oceanogr.*, **41**, 2307–2327, doi:10.1175/JPO-D-10-05004.1.

Marshall, J. and F. Schott, 1999: Open-ocean convection: Observations, theory, and models. *Reviews of Geophysics*, **37**, 1–64, doi:10.1029/98RG02739.

Martin, R. and G. W. K. Moore, 2006: Transition of a synoptic system to a polar low via interaction with the orography of Greenland. *Tellus A*, **58**, 236–253, doi:10.1111/j.1600-0870.2005.00169.x.

Martin, R. and G. W. K. Moore, 2007: Air-sea interaction associated with a Greenland reverse tip jet. *Geophysical Research Letters*, **34**, L24 802, doi:10.1029/2007GL031093.

Moore, G. W. K., 2003: Gale force winds over the Irminger Sea to the east of Cape Farewell, Greenland. *Geophysical Research Letters*, **30**, 1894, doi:10.1029/2003GL018012.

Moore, G. W. K., R. S. Pickart, and I. A. Renfrew, 2008: Buoy observations from the windiest location in the world ocean, Cape Farewell, Greenland. *Geophysical Research Letters*, **35**, L18 802, doi:10.1029/2008GL034845.

Moore, G. W. K. and I. A. Renfrew, 2005: Tip Jets and Barrier Winds: A QuikSCAT Climatology of High Wind Speed Events around Greenland. *Journal of Climate*, **18**, 3713–3725, doi:10.1175/JCLI3455.1.

Mysak, L., 1980: Topographically Trapped Waves. *Annual Review of Fluid Mechanics*, **12**, 45–76, doi:10.1146/annurev.fl.12.010180.000401.

National Geospatial-Intelligence Agency, 2004: Handbook of Magnetic Compass Adjustment. Tech. rep., National Geospatial-Intelligence Agency.

Ólafsson, H., 1998: Different predictions by two NWP models of the surface pressure field east of Iceland. *Meteorological Applications*, **5**, 253–261, doi:10.1017/S1350482798000875.

Ólafsson, H. and P. Bougeault, 1996: Nonlinear Flow Past an Elliptic Mountain Ridge. *Journal of the Atmospheric Sciences*, **53**, 2465–2489, doi:10.1175/1520-0469(1996)053<2465:NFPAEM>2.0.CO;2.

Ólafsson, H. and P. Bougeault, 1997: The Effect of Rotation and Surface Friction on Orographic Drag. *Journal of the Atmospheric Sciences*, **54**, 193–210, doi:10.1175/1520-0469(1997)054<0193:TEORAS>2.0.CO;2.

Olson, J. B. and B. A. Colle, 2009: Three-Dimensional Idealized Simulations of Barrier Jets along the Southeast Coast of Alaska. *Monthly Weather Review*, **137**, 391–413, doi:10.1175/2008MWR2480.1.

Olson, J. B., B. A. Colle, N. A. Bond, and N. Winstead, 2007: A Comparison of Two Coastal Barrier Jet Events along the Southeast Alaskan Coast during the SARJET Field Experiment. *Monthly Weather Review*, **135**, 3642–3663, doi:10.1175/MWR3448.E1.

Outten, S. D., I. A. Renfrew, and G. N. Petersen, 2009: An easterly tip jet off Cape Farewell, Greenland. II: Simulations and dynamics. *Quarterly Journal of the Royal Meteorological Society*, **135**, 1934–1949, doi:10.1002/qj.531.

Outten, S. D., I. A. Renfrew, and G. N. Petersen, 2010: Erratum: An easterly tip jet off Cape Farewell, Greenland. II: Simulations and dynamics. *Quarterly Journal of the Royal Meteorological Society*, **136**, 1099–1101, doi:10.1002/qj.629.

Parish, T. R., 1982: Barrier Winds Along the Sierra Nevada Mountains. *Journal of Applied Meteorology*, **21**, 925–930, doi:10.1175/1520-0450(1982)021<0925:BWATSN>2.0.CO;2.

Parish, T. R., 1983: The Influence of the Antarctic Peninsula on the Wind Field Over the Western Weddell Sea. *Journal of Geophysical Research*, **88**, 2684–2692, doi:10.1029/JC088iC04p02684.

Parish, T. R. and J. J. Cassano, 2003: The Role of Katabatic Winds on the Antarctic Surface Wind Regime. *Monthly Weather Review*, **131**, 317–333.

Pelly, J. L. and B. J. Hoskins, 2003: A New Perspective on Blocking. *Journal of the Atmospheric Sciences*, **60**, 743–755, doi:10.1175/1520-0469(2003)060<0743:ANPOB>2.0.CO;2.

Petersen, G. N., J. E. Kristjánsson, and H. Ólafsson, 2004: Numerical simulations of Greenland's impact on the Northern Hemisphere winter circulation. *Tellus A*, **56**, 102–111, doi:10.1111/j.1600-0870.2004.00047.x.

Petersen, G. N., J. E. Kristjánsson, and H. Ólafsson, 2005: The effect of upstream wind direction on atmospheric flow in the vicinity of a large mountain. *Quarterly Journal of the Royal Meteorological Society*, **131**, 1113–1128, doi:10.1256/qj.04.01.

Petersen, G. N., H. Ólafsson, and J. E. Kristjánsson, 2003: Flow in the lee of idealised mountains and Greenland. *Journal of the Atmospheric Sciences*, **60**, 2183–2195, doi:10.1175/1520-0469(2003)060<2183:FITLOI>2.0.CO;2.

Petersen, G. N. and I. A. Renfrew, 2009: Aircraft-based observations of air-sea fluxes over Denmark Strait and the Irminger Sea during high wind speed conditions. *Quarterly Journal of the Royal Meteorological Society*, **135**, 2030–2045, doi:10.1002/qj.355.

Petersen, G. N., I. A. Renfrew, and G. W. K. Moore, 2009: Overview of barrier winds off southeastern Greenland during GFDEx. *Quarterly Journal of the Royal Meteorological Society*, **135**, 1950–1967, doi:10.1002/qj.455.

Pickart, R. S., M. A. Spall, G. W. K. Moore, T. J. Weingartner, R. A. Woodgate, K. Aagaard, and K. Shimada, 2011: Upwelling in the Alaskan Beaufort Sea: Atmospheric forcing and local versus non-local response. *Progress In Oceanography*, **88**, 78–100, doi:10.1016/j.pocean.2010.11.005.

Pickart, R. S., M. A. Spall, M. H. Ribergaard, G. W. K. Moore, and R. F. Milliff, 2003: Deep convection in the Irminger Sea forced by the Greenland tip jet. *Nature*, **424**, 152–156, doi:10.1038/nature01729.

Pickart, R. S., D. J. Torres, and P. S. Fratantoni, 2005: The East Greenland Spill Jet. *Journal of Physical Oceanography*, **35**, 1037–1053, doi:10.1175/JPO2734.1.

Pierrehumbert, R. T. and B. Wyman, 1985: Upstream Effects of Mesoscale Mountains. *Journal of the Atmospheric Sciences*, **42**, 977–1003, doi:10.1175/1520-0469(1985)042<0977:UEOMM>2.0.CO;2.

Rabier, F., J.-N. Thépaut, and P. Courtier, 1998: Extended assimilation and forecast experiments with a four-dimensional variational assimilation system. *Quarterly Journal of the Royal Meteorological Society*, **124**, 1861–1887, doi:10.1002/qj.49712455005.

Rasmussen, L., 1989: Den dag, Angmagssalik naesten blaeste i havet. *Vejret, Danish Meteorological Society*, **2**, 3–14.

Renfrew, I. A., G. W. K. Moore, P. S. Guest, and K. Bumke, 2002: A Comparison of Surface Layer and Surface Turbulent Flux Observations over the Labrador Sea with ECMWF Analyses and NCEP Reanalyses. *Journal of Physical Oceanography*, **32**, 383–400, doi:10.1175/1520-0485(2002)032<0383:ACOSLA>2.0.CO;2.

Renfrew, I. A., S. D. Outten, and G. W. K. Moore, 2009a: An easterly tip jet off Cape Farewell, Greenland. I: Aircraft observations. *Quarterly Journal of the Royal Meteorological Society*, **135**, 1919–1933, doi:10.1002/qj.513.

Renfrew, I. A., G. N. Petersen, D. Sproson, G. W. K. Moore, S. Adiwidjaja, H. Zhang, and R. North, 2009b: A comparison of aircraft-based surface-layer observations over Denmark Strait and the Irminger Sea with meteorological analyses and QuikSCAT winds. *Quarterly Journal of the Royal Meteorological Society*, **135**, 2046–2066, doi: 10.1002/qj.444.

Renfrew, I. A., et al., 2008: The Greenland Flow Distortion Experiment. *Bulletin of the American Meteorological Society*, **89**, 1307–1324, doi:10.1175/2008BAMS2508.1.

Revell, M. J., J. H. Copeland, H. R. Larsen, and D. S. Wratt, 2002: Barrier jets around the Southern Alps of New Zealand and their potential to enhance alpine rainfall. *Atmospheric Research*, **61**, 277–298, doi:10.1016/S0169-8095(01)00142-9.

Rex, D. F., 1950a: Blocking action in the middle troposphere and its effect upon regional climate. I. An aerological study of blocking action. *Tellus*, **2**, 196–211, doi:10.1111/j. 2153-3490.1950.tb00331.x.

Rex, D. F., 1950b: Blocking action in the middle troposphere and its effect upon regional climate. II. The climatology of blocking action. *Tellus*, **2**, 275–301, doi: 10.1111/j.2153-3490.1950.tb00339.x.

Reynolds, R. W., N. A. Rayner, T. M. Smith, D. C. Stokes, and W. Wang, 2002: An Improved In Situ and Satellite SST Analysis for Climate. *J. Climate*, **15**, 1609–1625, doi:10.1175/1520-0442(2002)015<1609:AIISAS>2.0.CO;2.

Sahsamanoglou, H. S., 1990: A contribution to the study of action centres in the North Atlantic. *International Journal of Climatology*, **10**, 247–261, doi:10.1002/joc. 3370100303.

Sampe, T. and S.-P. Xie, 2007: Mapping High Sea Winds from Space: A Global Climatology. *Bulletin of the American Meteorological Society*, **88**, 1965–1978, doi: 10.1175/BAMS-88-12-1965.

Schott, F., M. Visbeck, and J. Fischer, 1993: Observations of Vertical Currents and Convection in the Central Greenland Sea During the Winter of 1988–1989. *Journal of Geophysical Research*, **98**, 14 401–14 421, doi:10.1029/93JC00658.

Schwerdtfeger, W., 1975: The Effect of the Antarctic Peninsula on the Temperature Regime of the Weddell Sea. *Monthly Weather Review*, **103**, 45–51, doi:10.1175/1520-0493(1975)103<0045:TEOTAP>2.0.CO;2.

Scorer, R. S., 1988: Sunny Greenland. *Quarterly Journal of the Royal Meteorological Society*, **114**, 3–29, doi:10.1002/qj.49711447902.

Serreze, M. C., F. Carse, R. G. Barry, and J. C. Rogers, 1997: Icelandic Low Cyclone Activity: Climatological Features, Linkages with the NAO, and Relationships with Recent Changes in the Northern Hemisphere Circulation. *Journal of Climate*, **10**, 453–464, doi:10.1175/1520-0442(1997)010<0453:ILCACF>2.0.CO;2.

Shaffrey, L. C., et al., 2009: U.K. HiGEM: The New U.K. High-Resolution Global Environment Model – Model Description and Basic Evaluation. *Journal of Climate*, **22**, 1861–1896, doi:10.1175/2008JCLI2508.1.

Skeie, R. B., J. E. Kristjánsson, H. Ólafsson, and B. Røsting, 2006: Dynamical processes related to cyclone development near Greenland. *Meteorologische Zeitschrift*, **15**, 147–156, doi:10.1127/0941-2948/2006/0114.

Smith, P. C., 1976: Baroclinic instability in the denmark strait overflow. *J. Phys. Oceanogr.*, **6**, 355–371, doi:10.1175/1520-0485(1976)006<0355:BIITDS>2.0.CO;2.

Smith, R. B., 1989: Hydrostatic airflow over mountains. *Advances in Geophysics*, **31**, 1–41, doi:10.1016/S0065-2687(08)60052-7.

Spall, M. A. and J. F. Price, 1998: Mesoscale Variability in Denmark Strait: The PV Outflow Hypothesis. *Journal of Physical Oceanography*, **28**, 1598–1623, doi:10.1175/1520-0485(1998)028<1598:MVIDST>2.0.CO;2.

Sproson, D. A. J., I. A. Renfrew, and K. J. Heywood, 2008: Atmospheric conditions associated with oceanic convection in the south-east Labrador Sea. *Geophysical Research Letters*, **35**, L06 601, doi:10.1029/2007GL032971.

Stark, J., C. Donlon, M. Martin, and M. McCulloch, 2007: OSTIA : An operational, high resolution, real time, global sea surface temperature analysis system. *OCEANS 2007 - Europe DOI - 10.1109/OCEANSE.2007.4302251*, 1–4.

Steingrimur, J. and H. Valdimarsson, 2004: A new path for the Denmark Strait overflow water from the Iceland Sea to Denmark Strait. *Geophysical Research Letters*, **31**, L03 305, doi:10.1029/2003GL019214.

Straneo, F., G. S. Hamilton, D. A. Sutherland, L. A. Stearns, F. Davidson, M. O. Hammill, G. B. Stenson, and A. Rosing-Asvid, 2010: Rapid circulation of warm subtropical waters in a major glacial fjord in East Greenland. *Nature Geoscience*, **3**, 182–186, doi:10.1038/ngeo764.

Våge, K., R. S. Pickart, G. W. K. Moore, and M. H. Ribergaard, 2008: Winter Mixed Layer Development in the Central Irminger Sea: The Effect of Strong, Intermittent Wind Events. *Journal of Physical Oceanography*, **38**, 541–565, doi:10.1175/2007JPO3678.1.

Våge, K., R. S. Pickart, M. A. Spall, H. Valdimarsson, S. Jónsson, D. J. Torres, S. Østerhus, and T. Eldevik, 2011: Significant role of the North Icelandic Jet in the formation of Denmark Strait overflow water. *Nature Geoscience*, **4**, 723–727, doi:10.1038/ngeo1234.

Våge, K., T. S. Spengler, H. C. Davies, and R. S. Pickart, 2009: Multi-event analysis of the westerly Greenland tip jet based upon 45 winters in ERA-40. *Quarterly Journal of the Royal Meteorological Society*, **135**, 1999–2011, doi:10.1002/qj.488.

van den Broeke, M. R. and H. Gallée, 1996: Observation and simulation of barrier winds at the western margin of the Greenland ice sheet. *Quarterly Journal of the Royal Meteorological Society*, **122**, 1365–1383, doi:10.1002/qj.49712253407.

Webster, F., 1968: Observations of inertial-period motions in the deep sea. *Rev. Geophys.*, **6**, 473–490, doi:10.1029/RG006i004p00473.